UNIVERSITY OF LEICESTER

Graduate School

AN ENGINEERING ASSET MANAGEMENT APPROACH TO THE EVALUATION OF UNDERGROUND POWER TRANSMISSION CABLES

Thesis submitted for the degree of

Doctor of Philosophy

At the University of Leicester

by

Hang ZHOU

Department of Engineering

University of Leicester

June 2018

Acknowledgements:

First of all, I would like to express my sincere gratefulness to my supervisor, Prof. Jingzhe PAN. His brilliant ideas and patient instructions allowed me to build up my PhD research with a solid foundation. He supplied me with generous resources from academia and industry while also allowing me great freedom in exploring the research field. He had the vision and offered support whenever it was needed. It was a great pleasure discussing research difficulties with him as he could always discover the key issues of obstacle, and at the same time would provide valuable and constructive suggestions. The way he encouraged me in my early research is indeed a philosophy that will influence my style of continuous work: be modest, subtle, honest, polite and grateful, as well as having an eternally curious heart.

This PhD project was carried out in close interaction with a research team led by Dr. Sivashangari Gnanasambandam. My research work benefited enormously through discussions with the team. These interactions have led to the two joint papers which were approved by National Grid Ltd. For publication, to which I am very grateful. The interactions and discussion were limited to either information that were in the public domain, or on information approved for publications in the three joined papers by National Grid Ltd. I would like to thank Mr. Maurizio Foresta, Dr. David Weston, Dr. Fan Li, and Dr. Michelle Le Blanc for their support and guidance throughout my research.

In addition, I would like to thank two funding bodies, the Great Britain China Educational Trust and the Henry Lester Trust Ltd. for their partial financial support during my PhD studies.

Finally, I would especially thank my family and friends. It is their continuous supports that made the completion of my PhD possible. My parents, grandparents, my uncles, aunts and cousins, their mental and psychological support in never doubting myself and staying strong when there are obstacles are extra special and was of great need to me. The patience they had and the enthusiasm to my career allowed me to focus and stay passionate. In particular, I would like to thank my girlfriend, Viola Wiegand, who is also doing a PhD the same time with me. She is always by my side, with happiness or with sorrow, with sunshine or with rain. If there is anything that I trust and believe would not let me down even in the bottom of my life, it is her faithful opinion and her earnest characteristic. The sparkle and delightfulness she keeps bringing into my life is forever and ever the greatest motivation for me in approaching what I am dreaming, till a dream is no longer a dream, till a determination with dedication.

Table of Contents：

1. Introduction.....20

1.1 General information of underground power transmission cable.....20

1.2 Objective of the PhD research and structure of thesis.....27

2. Literature Review 29

The above URLs lead to information from Ofgem, KEMA, National Grid Ltd., FOREWIND etc. which all play an important role in the U.K. power transmission industry. 29

2.1 Engineering asset management.....30

2.1.1 A typical asset management method by the power supply industry 31

2.1.2 Ofgem DNO Common Network Asset Indices Methodology.....32

2.2 Corrosion of materials 41

2.2.1 Hazards and consequences of corrosion 41

2.2.2 Corrosion mechanism and types of corrosion.....42

2.2.3 Caustic corrosion 53

2.3 Background of pitting corrosion and corrosion fatigue 53

2.3.1 Pit initiation.....54

2.3.2 Pitting corrosion.....56

2.3.3 Pit-crack transfer.....59

2.3.4 Crack propagation.....60

2.4 Research methodologies for engineering asset management against corrosion 61
2.5 Models for corrosion and fatigue 64
2.5.1 Models for corrosion 65
2.5.2 Models for fatigue 65
2.5.3 A modified crack growth model by author's research team within the project 66
2.6 Unresolved issues and the purpose of this thesis 69
3. Modelling of pit depth distribution for phosphor bronze tapes used in underground power transmission cables 73
3.1 Laboratory measurement of pit depths and data collection 73
3.2 Mathematical simulation on pit depth distribution model 75
3.3 Simulation results and discussion of the model 79
3.3.1 Experimental pit depth distribution 79
3.3.2 Pit growth modelling: Determination of pit growth parameter β and selection of probability distribution for α 87
3.3.3 Pit depth evolution and distribution 90
3.3.4 Pit depth distribution at different environmental conditions 96
4. Life prediction of phosphor bronze reinforcing tape used in underground power cables: - applying the pit to crack transfer probability 105
4.1 Model description 106

4.1.1 Pit Initiation 108
4.1.2 Pitting Corrosion 109
4.1.3 Fatigue 112
4.1.4 Procedure to calculate cable life 113
4.2 Results and discussions 116
4.2.1 Results for pit growth modelling 116
4.2.2 Results for pit to crack transfer 120
4.2.3 Determination of crack growth (Paris Law) parameters 126
4.2.4 Cable life prediction 127
4.2.5 Validation of life prediction model on existing circuit 127
4.3 Achievements of this research chapter 140
5. Defining probability of failure for both the empirical-based model and the mechanism-based model 141
5.1 A hypothesis based on the current industrial asset management model 141
5.2 A corrosion fatigue mechanism-based model on cable life estimation 153
5.2.1 Obtaining the pit depth distribution 153
5.2.2 Obtaining the pit-crack transfer pit depth 154
5.2.3 Processing the existing data for cable sections 154
5.2.4 Defining mechanism-based probability of failure model 158

6. A machine-learning algorithm approach on power cable probability of failure updating 167

6.1 Fundamental Bayesian Inference modelling 167

6.2 Probability density function models 169

6.2.1 PDF for empirical-based model 169

6.2.2 PDF for mechanism-based model 170

6.3 Assumptions and results of Bayesian Inference modelling 171

6.3.1 Markov Chain Monte Carlo (MCMC) method 172

6.3.2 Expression of the Bayesian Inference updated model 176

6.4 Explanation of the Bayesian Inferenced models 177

7. Conclusions 181

7.1 Conclusion on modelling the pit depth distribution (Chapter 3) 181

7.2 Conclusion on modelling pit growth and pit to crack transfer probability (Chapter 4) 181

7.3 Conclusion on modelling power transmission cable probability of failure (Chapter 5) and a machine learning approach (Bayesian Inference) to power cable probability of failure (Chapter 6) 182

Future Work: 184

Appendix I 185

Appendix II 204

References: 211

List of Publications:

1) Hang Zhou, Sivashangari Gnanasambandam, Maurizio Foresta, David Weston, Fan Li, Jingzhe Pan, Michelle Le Blanc, *Measurement and Modelling of Pitting Depth Distribution for Phosphor Bronze Tapes Used in Underground Power Transmission Cables*, CORROSION. 2017; 73(7):844-852.

2) Hang Zhou, Sivashangari Gnanasambandam, Maurizio Foresta, Fan Li, Michelle Le Blanc, David Weston, Jingzhe Pan, *Life Prediction of Phosphor Bronze Reinforcing Tape Used in Underground Power Cables*, CORROSION. 2018; 74(5):530-542.

3) Hang Zhou, Fan Li, Michelle Le Blanc, Jingzhe Pan, *A machine learning approach proposing the 'Intelligent Power Grid' in engineering asset management*, (Submitted to IEEE Transactions on Power Systems and under review).

List of Conference Presentation:

1) Hang Zhou (2016). Pitting corrosion in phosphor bronze tape used in underground power transmission cables – A Monte Carlo study, Paper presented at the NACE Milano Italia Section Conference & Expo 2016, Genoa, Italy.

List of Awards and Funding Bodies:

1) **Chinese Student Award** on Excellence of Ph.D. research (2017)

   Great Britain-China Educational Trust (GBCET)

2) **The Henry Lester Trust Award** (2017)

   Henry Lester Trust Ltd.

List of Figures:

Chapter 1:

Figure 1-1: A typical underground power cable layout

Figure 1-2: a) 3D representation for the components in the underground power transmission cable b) Cut-section of the underground power transmission cable

Figure 1-3: Gas and electricity network route maps

Chapter 2:

Figure 2-1: Galvanic series

Figure 2-2: Crevice in metal under water

Figure 2-3: Crevice corrosion process

Figure 2-4: Pitting corrosion under microscope

Figure 2-5: Through pits

Figure 2-6: Sideway pits

Figure 2-7: Intergranular corrosion of a failed aircraft component made of 7075-T6 aluminium

Figure 2-8: Flowchart of cable failure process

Figure 2-9: Penetration mechanism and phase diagram of a passive film with related processes of ion and electron transfer within the film and at its phase boundaries

Figure 2-10: Mechanical film breakdown mechanism and related competing processes

Figure 2-11: Adsorption mechanism with increased local transfer of metal ions and related corrosion current density, i_c, caused by complexing aggressive anions leading to thinning of the passive layer and increases in field strength and final free corrosion current density $i_{c,h}$ within the pit

Figure 2-12: (a) Outer and inner surface of the tape covered with bitumen (b) Outer and inner surface of the tape after bitumen removal with pentane (c) Example of tape in the mounting machine. Note the supporting clips necessary due to the small thickness of the tape (d) Cross-sectional view of the corrosion pits that are taken perpendicularly to the longitudinal axis of the tape (e) Corroded reinforcing phosphor bronze tape surface with a fracture end on the left (thickness of the tape about 150 µm)

Chapter 3:

Figure 3-1: Flowchart for pit growth modelling using Monte Carlo simulations

Figure 3-2: Pit depth measurement of Site 1 at 38 years (first failure)

Figure 3-3: Pit depth measurement of Site 1 at 44 years (second failure)

Figure 3-4: Pit depth measurement of Site 2 (43 years)

Figure 3-5: Pit depth measurement of Site 3 (28 years)

Figure 3-6: Pit depth measurement of Site 4 (41 years)

Figure 3-7: Pit depth distributions for 2 sets of samples belonging to the same piece of

tape

Figure 3-8: A representation of pit growth in hemispherical geometry

Figure 3-9: Comparison between experiment and simulation pit depth distribution of reinforcing tape of age 38 years

Figure 3-10: Comparison between experiment and simulation pit depth distribution of reinforcing tape of age 44 years

Figure 3-11: Comparison between simulation pit depth distribution of reinforcing tape of both age 38 years and 44 years

Figure 3-12: Theoretical pit depth distribution with evolution of time

Figure 3-13: Comparison between experiment and simulation pit depth distribution of reinforcing tape of age 43 years (Site 1)

Figure 3-14: Comparison between experiment and simulation pit depth distribution of reinforcing tape of age 28 years (Site 2)

Figure 3-15: Comparison between experiment and simulation pit depth distribution of reinforcing tape of age 41 years (Site 3)

Chapter 4:

Figure 4-1: (a) 3D optical microscopy image showing pits on the outer surface of the tape (b) SEM image of corrosion fatigue crack starting from a pit. The crack in the cross section shown was normal to the direction of the applied load (longitudinal axis of the tape).

Figure 4-2: Pictorial representation for the structure of the methodology in this chapter

Figure 4-3: Example plot for time related pit depth distribution calculation

Figure 4-4: The theoretical pit depth distribution with time model compared to the Monte Carlo simulation pit depth distribution model with an initial pit number of 100

Figure 4-5: The theoretical pit depth distribution with time model compared to the Monte Carlo simulation pit depth distribution model with an initial pit number of 1 million

Figure 4-6: Two stages of failure case where pitting corrosion transfers into crack propagation

Figure 4-7: A representative curve among all the potential pit to crack transfer probability functions (cumulative distribution function of the Weibull distribution)

Figure 4-8: Potential pit to crack transfer probability functions represented in Weibull CDF plots

Figure 4-9: Possible transfer curves

Figure 4-10: Determined pit to crack transfer probability function plot

Figure 4-11: Validation of life prediction model by prediction year at which $P_{failure} = P_{failure\ at\ calibration}$ of different cable sections at Location 1

Figure 4-12: Validation of life prediction model by prediction year at which $P_{failure} = P_{failure\ at\ calibration}$ of different cable sections at Location 2

Figure 4-13: Validation of life prediction model by prediction year at which $P_{failure} = P_{failure\ at\ calibration}$ of different cable sections at Location 3

Figure 4-14: Validation of life prediction model by prediction year at which $P_{failure} = P_{failure\ at\ calibration}$ of different cable sections at Location 4

Figure 4-15: Validation of life prediction model by prediction year at which $P_{failure} = P_{failure\ at\ calibration}$ of different cable sections at Location 5

Figure 4-16: Validation of life prediction model by prediction year at which $P_{failure} = P_{failure\ at\ calibration}$ of different cable sections at Location 6

Figure 4-17: Validation of life prediction model by prediction year at which $P_{failure} = P_{failure\ at\ calibration}$ of different cable sections at Location 7

Figure 4-18: Validation of life prediction model by prediction year at which $P_{failure} = P_{failure\ at\ calibration}$ of different cable sections at Location 8

Figure 4-19: Validation of life prediction model by prediction year at which $P_{failure} = P_{failure\ at\ calibration}$ of different cable sections at Location 9

Figure 4-20: Validation of life prediction model by prediction year at which $P_{failure} = P_{failure\ at\ calibration}$ of different cable sections at Location 10

Chapter 5:

Figure 5-1: Pictorial representation of the cable replacement model in the power supplement industry

Figure 5-2: Assumed AHI=1 cable with the life anticipation distribution

Figure 5-3: Cable with criticality evaluation of severe line plot explaining the assumed condition of Figure 5-2

Figure 5-4: Conservative probability of failure by empirical-based model for cable with a criticality evaluation of severe

Figure 5-5: Liberal estimation shift from the original criticality severe evaluated plot

Figure 5-6: Liberal and conservative PoF by industry applied empirical model (upper and lower boundaries for criticality severe evaluated cables)

Figure 5-7: The comparison of original plot and both the conservative and liberal interpretation of estimation

Figure 5-8: PoF plot for criticality light evaluated cable (both conservative and liberal estimations)

Figure 5-9: Empirical model on probability of failure for cables with light and severe criticality evaluation interpreted from industry

Figure 5-10: Geological data for Cable 1

Figure 5-11: Mean stress vs Length of cable for Cable 1 (curves connecting mean stresses are simulated by natural cubic splines algorithm)

Figure 5-12: Life estimation by length of cable of Cable 1

Figure 5-13: Life estimation by length of cable of Cable 1

Figure 5-14: Mechanism-based probability of failure for Cable 2

Figure 5-15: Mechanism-based probability of failure for Cable 1

Figure 5-16: The probability of failure for Cable 1 under the definition from the mechanism-based model (Left) The fitted function comparing to the conservative and liberal probability of failure function by empirical-based model (Right)

Chapter 6:

Figure 6-1: One trial of Markov Chain construction by Metropolis Hastings algorithm sampling with trial elements of 10000, among which only the accepted values are plotted (upper)Fluctuation of all the accepted values (bottom)

Figure 6-2: Values of $G(t_i)$ corresponding to the samplings shown in Figure 6-1

Figure 6-3: The plot of the Bayesian Inferenced probability density function of the liberal estimated model of Cable 1

Figure 6-4: Comparison of Bayesian Inferenced model and original industrial replacement priority model for probability of failure estimation (both conservative and liberal of Cable 1)

Figure 6-5: Comparison of Bayesian Inferenced model and original industrial replacement priority model for probability of failure estimation (both conservative and liberal of Cable 2)

List of Tables:

Chapter 2:

Table 2-1: Asset Health Index

Table 2-2: Estimated remaining service life (Years) to Asset Health Index

Chapter 3:

Table 3-1: T test table

Table 3-2: T test value table showing the results of simulation for 5 different types of distributions

Table 3-3: Calculated mean pit depth of the reinforcing tapes at different environments

Chapter 4:

Table 4-1: Basic information of samples from Location A and Location B

Table 4-2: Location parameter μ for cables and corresponding transfer pit depths

Chapter 5:

Table 5-1: Summary of existing cable data used in this chapter

Table 5-2: Coefficient matrix $\boldsymbol{A_1}$ for cubic spline curve fitting of Cable 1 mean stress vs length of cable data

Table 5-3: Coefficient matrix $\boldsymbol{A_2}$ for cubic spline curve fitting of Cable 2 mean stress

vs length of cable data

Table 5-4: Statistical evaluation of similarity between the actual PoF and the fitted function describing the probability of failure for the mechanical-based model

Chapter 6:

Table 6-1: ‘Tailored probability of failure function’ for all critical locations

1. Introduction

This thesis focuses on the engineering asset management approach, specifically, the improvement of the probability of failure model evaluating underground power transmission cables. This chapter introduces the background information of the underground power transmission cable, as well as outlines the structure of this Ph.D. thesis.

1.1 General information of underground power transmission cable

Underground power cables are widely used in power transmission and distribution networks because they provide reliable, safe, and incur minimum aesthetic impact. Oil-impregnated paper-insulated cables have been installed for carrying high voltages since 1960s [1]. The nature of the underground power transmission cable is introduced in three sections: a) Design of underground power transmission cable. b) Power transmission cable for civil and commercial use. c) Failure of power transmission cable and its consequences.

a) Design of underground power transmission cable

Power transfer, here specifically the electricity transfer, is a complicated engineering task on a very large scale. Due to its complexity, there is a variety of types to fulfil the requirements of usage diversities.

One industry leading company classifies the cables in use in five types [2]:

- XLPE cables (Cross Linked Polyethylene Extruded) 33kV to 400kV
- FFC (Fluid Filled Cables) 33kV to 400kV
- PPL-FFC (Paper Polyethylene Laminated) 275kV and 400kV
- MIND (Mass Impregnate Non Draining) up to 33kV
- GIL (Gas Insulated Lines)

This research focuses on the cables started commission around the 1970s, and during this period of time, the major cable designs follow FFC (Fluid Filled Cables). According to [2], of all the installed cables within the electricity network, the majority of the fluid filled cables were installed in the 1970s. Figure 1-1 gives a visualization of underground power cables.

The power transmission cable has a central oil duct inside a copper conductor which carries the load current. The conductor is insulated using successive layers of paper which are impregnated with pressurized oil in order to provide dielectric insulation. These cables generally have a lead or aluminium metallic sheath, which serves a number of purposes such as; retaining the insulating oil within the cable insulation, allowing oil pressurization, preventing the ingress of air and moisture into the insulation and providing mechanical support for the cable. The particular design of the cable considered in this thesis uses a lead sheath. Due to poor creep resistance, the lead sheath is not able to hold the internal pressure alone. To overcome this limitation, phosphor-bronze reinforcing tapes (tin - 0.93%, phosphorus - 0.02%, copper – to balance the rest) are wound over the cable's lead sheath after bitumen impregnated bedding tape has been applied. These reinforcing tapes are vital to the hydraulic security of the cable. If they are damaged the lead sheath will creep and eventually crack, leading to a fluid leak. The cable is finally given extruded PVC/PE over sheath.

Oil-filled power transmission cable can be identified as two sub-categories with each individual range of inner oil pressure [3]:

1. A single cable with a centrally located oil channel, with the oil under low or medium pressure ($0.1{\sim}0.3\ MN/m^2 = 100{\sim}300\ kPa$).
2. Multicore high-pressure cable ($1.4{\sim}1.5\ MN/m^2 = 1400{\sim}1500\ kPa$).

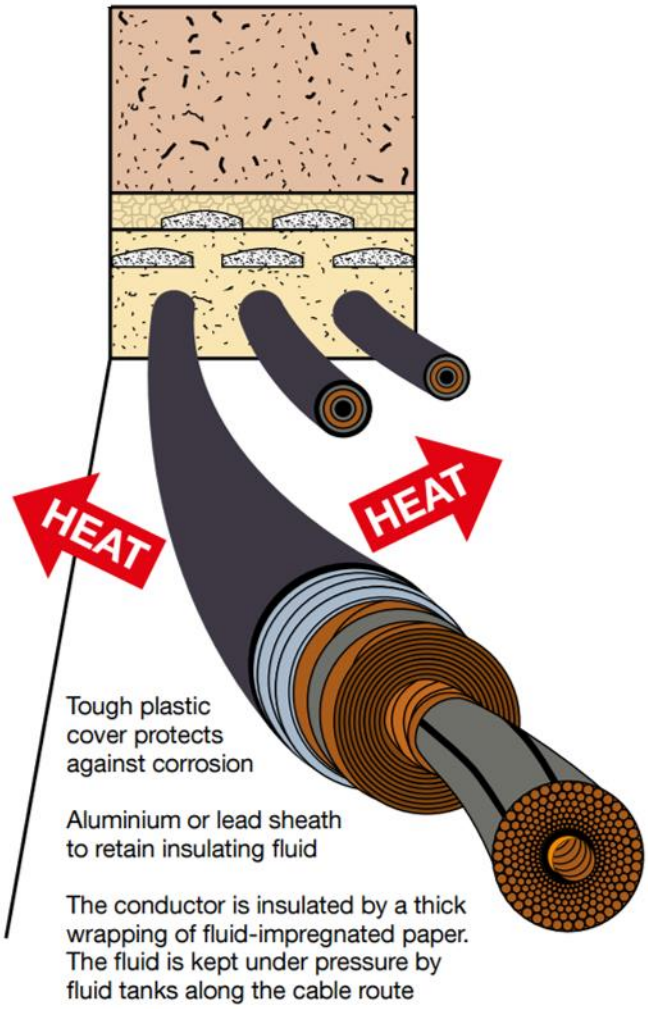

Figure 1-1: A typical underground power cable layout [2]

Further of Figure 1-1, a cut-section of the general Fluid Filled Cable design is shown in Figure 1-2 below, which explains the inner structure of the power cables under research. The protection phosphor bronze tape has a thickness of 0.15mm. According to TAIHAN Electric Wire Co., Ltd [4], for 275 kV underground power transmission cables, the nominal area is between 600 and 2000 mm^2, the paper insulation thickness is about 17.5 mm to 19.5 mm, the thickness of the sheath is around 2.0 to 2.5 mm, and the approximate overall diameter of the power cable is between 99 to 128 mm.

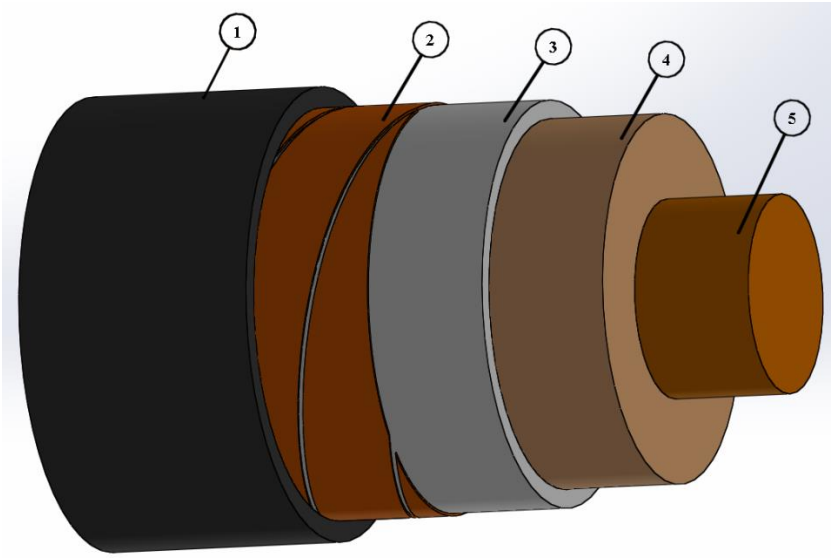

1. PVC over sheath
2. **Tin bronze tape with bitumen layer**
3. **Lead sheath**
4. Paper insulation
5. Conductor + oil duct

a)

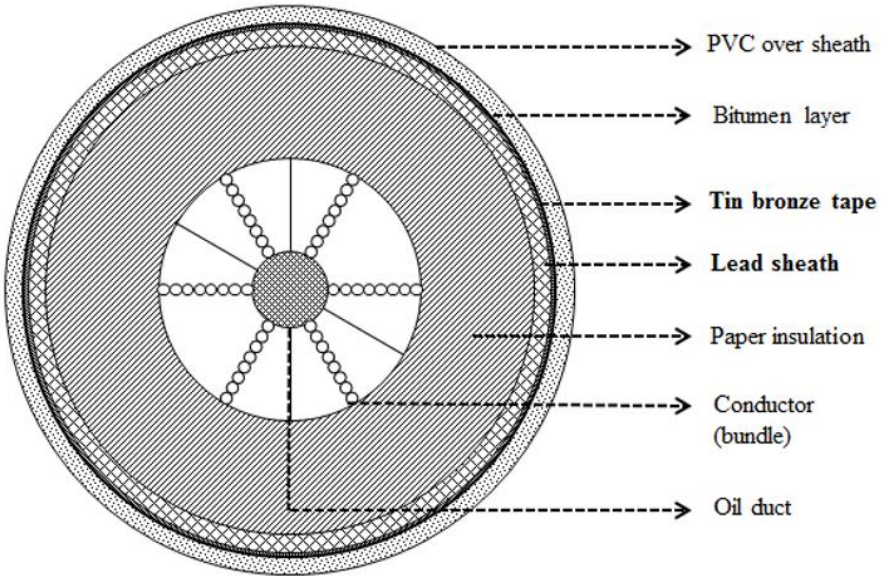

b)

Figure 1-2: a) 3D representation for the components in the underground power

transmission cable [5] b) Cut-section of the underground power transmission cable [6]

These cables have a paper insulation, wrapped around the central copper conductor and impregnated with fluid under pressure. The metallic tapes are wrapped around the paper insulation to reinforce the papers and retain the fluid pressure.

Outside the paper insulation, lead sheath covers the paper components. If it is exposed to ground water and other substances, the lead will deteriorate resulting in the ingress of water. To prevent this a layer of outer platic sheath wraps the inner layers for providing further insulation and prevent the potential corrosion, which is the PVC over sheath, shown in Figures 1-2 a) and 1-2 b).

Between the PVC over sheath and the lead sheath there is usually an additional layer of copper tapes (phospher bronze to be more accurate), this is to help the support of lead sheath and to prevent swelling as a result of the internal fluid pressures. [7]

To ensure the integrity of the cable, the outer sheath is covered in a semi-conductive material, which allows any defects in the outer sheath to be detected.

b) Power transmission cable for civil and commercial use

According to [2], currently the major power supplier, the National Grid plc. owns the high voltage electricity transmission system in England and Wales and operates the system throughout Great Britain at 275,000 and 400,000 volts (275kV and 400kV). This system contains approximately 7,200 kilometres (4,470 miles) of overhead line, 1,400 kilometres (870 miles) of underground cable and about 330 substations. A map is provided here which shows an overview of the energy operations geographically below in Figure 1-3 [8].

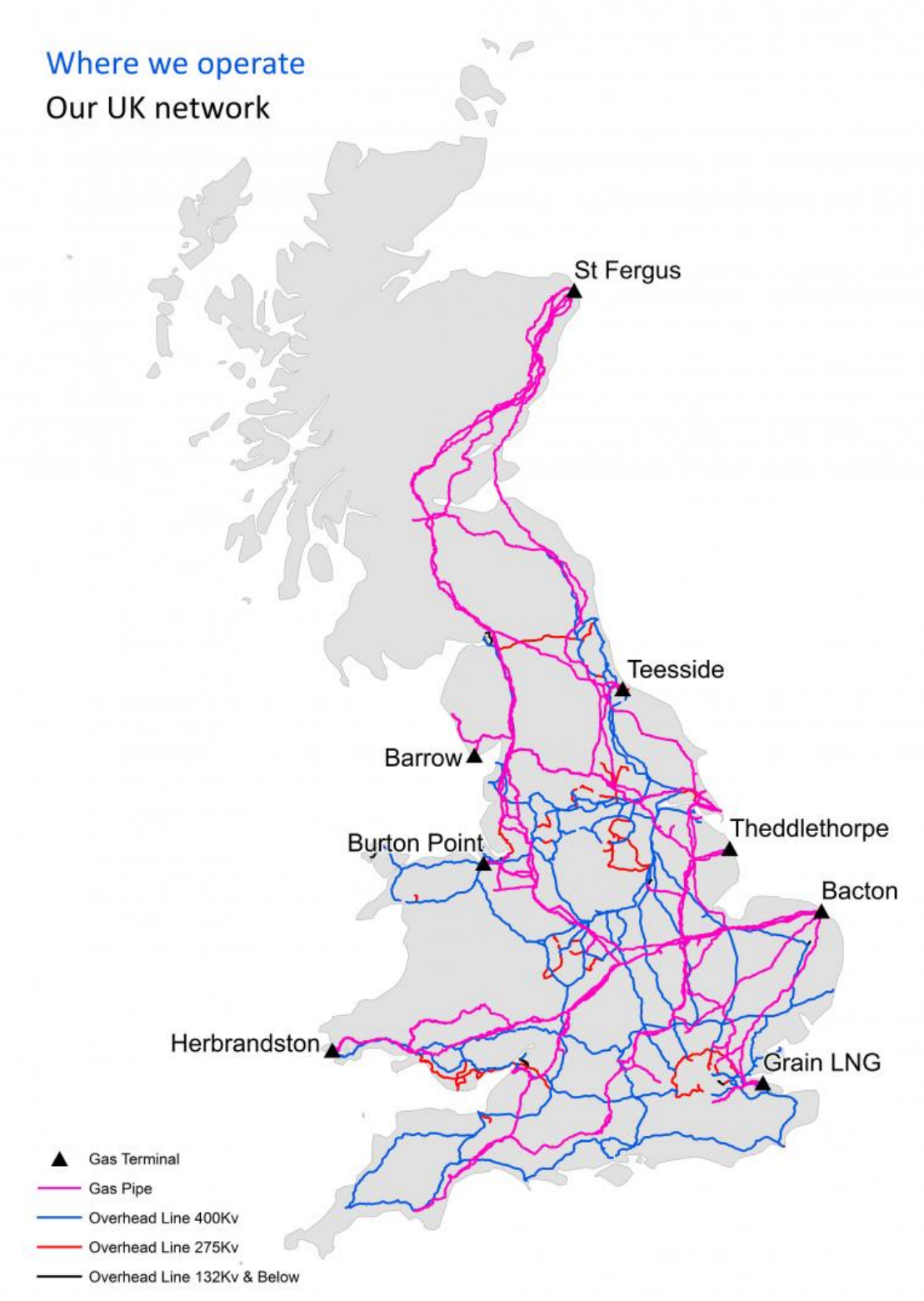

Figure 1-3: Gas and electricity network route maps [8]

According to the studies by the Institution of Civil Engineers [9], electricity transmission started around 1926. The initial national grids had 132kV in voltage. Due to the significant growth in gross domestic product and electricity demand in the 1950s, the UK created the Central Electricity Generating Board (CEGB) and started the building of a 400kV supergrid. Following the initial national grid developments in the 1920s, the distribution of electricity is generally through three voltage levels, the 33kV, 11kV and low voltage. Currently there are approximately 25 million customers in Great Britain.

Apart from the domestic users, Great Britain is also involved in interconnections with other countries for example, by the year 2014, there were four interconnectors from Great Britain:

- 2GW to France
- 1GW to Netherlands
- 500MW to Northern Ireland
- 500MW to the Republic of Ireland
- A fifth interconnector to Belgium is under consideration

c) Failure of power transmission cable and its consequences

According to [2], cables have an asset life of around 60 years, and they are regularly inspected and tested to ensure the cable insulation and joints are operating correctly. If a failure occurs on a 400kV underground cable, on average, due to the difficulty in locating, excavating and undertaking technically involved repairs, it will be out of service for a period 25 times longer than 400kV overhead lines.

Among all the failure reasons for underground power transmission cables, fluid leaks, faulty joints and accessories, sheath faults, water cooling failures and third-party damages are the majority causes. After a failure is detected, it takes from two to six weeks to locate the fault or fluid leak and repair the cable. At the same time, excavations

may be required, which will lead to road closures and traffic management measures. Based on the experience of construction, some of the excavations could be at the scale of $4m \times 30m$. [2]

The emergency failure of underground cables can cause sudden power offs for which it takes a long period of time to recover. This not only causes costs for the power supplying companies, but can create inconvenience and disturbance to civilians' everyday life as well as the functioning of public services, factory productions, industrial facilities etc.

To avoid such costly consequences, the best solution is to avoid failure and process the maintenance before failure occurs, where the accuracy of engineering asset management plays a significant role. This research puts the focus on the improvement of engineering asset management accuracy and feasibility.

1.2 Objective of the PhD research and structure of thesis

The aim of this research is to improve the existing model currently applied in the industry in the practise of 'Engineering Asset Management', which is to estimate the probability of failure on power cables throughout their servicing lives, in order to enable a more accurate prediction of cable lives or the probability of failure of cables to assist the asset management decisions.

This thesis will follow the following structure, excluding Chapter 1 as the introduction chapter:

Chapter 2 gives the information of Literature Review, including the available data and the experimental results of related research topic. **Chapter 3** is the first research result chapter, it gives details for the simulation of pit depth distribution on the surface of the phosphor bronze protection layer. **Chapter 4** discusses the pit to crack transfer probability, this is a novel explanation to explain the experimental results that do no follow the conventional crack propagation theory. **Chapter 5** provides the definition of

probability of failure according to the mechanism-based model, this model is summarised from the research results in Chapter 3 and Chapter 4. **Chapter 6** provides a machine learning approach (Bayesian Inference) to the asset management evaluation of the underground power transmission cable, this is a fundamental concept for developing a 'Intelligent Power Grid' which the asset probability of failure and the engineering asset pricing can be dynamically updated and be more up to date. **Chapter 7** is the conclusion chapter and the **Chapter 8** provides an overview of the future work.

2. Literature Review

In this literature review chapter, the following fundamental topics are presented:

- Engineering asset management
- Corrosion of materials
- Pitting corrosion and corrosion fatigue
- Research methodologies for engineering asset management against corrosion
- Existing data (from published documents, e.g the dimension of cables, the inner pressure, etc.)
- Experimental data (collected from provided samples in this study, e.g pit depth distribution)

This thesis uses data obtained from open literature and internet sources, including the designed life of typical underground power transmission cables, the existing asset management strategy by Ofgem, the typical section lengths of the underground power transmission cables, the Asset Health Index concept and relevant estimation of remaining life of cables in service, etc, listed below:

- https://www.nationalgrid.com/sites/default/files/documents/39111-Undergrounding_high_voltage_electricity_transmission_lines_The_technical_issues_INT.pdf
- https://www.ofgem.gov.uk/ofgem-publications/56018/15735-kemangetassetmgtpub.pdf
- https://www.ofgem.gov.uk/ofgem-publications/54026/tx-ntwk-output-measures-nget-appendix.pdf
- http://www.forewind.co.uk/uploads/files/TeessideAB/Application_Documents/7.Other_Statutory_Documents/7.2_Cable_Details_and_Grid_Connection_Statement.pdf

The above URLs lead to information from Ofgem, KEMA, National Grid Ltd.,

FOREWIND etc. which all play an important role in the U.K. power transmission industry.

2.1 Engineering asset management

Amadi-Echendu et al. [10] define engineering asset management as 'the total management of physical, as opposed to financial, assets'. It is an association of engineering capability and economic cost and value. This is especially an important concept for governments and profitable engineering-based companies. Due to the diversity of the engineering industry, various methods to link engineering capability and financial cost exist.

The concept of asset management is fundamentally to achieve the greatest return for all investments, including the monitoring and maintaining facilities systems and providing the best possible service to users.

The typical asset management can be further divided into

a. Financial asset management: Or in another word, the investment management. This type of investment manages investment funds, in chasing the best return/investment ratio in the financial sector.
b. Infrastructure asset management: This is a combination of management, financial, economics, engineering and other practices applied to physical assets with the objective of providing the required level of service in the most cost-effective manner. The infrastructure asset management focuses on the entire lifecycle monitoring – including design, construction, commissioning, operating, maintaining, repairing, modifying, replacing and decommissioning/disposal.
c. Enterprise asset management: This is the business of processing and enabling information systems that support management of an organization's assets, both physical assets and non-physical assets. This asset management category owns its specific International Organization for Standardization, the ISO 55000 series

provides terminology, requirements and guidance for implementing, maintain and improving an effective asset management system.

d. Public asset management: This is an expension of the enterprise asset management (EAM) by incorporating the management of all things of value to a municipal jurisdiction and its citizens' expectations. An EAM requires and asset registry (inventory of assets and their attributes) combined with a computerized maintenance management system (CMMS). All public assets are interconnected and share proximity, possible through the use of geographic information system (GIS).

In this section, the management method of the industry and Office of Gas and Electricity Markets (Ofgem) on the evaluation of underground power cable capabilities are introduced.

2.1.1 A typical asset management method by the power supply industry

One typical method applied by the industry is a system known as the Asset Health Index (AHI) to evaluate the condition of underground power cables [11]. The base of this evaluation is shown in the following Table 2-1. In this table, AHI value equals to 1 being the most critical and equals to 3 or 4 being on the safe side [11].

Table 2-1: Asset Health Index [11]

Score	Condition Criteria
1	Remaining useful life 0~2 years
1R	Remaining useful life 2~5 years
2	Remaining useful life 5~10 years
3 & 4	Remaining useful life > 10 years

Relevant to the Asset Health Index above the estimation of remaining lives of the cables is shown in Table 2-2.

Table 2-2: Estimated remaining service life (Years) to Asset Health Index [11]

Criticality / AHI	Very High	High	Medium	Low
1	0~2	0~2	2~5	2~5
2	5~10	5~10	5~10	10+
3	10+	10+	10+	10+
4	10+	10+	10+	10+

To summarize the above method, cables are being evaluated under four levels of criticality by observation, which will automatically lead to the related estimation of remaining life. Criticality is based on the historical record of maintenance, the observed condition of the power cables and the locations of specific power supplement lines. This is an industry defined classification.

2.1.2 Ofgem DNO Common Network Asset Indices Methodology

The following is a summary of the methodology proposed by Ofgem from its publication for asset management [12]. The general method is introduced in this section, and the application of this method is given as a working example in Appendix I in this thesis. This method contains a large amount of table referencing for the correct categories of evaluated cables. These tables are not given in this thesis, but they are publicly available. (Sentences are deleted)

The Ofgem method follows the 9 major steps below (with reference to the specific page of the manual, which is represented by the word ‘Code’):

1) Calculation of general probability of failure

From the Design Code, the possibility of failure is calculated as (Code, p.30)

$$PoF = K \times \left[1 + (C \times H) + \frac{(C \times H)^2}{2!} + \frac{(C \times H)^3}{3!}\right]$$

By observation of this mathematical expression, it is easy to recognize as the Taylor Series Expansion of an exponential function, with the first four terms kept. C is a constant that controls the shape of the curve and H represent the Health Score.

Where :

- $If\ Health\ Score > 4, then\ H =$

$Health\ Score\ (Current\ or\ Future)$

- $If\ Health\ Score \leq 4, then\ H = 4$
- $K\ and\ C\ are\ constants$

The Value of both K and C are to the Code Table 21 in Appendix B (Code, p.106). From this it can be concluded that for *Pressurized Cable (EHV UG Cable (Oil) and 132 kV UG Cable (Oil))*, K-value is 2.0944%, C-value is 1.087 and Health Score Limit is 4.

2) Calculation of normal expected life

Normal Expected Life is to be found in Table 20 Appendix B of the Code, corresponds to a Health Score of 5.5.

For *33kv UG Cable (Oil) with Lead sheath-Copper conductor*, *66kv UG Cable(Oil) with Lead sheath- Copper conductor* and *132kv UG Cable(Oil) with Lead sheath- Copper conductor*, the Normal Expected Life are all 80 years.

3) Calculation of expected life

The Expected Life calculation involves the Location Factor and the Duty Factor, and the calculation method is (Code, p.32)

$$Expected\ Life = \frac{Normal\ Expected\ Life}{(Duty\ Factor \times Location\ Factor)}$$

As in previous Step 2 the Normal Expected Life is 80 years.

$$\therefore Expected\ Life = \frac{80}{(Duty\ Factor \times Location\ Factor)}$$

Calculation of Location Factor

The general Location Factor consists of four different aspects, including:

i) Distance from coast factor

ii) Altitude factor

iii) Corrosion category factor

iv) Environment factor (indoor/outdoor)

The Distance from Coast Factor can be found in Table 22 (Code, p.106)

As the underground cable shall not be influenced by the distance from coast, it is chosen as default and equals to 1.

The Altitude Factor can be found in Table 23 (Code, p.107)

As the underground cables are buried and so should not be influenced by the altitude, therefore, the default value is also chosen here as 1.

The Corrosion Category Factor can be found in Table 24 (Code, p.107).

Although no category listed in the table fits the underground cable environment for corrosion, the underground environment is complicated, and can vary from the lowest value to the highest value. In this working example, three values are chosen for the evaluation of cable in Location 1, the lower limit value of 0.75, the upper limit value of 1.6 and the typical default value of 1.

The Environment Factor is determined directly as the underground power transmission cables are buried outdoor.

After obtaining all the necessary values for the Location Factor determination, under the Environment Factor classified as ‘Outdoor’, the calculation of Location factor is as follows in two categories (Code, p.43):

1) If the maximum of the Distance From Coast Factor, Altitude Factor and Corrosion Factor is greater than 1, which in this study case would be when $Corrosion\ Factor_{max} = 1.60$, then

$$Location\ Factor = MAX(Distance\ From\ Coast\ Factor, Altitude\ Factor, Corrosion\ Factor) + \Big(\big((COUNT\ of\ factors\ greater\ than\ 1) - 1\big) \times INC\Big)$$

Here in this example only one factor is greater than one, INC in the above equation represents for Increment Constants, and can be found in Table 25 (Code, p.107). Except the Switchgear, Transformers, Submarine Cables which has an INC of 0.05, the rest of the infrastructures are with an INC of 0, as with the study of underground cables, the INC is 0.

Condition 1:

$$Location\ Factor_{Condition\ 1} = 1.6$$

2) If the maximum of the Distance From Coast Factor, Altitude Factor and Corrosion Factor is not greater than 1, which in this study case would be when $Corrosion\ Factor_{min} = 0.75$ and $Corrosion\ Factor_{typ} = 1.00$ then

$$Location\ Factor = MIN(Distance\ From\ Coast\ Factor, Altitude\ Factor, Corrosion\ Factor)$$

Here

$$Location\ Factor_{Condition\ 2} = 0.75$$

And

$$Location\ Factor_{Condition\ 3} = 1$$

Calculation of Duty Factor (Code, p47)

For the Duty Factor calculation, when dealing with cables, there are two duty factors to be considered, DF1 and DF2. The calculation for Duty Factor with both DF1 and DF2 is as follows (Code, p.48):

$$Duty\ Factor = 0.5 \times DF1 + 0.5 \times DF2$$

The Duty Factor can be checked from Table 30 (Code, p.49)

4) Calculation of β_1 (initial ageing rate)

The equation calculating the initial ageing rate is as follows (Code, p.32):

$$\beta_1 = \frac{\ln\left(\frac{H_{expected\ life}}{H_{new}}\right)}{Expected\ Life}$$

Where:

- $H_{new}\ is\ the\ Health\ Score\ of\ a\ new\ assest, equal\ to$ 0.5
- $H_{expected\ life} is\ the\ Health\ Score\ of\ the\ asset\ when\ it\ reaches\ its\ expected\ life, equal\ to$ 5.5

5) Calculation of initial health score

The calculation for the Initial Health Score is as (Code, p.32):

$$Initial\ Health\ Score = H_{new} \times e^{(\beta_1 \times age)}$$

Where:

- $H_{new}\ is\ the\ health\ Score\ of\ the\ new\ asset, equal\ to$ 0.5
- $Initial\ Health\ Score\ is\ capped\ at\ a\ value\ of$ 5.5
- $\beta_1\ is\ the\ initial\ ageing\ rate$

- $age\ is\ the\ current\ age\ of\ the\ asset\ in\ years$

6) Calculation of current health score

The current Health Score is modified from the Initial Health Score, the calculation for this is (Code, p.33):

$$Current\ Health\ Score = Initial\ Health\ Score \times Health\ Score\ Factor \times Reliability\ Factor$$

Where

$$IF\ Current\ Health\ Score > Health\ Score\ Cap$$
$$THEN\ Current\ Health\ Score = Health\ Score\ Cap$$

- Current Health Score is capped at 10

Then the Current Health Score is compared with the Health Score Collar (Code, p.34)

$$IF\ Current\ Health\ Score < MAX(Health\ Score\ Collar, Reliability\ Collar)$$
$$THEN\ Current\ Health\ Score = MAX(Health\ Score\ Collar, Reliability\ Collar)$$

To calculate the Current Health Score, the Health Score Factor, or the Health Score Modifier is determined by: (Code, p.49)

i. Observed Condition Modifier
ii. Measured Condition Modifier

Each of the condition modifier would contain three elements:

i. A Condition Input Factor

ii. A Condition Input Cap

iii. A Condition Input Collar

As stated on (Code, p.60), there are no Observed Condition Inputs for cable assets other than Submarine Cables. For these assets:

i) The Observed Condition Factor shall be set to 1

ii) The Observed Condition Cap shall be 10

iii) The Observed Condition Collar shall be 0.5

From (Code, p.62), the Measured Condition for both EHV cable (oil) and 132kV cable (oil) are 'Leakage'.

The Measured Condition Modifier, from Table 15 (Code, p.63), for both EHV cable (oil) and 132kV cable (oil),

$$\begin{cases} Factor\ Divider\ 1 = 1.5 \\ Factor\ Divider\ 2 = 1.5 \\ Max.No.of\ Combined\ Factors = 1 \end{cases}$$

The next step is to find out the maximum and minimum value for Measured Condition Input, from Table 172 (Code, p.142), for EHV Cable (Oil) under the condition of Leakage:

$$\begin{cases} Condition\ Input\ Factor_{min} = 1.0 \\ Condition\ Input\ Factor_{max} = 2.0 \end{cases}$$
$$\begin{cases} Condition\ Input\ Cap_{min} = 10 \\ Condition\ Input\ Cap_{max} = 10 \end{cases}$$
$$\begin{cases} Condition\ Input\ Collar_{min} = 0.5 \\ Condition\ Input\ Collar_{max} = 8.0 \end{cases}$$

From Table 179 (Code, p.143), for 132kV Cable (Oil) under the condition of Leakage

$$\begin{cases} Condition\ Input\ Factor_{min} = 1.0 \\ Condition\ Input\ Factor_{max} = 2.0 \end{cases}$$

$$\begin{cases} Condition\ Input\ Cap_{min} = 10 \\ Condition\ Input\ Cap_{max} = 10 \end{cases}$$
$$\begin{cases} Condition\ Input\ Collar_{min} = 0.5 \\ Condition\ Input\ Collar_{max} = 8.0 \end{cases}$$

It can be concluded that for the cables protected by oil the factors being used are the same.

After obtaining all the factors in the Health Score Factor section, a 'Combining Factors Using a Modified Maximum and Increment (MMI)' Technique is applied for the calculation of the real Health Score Factor. (Code, p.50 & 51)

(a) Calculating the minimum value for Health Score Factor

- $Var_1 = Minimum\ of\ Factors =$

$$\min_{condition\ factor}\left(\frac{Observation\ Factor}{Leakage\ factor}\right)=1.0$$

- $Var_2 = 2nd\ Lowest\ of\ Factors = 1$
- $Var_3 = \frac{Var_2 - 1}{Factor\ Divider\ 2} = \frac{0}{1.5} = 0$
- $Combined\ Factor_{min} = Var_1 + Var_3 = 1$

(b) Calculating the maximum value for Health Score Factor

- $Var_1 = Maximum\ of\ Factors =$

$$\max_{condition\ factor}\left(\frac{Observation\ Factor}{Leakage\ factor}\right) = 2.0$$

- $Var_2 = Excluding\ Var_1$
  - $For\ remaining\ Factors\ where\ (Factor - 1) > 0, which\ is\ another\ 1$

- $Sum\ (Factor - 1)\ for\ the\ highest\ n - 1\ of\ these; where\ n =$ $Max.No.of\ Combined\ Factors, in\ this\ case, n = 1, \therefore$ $need\ to\ sum\ up\ in\ total\ of\ 0\ factors, which\ gives\ Var_2 = 0$

- $Var_3 = \frac{Var_2}{Factor\ Divider\ 1} = 0$
- $Combined\ Factor_{max} = Var_1 + Var_3 = 2.0$

The Reliability Factor (Code, p.69) has a value between 0.6 and 1.5 with a default value of 1, written as

$$\begin{cases} Reliability\ Factor_{min} = 0.6 \\ Reliability\ Factor_{max} = 1.5 \\ Reliability\ Factor_{dft} = 1.0 \end{cases}$$

7) Calculation of β_2 (current ageing rate)

It can be regarded that for the current asset the age is over 10 years (Code, p.34).

$$\beta_2 = \frac{\ln\left(\frac{Current\ Health\ Score}{H_{new}}\right)}{Age}$$

8) Calculation of future health score

The Future Health Score is calculated as (Code, p.36):

$$Future\ Health\ Score = Current\ Health\ Score \times e^{\left(\beta_2/r\right)\times t}$$

Where:

- $t\ is\ the\ number\ of\ future\ years$

- $Future\ Health\ Score\ is\ capped\ at\ 15$
- r is the Aging Reduction Factor

The Aging Reduction Factor is found from Table 209 (Code, p.149)

- $IF\ Current\ Health\ Score < 2, THEN\ Ageing\ Reduction\ Factor_{min} = 1$
- $IF\ Current\ Health\ Score > 5.5, THEN\ Ageing\ Reduction\ Factor_{max} = 1.5$
- $IF\ 2 \leq Current\ Health\ Score \leq 5.5, THEN\ Ageing\ Reduction\ Factor_{max} = \frac{Current\ Health\ Score - 2}{7} + 1$

9) Calculation of current and future possibility of failure

It can be observed from the above calculation that the distribution of the probability of failure is of the function

$$PoF = K \times \left[1 + (C \times H) + \frac{(C \times H)^2}{2!} + \frac{(C \times H)^3}{3!}\right]$$

2.2 Corrosion of materials

In this section, a brief introduction of the corrosion effect on materials are introduced, including:

- Hazards and consequences of corrosion
- Corrosion mechanism and types of corrosion
- Caustic corrosion

2.2.1 Hazards and consequences of corrosion

According to ASM International [13], corrosion is defined as 'A chemical or electrochemical reaction between a material, usually a metal, and its environment that produces a deterioration of the material and its properties'. With this definition, the deterioration of the material and its properties lead to hazards, and will especially cause consequences. For example, metal corrosion has an impact on U.S. economy with almost $300 billion loss per year. By applying the corrosion-resistant materials and the best corrosion-related technics, this cost can reduce by approximately one-third [13]. According to the project led by Chinese Academy of Science, introduced by Wei Ke [14], in 2002, the direct cost by corrosion damage in China exceeded 500 billion CNY, occupying 5% of GNP of the same year.

All material will react with the surrounding medium, from everyday life, to industrial productions. Especially in industrial production, corrosion causes leakage to equipment, leading to the failure of equipment, and can even cause the injury or deaths of operating technicians. In such reason, the research of corrosion is highly focused and valued in all countries.

2.2.2 Corrosion mechanism and types of corrosion

2.2.2.1 Corrosion mechanism

Corrosion can be regarded as the process of two kinds of mechanisms, the chemical corrosion and the electrochemical corrosion.

Chemical corrosion:

The chemical corrosion mechanism is the corrosion process without the production of electricity currents. As for the material, the surface reacts with the material it contacts, produces an oxidation-reduction reaction and this reaction consumes the material surface. For example, in chemical plants the process that steel reacts with chlorine:

$$3Cl_2 + 2Fe = 2FeCl_3$$

The above chemical reaction produces no electricity current, hence it is a type of chemical corrosion.

Electrochemical corrosion:

Electrochemical corrosion involves the release of ions to the environment and movement of electrons within the material, this mechanism can occur only if the environment can contain ions and the material can conduct electrons [15].

For example, submerge iron (material property not well-distributed) into hydrochloric acid, there is the following reaction:

$$Fe + 2HCl \rightarrow FeCl_2 + H_2 \uparrow$$

Which can be further written as:

$$Fe + 2H^+ + 2Cl^- \rightarrow Fe^{2+} + Cl_2^{2-} + H_2 \uparrow$$

In the above electrochemical reaction, Cl^- was not involved in the reaction, the real reaction is:

$$Fe + 2H^+ \rightarrow Fe^{2+} + H_2 \uparrow$$

Which leads to the real electrochemical reaction as:

$$\begin{cases} Anode: Fe \rightarrow Fe^{2+} + 2e & (oxidation) \\ Cathode: 2H^2 + 2e \rightarrow H_2 \uparrow & (reduction) \end{cases}$$

2.2.2.2 Types of corrosion

- **General corrosion**

Also called the 'uniform corrosion', general corrosion is the uniform loss of metal over an entire surface, and it is characterized and expressed as a mass loss per unit area and unit of time [16]. This type of corrosion is developed at a uniform speed, yet slow in progress. It is considered as the most common form of corrosion and particularly responsible for most material loss.

- **Local corrosion**

Local corrosion happens when a passive metal meets corrosive environment, it develops at discrete sites where other protective passive film has broken down. This type of corrosion usually accelerates with the progress of time [17].

Local corrosion can be further sub-divided into the following types:

i) Galvanic corrosion
ii) Crevice corrosion
iii) Pitting corrosion
iv) Intergranular corrosion
v) Selective corrosion
vi) Stress corrosion
vii) Corrosion fatigue
viii) Hydrogen damage

i) <u>Galvanic corrosion</u>

'Galvanic corrosion (also called 'dissimilar metal corrosion' or wrongly 'electrolysis') refers to corrosion damage induced when two dissimilar materials are coupled in a corrosive electrolyte' [18]. Due to the effect of oxygen concentration difference, this forms a concentration cell. The electrode reaction of galvanic corrosion is similar to that of the general corrosion. For example, the reaction between carbon steel tube and titanium tube under sea water, according to the galvanic series shown in the following Figure 2-1.

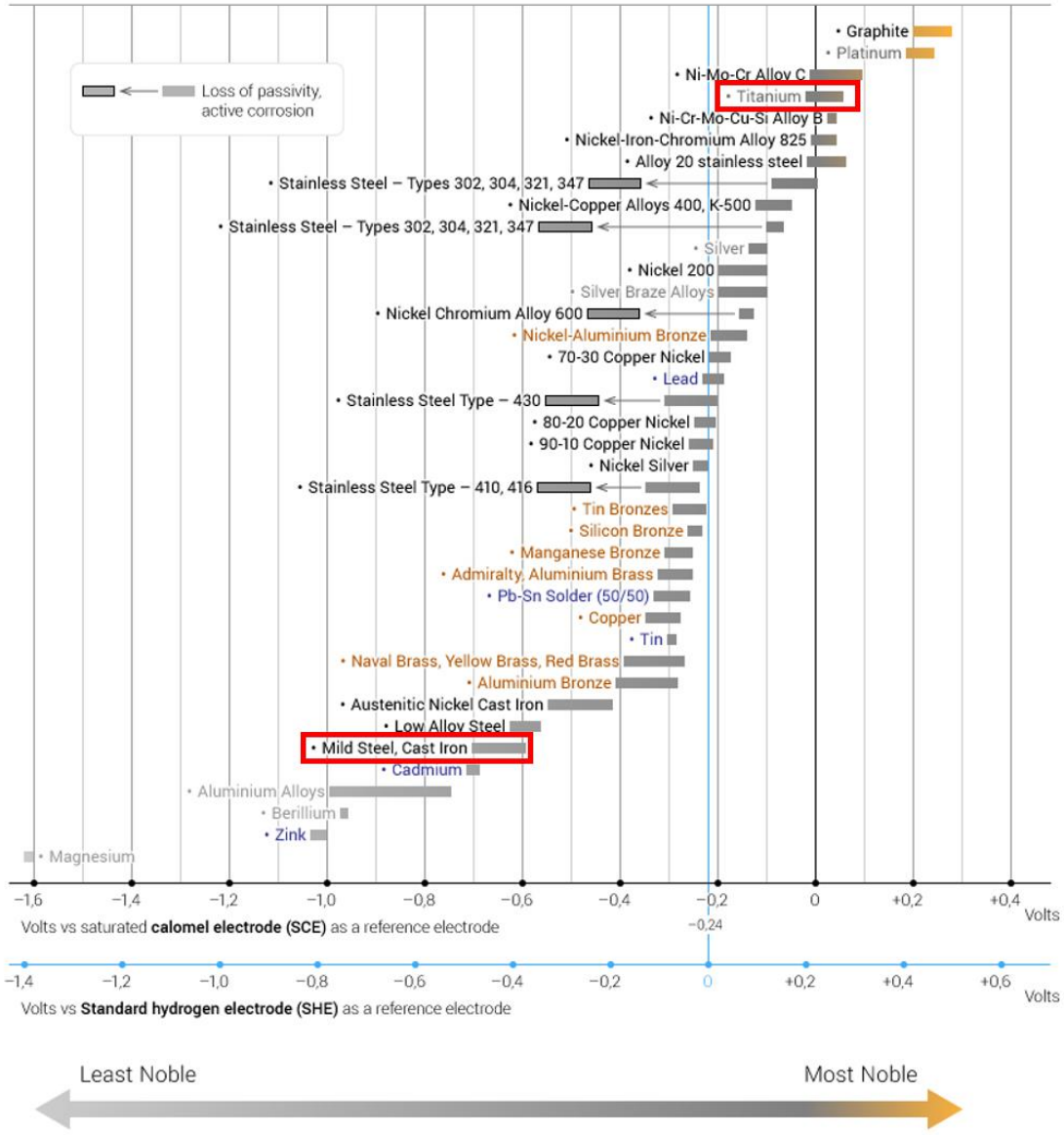

Figure 2-1: Galvanic series [19]

The electrode reaction is as follows:

- $$\begin{cases} Anode: & Fe \rightarrow Fe^{2+} + 2e \\ Cathode: & 0.5O_2 + H_2O + 2e \rightarrow 2OH^- \\ Reaction: & Fe^{2+} + 2OH^- \rightarrow Fe(OH)_2 \\ & 4Fe(OH)_2 + 2H_2O + O_2 \rightarrow 4Fe(OH)_3 \end{cases}$$

- Further reaction:

$$\begin{cases} 3Fe^{2+} + 4H_2O \rightarrow Fe_3O_4 + 8H^+ + 2e \\ Fe^{2+} \rightarrow Fe^{3+} + e \\ Fe^{3+} + 3H_2O \rightarrow Fe(OH)_3 + 3H^+ \end{cases}$$

It is unavoidable in industry to use a combination of metal materials. For example, at the connection of tube and cast iron/steel plate in heat exchangers, the plate is under potential accelerated corrosion.

ii) Crevice corrosion

'Crevice corrosion is a localized form of corrosion usually associated with a stagnant solution on the micro-environmental level. Such stagnant microenvironments tend to occur in crevices. Process such as those formed under gaskets, washers, insulation material, fastener heads, surface deposits, disbonded coatings, threads, lap joints and clamps. Crevice corrosion is initiated by changes in local chemistry within the crevice' [20].

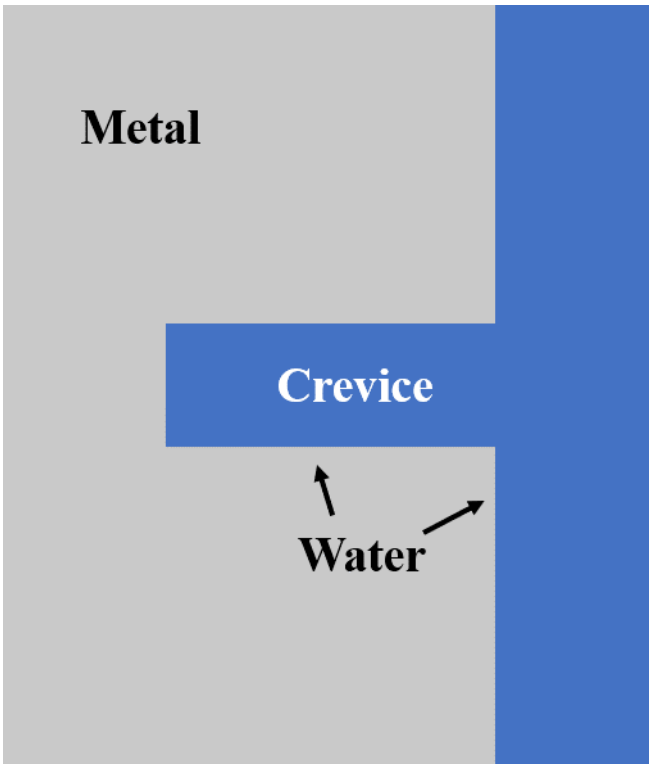

Figure 2-2: Crevice in metal under water (adapted from [20])

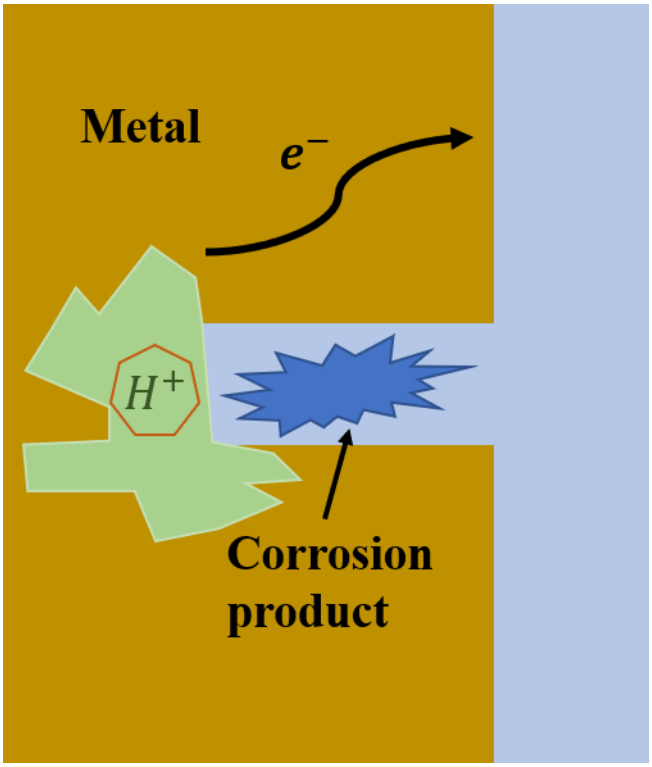

Figure 2-3: Crevice corrosion process (adapted from [20])

A typical electrode reaction is as follows:

- $Anode: \begin{cases} Fe \rightarrow Fe^{2+} + 2e \\ MCl + H_2O \rightarrow MOH + H^+ + Cl^- \end{cases}$ $(In\ crevice)$
- $Cathode: H_2O + 0.5O_2 + 2e \rightarrow 2OH^-$ $(Out\ of\ crevice)$

Anode reaction is within the crevice and is an accelerated corrosion, the cathode reaction is outside the crevice and is a minor corrosion. Crevice corrosion often happens at the contact area under screw caps, also under the sea. It can happen at the position where sea plants grow on the metal.

iii) Pitting corrosion

'Pitting corrosion is a localized form of corrosion by which cavities or "holes" are produced in the material. Pitting is considered to be more dangerous than uniform corrosion damage because it is more difficult to detect, predict and design against of. Corrosion products often cover the pits. A small, narrow pit with minimal overall metal

loss can lead to the failure of an entire engineering system' [21]. It happens the most in the environment with the existence of Cl^-, the reaction process is similar to that of the crevice corrosion:

$M^+ + Cl^- \rightarrow MCl$ $(In\ pit)$

$MCl + H_2O \rightarrow MOH + H^+ + Cl^-$ $(Out\ of\ pit)$

The unevenness of the metal surface, e.g. scratch, sunken, impurity, are commonly the start points of pitting corrosion. When the medium is with both halogen ions and oxidant, it is easy for pitting corrosion to happen, for example, $CuCl_2$ and $FeCl_3$ are both strong pitting corrosion agents.

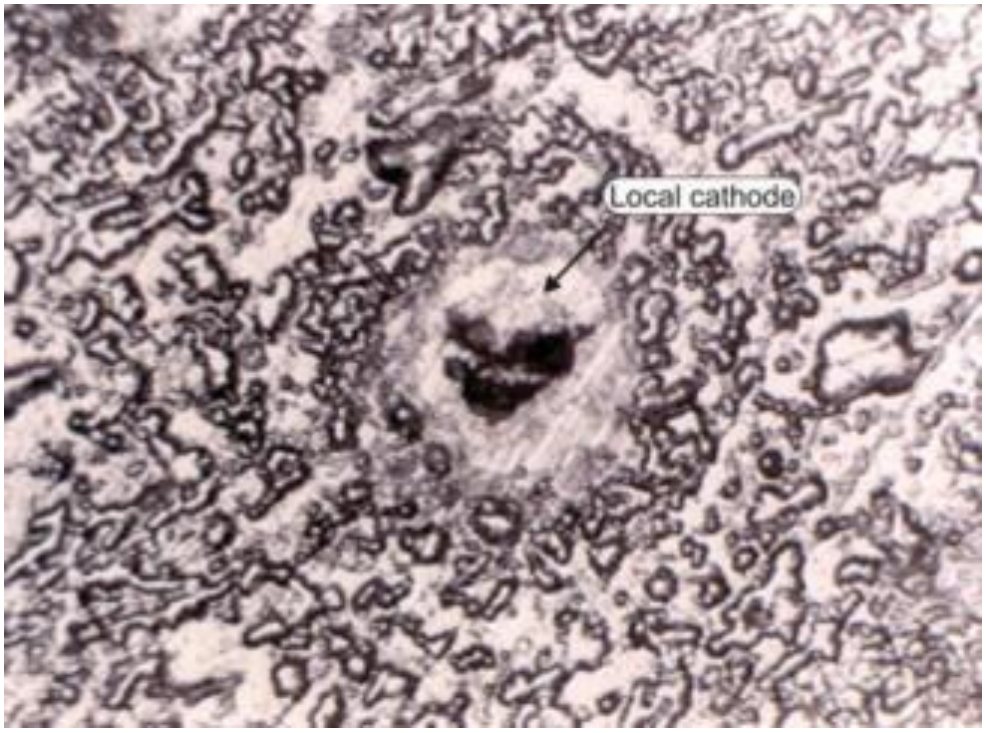

Figure 2-4: Pitting corrosion under microscope [21] (the black area the arrow is pointed at shows a deep pit, with a circle of white corrosive reaction products surrounding the deep pit, other small sunken in this figure shows the imperfection of metal surface, which are the external scratch and light damage to the surface of the metal)

Pits developed from pitting corrosion can be different in shapes, e.g. through pits shown in Figure 2-5 and sideway pits shown in Figure 2-6.

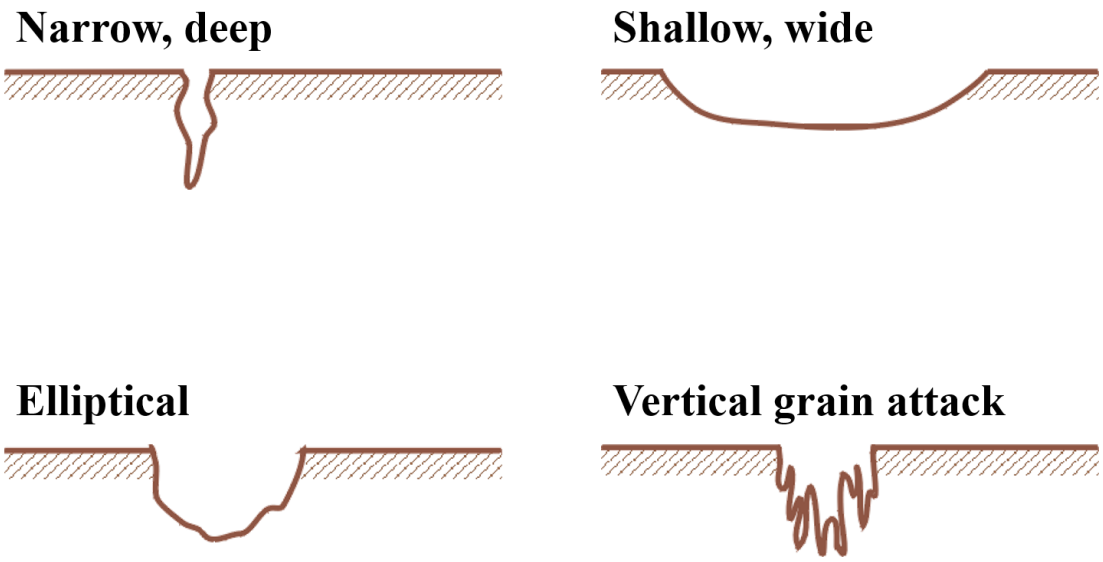

Figure 2-5: Through pits (adapted from [21])

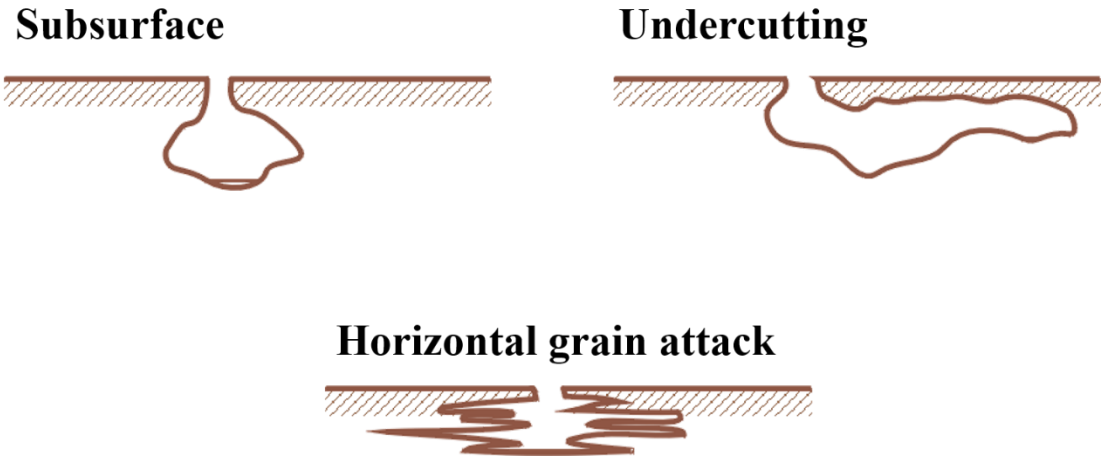

Figure 2-6: Sideway pits (adapted from [21])

The pitting corrosion is the major type of corrosion in this research, and will be discussed in more details in Section 2.3.

iv) Intergranular corrosion

'The microstructure of metals and alloys is made up of grains, separated by grain boundaries. Intergranular corrosion is localized attack along the grain boundaries, or immediately adjacent to grain boundaries, while the bulk of the grains remain largely unaffected' [22].

When intergranular corrosion appear, the appearance and the shape of the metal stay almost unchanged, most metal remains its metallic lustre. However, the strength and the ductility of the metal decrease severely, when cold bended, there are cracks appear on metal surfaces, the metal can even lose its metallic lustre. For nonferrous metal aluminium, if small amount of iron sediments appear at the grain boundary, this will cause intergranular corrosion.

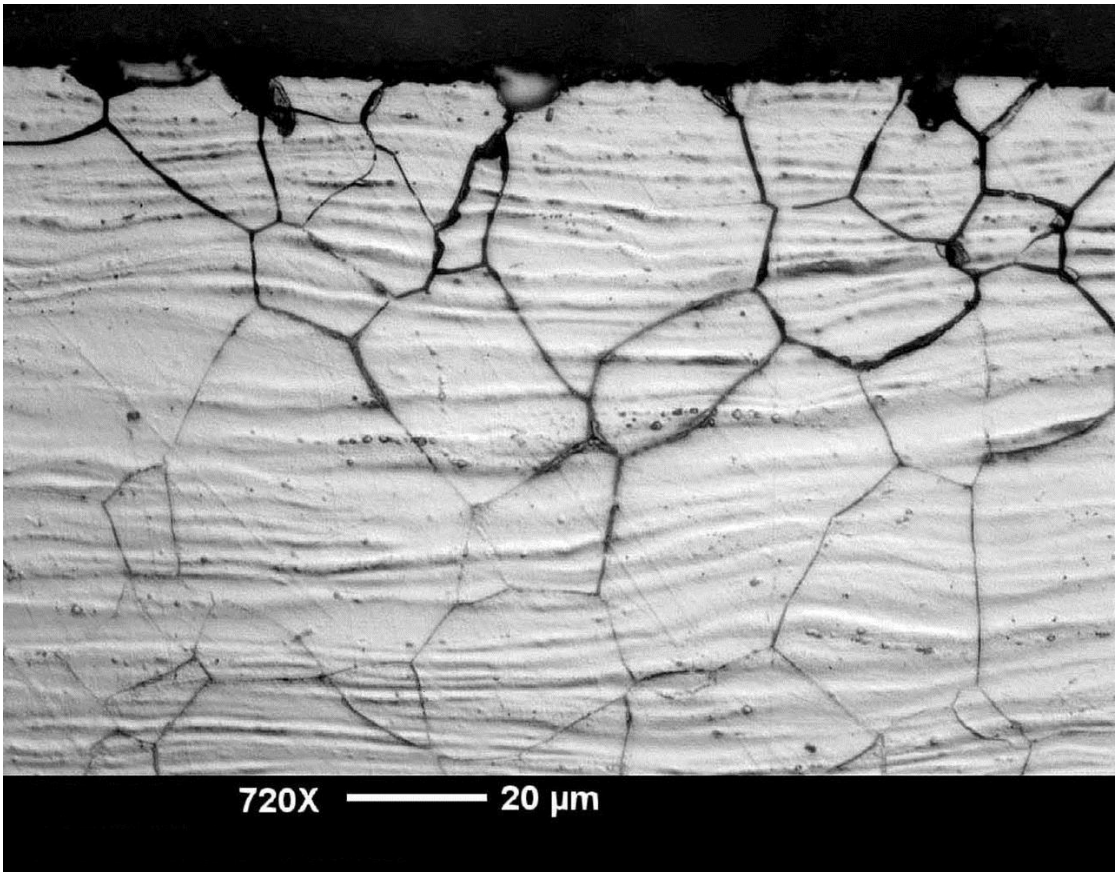

Figure 2-7: A typical figure of intergranular corrosion [23]

Each individual grain is a distinct crystal with its own orientation. The areas between the grains are known as grain boundaries. Within each grain, the individual atoms form a crystalline lattice. Corrosion happening among the gaps of these grain boundaries are the fundamental mechanisms of the intergranular corrosion effects.

v) Selective corrosion

Selective corrosion, also known as dealloying or selective leaching, refers to the selective removal of one element from an alloy by corrosion processes [24]. There are three common selective corrosion forms.

- Brass is an alloy with 30% Zn and 70% Cu. Among the two elements, Zn is more active, therefore will dissolve with corrosion reaction. When selective corrosion is happening to brass alloy, it will turn from yellow brass colour into purple/red/copper colour.
- Graphitization corrosion. 'When steel is exposed to elevated temperatures for long periods, metallurgical degradation of the steel's microstructure matrix occurs to form free graphite (carbon) and iron (ferrite). At elevated temperatures, carbon tends to migrate to the grain boundaries, leading to the formation of graphite nodules, which have an embrittling effect on metal' [25].

vi) Stress corrosion

Stress corrosion, also known as stress corrosion cracking (SCC), is the cracking induced from the combined influence of tensile stress and a corrosive environment [26]. Materials in certain corrosive medium, when under no external forces, the corrosion effect is minor, but when the tensile stress reaching certain limits, brittle cracking can even happen on ductile metals. The brittle cracking does not usually show any sign before happening, hence can cause catastrophic consequences. Three requirements are usually fulfilled for SCC: sensitive material, tensile stress and certain

corrosive medium.

vii) Corrosion fatigue

'Corrosion-fatigue is the result of the combined action of an alternating or cycling stresses and a corrosive environment' [27].

Corrosion fatigue has the following features:

a. There is no fatigue limit.
b. Different from SCC, as long as there is existence of corrosive medium, corrosion fatigue can still happen on pure metal.
c. The corrosion fatigue strength of a metal is related to its corrosion resistance.
d. Normally, corrosion fatigue starts from scratch or sunken at the surface of metal. There are many sources of cracking. The corrosion fatigue cracks are mostly trans-granular, with small amount of cracks being intergranular fractures.
e. Corrosion fatigue cracking is brittle fracture. There is no macroscopic plastic deformation. Along the crack there is corrosion product.

viii) Hydrogen damage

Hydrogen damage is caused by the existence of hydrogen or the reaction between hydrogen and certain components in the material, which affects the mechanical properties of materials with reduction in ductility and toughness [28]. Hydrogen damage can be further divided into, hydrogen corrosion, hydrogen blistering, and hydrogen embrittlement.

- Hydrogen corrosion: Hydrogen particle release H^+ ion, cause acid environment which enables corrosion.

- Hydrogen blistering: Metal infused H atom in hydrogen environment, temperature decreases gather and form H_2 bubbles like blisters near surfaces.
- Hydrogen embrittlement: Metal becomes brittle and fracture due to the introduction and subsequent diffusion of hydrogen into the metal.

2.2.3 Caustic corrosion

Caustic corrosion can be described as the corrosive interaction of sufficiently concentrated sodium hydroxide with a metal, producing distinct hemispherical or elliptical depressions [29]. Caustic corrosion is also known as “caustic attack”, “caustic gouging” or “ductile gouging” [30, 31].

In caustic corrosion, except the fundamental reaction product of $Fe(OH)_2$, the following reaction also happens, which produces large amount of hydrogen:

$$\begin{cases} 3Fe + 7NaOH \rightarrow Na_3FeO_3 \cdot 2Na_2FeO_2 + 7H \\ Na_3FeO_3 \cdot 2Na_2FeO_2 + 4H_2O \rightarrow 7NaOH + Fe_3O_4 + 8H \\ H + H \rightarrow H_2 \\ 3Fe + 4H_2O \rightarrow Fe_3O_4 + 4H_2 \end{cases}$$

2.3 Background of pitting corrosion and corrosion fatigue

The flowchart of the cable failure process under the corrosion fatigue influence is shown in Figure 2-8:

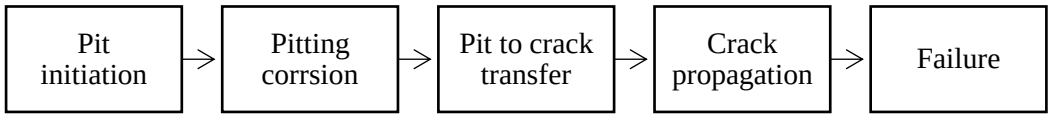

Figure 2-8: Flowchart of cable failure process [6]

2.3.1 Pit initiation

According to Soltis's [32] review on the mechanisms of pit initiation, the widely-recognised cause of pit initiation is the passivity breakdown. It was summarised by Böhni that the passivity breakdown is caused by three main mechanisms [33]: the penetration mechanism, the film mechanism and the adsorption mechanism. These are illustrated in Figure 2-9 to Figure 2-11.

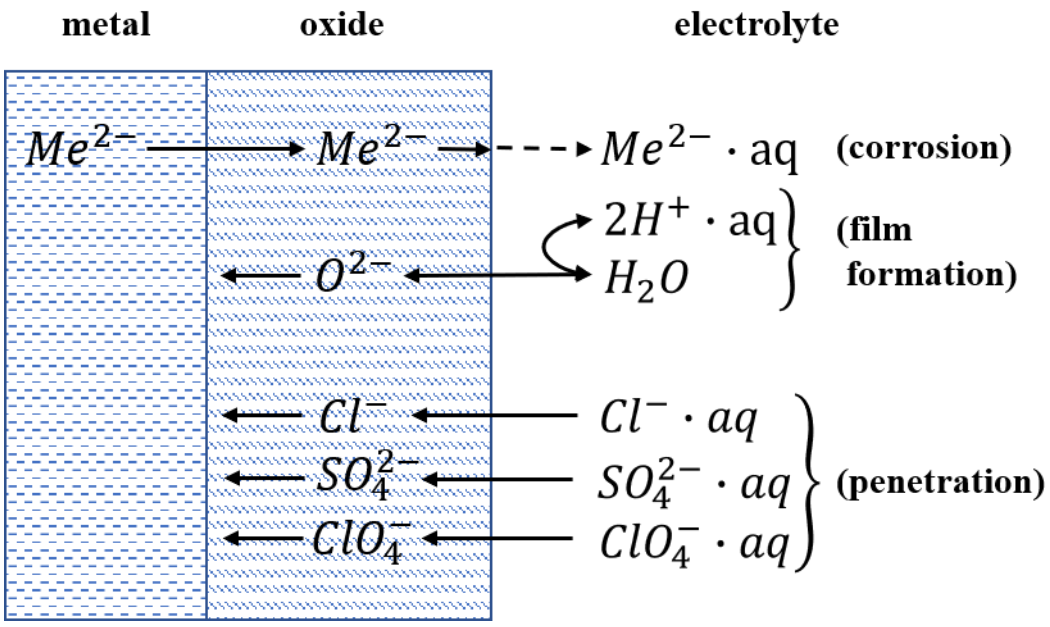

Figure 2-9: Penetration mechanism and phase diagram of a passive film with related processes of ion and electron transfer within the film at its phase boundaries (adopted from [33])

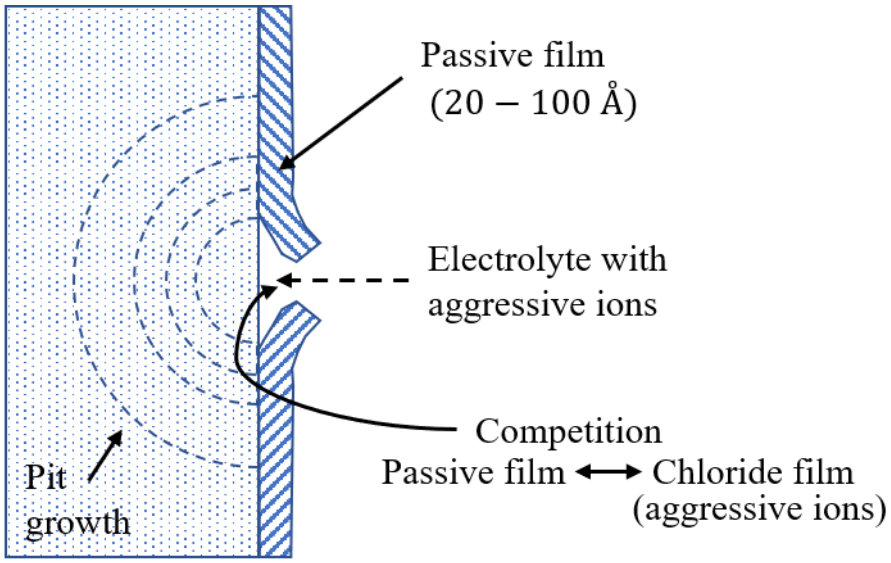

Figure 2-10: Mechanical film breakdown mechanism and related competing processes (adapted from [33]) the passive film protecting the surface of metal is damaged due to external reasons, this gives the gap for electrolyte with aggressive ions to enter the gap created and react with the inner active metal atoms. This eventually leads to the pit initiation and cause pit growth.

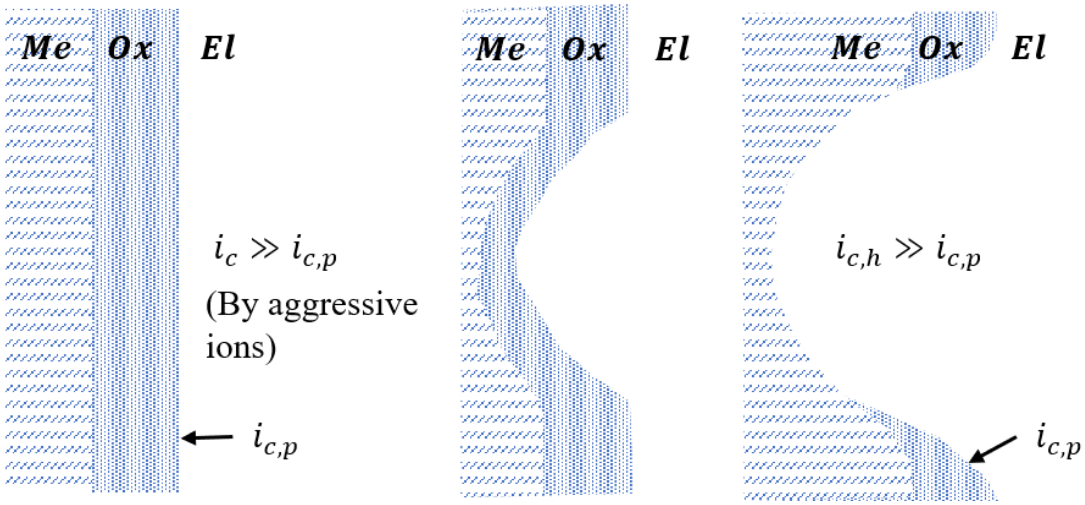

Figure 2-11: Adsorption mechanism with increased local transfer of metal ions and related corrosion current density, i_c, caused by complexing aggressive anions leading

to thinning of the passive layer and increases in field strength and final free corrosion current density $i_{c,h}$ within the pit (adapted from [33])

In this research, although the study is about the total process of metal failure, the pit initiation time is ignored because this has little influence. Pitting initiation is considered to be happening in a sudden immediately after the initiation mechanism, the time is considered as to short to impact the servicing life which is as long as decades. The mechanism and electro-chemical reaction is not considered at the first stage of the failure process, and here the pit initiation will not be discussed in further details.

2.3.2 Pitting corrosion

Pitting corrosion is commonly considered as the most damaging form of corrosion for metals used in underground applications because it is very difficult to detect, predict and mitigate [34]. It is characterized as a localized accelerated dissolution of metal that occurs due to the breakdown of the protective passive film on a metal surface [35]. Most of the pitting corrosion behaviours are studied on materials such as aluminium alloy [36-40] and stainless steel [41-44]. Few studies have been carried out on the phosphor bronze [45, 46].

When the cable is buried underground, moisture can penetrate through the outer polymer sheath and initiate corrosion on the phosphor bronze reinforcing tapes [45-47]. Hence the tape is under the risk of combined effect of a slow rate localized environmental corrosion and mechanical fatigue due to the cyclic pressure resulted from the oil.

It is essential to measure the pit depth distribution, since only a small part of the long cable can be experimentally analysed. Many methods and tools are found in the literature for measuring the pit depth, mainly for ferrous materials. Magnetic Flux

Leakage is used in a data fitting work for steel [48]. X-Ray Computed Tomography (XCT) or Scanning Electron Microscopy (SEM) can be used to observe single pit morphology. The majority of the literature deals with the pit penetration problem, where the deepest pit causes failure [49]. Non-destructive Testing (NDT) methods such as ultrasonic, tangential radiography and eddy current techniques are not applicable due to less thickness of the material and the fact that the pits are filled in with corrosion products [50, 51]. Optical and mechanical profilometers, 3D Laser Scanner, and pit gauge cannot be used due to the difficulty of removing the corrosion products within the pits [51]. Moreover, measurement tools are usually available for relatively large pits (> 100 μm). In contrast, on the surface of the reinforcing phosphor bronze tapes, the pits of interest are very small (less than about 100 microns) and filled with corrosion products. For these reasons metallographic examination is found to be suitable for the pit depth measurement of the tapes because it allows to overcome the problem of removing the corrosion products, while at the same time allowing to obtain the pit depth distribution in a systematic way.

A number of oil leak events have been detected over the years on cable circuits due to rupturing of the lead sheath under the oil pressure. The vulnerability of phosphor-bronze reinforcing tapes to corrosion has been identified as the cause of these failures [52, 53]. The corroded reinforcing tape with the fractured face is shown in Figure 2-12.

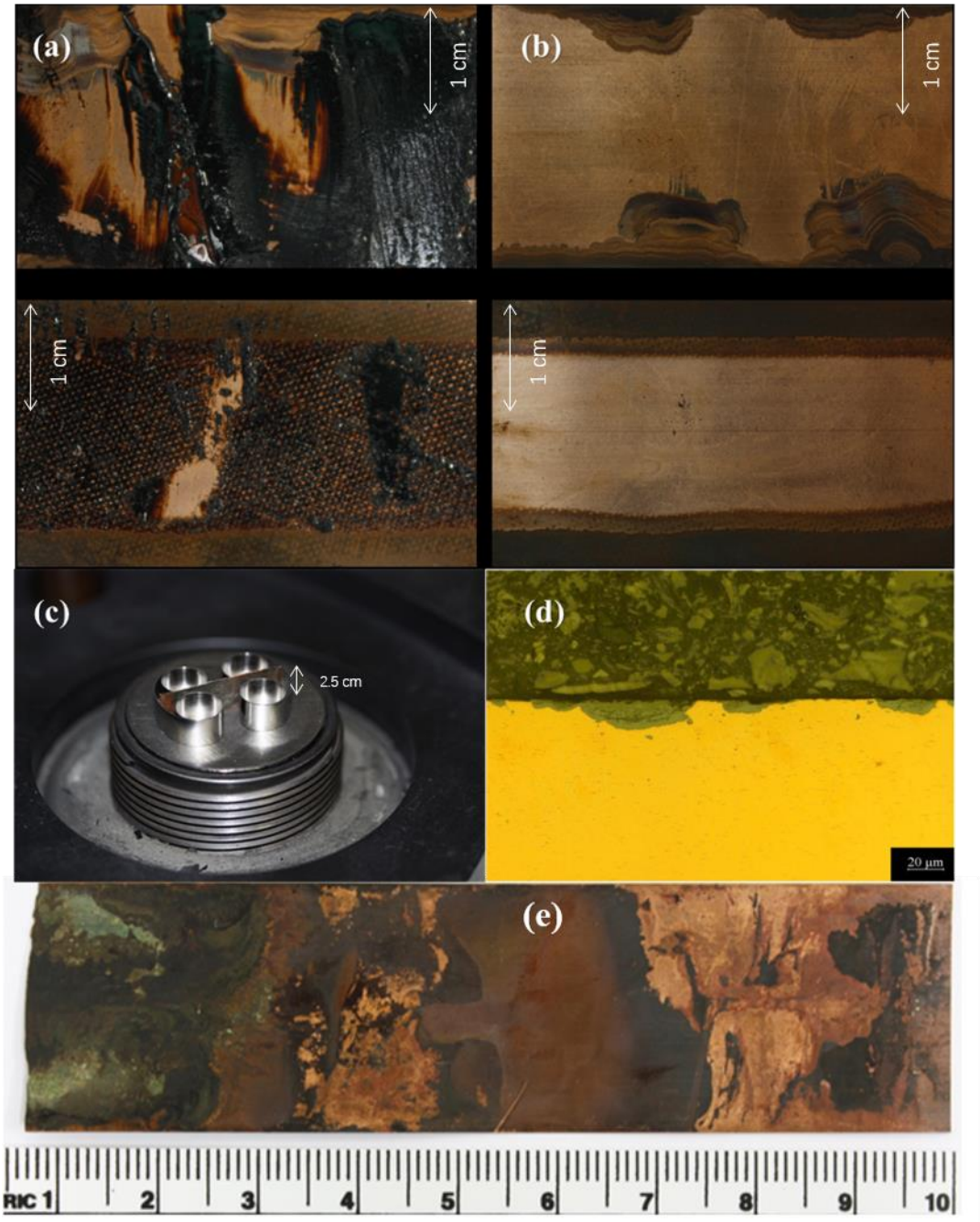

Figure 2-12: (a) Outer and inner surface of the tape covered with bitumen (b) Outer and inner surface of the tape after bitumen removal with pentane (c) Example of tape in the mounting machine. Note the supporting clips necessary due to the small thickness of the tape (d) Cross-sectional view of the corrosion pits that are taken perpendicularly to the longitudinal axis of the tape (e) Corroded reinforcing phosphor bronze tape surface with a fracture end on the left (thickness of the tape about 150 µm) [5]

2.3.3 Pit-crack transfer

There models existing for the pit-crack transfer all originating from two basic ones which characterize the corrosion fatigue crack nucleation process: a critical pit size model [7, 54] and a pit growth/crack growth competition model [55, 56]. Both models consider corrosion pit as an equivalent surface crack and its growth rate is described by the pit kinetics. In the critical pit size model, the pit grows to a critical size; a corrosion fatigue crack is considered to have nucleated from it when the local mechanical condition is adequate for the onset of the crack growth. The critical condition is defined in terms of the threshold stress intensity factor for corrosion fatigue (ΔK_{th})[57-59]. On the other hand, in the competition model the pit growth law of a corrosion pit is formulated using fracture mechanics. The occurrence of corrosion fatigue nucleation is defined by a critical pitting condition (ΔK_p) at which the crack growth rate exceeds the pit growth rate. These two models provide a framework for predicting corrosion fatigue life by correlating fracture mechanics parameters to the crack nucleation [55, 56]. However, the usefulness and applicability of these models is not yet fully established, because quantitative evidence is still missing.

Kondo [56] introduced the basic requirements for predicting the pit-crack transfer, consisting of two rules: first, the pit depth must reach a threshold value in order to initiate the transition. Second, at the transfer depth, the crack propagation rate is larger than the growth rate of pitting corrosion. The pitting corrosion growth rate is estimated using a basic power law, which was first introduced by Romanoff [60]. The power law model has proved to be successful in a variety of materials, for example, aluminium alloy [61-63], steel [44, 64, 65] and tin bronze in the author's previous work [6].

2.3.4 Crack propagation

The most basic and widely applied model in crack propagation is Paris' Law. For example, Bechhoefer et al. [66] modified Paris' Law and applied it to life prediction on aircraft components. Researchers have also discussed the determination and influence of stress intensity factor K on crack propagation in different materials, e.g. microcapsule-toughened epoxy [67] and aluminum alloy foams [68]. Furthermore, Pugno et al. [69] provided a complete discussion of Paris' Law and proposed a new equation to generalize it.

To monitor the total failure process of specific materials in engineering applications, some researchers proposed to combine pitting corrosion and crack propagation [58, 59, 70]. Among these works, pit-crack transfer is a crucial factor, as it influences the prediction of material life before failure.

Recently, a combination of deterministic and statistical approaches was developed by Engelhardt and Macdonald [71] and applied to model the evolution of cracks in steam turbines starting from pits [72]. Similarly, Turnbull [70] developed a model based on deterministic equations with statistically distributed input parameters. The model uses Kondo's condition for the pit to crack transition and captures the statistical variability of pit and crack growth using a Monte Carlo method where input values are chosen at random from statistical distributions. It is successfully applied to the simulation of the time-evolution of the pit depth distribution and percentage of pits that transform into stress corrosion cracks for the case of steam turbine steel discs. The simulation not only reflected the trends in the experimental measurement, but also reproduced the statistical variability or noise associated with the measurements. These models are rarely tested over long term real data on corrosion fatigue life. In addition to this, Turnbull [73] used a probability theory to describe the transfer ('Transfer Probability'), suggesting that it is not always the pit with the largest depth that transfers from pitting corrosion to crack propagation. All pits with different depths have a certain probability of transfer. A

cumulative distribution function (CDF) from the Weibull distribution was applied by Turnbull to describe this transition.

2.4 Research methodologies for engineering asset management against corrosion

Probabilistic and statistical techniques are used to model the pit growth because of a) the stochastic nature of pit growth [74] and b) lack of precise electrochemical technique to measure the pit depth [75]. Nathan and Dulaney [76] emphasised the importance of using statistical approaches to model the localized pitting corrosion. Sheikh et al. [77] modelled the stochastic nature of the growth of the deepest pit. Johnsen and Hilfer [78] predicted the stochastic evolution of corrosion front using statistical methods by a time sequence of random corrosion events. Wei [79] presented a probabilistic model to predict the growth of corrosion pits in aluminium alloys in aqueous environments. Engelhardt and Macdonald [80] modelled pit depth distribution using damage function analysis, which was successfully applied to the pitting corrosion of iron in neutral chloride solutions. Komukai and Kasahara [81] as well as Isogai, Katano and Miyata [82], applied extreme value models to study pitting corrosion. Valor et al. [83] introduced Markov Chain models for the stochastic modelling and Cavanaugh et al. [84] used neural network approaches for modelling pit growths.

Monte Carlo simulation is widely used to determine a statistical distribution that can best fit the real-life corrosion phenomenon. The Monte Carlo method has shown to give simulation results that are consistent with experimental data; in the process, a better understanding - at least qualitative - of pitting corrosion can be achieved and, more importantly, predictions can be made. Shibata [85] applied the Monte Carlo simulation to validate the pit depth distribution obtained from experiments. Monte Carlo simulations are successfully used to model the pit growth of the most common industrial

materials such as aluminium alloy [79, 86, 87] and steel [44, 64, 65]. These simulations can also be combined with degradation models to perform reliability analysis for infrastructures [88]. Davey et al. [89] used the Monte Carlo method to model the initiation of pitting corrosion, and established an atlas of risk for undersea metals. Ossai et al. [90] developed a 2D fussy Monte Carlo simulation to estimate a corrosion wastage rate for pipelines using both Markov modelling and Monte Carlo simulation. Murer and Buchheit [91] applied Monte Carlo to fit the experimental pit depth distribution for aluminium alloy. These simulations were also used to characterize the randomness of pit growth in different environmental conditions. The distributions applied for these simulations are determined by certain parameters which include the type, mean, variance, location, scale, shape, etc. According to Caleyo et al. [82] and Velazquez et al. [75], these parameters can vary due to environmental effects.

The estimation of the remaining life of engineering assets is an important assistance to decision making in the modern industry. The precision in life estimation, especially when interpreted as the probability of failure of engineering assets, enhances the confidence to the decisions on the reliabilities of infrastructures. The decisions are closely related to the living quality of civilians, the financial budgets of governments and the profits of companies. This study focuses on estimating the probability of failure of underground power transmission cables, with results based on existing data from the industry. The foundation of this research is an existing experience-based probability of failure model investigated and summarised by KEMA [92]. This model generalises the probability of failure of all cables into one universal function. The disadvantage is obvious: such a model cannot account for the variety of cable conditions. As more cables approach the designed servicing age, the predictions fail to be convincing. In the author's recent work, life estimation of power cables was based on computer modelling of a pit depth distribution using Monte Carlo simulations [5] and a complete failure process analysis based on the concept of pit-crack transfer probability [6]; these two

topics will be further discussed in details in Chapter 5 and Chapter 6. Compared to the experience-based model, these research results are considered as the information with a different approach to the same engineering asset data. The Bayesian Inference method is applied as a conjunction to update the experience-based model with the mechanism-based model.

When discussing engineering asset management, there are two major approaches in the assistance of decision making: the remaining life estimation (can be seen in section 2.1.1 which discussed the industry application of asset management strategy) and the probability of failure estimation (can be seen in section 2.1.2 which discussed the Ofgem approach on asset management). The approach of remaining life estimation has been researched widely in different engineering disciplines. Martin et al. [93] studied the remaining life of the transformer insulation and concluded that the remaining life is strictly related to paper insulation degradation. Khalifa et al. [94] developed a quantitative model for gas turbines on a risk-based maintenance and remaining life assessment. Segovia et al. [95] created a Cox model based on corrosion studies estimating the remaining life of power transmission towers. Ahmadzadeh and Lundberg [96] applied an artificial neural network (ANN) method in the remaining useful life estimation of grinding mills. Animah and Shafiee [97] discussed the remaining life estimation for offshore oil and gas assets, with a proposal for the decision making of life extension.

The other approach - probability of failure estimation - is discussed by the following researchers. Su et al. [98] applied a one-dimensional integral approach to the probability of failure estimation for geotechnical structures. Wang et al. [99] discussed the failure probability for an ethylene cracking furnace tube, which is a key component in the petrochemical industry. Zhou et al. [100] analysed the probability of failure of multi-storied reinforcement-concrete structures based on the evaluation of seismic control effect. Liang et al. [101] evaluated the failure rate of a power transformers and proposed

a decision strategy for replacement. Seo et al. [102] studied the probability of failure model based on the safety factor in a water supply network; the determination of safety factor was related to the fundamental mechanism of corrosion in water pipes. Furthermore, based on the same fundamental pitting corrosion studies, Kioumarsi et al. [103] discussed the failure probability of steel bars in a reinforced concrete beam.

Among the proposals of remaining life estimation and the probability of failure estimations, the following methods have proved to be the popular approaches. The Monte Carlo method is used in near-reality data simulations [99, 104], the neural network algorithm is applied to data processing [104, 105] and the Weiner process is used in remaining-life model building [8, 106]. Currently, the Bayesian Inference approach to update the old-information model with new information model is not widely used, especially in engineering disciplines. Mosallam et al. [107] applied a Bayesian approach to remaining life estimation, but mainly focused on the algorithm of discrete Bayesian filtering. Wang et al. [106] applied the Bayesian Inference algorithm to model updating. However, with insufficient pre-processing of data, an over-simplified assumption, and the simplification in handling the Bayesian Inference function, the process of this algorithm is not suitable to provide the potential of general application in the engineering field. Apart from the engineering field, Bayesian Inference is a key algorithm in the machine learning field, for example used for the prediction of human behaviour [108, 109], public application like credit card applications and artificial intelligence [110-112], and the extension of machine-learning related fundamental theories [113-116], etc.

2.5 Models for corrosion and fatigue

In this section the fundamental models are discussed. As the major mechanism for the failure of the phospher bronze is corrosion fatigue, the sub-sections will be divided into the fundamental model of pitting corrosion, and the fundamental model of mechanical

fatigue.

2.5.1 Models for corrosion

The corrosion model, fundamental to Chapter 3 for the simulation of pit depths distribution, is the power law first proposed by Romanoff [60]:

$$y(t) = \alpha \times t^{\beta} ------(2-1)$$

where *y* is the pit depth, *t* is the time and α and β are constants. This is a mathematical model describing the pit depth growth to be time dependent. This is a simple model regardless of multiple mechanisms that caused the pitting, for example, the pit initiation, the electro-chemical reactions of pit growth etc. It can be regarded as a statistical model which focuses on describing the pattern of pits. The parameter α is normally represented by a type of distribution, this distribution with certain numbers of parameters is usually curve fitted via laboratory experimental data. The parameter β is a geometry related value, usually within the range of 0.2 to 1.

2.5.2 Models for fatigue

a) Paris' Law for crack propagation

The fundamental yet classical theory in the fatigue crack propagation is the Paris' Law, also called the Paris-Erdogan Law. It was first introduce by Paris [117] in 1961. The model is related to the stress intensity factor and is expressed as:

$$\frac{da}{dN} = C\Delta K^{m} -------(2-2)$$

In which a is the crack length, $\frac{da}{dN}$ is the crack growth rate, C and m are material, environment and stress ratio related constants, and Δk represents the stress intensity factor.

b) Kondo's theory on the pitting corrosion to crack propagation transfer

Kondo [56] introduced the basic requirements for predicting the pit-crack transfer,

consisting of two rules: first, the pit depth must reach a threshold value in order to initiate the transition. Second, at the transfer depth, the crack propagation rate is larger than the growth rate of pitting corrosion.

c) Turnbull's proposal on pitting corrosion to crack propagation transfer

Turnbull [73] used a probability theory to describe the transfer ('Transfer Probability'), suggesting that it is not always the pit with the largest depth that transfers from pitting corrosion to crack propagation. All pits with different depths have a certain probability of transfer.

2.5.3 A modified crack growth model by author's research team within the project

A member of the author's research team[1] provided a modified crack propagation model which is the fundamental theory of Chapter 5, the following is the description of this modified crack propagation model. It is referred to as 'Crack growth rate under high mean stress'.

From the work of Turnbull the crack growth rate is given by [70, 73]

$$\frac{\mathrm{d}x}{\mathrm{d}t} = C\Delta\sigma^{p}x^{q} \quad ------(2-3)$$

where x is the crack length (for consistency with pit depth), $\Delta\sigma$ is the stress amplitude, C is a constant for the same type of crack and $p=2q$ (same as for long cracks used in Linear Elastic Fracture Mechanics [70]) and q are material constants. Since for the same pit depth, the pit growth rate is statistically distributed, it would be expected that the crack growth rate will also follow a similar distribution. The above equation cannot be used in the cable life prediction as the failure is dominated by the effect of mean stress.

[1] Sivashangari Gnanasambandam, co-author of the author's two publications.

Various empirical approaches have been proposed in the literature to address the effect of mean stress. For example, Zhang et al. [118] suggested to modify the stress amplitude such that

$$\Delta\sigma^* = \frac{\Delta\sigma}{\left[\frac{1-R}{1+R}\right]^s} - - - - - - (2-4)$$

where $R = \frac{\sigma_{min}}{\sigma_{max}}$ and s = 0.5 for copper alloys [119]. Different modifications have also been put forward by Smith, Watson and Toppers [120] who proposed the effect of mean stress as a geometric mean of the maximum stress and the stress amplitude and is given below

$$\Delta\sigma^* = \sqrt{\sigma_{max}\Delta\sigma} - - - - - - (2-5)$$

This approach is called SWT method and it does not depend on any material property. Walker [121] introduced an additional material property γ into the above equations as shown in equation (2-6). The value of γ ranges from 0.4 to 0.8.

$$\Delta\sigma^* = {\sigma_{max}}^{1-\gamma}\Delta\sigma^{\gamma} - - - - - - (2-6)$$

Klesnil and Lukas [122] proposed an empirical relation to account the effect of mean stress as shown below

$$\Delta\sigma^* = \frac{\Delta\sigma}{(1-R)^{\gamma}} - - - - - (2-7)$$

where the value of γ lies between 0.5 to 0.75. We have tested all these empirical equations and concluded that none of them is valid for the cable failure. A possible reason is perhaps that the mean stress in the underground cable is much higher than the stress amplitude. In order to capture the cable failure observed in the field data over the long term, it is proposed to modify equation (2-3) similar to the ripple loading with high mean stress and very small amplitude loading as follows

$$\frac{\mathrm{d}x}{\mathrm{d}t} = C(\Delta\sigma^*)^p x^q - - - - - (2-8)$$

where $\Delta\sigma^* = \sigma_{mean} + \Delta\sigma$. The exponents for $\Delta\sigma$ and x have been separated and we represented the effective stress as a sum of mean stress and daily alternating stress. Equation (2-8) can be interpreted as an empirical rate equation for crack propagation under a combination of high mean stress and small stress amplitude. Its justification is the fact that it can capture the field data collected over 30 years in this work.

In particular, two failure cases at two different cable locations are studied for asset management modelling. The material properties and geometries of the tape and lead sheath used in calculations for the two specific cables were listed previously in Table 2-3.

Mean (σ_{mean}) and alternating stress ($\Delta\sigma$) are calculated as follows [53]: The reinforcing tapes experience variation in stress because of the cable internal oil pressure and temperature variation (due to variation of electricity demand with time),

$$\sigma_{static\ pressure} \cong \frac{r_t}{t_t} - - - - - (2-9)$$

$$\Delta\sigma = \sigma_{dynamic\ pressure} + \sigma_{thermal} - - - - - (2-10)$$

$$\sigma_{thermal} \cong \frac{\alpha_s' - \alpha_t'}{\frac{1}{E_t} + \frac{1}{E_s}\frac{t_t}{t_s}} \Delta T - - - - - - - (2-11)$$

where r_t is the radius at which the tape is wrapped around the lead sheath, t_t is the tape thickness, p is the inner pressure, T is the temperature in K, α' is the linear expansion coefficient, E is the Young modulus, t is the thickness, and the subscripts s and t indicate the lead sheath and the phosphor bronze tape respectively. Mean (σ_{mean}) stress is calculated from the average of the stress exerted due to static pressure over the operating period and the $\sigma_{dynamic\ pressure}$ is calculated from the daily variation of stress due to static pressure. The measured values of mean stresses and alternating stresses of the two failed cables were provided in Table 2-4.

2.6 Unresolved issues and the purpose of this thesis

Following the previous sections, it can be observed that there are several issues existing regarding the in-depth of the researches. These unsolved issues are listed and explained below:

Macroscopic mathematical description of pit depth distribution of bronze

First of all, the current research in the corrosion filed focuses on the microscopic reaction observation. The electro-chemical reactions on metal material surfaces are studied, though they are normally focusing on individual pit. The issue of researching on individual pit is: corrosion pits are at small scales, in the size of micrometres, normally on the surface of any material with a period of time of usage, the number of corrosion pits is large, each pit can be a result of complicated electro-chemical reactions, which means that they are microscopically random. The study of single pit corrosion may not be able to explain the majority of randomness in the corrosion phenomenon. Furthermore, steel and aluminium are among the most popular materials in the researching of corrosion phenomenon and they are considered as the most important fundamental materials in the engineering industry. The power transfer cables being researched in this thesis, fails due to the corrosion fatigue effect of a reinforcing tape layer within the cables. The layer is of the phosphor bronze material which has limited amount of research track records. As the study of this phosphor bronze material is crucial to the understanding of the failure mechanism in power transmission cables, the research in this thesis is carried out.

In Chapter 3 of this thesis, the modelling of pit depth distribution in a macroscopic scale for the phosphor bronze material is carried out in order to fill the blank of research on macroscopic pit depth distribution on phosphor bronze material.

The understanding of the corrosion pit transfer to crack propagation mechanism

The current classical understanding for the corrosion fatigue mechanism is proposed by Kondo [56] which states that when pitting corrosion and fatigue cracking happening at the same time (corrosion fatigue), it is always the fastest growing corrosion pit (which is also the deepest pit) that transfers into a more serious condition of crack propagation, and this is the main cause of the failure of the material. The experiment carried out during the research of this thesis showed different phenomenon, which for many phosphor bronze reinforcing tapes being studied is not the deepest pit measured that caused the final failure, but rather pits that grew slower and of less depth.

To solve the issue that the experimental phenomenon cannot be explained by the classical theory, in this thesis, a statistical approach is proposed on the explanation. This approach assumed that for every pit on the surface of metal there is a probability that it would transfer to crack propagation under cyclic loading, it is just that deeper pits have larger probabilities than smaller pits for the transfer, which enhanced the classical theory so to explain the actual experimental phenomenon.

The limits of the probability of failure model for power transmission cables in the industry

Currently there are several models used in the industry for the estimation of probability of failure for underground power transmission cables, for example, a single normal distribution applying to all underground cables, or, define cables at 4 criticality levels and define a fixed remaining life estimation for each level.

The limits and disadvantages are obvious. The environment of all underground power transmission cables are different and complicated, therefore, a universal single function model cannot give the most complete information for the varieties of situations. Also to classify cables in four criticality levels show the problem of too ambiguous too. The

fact is, each cable is with a unique condition and the development to failure in each cable is not identical.

To solve this problem, I proposed a new definition of the probability of failure based on the chemical and physical characters of each individual cable. In addition, these individual models are combined with the existing industry models for a most complete inclusive of cable information and data. I name these combined models 'Tailored probability of failure model' which gives the most fitted estimation on the probability of failure for each individual cable.

The objective of this thesis

First of all, from the literature, there is little research done on the pitting corrosion of phosphor bronze material. The lack of such information meaning the existing model for failure prediction is inaccurate at a industrial level of application. With this issue in mind, the initial motivation of this thesis is to provide the novel simulation of pit depth distribution on phosphor bronze material which is a vital component in the underground power transmission cables.

Second, by acknowledging the pit depths distribution, it is essential in failure prediction that the crack propagation should follow the pitting corrosion procedure. The experimental results cannot be perfectly explained by the existing theory of pit to crack propagation, which requires a novel theory in explanation. A statistical approach is applied to link the pitting corrosion and crack propagation in a reasonable way.

Last, the result of the two motivations leads to life estimation of underground power transmission cables, which then leads to the calculation of probability of failure of the cables. However, there are existing industry-level models which discuss the same goal. To enable the research output is of use in the energy industry, the final motivation is to integrate the research results into the existing models, which leads to the machine

learning approach, specifically the Bayesian network approach in updating the empirical industry model by the research output of this thesis.

To represent the procedure of the research chapters, a flowchart is provided below.

Flowchart of research output:

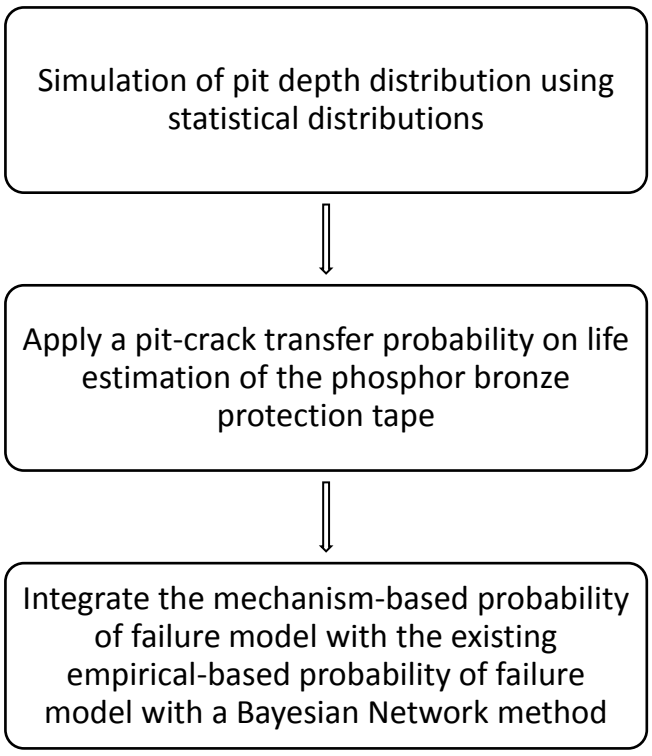

3. Modelling of pit depth distribution for phosphor bronze tapes used in underground power transmission cables

The purpose of this chapter is to develop a mathematical model describing the pit depth distribution on the surface of the phosphor bronze material. A simple power law involving two parameters is applied, to achieve a balance between simplicity and accuracy. It is of the interests of both industry and research output that when a certain model can explain the physical phenomenon, then the simpler the model the better. The power law applied in this chapter is a statistical model, this approach is made as the real mechanism is complicated and the data is limited in discovering the effects of all mechanisms. The modelling procedure consists of the following major steps:

1) Laboratory measurement of pit depths on available phosphor bronze tape samples and data collection.
2) Mathematical simulation on pit depth distribution model.
3) Simulation results and discussion of the model.

The laboratory scanning of pit depth, done by the co-authors of the jointly published paper [5], is greatly acknowledged. A brief description of the experimental work is included in this chapter for completeness. This chapter is entirely based on one publication of the author (first-author publication) [5], extended with additional details in the methodology and result sections. In this chapter, Figure 2-11 (re-print), Figure 3-1, Figure 3-7, Figure 3-9, Figure 3-10, Figure 3-11, Figure 3-12, Figure 3-13, Figure 3-14 and Figure 3-15 are in the published journal paper, the rest of the figures shown here are for extended details.

3.1 Laboratory measurement of pit depths and data collection

The measurement presented in this sections was performed by the co-authors of a joint paper [5].

Reinforcing tapes of different service ages and from different environments are analysed to find the pit depth distribution using metallographic methods as discussed below.

The pit depth data extraction follows a three-step procedure: tape cleaning, sample preparation and pit depth measurement. For the tape cleaning, sample preparation and pit depth measurement, the methods discussed in ASTM standard is followed [123].

Tape cleaning: The tape was cleaned as it was initially covered by bitumen. In this process, bitumen is dissolved and removed with extra pure n-pentane by immersion of the tape sample in a sequence of three pentane baths and gently removing all the sticky bitumen with the aid of cotton buds. The process takes from 10 to 30 seconds and the tape does not show any signs of corrosion due to the cleaning process.

Sample preparation: Once a piece of tape has been cleaned, samples can be prepared by cutting the tape in small rectangular samples every 0.5 cm along the tape's longitudinal axis. Each tape sample is mounted in groups of two sections per mounting by keeping the upper sides of the tape in the same direction and marking the lower side so to distinguish between the two after the mounting is complete. A conductive phenolic mounting resin was used. The sample was then ground/polished with a succession of SiC paper starting form 240 grit to a 1 micron finishing. The area immediately next to the cut edge will be removed in the grinding process, so that local plastic deformation near the cut will not alter the pit depth measurement. Finally the samples were immersed in an ultrasonic bath with methanol for 3 minutes at room temperature in order to remove any polishing residue from the polished surface. The tape before and after the cleaning is shown in Figure 2-11 (a) and 2-11 (b), the mounted sample is shown in Figure 2-11 (c).

Pit depth measurement: The procedure listed in the ASTM standard G46 [124] to

measure the pit depth is followed as below.

- Locate the mounted reinforcing tape under the optical microscope.
- Start from the top surface section edge with 5x lens and sequentially increase the lens magnification and refocus till the edge is visualised with a 50x lens. Focus is obtained with the coarse focusing knob for the 5x, 10x, and 20x lens, while the fine-focusing knob is necessary for the 50x lens.
- Start from the edge, use the X-Y knobs to move the image along the tape top surface, stop and measure each pit encountered till the entire top surface length of the sample has been scanned.
- Perform the readings by drawing multiple measuring lines and measuring each pit on the deepest point. In this way there is no need to stop and record each pit dimension singularly, but the measurements for a single sample can be recorded altogether at the end of the analysis of the sample.
- Calculate the probability of occurrence for a pit depth range which is the number of pits counted in the given pit range divided by the total number of pits in the tape.

3.2 Mathematical simulation on pit depth distribution model

The modelling consists of three stages as shown in the flowchart (as Figure 3-1) and explained in detail below:

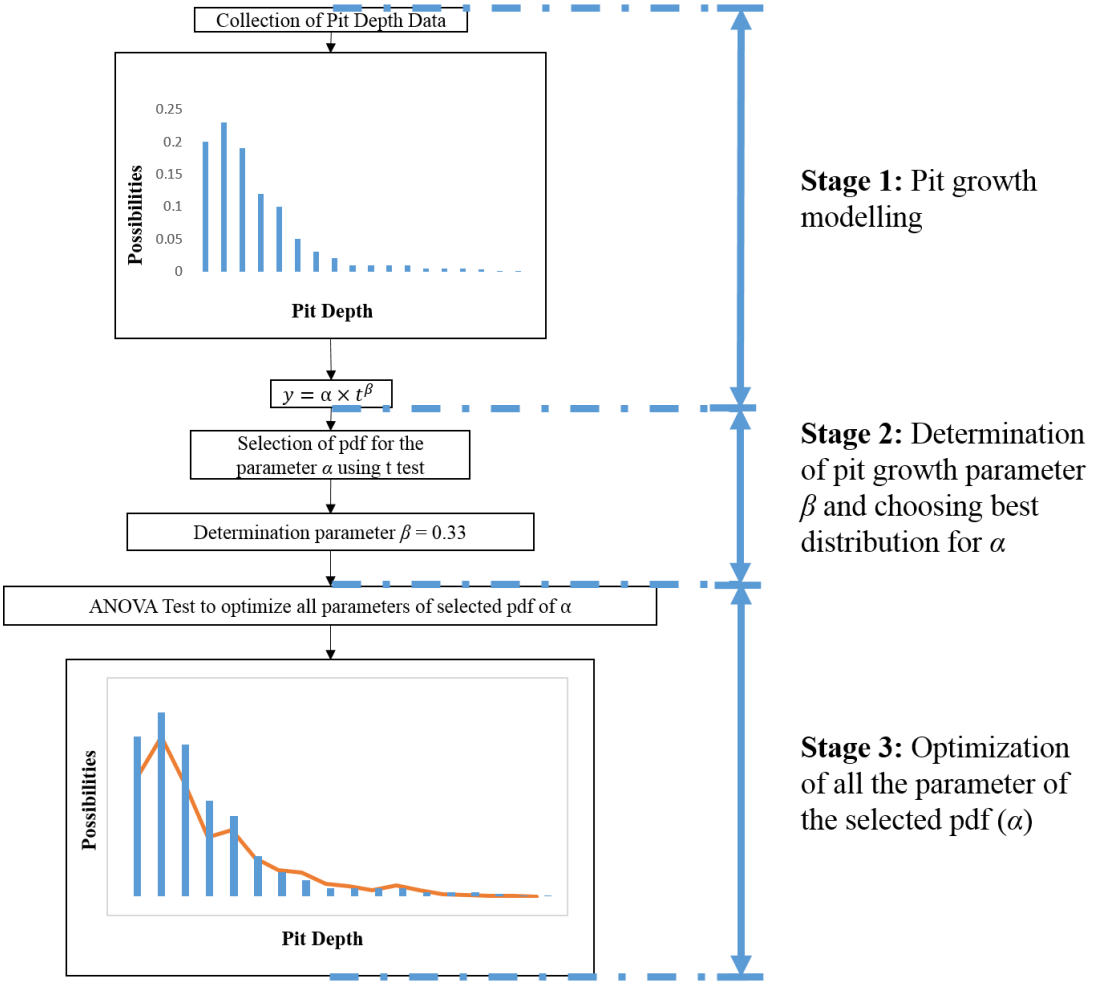

Figure 3-1: Flowchart for pit growth modelling using Monte Carlo simulations [5]

Stage 1: Pit growth modelling

The mathematical model used to calculate the pit depth is a time dependent power law which was first introduced by Romanoff [60].

$$y(t) = \alpha \times t^{\beta} \qquad (3-1)$$

where y is the pit depth, t is the time and α and β are constants. In this model, β is an unknown constant and α is also unknown but chosen from a random distribution and both the parameters are determined by the best statistical fit to the experimental pit depth distributions using Monte Carlo simulations.

Stage 2: Determination of pit growth parameter β and choosing best distribution for α

Monte Carlo simulations are used to simulate the pit growth which is modelled by Equation (3-1). For most of the materials the value β is in the range of 0.2 to 1 [44]. The parameter α is unknown and is assumed to follow a probability density function (PDF) which gives the best fit to the experimental pit depth distribution.

The probability distributions considered for selection of α are shown here. Each general distribution function is given for reference:

- Exponential distribution with one parameter

$$f(x|\lambda,k) = \begin{cases} 0 & x < 0 \\ \lambda e^{-\lambda x} & x \geq 0 \end{cases} \quad (3-2)$$

  Where

  - λ *is the scale parameter*

- Normal distribution with two parameters

$$f(x|\mu,\sigma^2) = \frac{1}{\sqrt{2\pi\sigma^2}} e^{-\frac{(x-\mu)^2}{2\sigma^2}} \quad (3-3)$$

  Where

  - $\mu \in \boldsymbol{R}$ *is the location parameter, equals to the mean of the dataset*
  - σ *is the scale factor, also representing the standard deviation*

- Gamma distribution with two parameters

$$f(x|k,\theta) = \frac{1}{\Gamma(k)\theta^k} x^{k-1} e^{-\frac{x}{\theta}} \quad (3-4)$$

  Where

  - k *is the shape factor*
  - θ *is the scale factor*
  - $\Gamma(k)$ *is the Gamma function*

$$\Gamma(k) = \int_0^\infty \frac{t^{k-1}}{e^k} dk \quad (3-5)$$

- Weibull distribution with two parameters

$$f(x|\lambda,k)=\begin{cases}0 & x<0\\ \frac{k}{\lambda}\left(\frac{x}{\lambda}\right)^{k-1}e^{-\left(\frac{x}{\lambda}\right)^{k}} & x\geq 0\end{cases} \quad (3-6)$$

- $\lambda\ is\ the\ scale\ factor$
- $k\ is\ the\ shape\ factor$

- Generalized Extreme Value (GEV) distribution with three parameters

$$f(x|\mu,\sigma,\xi)=\frac{1}{\sigma}t(x)^{\xi+1}e^{-t(x)} \quad (3-7)$$

Where

$$t(x)=f(x)=\begin{cases}\left(1+\xi\left(\frac{x-\mu}{\sigma}\right)\right)^{-1/\xi} & if\ \xi\neq 0\\ e^{-(x-\mu)/\sigma} & if\ \xi=0\end{cases} \quad (3-8)$$

- $\mu\in\boldsymbol{R},is\ the\ locaiton\ factor$
- $\sigma>0,is\ the\ scale\ facotr$
- $\xi\in\boldsymbol{R},is\ the\ shape\ factor$

The Monte Carlo simulation protocol to find β and the best distribution for the parameter α is as follows. At known time (t), number of pits (n), number of iterations (N), and by varying β from 0.2 to 1, the pit depth is calculated from Equation (3-1) for each distribution of α listed above. The generated pit depth is compared with the actual pit depth distribution to find the value of β using the best fit from the statistical t test. The same procedure is followed for all the five distributions of α and their corresponding t test values for the best fitted β are compared to get the appropriate distribution for α.

A very important application of the Student's t test is to determinate whether two sets of data are significantly different from each other. This test can be applied to samples with a normal distribution, or samples with a normal distribution tendency proved by the central limit theory [125].

Stage 3: Optimization of all the parameter of the selected pdf (α)

The parameters of the best distribution are derived by fitting the data obtained into the actual pit depth distribution. The Monte Carlo simulation protocol to optimize all the parameters of best distribution is as follows. At known time (t), number of pits (n), number of iterations (N), and a determined value of β from stage 2, the pit depth is calculated from Equation (3-1) by varying three parameters of α. At a given value of α and for each iteration, the generated 1 million pit depths are compared with the actual pit depth distribution and the optimized parameters for the distribution is obtained using the best fit from the statistical method.

In the literature, a number of statistical methods such as ANOVA [126], K-S test [44] and Anderson Darling goodness-of-fit test [127] are used to compare the difference between experiment and simulated pit depth distribution. The statistical test applied in our method for comparing the experimental data is the ANOVA (analysis of variance), a method which is commonly used in pitting corrosion.

3.3 Simulation results and discussion of the model

Pit depths were extracted from the tape samples with different service age and also from different locations using metallographic methods as discussed in section 3.1. The obtained pit depth distributions were modelled using Monte Carlo simulations as described in section 3.2. The results obtained from pit depth extraction and the modelling are elaborated in detail in the following sections.

3.3.1 Experimental pit depth distribution

The pit depths are extracted from the various samples of reinforcing tapes using metallographic methods. According to Chapter 2, the experimental data is already provided. First of all, the measurement pit depths data for all failure cases are plotted in

bar charts below, for a universal comparison of data. Instead of comparing the number of pits being counted within each pit depth range, a probability of occurrence of pits is introduced. The probability of occurrence is calculated as the number of pits occurring within a pit range divided by the total number of pits measured at one location. These experimental results are shown in the following figures for visual assistance.

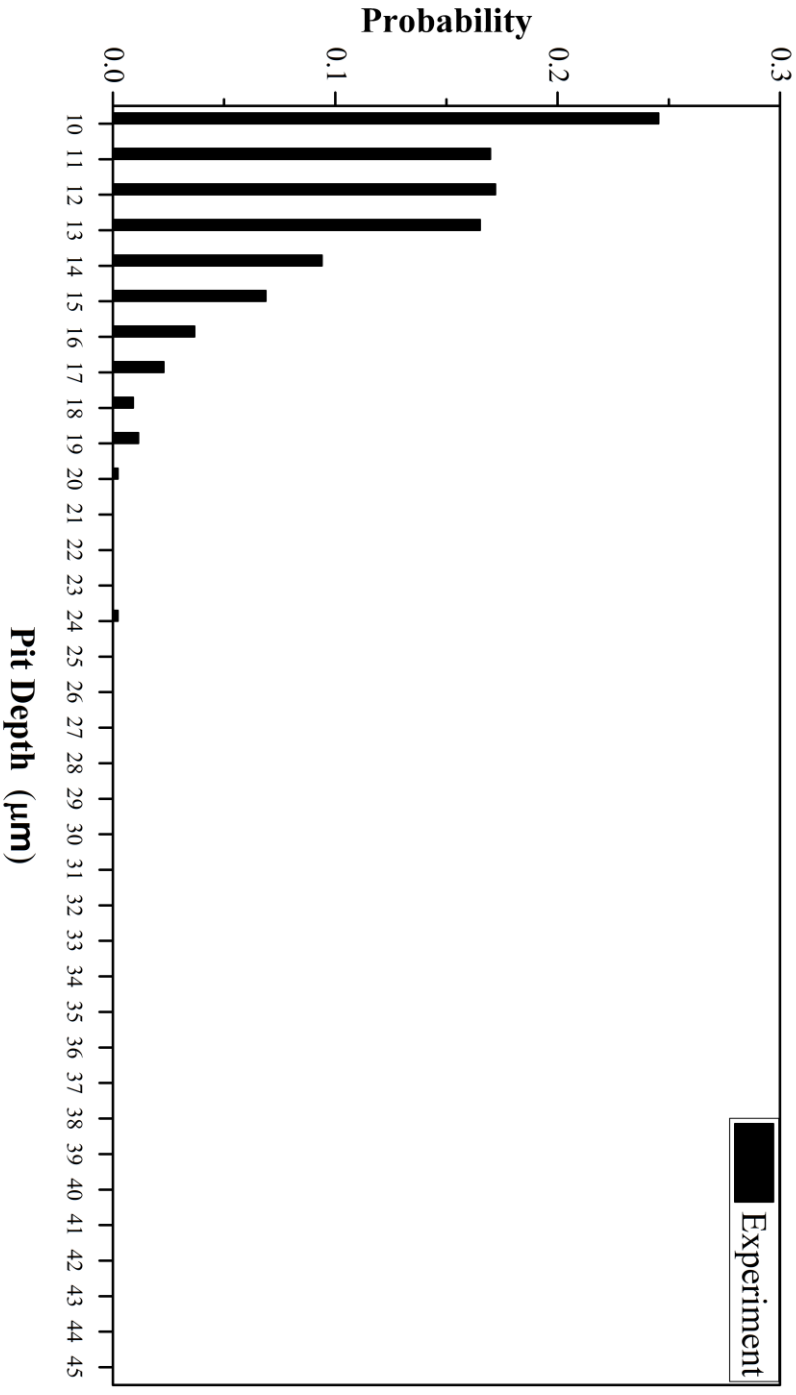

Figure 3-2: Pit depth measurement of Site 1 at 38 years (first failure) (re-produced from [5]

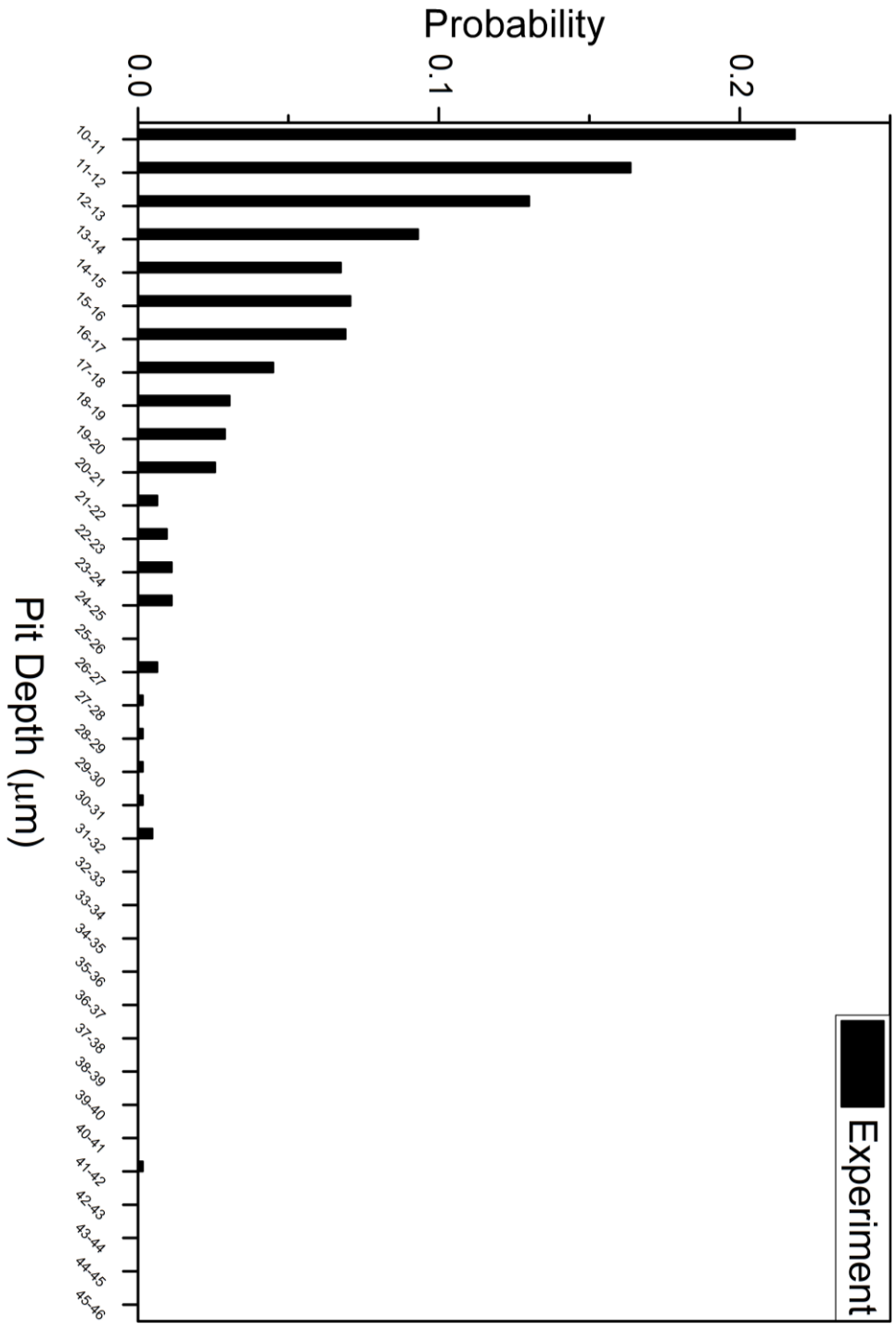

Figure 3-3: Pit depth measurement of Site 1 at 44 years (second failure) (reproduced from [5])

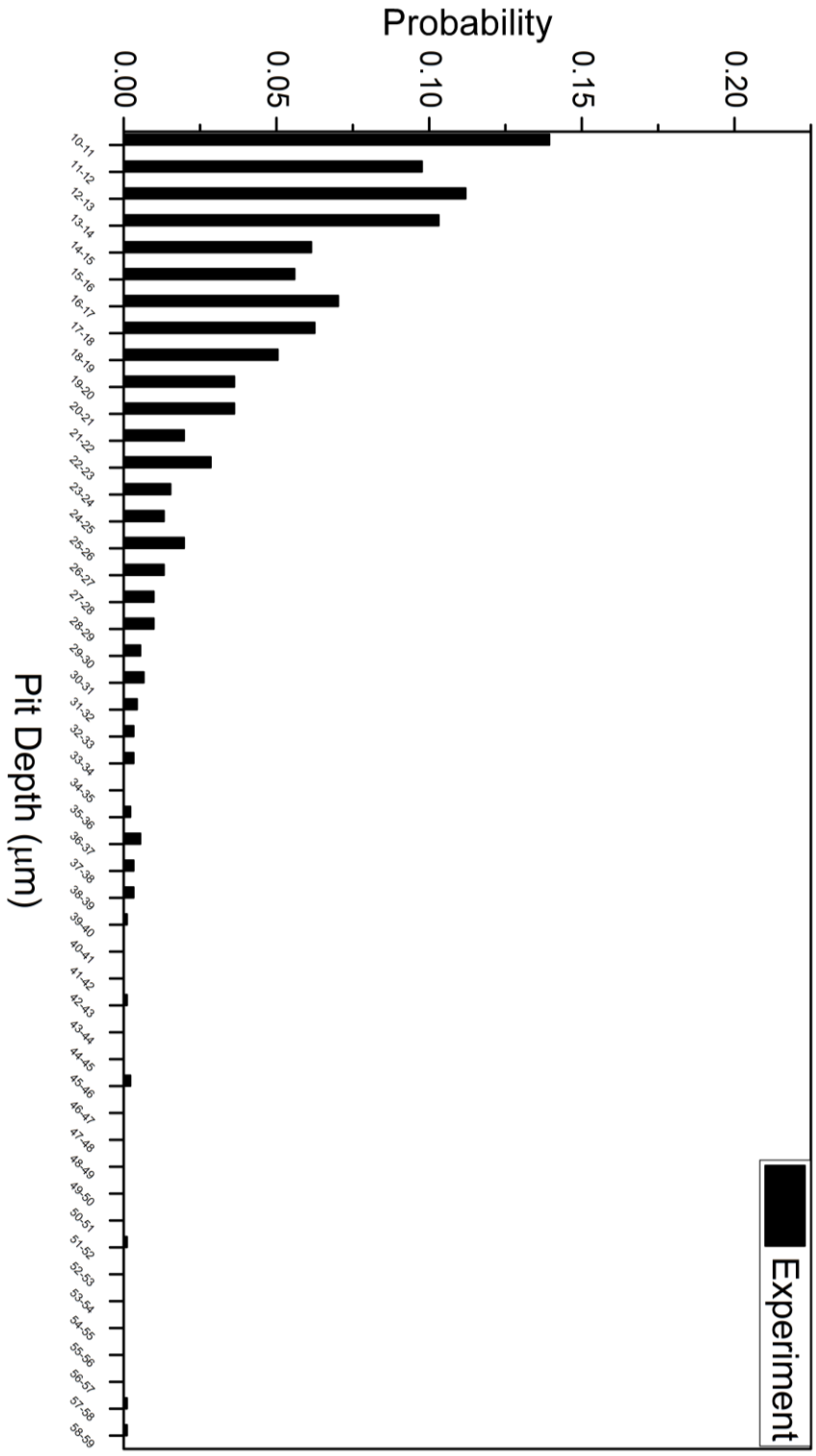

Figure 3-4: Pit depth measurement of Site 2 (43 years) (re-produced from [5])

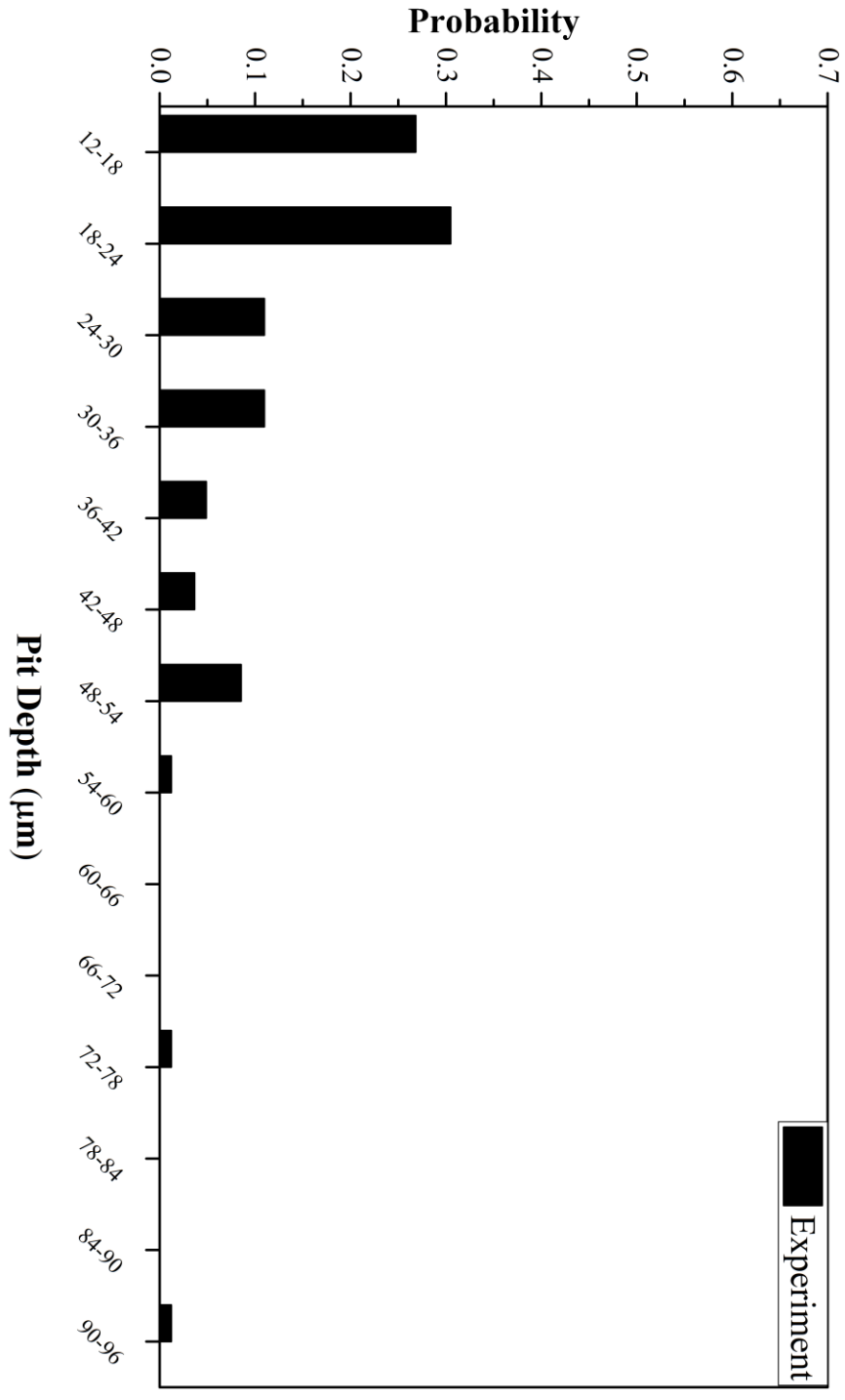

Figure 3-5: Pit depth measurement of Site 3 (28 years) (re-produced from [5])

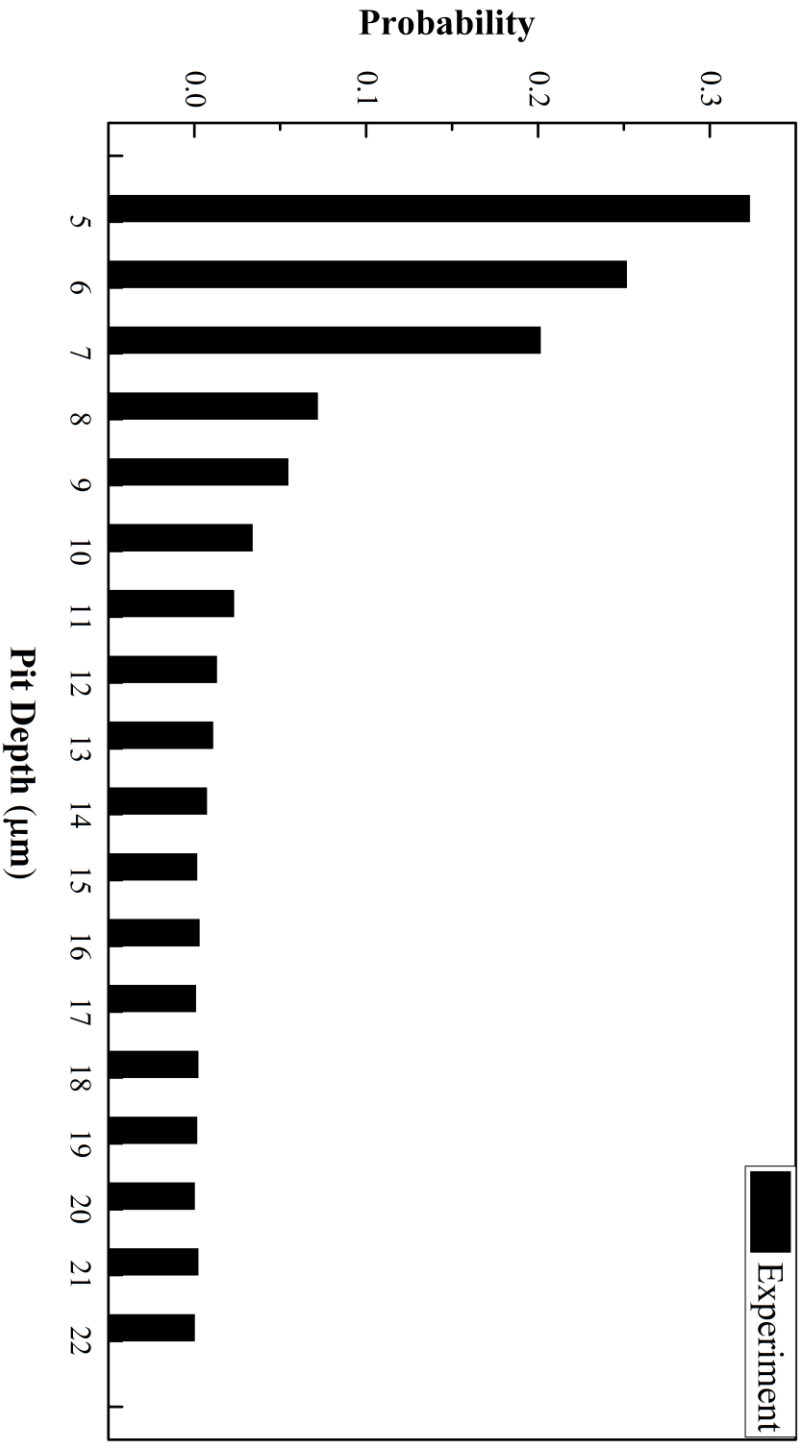

Figure 3-6: Pit depth measurement of Site 4 (41 years) (re-produced from [5])

In addition to the pit distributions above, Figure 3-7 is plotted to validate that the experimental pit depth distribution follow a constant pattern. Taken from the same phosphor bronze tape, two experiments count pit depths each containing 16 samples are carried out. This is the original measurement of Site 2 phosphor bronze samples.

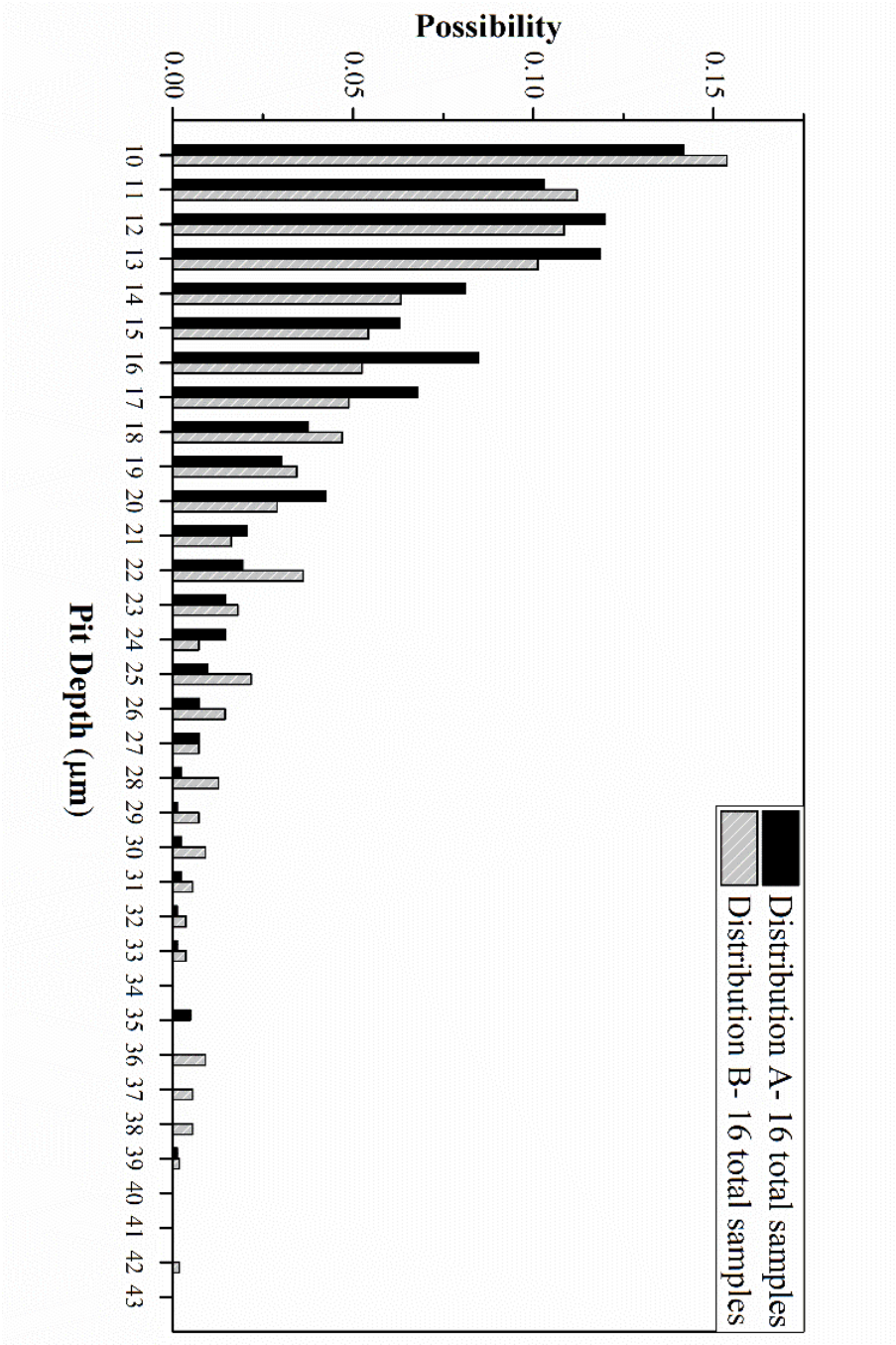

Figure 3-7: Pit depth distributions for 2 sets of samples belonging to the same piece of tape (re-produced from [5])

The above figures, Figure 3-2 to Figure 3-7, are plotted for the observation of a pattern of distributions. The observed pattern is used as an initial assumption of the potential statistical distributions for further simulation. Especially Figure 3-7 is regarded as an evidence that the pit depths remain the same pattern of distribution throughout the years of developing, which provides the an assumption that one statistical distribution can be used to simulate the entire process of pitting corrosion phenomenon.

3.3.2 Pit growth modelling: Determination of pit growth parameter β and selection of probability distribution for α

Monte Carlo simulations are performed to calculate the pit depth using Equation (3-1) with the parameters:

- β varying from 0.2 to 1.
- α is chosen from one of the 5 distributions mentioned in Section 3.2

First of all, the comparison of simulation results and experimental data is done for Site 1. For each distribution, by varying β, the pit depth distribution is calculated for a reinforcing tape of service age 38 and compared with their corresponding experimental pit depth distribution using the t test.

One of the t test applications is the comparison of the similarity between two sets of data. One major step in the t test application is to reference the t test table which is given here.

Table 3-1: T test table [128]

cum. prob	$t_{.50}$	$t_{.75}$	$t_{.80}$	$t_{.85}$	$t_{.90}$	$t_{.95}$	$t_{.975}$	$t_{.99}$	$t_{.995}$	$t_{.999}$	$t_{.9995}$
one-tail	0.50	0.25	0.20	0.15	0.10	0.05	0.025	0.01	0.005	0.001	0.0005
two-tails	1.00	0.50	0.40	0.30	0.20	0.10	0.05	0.02	0.01	0.002	0.001
df											
1	0.000	1.000	1.376	1.963	3.078	6.314	12.71	31.82	63.66	318.31	636.62
2	0.000	0.816	1.061	1.386	1.886	2.920	4.303	6.965	9.925	22.327	31.599
3	0.000	0.765	0.978	1.250	1.638	2.353	3.182	4.541	5.841	10.215	12.924
4	0.000	0.741	0.941	1.190	1.533	2.132	2.776	3.747	4.604	7.173	8.610
5	0.000	0.727	0.920	1.156	1.476	2.015	2.571	3.365	4.032	5.893	6.869
6	0.000	0.718	0.906	1.134	1.440	1.943	2.447	3.143	3.707	5.208	5.959
7	0.000	0.711	0.896	1.119	1.415	1.895	2.365	2.998	3.499	4.785	5.408
8	0.000	0.706	0.889	1.108	1.397	1.860	2.306	2.896	3.355	4.501	5.041
9	0.000	0.703	0.883	1.100	1.383	1.833	2.262	2.821	3.250	4.297	4.781
10	0.000	0.700	0.879	1.093	1.372	1.812	2.228	2.764	3.169	4.144	4.587
11	0.000	0.697	0.876	1.088	1.363	1.796	2.201	2.718	3.106	4.025	4.437
12	0.000	0.695	0.873	1.083	1.356	1.782	2.179	2.681	3.055	3.930	4.318
13	0.000	0.694	0.870	1.079	1.350	1.771	2.160	2.650	3.012	3.852	4.221
14	0.000	0.692	0.868	1.076	1.345	1.761	2.145	2.624	2.977	3.787	4.140
15	0.000	0.691	0.866	1.074	1.341	1.753	2.131	2.602	2.947	3.733	4.073
16	0.000	0.690	0.865	1.071	1.337	1.746	2.120	2.583	2.921	3.686	4.015
17	0.000	0.689	0.863	1.069	1.333	1.740	2.110	2.567	2.898	3.646	3.965
18	0.000	0.688	0.862	1.067	1.330	1.734	2.101	2.552	2.878	3.610	3.922
19	0.000	0.688	0.861	1.066	1.328	1.729	2.093	2.539	2.861	3.579	3.883
20	0.000	0.687	0.860	1.064	1.325	1.725	2.086	2.528	2.845	3.552	3.850
21	0.000	0.686	0.859	1.063	1.323	1.721	2.080	2.518	2.831	3.527	3.819
22	0.000	0.686	0.858	1.061	1.321	1.717	2.074	2.508	2.819	3.505	3.792
23	0.000	0.685	0.858	1.060	1.319	1.714	2.069	2.500	2.807	3.485	3.768
24	0.000	0.685	0.857	1.059	1.318	1.711	2.064	2.492	2.797	3.467	3.745
25	0.000	0.684	0.856	1.058	1.316	1.708	2.060	2.485	2.787	3.450	3.725
26	0.000	0.684	0.856	1.058	1.315	1.706	2.056	2.479	2.779	3.435	3.707
27	0.000	0.684	0.855	1.057	1.314	1.703	2.052	2.473	2.771	3.421	3.690
28	0.000	0.683	0.855	1.056	1.313	1.701	2.048	2.467	2.763	3.408	3.674
29	0.000	0.683	0.854	1.055	1.311	1.699	2.045	2.462	2.756	3.396	3.659
30	0.000	0.683	0.854	1.055	1.310	1.697	2.042	2.457	2.750	3.385	3.646
40	0.000	0.681	0.851	1.050	1.303	1.684	2.021	2.423	2.704	3.307	3.551
60	0.000	0.679	0.848	1.045	1.296	1.671	2.000	2.390	2.660	3.232	3.460
80	0.000	0.678	0.846	1.043	1.292	1.664	1.990	2.374	2.639	3.195	3.416
100	0.000	0.677	0.845	1.042	1.290	1.660	1.984	2.364	2.626	3.174	3.390
1000	0.000	0.675	0.842	1.037	1.282	1.646	1.962	2.330	2.581	3.098	3.300
z	0.000	0.674	0.842	1.036	1.282	1.645	1.960	2.326	2.576	3.090	3.291
	0%	50%	60%	70%	80%	90%	95%	98%	99%	99.8%	99.9%
	Confidence Level										

The experimental data contains 39 samples (38 degrees of freedom). According to the t test distribution table, to reject the null hypothesis (the simulation results and experimental data do not have a significant difference), the t test value should be smaller than approximately 2.021 with pre-determined p value as 0.05. Any probability distribution for α with a certain value of β (between 0.2 to 1) which gives the value smaller the t test value will be selected as the best distribution for α and the corresponding β value is fixed as a constant value for β.

On a trial and error basis, the range of parameters in the probability distribution is fixed

based on the t test results. All the probability distributions are further tested with the pit depth data at 44 years and their applicability is assessed by t test.

Table 3-2: T test value table showing the results of simulation for 5 different types of distributions [5]

Distribution Type	38 Years distribution	44 Years distribution	Conclusion
Normal	$2.1061 > 2.021$	$2.3454 > 2.021$	Exceeding the T test value
Exponential	$2.0627 > 2.021$	$3.1495 > 2.021$	Exceeding the T test value
Two parameter Weibull	$1.6742 < 2.021$	$2.3805 > 2.021$	Exceeding the T test value
Three parameter GEV	$1.4283 < 2.021$	$2.0196 < 2.021$	***T test value under boundary value***
Gamma	$1.5544 < 2.021$	$2.4025 > 2.021$	Exceeding the T test value

From Table 3-2 it can be easily observed that all four distributions except for the GEV distribution rejected the null hypothesis. GEV distribution achieved an acceptable t- test results for both 38 and 44 years pit depth data obtained from the same location. So the GEV distribution with three parameters is selected for the random parameter α. The corresponding value of β for the GEV distribution varied from 0.3 to 0.32. Theoretically, $pit\ depth \propto t^{\frac{1}{3}}$, this is due to the geometry assumption of pit growth [129-140], which means the β value shall be approximately 0.33, provided that the pit shape is hemispherical in nature [141].

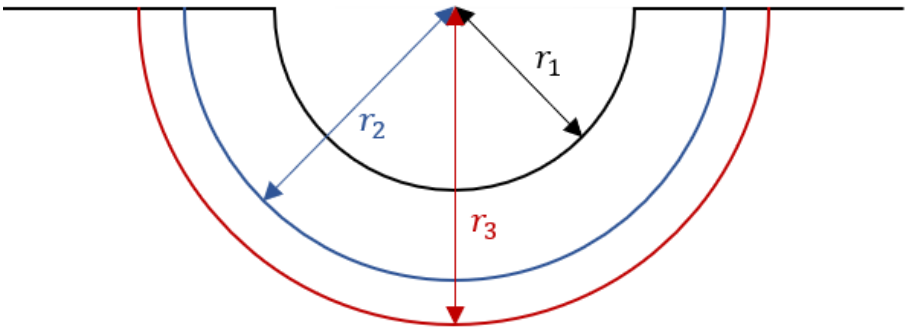

Figure 3-8: A representation of pit growth in hemispherical geometry

Pit depth is assumed to grow at a constant volume speed, which means a constant volume growth in unit time. The volume of hemisphere is:

$$V = \frac{2}{3}\pi r^3 \qquad (3-9)$$

According to the assumption of constant volume speed, it can be expressed as:

$$\frac{dV}{dt} = \frac{d\frac{2}{3}\pi r^3}{dt} = C\ (constant) \qquad (3-10)$$

Which leads to:

$$\frac{dr}{dt^{1/3}} = \left(\frac{C}{\frac{2}{3}\pi}\right)^{1/3} = C'\ (also\ regarded\ as\ a\ constant) \quad (3-11)$$

In the above equation (3-11) r is the radius of the hemisphere, which is the same as pit depth and t is time. This deduction procedure proves that pit depth is related to $t^{1/3}$. This hemispherical assumption can be further justified by the observed pit shape in the tape sample, shown in Figure 2-11 (d). It can be concluded that the pit growth follows the theoretical geometry assumption, and the β value is fixed as 0.33.

3.3.3 Pit depth evolution and distribution

Pit growth is modelled using Equation (3-1) and the Monte Carlo (MC) method, as explained in Section 3.2. Pit depth is calculated by keeping constant value for β as 0.33

and using the three parameter GEV distribution for α in Equation (3-1). The three parameters of α (scale parameter (σ), location parameter (μ) and shape parameter (ξ)) are optimized by comparing the experimental and simulated pit depth distributions using ANOVA test.

Although the simulation results suggested that the GEV distribution is the pattern that proved to be the most accurate, it is not a widely used distribution format in the corrosion field. The standard format of the possibility density function regarding to the GEV distribution was given previously in Equation (3-7) and Equation (3-8).

Each simulation uses 10000 number of pits and 1000 number of iterations. In total, 10000000 pits are involved in each simulation. All the pits follow the GEV distribution with the same three parameters. The probability of occurrence for a pit depth range is calculated similarly to the experiment data.

Monte Carlo simulations are performed to calculate the pit depth distribution of the reinforcing tape over two different years (38 and 44 years) under the same environmental conditions, which means that the samples taken for these two years are from the same location. First, GEV distribution is applied for the tapes of service at 38 years. The optimized parameters of α that gave the best fit to the experiment pit depth distributions using ANOVA tests are $\sigma = 0.5, \mu = 3.4$ and $\xi = 0.5$. Then, using the GEV distribution with the same three parameters ($\sigma = 0.5, \mu = 3.4$ and $\xi = 0.5$), the pit depth distribution for the tapes of service at 44 years is calculated. The simulated pit depth distribution fitted well with the experiment pit depth distribution of the reinforcing tapes of service life 44 years. Comparisons between the simulated pit depth and experimental pit depth distribution of age 38 and 44 years are shown in Figure 3-9 and Figure 3-10, respectively.

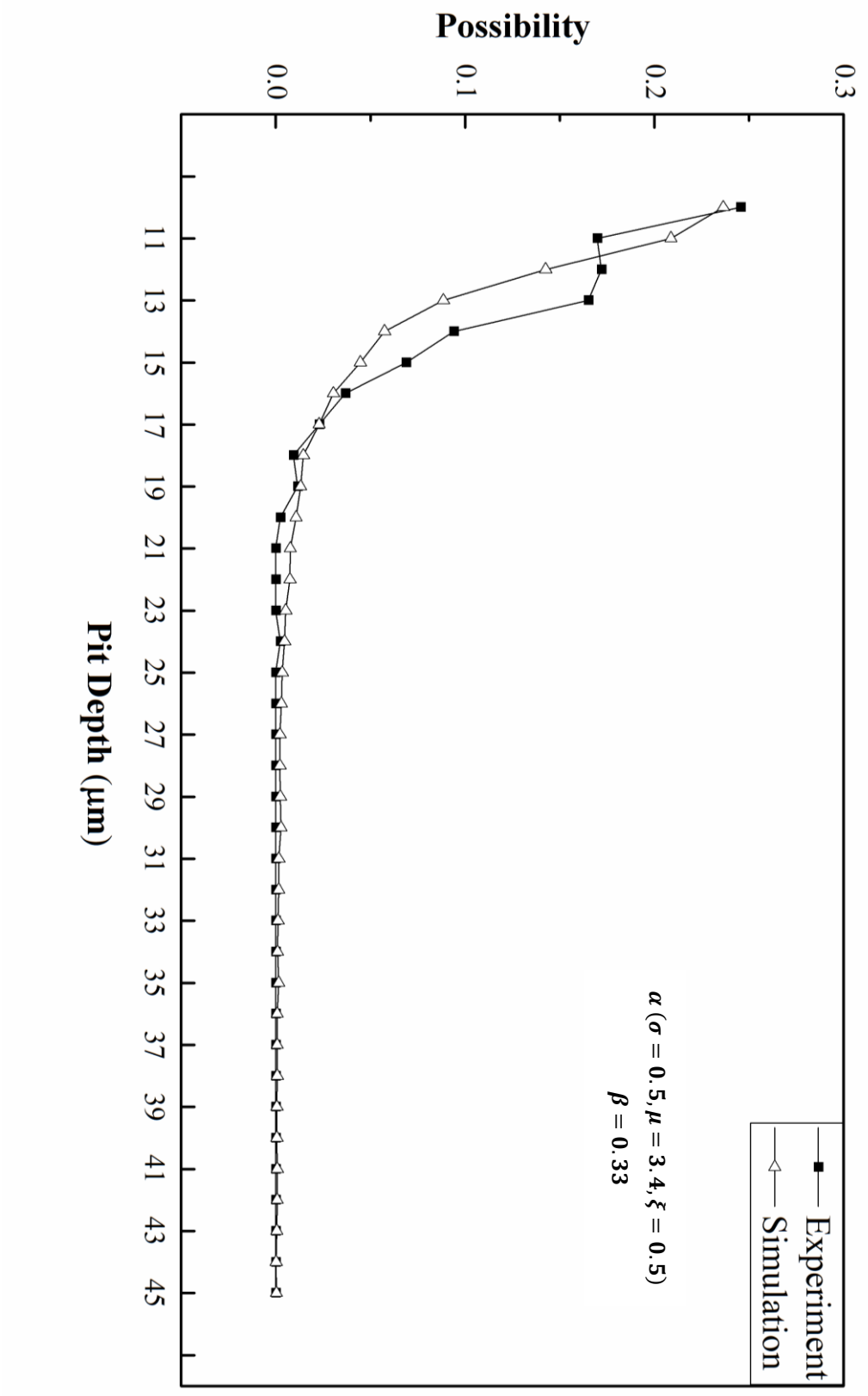

Figure 3-9: Comparison between experiment and simulation pit depth distributions of reinforcing tape of age 38 years [5]

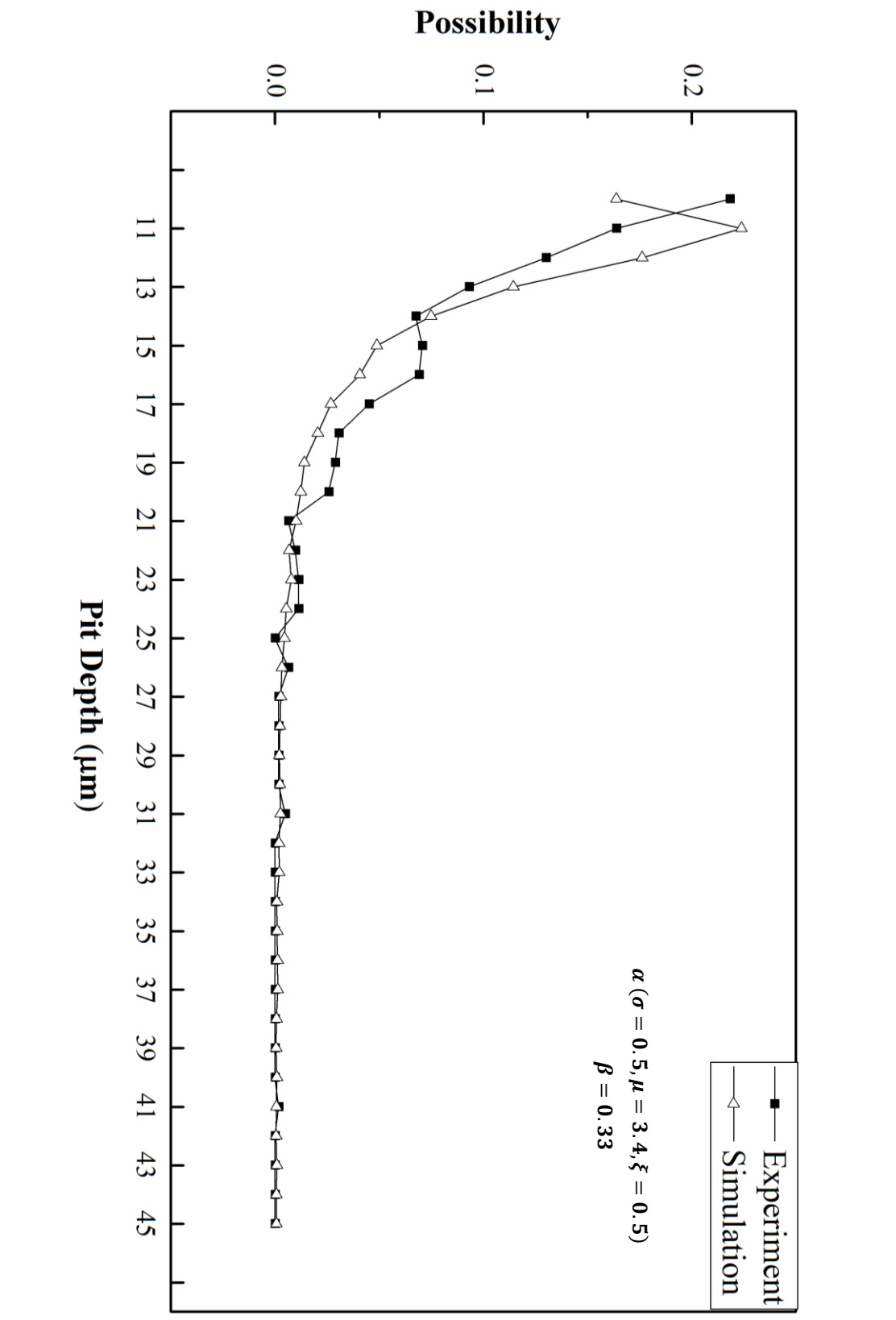

Figure 3-10: Comparison between experiment and simulation pit depth distributions of reinforcing tape of age 44 years [5]

It can be observed from both the figures that there is a relatively high probability for the shallower pits to appear and the probability of occurrence severely decreases with the increased depths of the pits. It can be observed that the difference between the experiment and simulation curves are relatively high at smaller pits compared to the tails of both curves; this is due to the difficulty in measuring shallow pits which normally results in counting errors. Further, the line plot in Figure 3-11 reflected the shifting of the distribution pattern with the progress of the time.

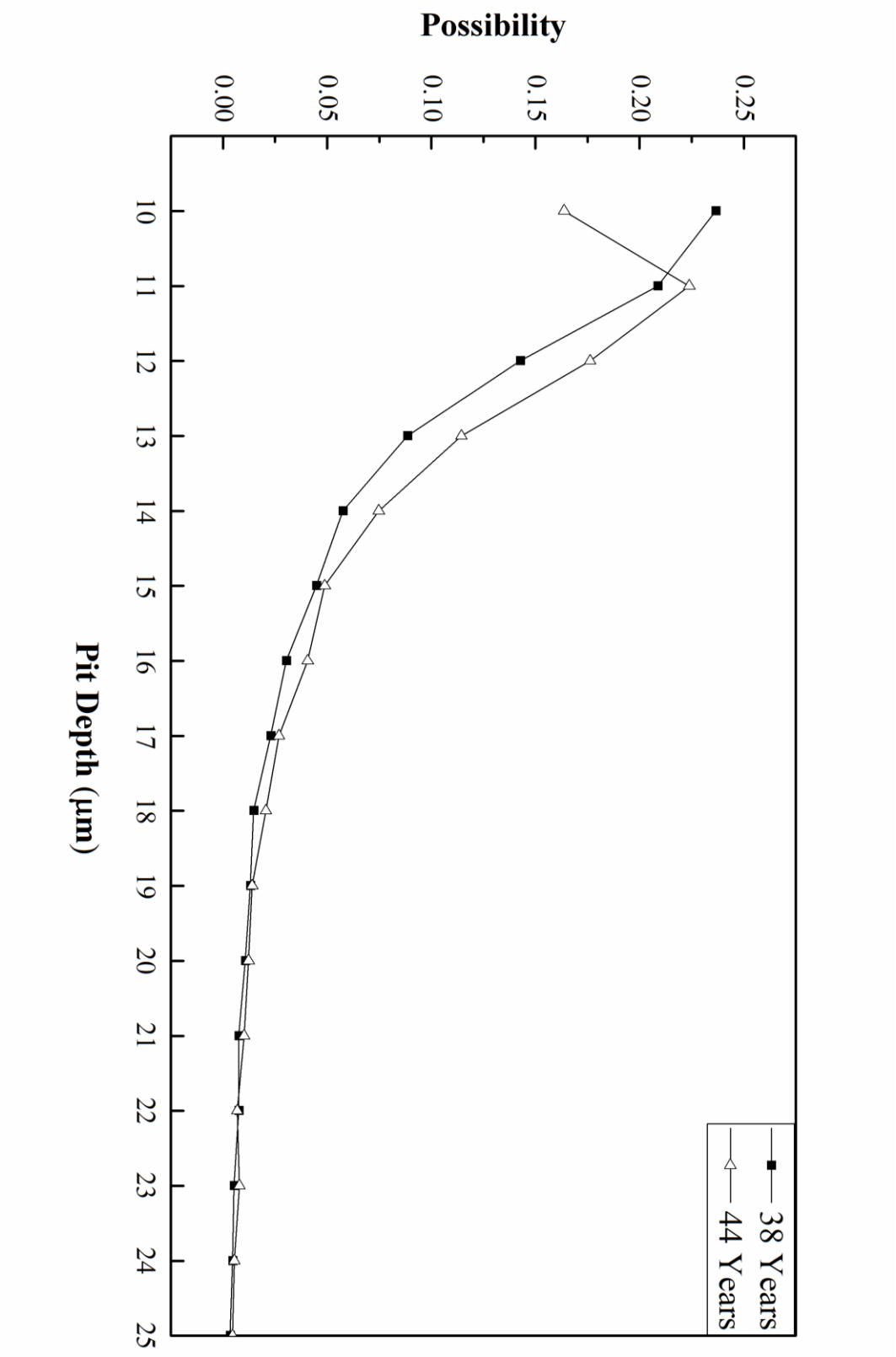

Figure 3-11: Comparison between simulation pit depth distributions of reinforcing tape of both age 38 years and 44 years [5]

In order to capture the growth of pit depth distribution over the time, an analytical mathematical model is developed. The theoretical pit depth distribution at 2-year, 5-year, 10- year, 20-year, 35-year and 50-year time are plotted in Figure 5-12.

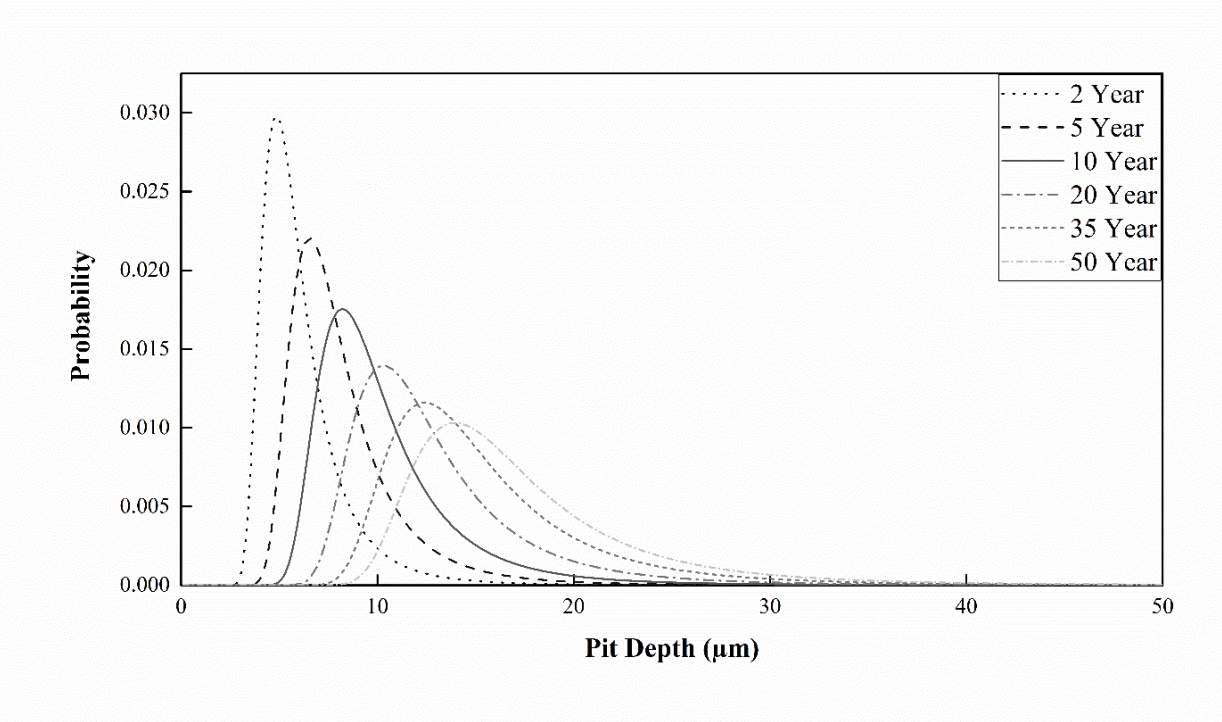

Figure 3-12: Theoretical pit depth distribution with evolution of time [5]

Therefore, we observed that the simple pit growth law in Equation (3-1) is capable of predicting the evolution of pit depth distribution consisted with the experimental observations. This result shows that the three parameters optimized by comparing the pit depth distribution at 38 years can be successfully applied to find the pit depth distribution at 44 years. It proves that the model is able to predict the evolution of pit depth with time.

3.3.4 Pit depth distribution at different environmental conditions

The same methodology is applied to fit the pit depth distributions of the reinforcing tape extracted from different environmental conditions (named as Site 1 to 3).

The change in the environmental condition is incorporated into the present approach by changing only location factor μ and by keeping the other two parameters (scale parameter (σ) and shape parameter (ξ)) as constants for the GEV distribution of α. The value of the two parameters were fixed based on previous calculations (σ = 0.5 and ξ = 0.5). The only changing parameter for optimization of simulation is the location factor μ for which the best value is identified using ANOVA test by comparing experimental and simulated pit depth distributions at different sites.

For Site 1, the parameters for the GEV distribution after fixing σ and ξ are $\sigma = 0.5, \mu = 4.7$ and $\xi = 0.5$ and the comparison between the simulated and experimental pit depth distributions is shown in Figure 3-13.

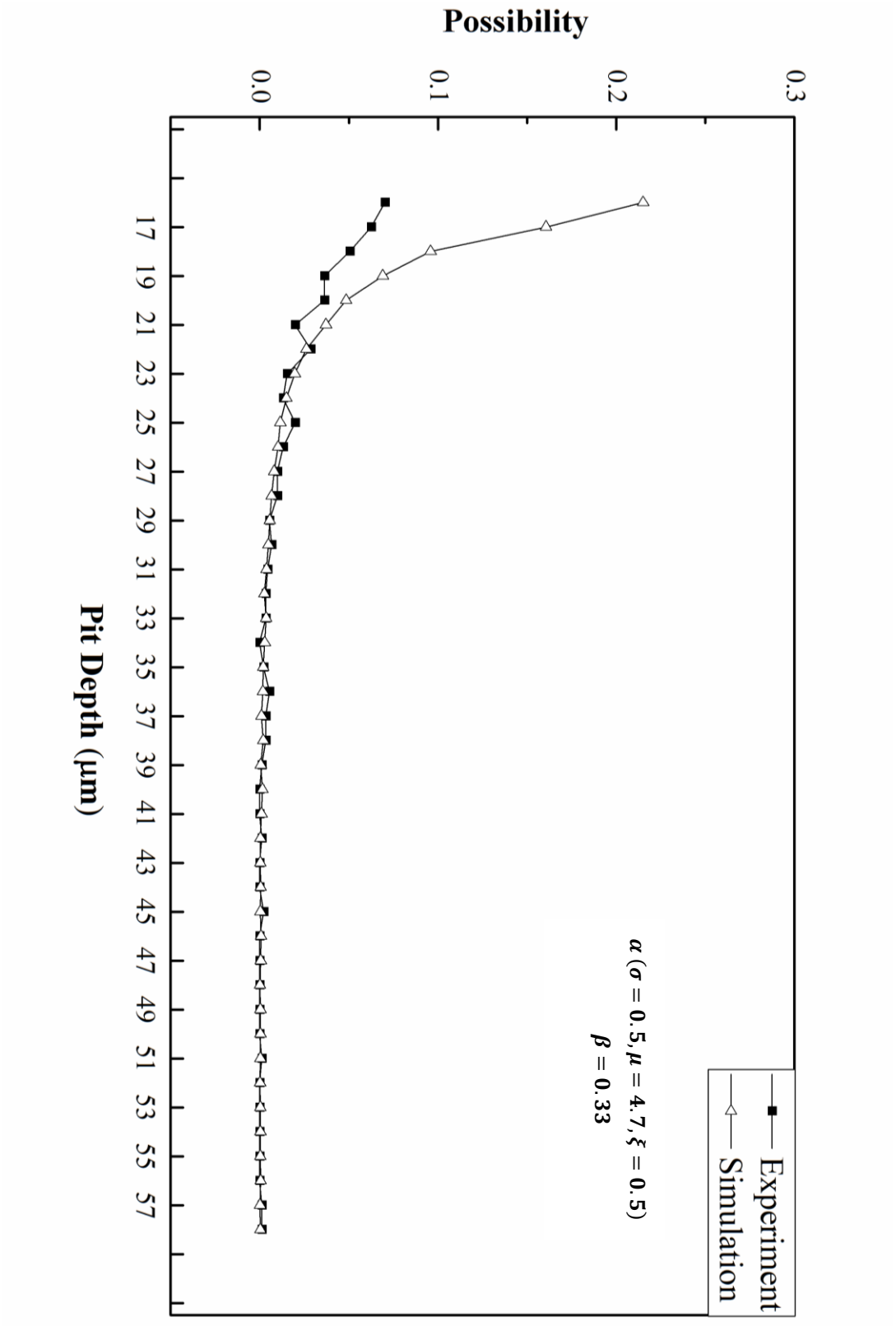

Figure 3-13: Comparison between experiment and simulation pit depth distributions of reinforcing tape of age 43 years (Site 1) [5]

It can be concluded from the Site 1 simulation that a fixed three parameter distribution for α may not be the best choice to fit the pit growth distribution in different environmental conditions. However, by changing only one of the three parameters, which is the location parameter μ, the fitting can achieve an optimum result. This can be explained as follows: the location parameter μ is influenced by multiple environmental factors, most likely the temperature and soil properties.

The same methodology is followed for Site 2, for which the optimized parameters are $\sigma = 0.5, \mu = 5.2$ and $\xi = 0.5$. The comparison between the simulated and experiment pit depth distributions are shown in Figure 3-14.

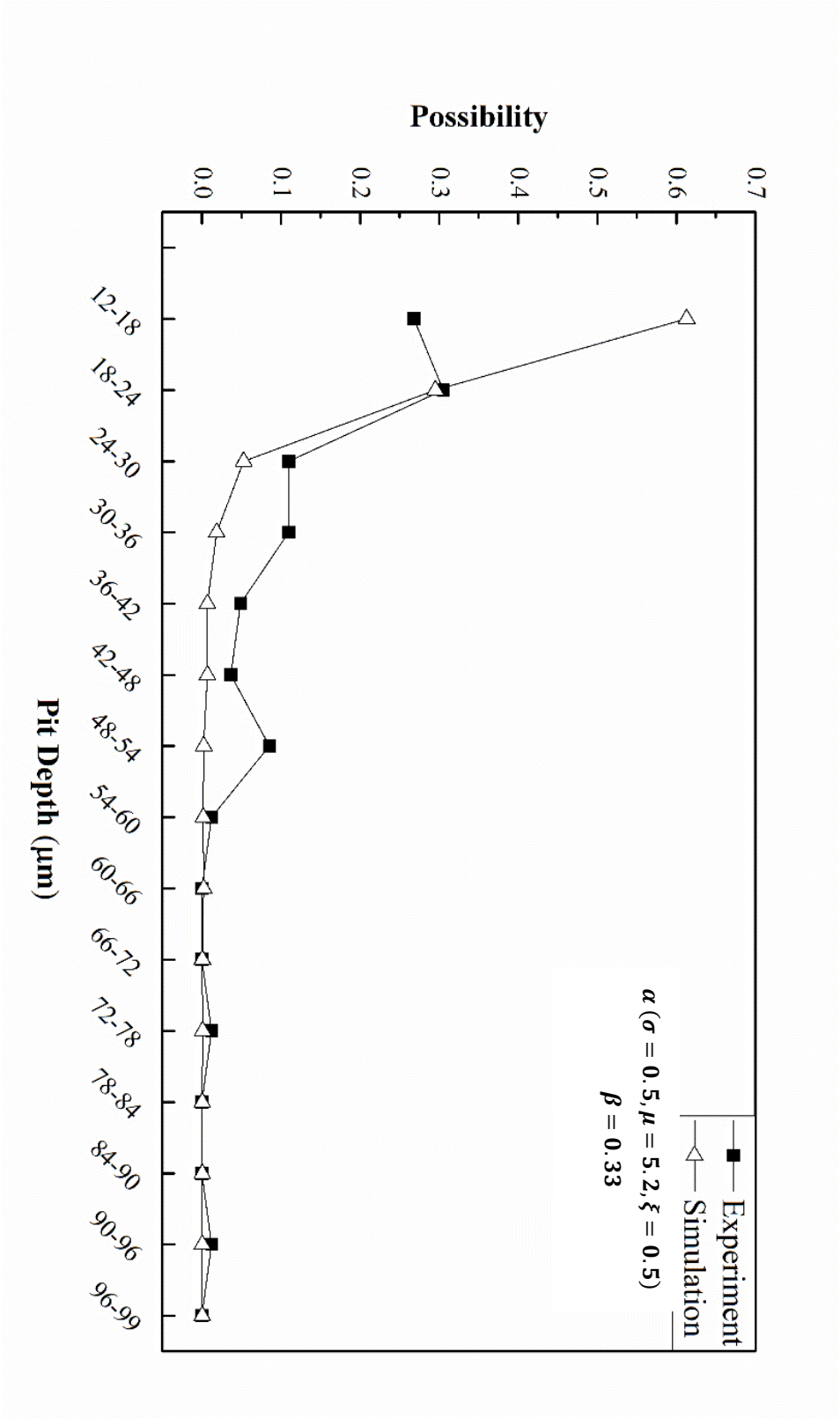

Figure 3-14: Comparison between experiment and simulation pit depth distributions of reinforcing tape of age 28 years (Site 2) [5]

At Site 2, the environmental condition makes the pits grow faster than at the other locations, as can be seen from the deepest pit reaching the range of 90-96 μm. The pit growth equation predicted the high pit growth rate very close to the experimental observation by only changing the parameter μ.

The comparison between the simulated and experimental pit depth distributions at Site 3 is shown in Figure 3-15 and the optimized parameters are $\sigma = 0.5, \mu = 1.9$ and $\xi = 0.5$.

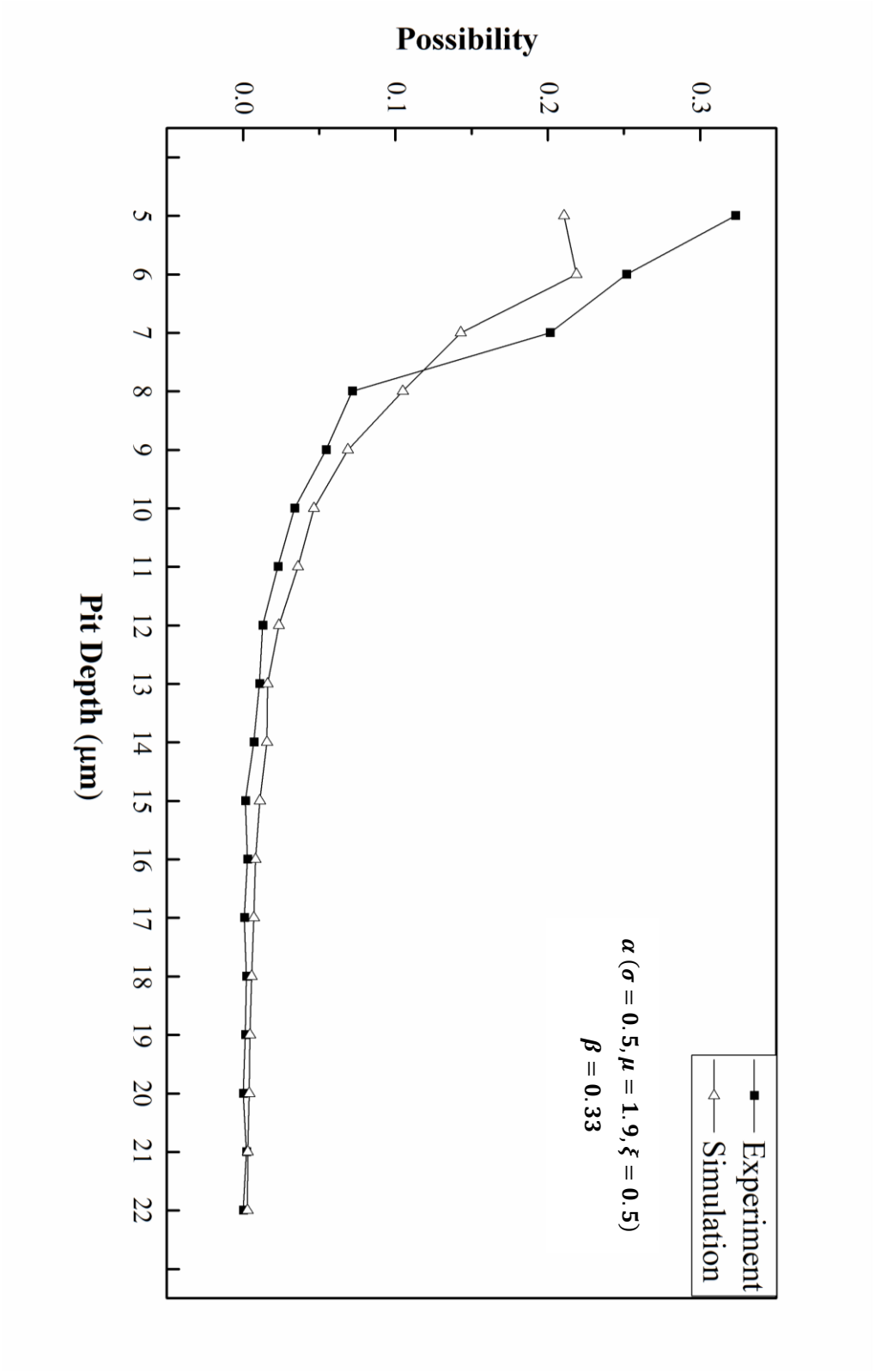

Figure 3-15: Comparison between experiment and simulation pit depth distributions of reinforcing tape of age 41 years (Site 3) [5]

The maximum pit depth measured on tape sample from site 3 is within the 22-23 μm range which is very low compared to other sites and it is well taken care of by the low value of the location factor (μ = 1.9) in the simulation. It can be observed that for smaller pits, unlike the larger pits, the agreement between the experimental results and the simulation results do not match.

From the above simulations in different sites corresponding to different environmental conditions, we can conclude that the power law equation simulated from the three parameter GEV distribution is successful in representing the evolution of pit depth over time and also pit depth in different environmental conditions. Furthermore, the mean of the GEV distribution gives the direct indication of the corrosion level of the environment. Mean pit depth of the reinforcing tape is calculated from the mean of the GEV distribution as

$$y_{mean} = \left(\mu + \sigma \times \frac{\Gamma(1-\xi) - 1}{\xi}\right) \times t^{\beta} \qquad (3-12)$$

From the simulation result already discussed above, the parameter σ is set as 0.5, ξ as 0.5, and β as 0.33. By substituting the values into the model, a specific pit growth model for the mean level of pit depths can be obtained for phosphor bronze material as,

$$y_{mean} = (\mu + \Gamma(0.5) - 1) \times t^{0.33} \qquad (3-13)$$

which gives,

$$y_{mean} = \left(\mu + \sqrt{\pi} - 1\right) \times t^{0.33} \qquad (3-14)$$

where μ is a measure of corrosion factors in different environments, with a close link to humidity, pH level, temperature, pressure, etc. The obtained mean pit depths for the reinforcing tapes at different environmental conditions is given in Table 3-3, indicating the extent of corrosion at the different sites.

Table 3-3: Calculated mean pit depths of the reinforcing tapes at different environments [5]

Time (Years)	$\boldsymbol{\mu}$	$\boldsymbol{y_{mean}}$ $(\boldsymbol{\mu m})$
38	3.4	13.8586
44	3.4	14.5456
43	4.7	18.9333
28	5.6	19.1368
41	1.9	9.1018

The parameter μ value in this chapter is the deterministic value to evaluate the corrosion criticality of the existing cables. The larger the location parameter μ is, the more corrosive the phosphor bronze layer wrapping the cable is. The value of parameter μ also leads to the results of mean pit depths y_{mean}, this provides a more straight forward comparison for the corrosive environment, the higher the mean pit depth is the more corrosive the environment the cable is buried in.

4. Life prediction of phosphor bronze reinforcing tape used in underground power cables: - applying the pit to crack transfer probability

In this chapter, a proposal is made to explain the entire procedure of the corrosion fatigue failure phenomenon. According to the conventional theory, the failure of metal material by corrosion fatigue mechanism is due to the deepest growing pit. The deepest corrosion pit eventually transfers into crack propagation, so that the pit growth speed will then be controlled by the fatigue mechanism. As the pit growth speed controlled by crack propagation is much faster than that of pitting corrosion, this fast propagation speed will lead to the final failure of the material. However, a new phenomenon is observed during this research and from laboratory experimental results. An underground power transmission cable fails due to the failure of the phosphor bronze protection layer, as stated in the previous chapters. The phosphor bronze protection layer has a dimension of 152.4 μm of thickness, which means that for the failure to occur, at a certain spot on the tape, a crack grows until a depth close to this thickness, resulting in the eventual failure. During the experiment on the pit depth scanning and measurement, described in Chapter 2, among all the pits being measured, only within the sample from Site 3 a relatively deep pit was observed which was 96 μm in depth. The rest of the failure cases did not provide very deep pit depth measurement results; for Site 1 on both years of failure cases, the deepest pits were 21 μm and 44 μm respectively. At Site 2 the deepest pit measured was 59 μm. These deepest depths merely reached 40% of the total thickness of the phosphor bronze layer. This was hardly the proof that the deepest pit was the main influential reason for the failure cases.

According to the above described observation, the proposal of ‘corrosion pit to crack propagation transfer probability’ is carried out. The main approach of this proposal is that throughout the entire process of corrosion fatigue on metal materials, at each time

point there is a probability for all depths of pits to transfer into crack propagation resulting in the final failure, but the smaller pits with shallower depths have smaller probability comparing to the larger pits with deeper depths.

This approach to analyse the entire failure process of corrosion fatigue mechanism is discussed in the following sub-sections, from pit initiation to failure, the process follows the sequence mentioned in Figure 2-7.

The objective of the work in this chapter is to develop an accurate model for determining the cable life, based on the corrosion fatigue failure mechanism. Here in this research the tape corrosion fatigue failure process is characterized using Kondo's criteria of pit to crack transition [55, 56] and the parameters of interest are modelled using Monte Carlo simulations. The proposed model is an integrated approach to use existing models with necessary modifications needed to predict the cable failure life of over 40 years old. Further, within this chapter validations are given on testing the hypothesis that the most likely pit-crack transfer may not happen at the largest pit, but at a pit of any size within the reasonable range.

4.1 Model description

In the previous work (Chapter 3), it was demonstrated that the failure mechanism of phosphor bronze reinforcing tapes is corrosion fatigue, based on stress calculation and analysing the morphology of the cracked surfaces [53]. Typical characteristics of corrosion fatigue, such as corrosion pits on tape surface, multi- cracks in association with corrosion pits, and fatigue striation on the fractured face, are found in the failed reinforcing tape (Figure 4-1a & 4-1b).

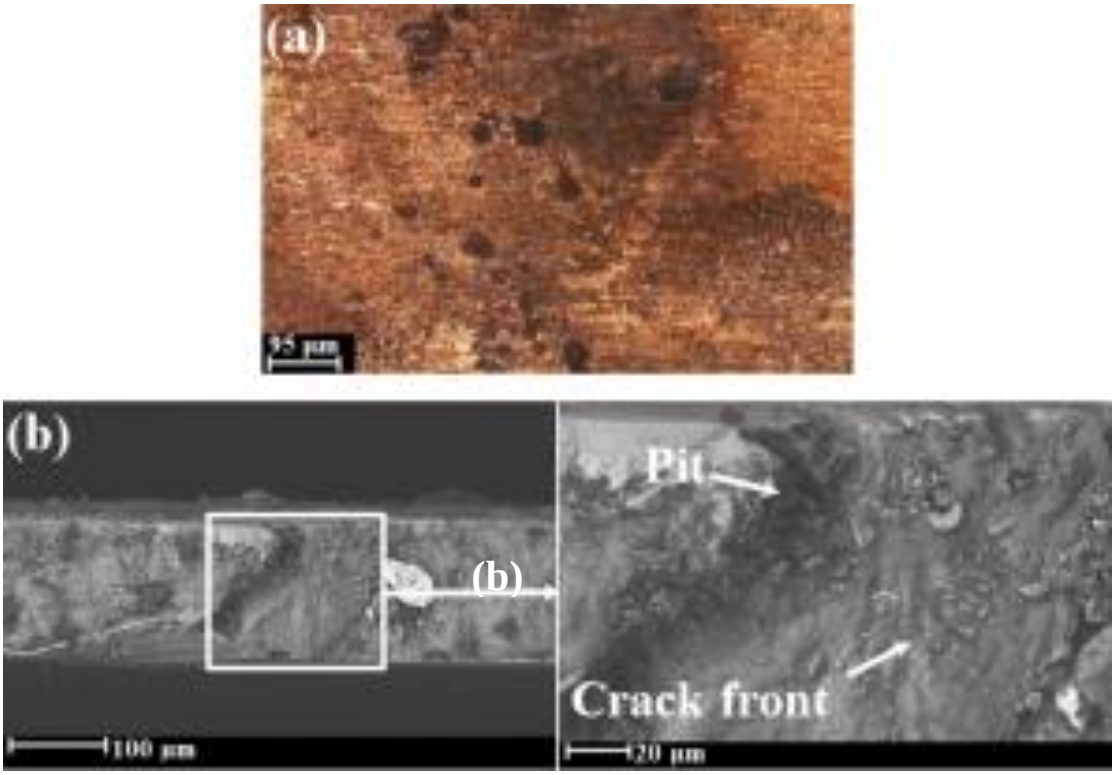

Figure 4-1: (a) 3D optical microscopy image showing pits on the outer surface of the tape (b) SEM image of corrosion fatigue crack starting from a pit [53]. The crack in the cross section shown was normal to the direction of the applied load (longitudinal axis of the tape). [6]

In this work, a probabilistic model similar to the Turnbull model [70, 73] was applied to find the corrosion fatigue life of the tapes. The essential features of modelling pit growth and its transition to crack are described in detail below. The structure of the methodology is shown as a flowchart in Figure 4-2.

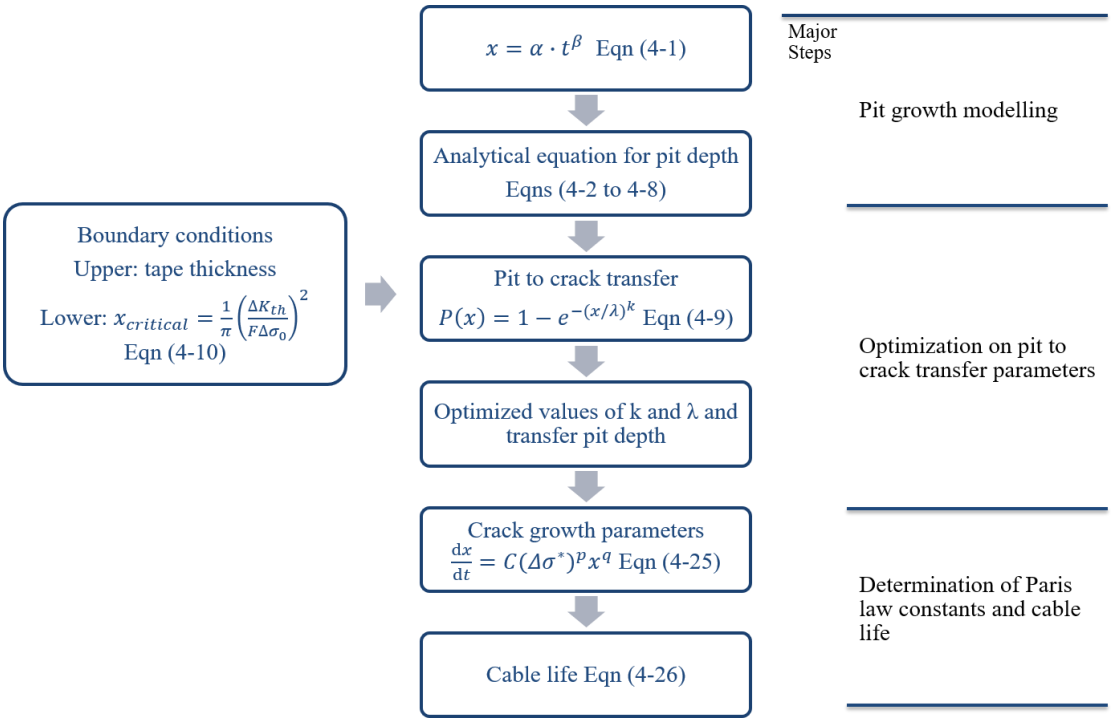

Figure 4-2: Pictorial representation for the structure of the methodology in this chapter [6]

4.1.1 Pit Initiation

The pit initiation is due to the electro-chemical reactions between the components of the metal material and the environment. The exact initiation mechanism is not fully understood and being continuously studied. For example, Soltis [32] provides a summary of existing information on pit initiation. Apart from the initiation theory, the pit initiation rate is another focus, which can be seen in the work of McCafferty [142] and Cavanaugh [143]. However, compared to the total service life of the power transmission cable in [6] and the present study, the pitting initiation time is short enough to be ignored. The pitting initiation will not be considered in the total service life calculation in the study within this chapter. Pitting initiation is considered to be happening in a sudden immediately after the initiation mechanism, the time is considered as to short to impact the servicing life which is as long as decades.

4.1.2 Pitting Corrosion

Pit growth is modelled using the power law and also a pit depth distribution model using analytical equations is developed.

It is important to deduce a general expression for the pit depth distribution through the power law. It is assumed that after initiation, all pits grow continuously. The average growth rate at year t is considered as the pit depth at year t divided by time, i.e., we have:

$$Pit\ growth\ rate = \frac{Pit\ depth\ at\ year\ t}{t} ------(4-2)$$

The probability density function (PDF) of α in Equation (3-1) is known as:

$$GEVPDF = \frac{1}{\sigma} g(x)^{\xi+1} e^{-g(x)} ------(4-3)$$

Where

$$g(x) = \begin{cases} (1 + \left(\frac{x-\mu}{\varphi}\right)\xi)^{-1/\xi} & if\ \xi \neq 0 \\ e^{-(x-\mu)/\varphi} & if\ \xi = 0 \end{cases} ------(4-4)$$

For example, the pit depth distribution at the end of Year 1 is given by:

$$P(x) = \alpha \times t^{\beta} = GEVPDF \times 1^{0.33} = GEVPDF\ of\ \alpha ------(4-5)$$

The above expressions are used to determine the distributions of the annual growth rate for all pits.

In Chapter 3, pit depth distributions for two failure cases at 38 years and 43 years respectively were described successfully by using the Monte Carlo simulation. In this chapter, the mathematical model is developed to calculate the pit depth distribution for tin bronze tape without repeatedly applying the rather time-consuming Monte Carlo simulation.

The concept of pit depth distribution is illustrated with a working example provided. In Figure 4-3, two curves represent the development of pit depth distribution of the same cable.

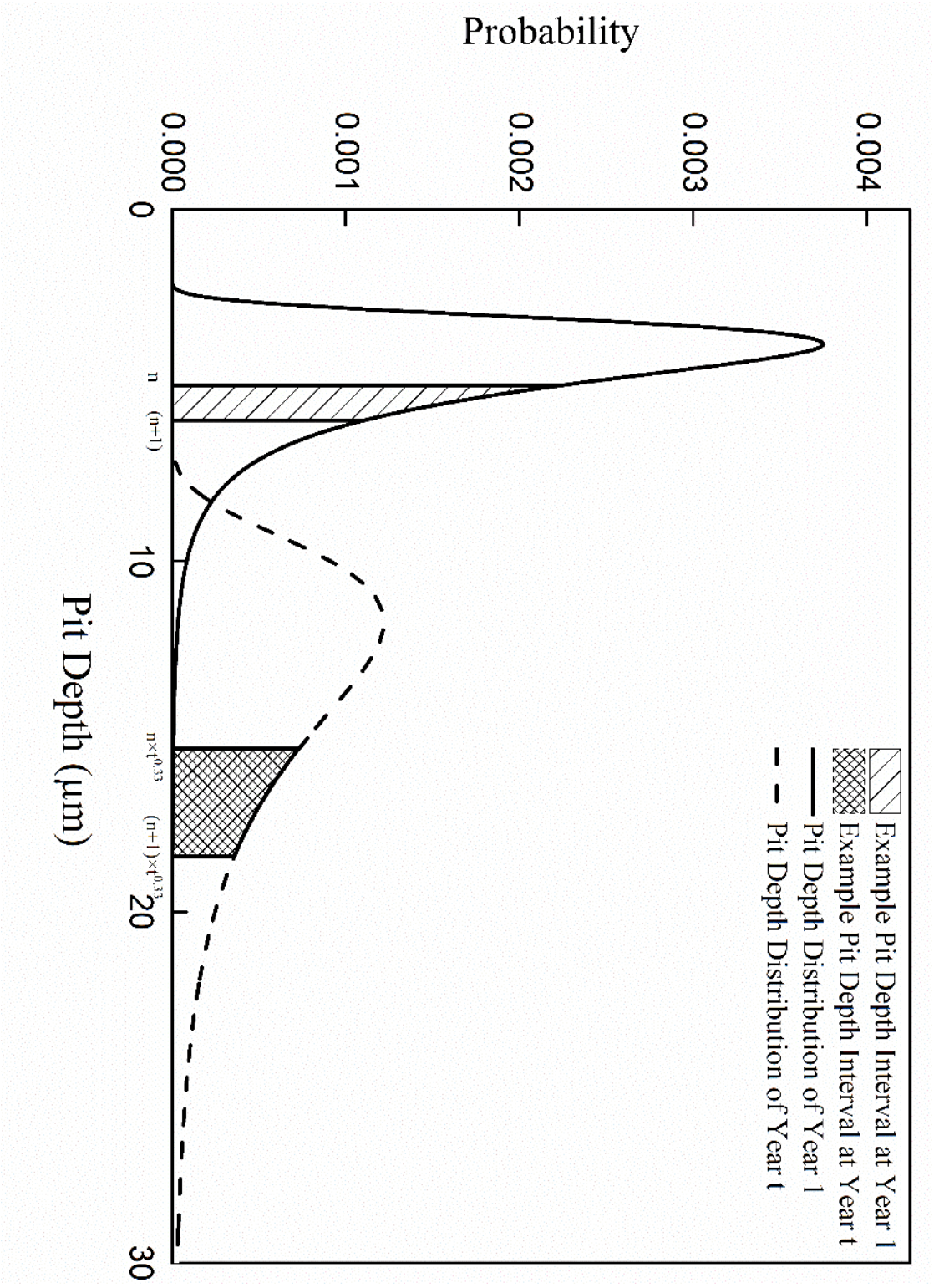

Figure 4-3: Example plot for time related pit depth distribution calculation [6]

The solid curve shows the pit depth distribution at the end of Year 1 and the dotted curve of Year t. Taking an interval of pit depth at Year 1, [n (n+1)] μm, the shadowed area represents the probability of occurrence of the range. At Year *t*, the lower boundary of the range grow to $n \times t^{0.33}\ \mu m$, the upper boundary of the range grow to $(n+1) \times t^{0.33}\ \mu m$, where the new shadowed area represents the probability of occurrence of the development of pit depths. Obviously, the two shadowed intervals take up the same area. This relationship can be repressed by the following equation:

$$\int_{n}^{(n+1)} (GEVPDF\ for\ \alpha)\ dx$$

$$= \int_{n\times t^{0.33}}^{(n+1)\times t^{0.33}} (New\ GEVPDF\ at\ t\ years)\ dx \quad --(4-6)$$

Applying this concept, a matrix can be written representing the probability of occurrence for all pit depth intervals. This matrix is referred to as 'Base Pit Depth Distribution', it represents the probability of occurrence of pits within all 1 μm of interval:

$$Base\ Pit\ Depth\ Distribution = \begin{bmatrix} \int_{0}^{1} (GEVPDF\ for\ \alpha)\ dx \\ \int_{1}^{2} (GEVPDF\ for\ \alpha)\ dx \\ \vdots \\ \int_{d-1}^{d} (GEVPDF\ for\ \alpha)\ dx \\ \int_{d}^{d+1} (GEVPDF\ for\ \alpha)\ dx \end{bmatrix} -----(4-7)$$

Then at any time *t* (years), the pit depth distribution matrix can be further expressed as:

$$Pit\ Depth\ Distribution\ Matrix\ at\ t = \begin{bmatrix} \int_{0/t^{0.33}}^{1/t^{0.33}} (GEVPDF\ for\ \alpha)\ dx \\ \int_{1/t^{0.33}}^{2/t^{0.33}} (GEVPDF\ for\ \alpha)\ dx \\ \vdots \\ \int_{d-1/t^{0.33}}^{d/t^{0.33}} (GEVPDF\ for\ \alpha)\ dx \\ \int_{d/t^{0.33}}^{d+1/t^{0.33}} (GEVPDF\ for\ \alpha)\ dx \end{bmatrix} - (4-8)$$

4.1.3 Fatigue

Fatigue is the weakening of a material caused by repeatedly applied loads. In this research, due to the oil protection being pump through the sheath of the cable, the pressure caused by the pumped oil is of cyclic effect. This leads to the fatigue of the protection phosphor bronze tape. This is especially dangerous when combined with pitting corrosion on the surface of the material, as the initiated corrosion pits provides initial crack mechanism and can be damaged severely in great speed by the fatigue mechanism.

An un-used piece of phosphor bronze tape is regarded of experiencing two major stage after pit initiation on the surface before failure. The first stage being corrosion speed over the crack propagation speed, which means corrosion speed controls, the bronze tape is serviceable but is weakening. The second stage being the crack propagation speed over corrosion speed, which means crack propagation speed controls. At the second stage the crack grows so fast that the time is neglectable on a 150 μm thickness.

The crack propagation model under fatigue in this chapter is a modification of the Paris' Law: $\frac{da}{dN} = C\Delta K^m$. In which a is the crack length, $\frac{da}{dN}$ is the crack growth rate, C and m are material, environment and stress ratio related constants, and Δk represents the stress intensity factor.

4.1.4 Procedure to calculate cable life

The cable life of the bronze tape is defined as the time for a pit to grow to the point of pit-crack transition and is calculated by using all the above equations as shown in a schematic diagram (flowchart). Three stages of the method are explained in detail below.

<u>Stage 1:</u> Determination of pit growth parameter and analytical equation

The pit depth distribution is modelled using the Equation (4-1) and the coefficients of the equations (β and α) are determined by Monte Carlo simulations [4]. The analytical form of the equation is derived using Equations (4-8).

<u>Stage 2:</u> Optimization of pit to crack transfer

Next step is to determine the two parameters which control the pit-crack transfer probability (CDF of Weibull distribution) of the tin bronze material as given in Equation (4-9). A global optimization algorithm is used with the detailed steps provided as follows:

i. A combination of 2 parameters (λ, k) determining the pit-crack transfer probability function is chosen from all the potential combinations. It is convenient to express the pit depth distribution in a matrix format with a 1 μm interval such that

$$Pit - crack\ transfer\ probability\ matrix$$

$$= \begin{bmatrix} \int_0^1 \left(1 - e^{-(x/\lambda)^k}\right) dx \\ \int_1^2 \left(1 - e^{-(x/\lambda)^k}\right) dx \\ \vdots \\ \int_{d-1}^{d} \left(1 - e^{-(x/\lambda)^k}\right) dx \\ \int_d^{d+1} \left(1 - e^{-(x/\lambda)^k}\right) dx \end{bmatrix} - - - (4-9)$$

ii. Pit depth distributions are obtained for each working year using the model described in section 4.1.2.2. As in the steps further on there will be definitions in the algorithm with names including the natural numbers 1 & 2 to avoid confusion in the labelling, all data related to Site 1 mentioned previously in all chapters will be re-named as Location A. Following the same principle, all data related to Site 2 will be re-named as Location B. i.e. from Year 1 to 38 for Location A and Year 1 to 43 for Location B, following the individual three parameters provided in Table 4-1.

Table 4-1: Basic information of samples from Location A and Location B [6]

Sample Label	Year of Failure	Pit Depth Distribution Parameter
Location A	38	φ = 0.5, μ = 3.4, k = 0.5
Location B	43	φ = 0.5, μ = 4.7, k = 0.5

iii. For the pit depth distribution of each working year, the pit depth distribution matrix at t (Equation (4-8)) is multiplied with the pit-crack transfer probability matrix in stage 1. The products of the two equations are named as 'Failure Likelihood'. Within this stage, a discriminant condition is applied from assumptions made in

section 4.1.4. For all the 'Failure Likelihood' calculations, only the results for the pits deeper than the minimum threshold pit depth of transfer are considered.

iv. For Location A, multiplying the probability matrix of each potential pit-crack transfer by the pit depth distribution Matrix at Year t_1 $(1 \leq t_1 \leq 38)$, creates a 'Failure Likelihood' consisting of 150 elements, representing pit depths intervals from [0 1] μm to [149 150] μm. The largest element is considered as 'Maximum Failure Likelihood Location A' under one potential pit-crack transfer probability function. Again the largest element among these 38 is the 'Maximum Failure Likelihood 2 Location A' of this function. For Location B, under the same potential pit-crack transfer function, except for the fact that there are 43 'Maximum Failure Likelihood 1 Location B' elements, because $1 \leq t_1 \leq 43$. The 'Maximum Failure Likelihood 2 Location B' is obtained in the same method.

v. With each potential pit-crack transfer function, a summation of the 'Maximum Failure Likelihood 2' is made:

$$\begin{aligned} &Sum\ Maximum\ Likelihood\ 2 \\ &\quad = Maximum\ Likelihood\ 2\ Location\ 1 \\ &\quad + Maximum\ Likelihood\ Location\ 2 - (4 - 10) \end{aligned}$$

Which means that with all potential functions, there are equal numbers of 'Sum Maximum Likelihood 2'. The largest value among them is the final result of the optimization. The corresponding transfer pit depths, year of transfer (t_1 and t_2), as well as the pit-crack transfer function are also the outcome of this analysis.

<u>Stage 3:</u> Determination of crack growth parameters (Paris law constants) and cable life

The transfer pit depth can be further used to determine parameters in Paris' Law and

also to establish a life prediction model for the power transmission cables.

The relationship between the pitting corrosion growth rate and the crack propagation growth rate can be established as:

$$Pitting\ corrsoion\ growth\ rate = V_p(x)$$
$$= Crack\ propagation\ growth\ rate$$
$$= V_c(x) - - - (4-11)$$

This leads to the expression of:

$$\frac{Transfer\ pit\ depth}{Year\ of\ transfer} = C(\Delta k)^m = - - - - - (4-12)$$

where C and m are Paris Law constants. The above equation is used to calculate the cable life for given Paris law constants.

4.2 Results and discussions

The pit depth distribution of the reinforcing tape is the starting point to calculate the life of the power cable. First the simulated pit depth distribution is modelled with an analytical equation and used to calculate the pit to crack transfer probability. Then, Paris constants are calculated to predict the cable life.

4.2.1 Results for pit growth modelling

Pit depth distribution is modelled using the power law (Equation (4-1)) as detailed in our previous work [4] using Monte Carlo simulations. The analytical equation for the pit depth distribution is derived using Equation (4-8).

To validate the analytical method, data from a working cable is used for comparison

between the mathematical analytical pit depth distribution model and the Monte Carlo simulation method. Shown in Figure 4-4, the red curves represent the Monte Carlo method, the blue curves represent the analytical pit depth distribution equation. Under the simulation of 100 pits, which is a relatively small number, both models appear to have a similar shape, but still with some differences. When increasing the simulation pit number to 1 million, as shown in Figure 4-5, there is basically no difference observed between the two models, which proves the validity of the model.

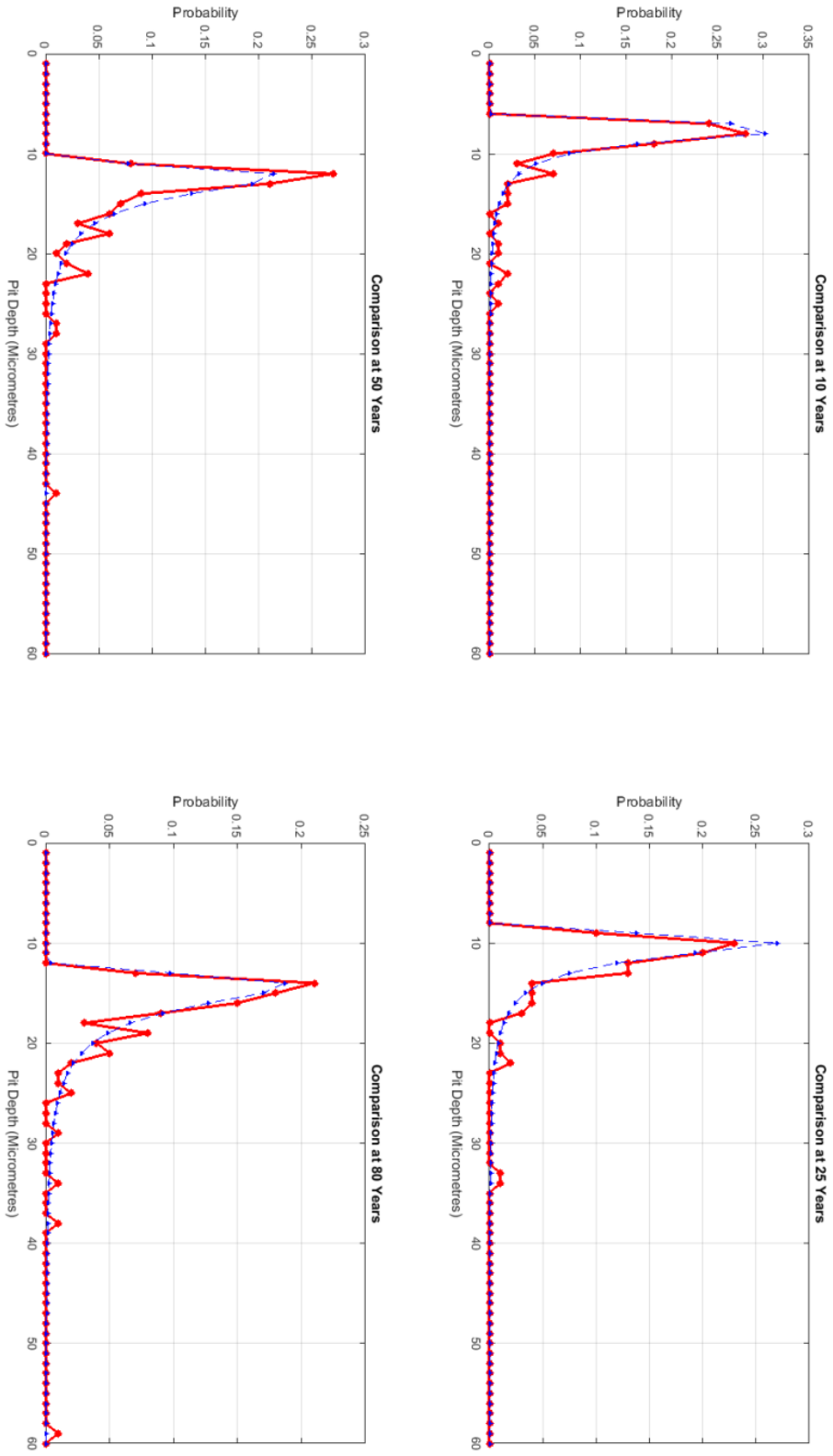

Figure 4-4: The theoretical pit depth distribution with time model compared to the Monte Carlo simulation pit depth distribution model with an initial pit number of 100 [6]

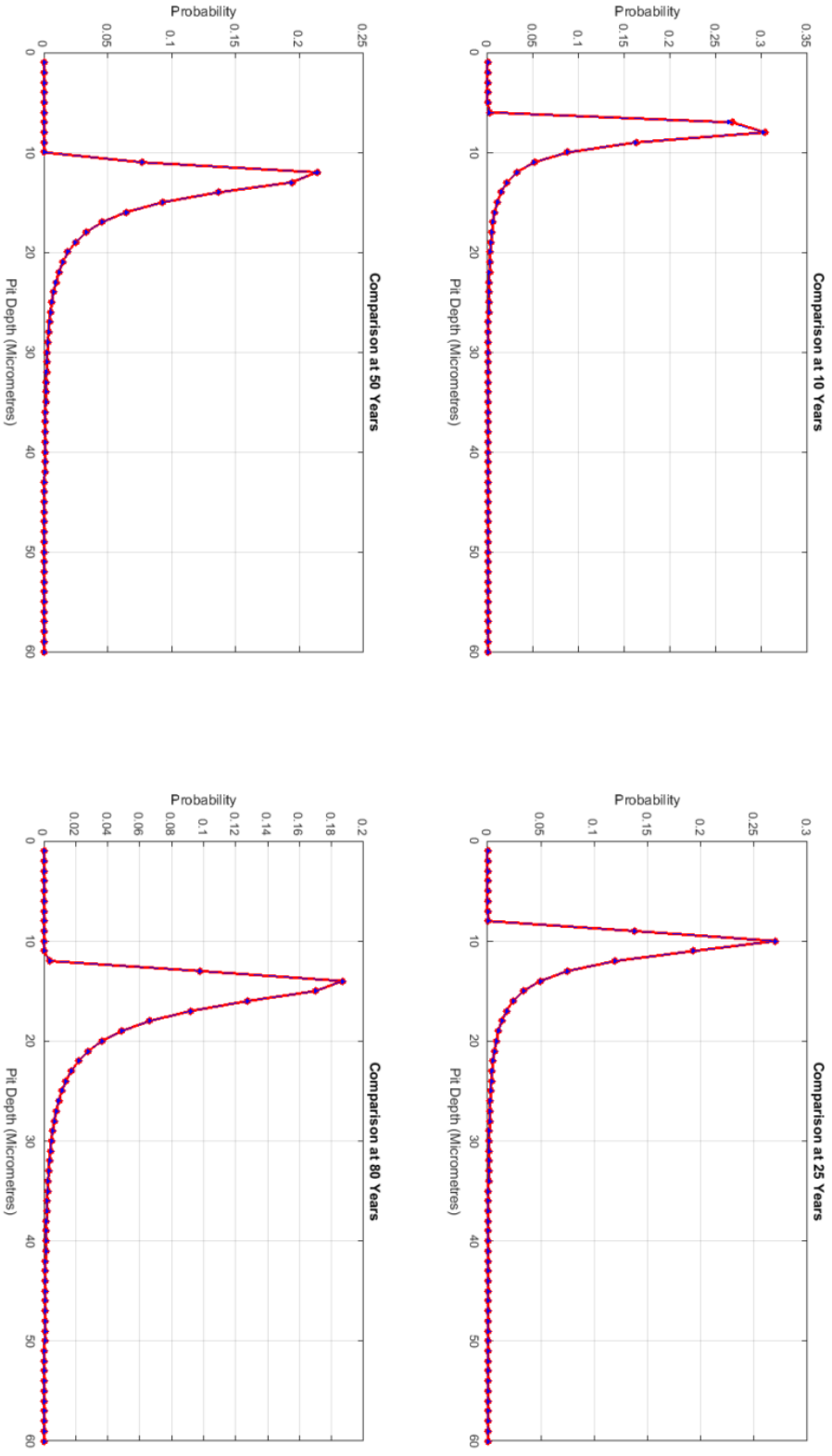

Figure 4-5: The theoretical pit depth distribution with time model compared to the Monte Carlo simulation pit depth distribution model with an initial pit number of 1 million [6]

4.2.2 Results for pit to crack transfer

A relationship between the pit growth speed and the crack propagation speed is shown in Figure 4-6. Pit to crack transfer is calculated using Equation (4-9).

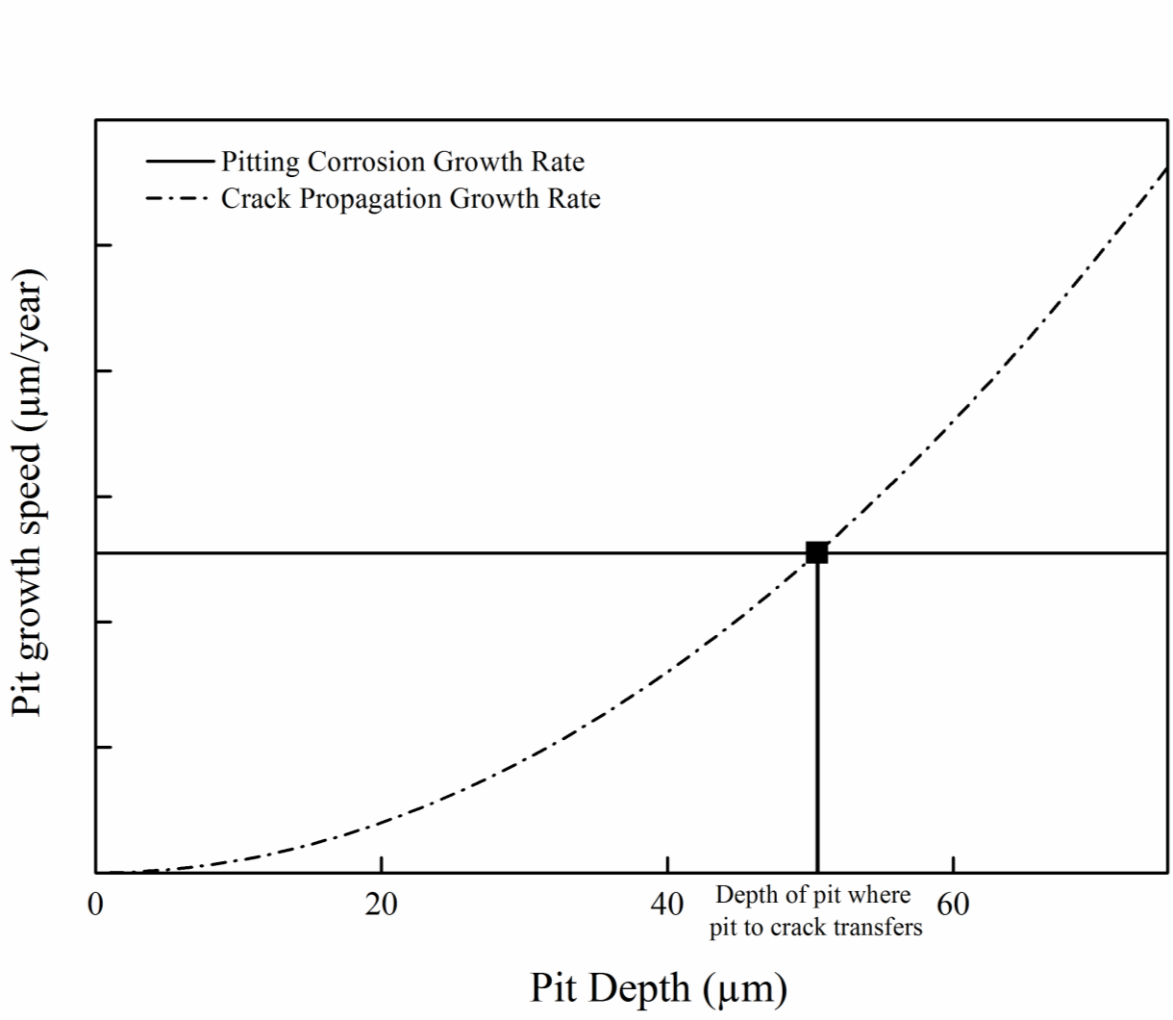

Figure 4-6: Two stages of failure case where pitting corrosion transfers into crack propagation [6]

An optimization procedure is carried out to calculate the two parameters (λ and k) used in the equation. The boundary condition is required to do the simulation and the derived parameters are explained below.

4.2.2.1 Boundary conditions for pit-crack transfer probability function

The thickness of the tin bronze tape is 150 μm. A pit depth of 150 μm is therefore the maximum limit. Moreover, any transfer function (Weibull CDF) reaching 100% when pit depth $x < 150\mu m$ is considered as invalid. This is regarded as the upper boundary of the transfer function. The lower boundary of the transfer function is determined by the threshold pit depth for both locations. As previously mentioned in Section 3.1.3, the only unknown information is the threshold of the stress intensity factor. However, according to Kunz and Collini [144], there are results obtained for threshold stress intensity factors of coarse grain (CG) copper and Annealed CG copper. The results rely on the R-ratio, which is the ratio of the minimum value of cyclic stress and the maximum value of the cyclic stress. In the case of Location A, $R_1 = 0.9856$ and for Location B, $R_2 = 0.9719$. For the results of these two *R*-ratios, it can be estimated that the threshold intensity factor can be as low as 1.5 $MPa\sqrt{m}$. Applying this threshold intensity factor value to Equation (3-10), it is estimated that the initial threshold pit depth for Location A is 35 μm and the threshold pit depth for Location B is 60 μm. These two values are used to select the valid (λ, k) combinations from all initial choices of λ and k combinations. A representative curve of pit-crack transfer probability is shown in Figure 4-7.

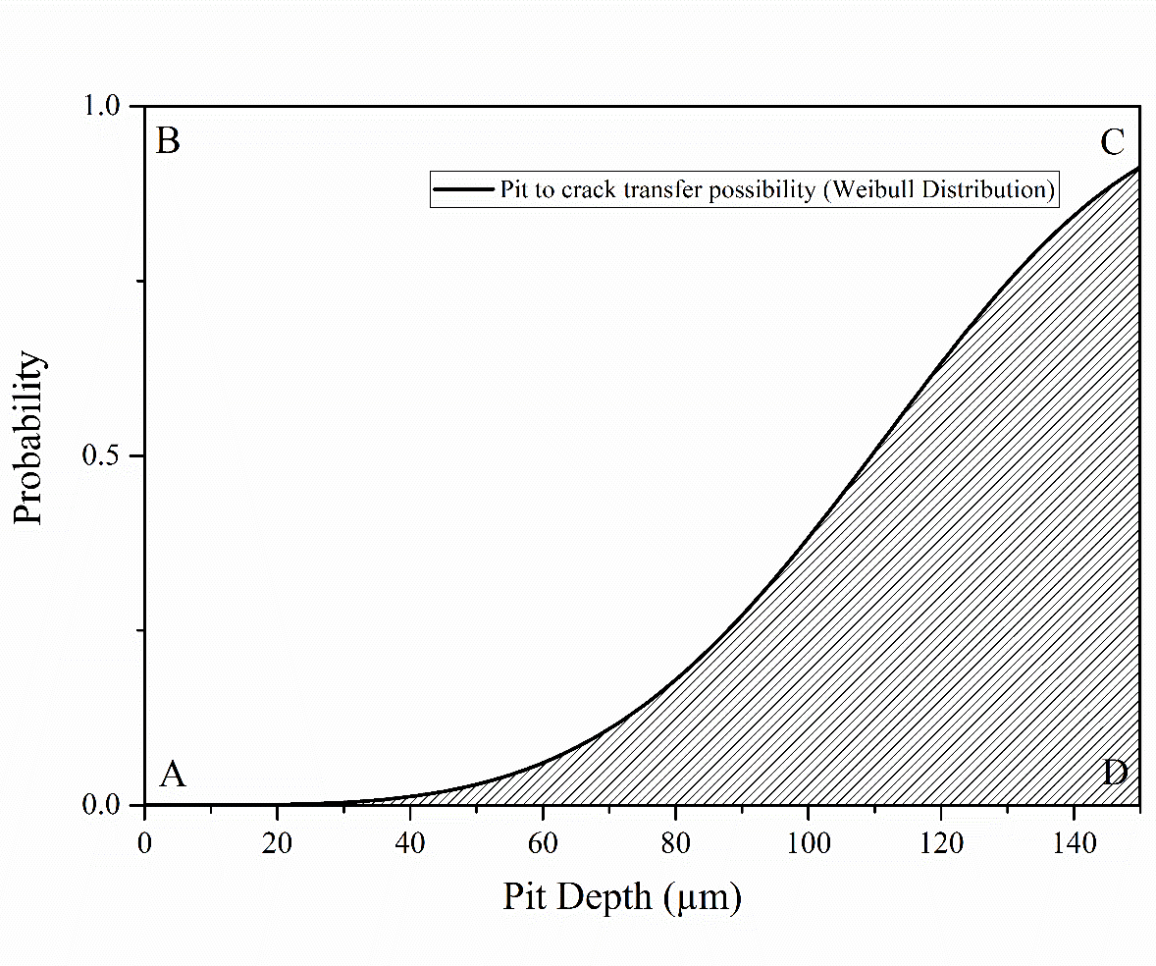

Figure 4-7: A representative curve among all the potential pit to crack transfer probability functions (cumulative distribution function of the Weibull distribution) [6]

The application of the above boundary conditions is considered as a pre-selection step with the purpose to accelerate the optimization. Without this step, the number of equations that are involved in optimization can be observed from Figure 4-8.

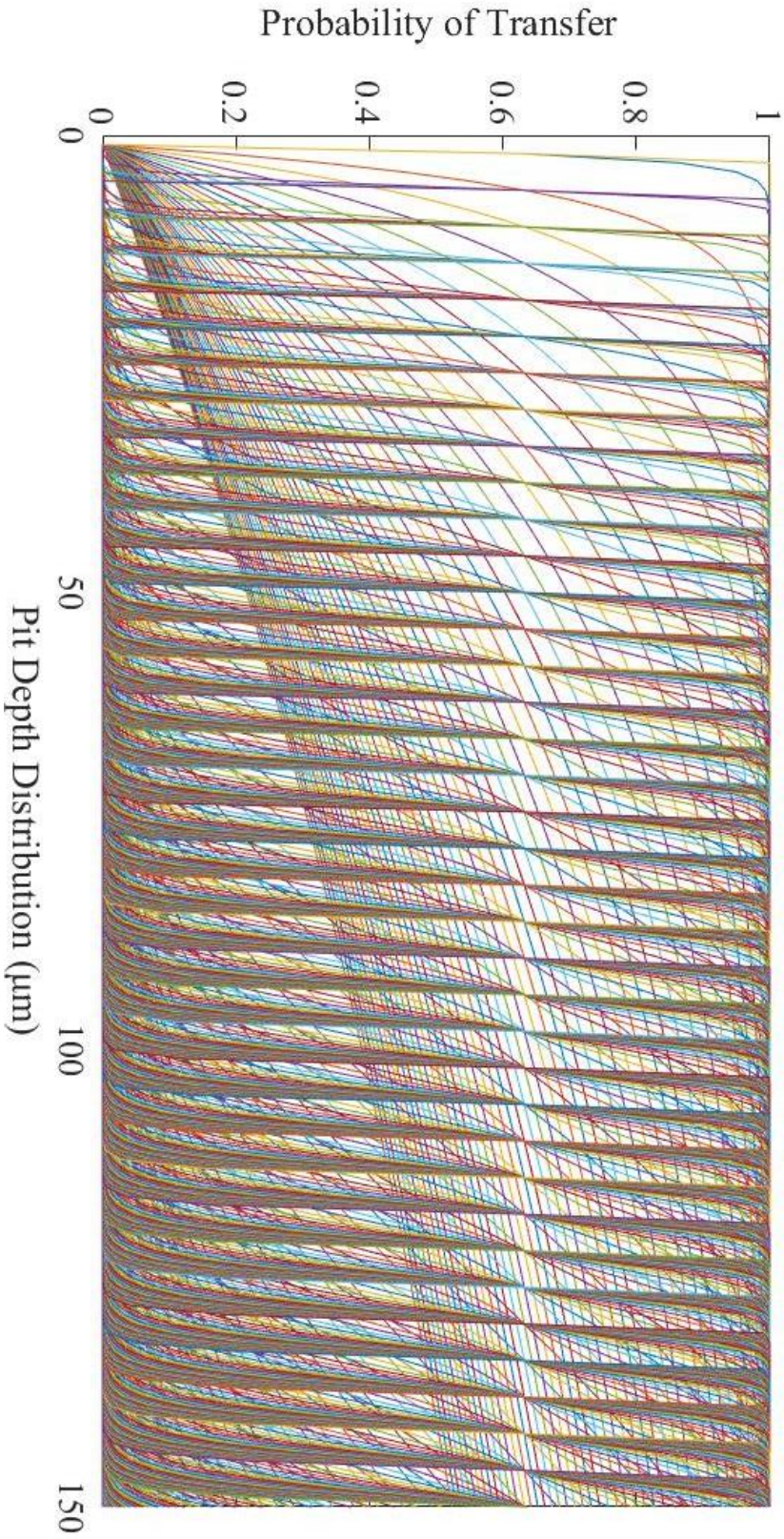

Figure 4-8: Potential pit to crack transfer probability functions represented in Weibull CDF plots [6]

To describe the boundary conditions in more detail, two conditions have to be fulfilled regarding the threshold pit depths for two locations:

1. The probability of transfer is 0 at a pit depth of 35 μm.

2. The probability of transfer is larger than 0 starting from pit depth of 60 μm. A range of the potential pit to crack transfer curves can be seen in Figure 4-9.

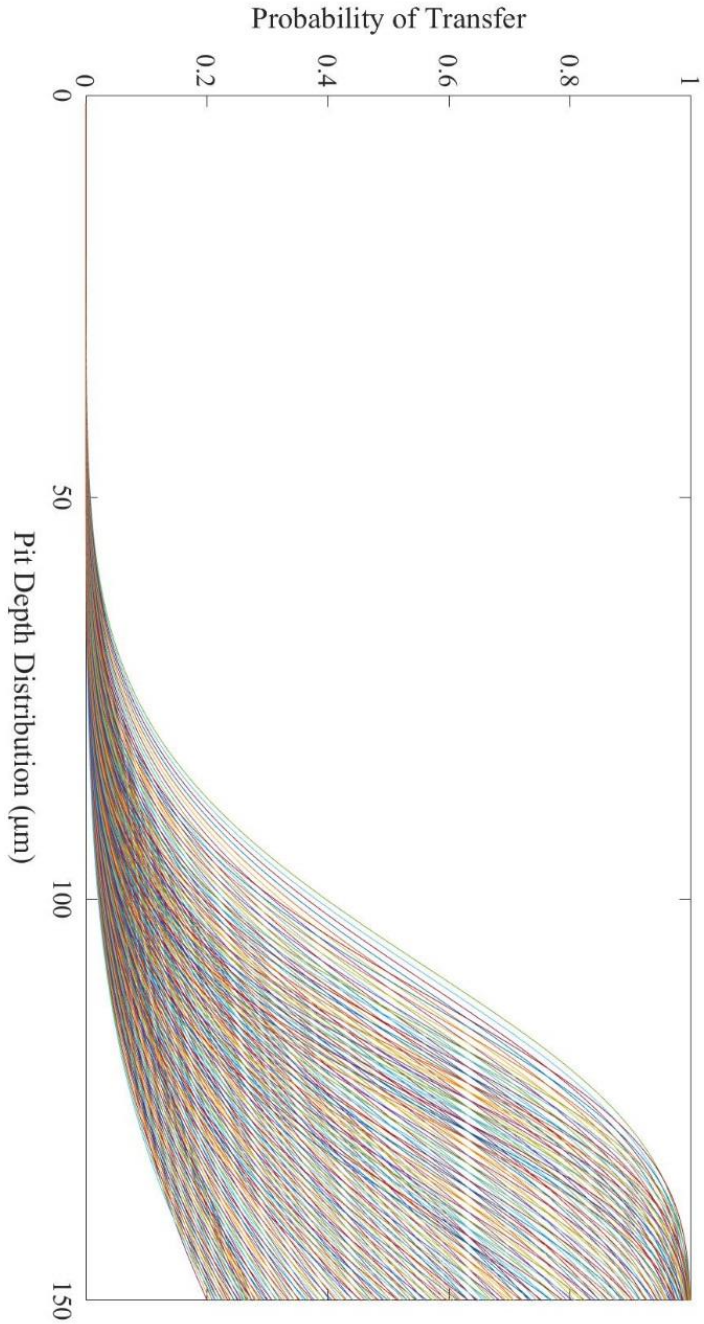

Figure 4-9: Possible transfer curves [6]

The above simulation requires a large number of calculations as the approach of the algorithm is simply universal optimization. During the process to obtain results of this chapter, coding skills to speed up the calculation are applied. It is calculated by parallel programming with the assistance of the High Performance Computing (HPC) ALICE from the University of Leicester. This speed up can be seen in the code provided related to this chapter of research in Appendix III.

4.2.2.2 Parameters (λ, k) for pit-crack transfer probability function

From section 4.1.5, one of the final results of the optimization algorithm is the identification of parameters (λ, k) in the transfer function. With the current data, the simulation result is $(\lambda, k) = (109.3, 6.1)$. A plot of the determined transfer function using these two parameters is shown in Figure 4-10.

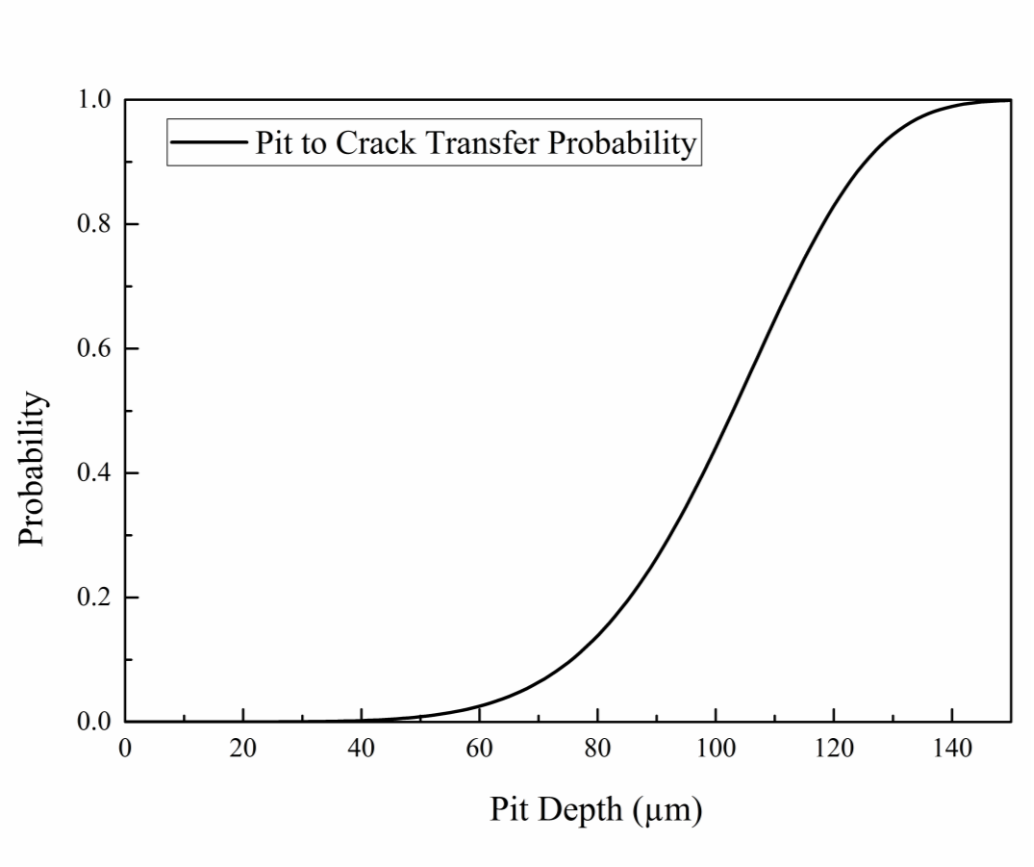

Figure 4-10: Determined pit to crack transfer probability function plot [6]

The mathematical expression for this pit-crack transfer probability function is therefore given by:

$$P(x) = 1 - e^{-(x/109.3)^{6.1}} \quad - - - - - - - (4-19)$$

The transfer pit depth for cables at Location A is 113 μm and the transfer pit depth for cables at Location B is 111 μm.

4.2.3 Determination of crack growth (Paris Law) parameters

With the simulation results mentioned above, the relationships between the pitting corrosion growth rate and the crack propagation growth rate can be established according to a general expression given in equation (4-18). The shape factor Y was

taken as 1 to be on the safe side. By the nature of Paris' Law, it can be assumed that $p = 2q$, which gives the parameters of the modified Paris' Law as: $C = 0.108, p = 0.453, q = 0.226$.

This gives the final expression of Paris' Law as:

$$V_c(x) = 0.108 \times (\sigma_{mean} + \Delta\sigma)^{0.453} \times {x_{transfer}}^{0.226} - -(4-20)$$

In this expression the pit depth is given in the unit of μm, time in the unit of years, and stress in the unit of MPa.

4.2.4 Cable life prediction

The above key parameters such as pit growth parameters, pit to crack parameters and transfer depth are critical to life prediction of power transmission cables. To calculate the service life of any working cable, the first step is to simulate the pit depth distribution on the surface of tin bronze tape by the method developed in [6]. The result is a combination of three parameters $(\sigma_{sample}, \mu_{sample}, k_{sample})$ which governs the GEV distribution. In the second step, upon obtaining the three governing parameters, a pit depth distribution of any year can be obtained using the model described in section 4.1.2. In the third step, multiplying the pit depth distribution with the determined pit-crack transfer function, the transfer pit depth of the sample can be obtained, naming it $x_{transfer}$. From Equation (4-20), the cable life prediction function can be written as:

$$t_{cable} = \frac{{x_{transfer}}^{0.774}}{0.108 \times (\sigma_{mean} + \Delta\sigma)^{0.453}} - - - -(4-21)$$

4.2.5 Validation of life prediction model on existing circuit

The life prediction model is applied to 10 existing cables to validate the accuracy of prediction. In Table 4-2, the key parameters for determining pit depth distribution are given, which from the previous results, are a variety of location parameters μ for the

GEV distribution. With the location parameters μ, the corresponding pit-crack transfer pit depths are also given in Table 4-2.

Table 4-2: Location parameter μ for cables and corresponding transfer pit depths [6]

Location	**Pit depth distribution parameters**	**Transfer pit depth (μm)**
Location 1	φ = 0.5, μ = 3.0, k = 0.5	114
Location 2	φ = 0.5, μ = 2.2, k = 0.5	115
Location 3	φ = 0.5, μ = 1.0, k = 0.5	115
Location 4	φ = 0.5, μ = 3.0, k = 0.5	114
Location 5	φ = 0.5, μ = 2.8, k = 0.5	114
Location 6	φ = 0.5, μ = 1.8, k = 0.5	115
Location 7	φ = 0.5, μ = 1.0, k = 0.5	115
Location 8	φ = 0.5, μ = 1.0, k = 0.5	115
Location 9	φ = 0.5, μ = 1.0, k = 0.5	115
Location 10	φ = 0.5, μ = 2.0, k = 0.5	115

It can be observed from Table 4-2 that the transfer pit depth are within a small range, from 114 μm to 115 μm. This may show that for the specific material – the phosphor bronze, it is the property of the material that the crack propagation starts to dominate at this depth after corrosion pitting initiated and grow to this depth. The evidence of this assumption shall be further evaluated through laboratory work.

The prediction years can be interpreted as a relative failure probability comparing to the solid failure cases. According to this concept, for the different cable sections shown in Figure 4-11 to Figure 4-20 it is possible to consider the failure probabilities relative to the failed section probabilities. The closer a prediction year of certain section is to the failed section, the higher probability of failure this specific section has. From Figure 4-

11 to Figure 4-20, the prediction year at which $P_{failure} = P_{failure\ at\ calibration}$ of cable sections are shown in the scatter plot format for all 10 locations. The cable data were referenced to the current year of 2017. A few known conditions of the cable sections are taken for the validation of the proposed life prediction model:

- Section 46 of Location 1 was known to be corroded; according to the model the predicted year is 2012, which falls below the referencing line of 2017. See Figure 4-11.
- Section 46 and Section 61 of Location 2 were decommissioned, the predicted years are 2015 and 2009; Section 65 of Location 2 were known failure, the predicted year is 2009, which falls below the referencing line of 2017. See Figure 4-12.
- Section 93 of Location 4 was decommissioned, the predicted year is 2015, which falls below the referencing line of 2017. See Figure 4-14.
- Section 176 of Location 5 was known failure, the predicted year is 2016, which falls below the referencing line of 2017. See Figure 4-15.
- Section 108 of Location 6 was known corroded, the predicted year is 2014, which falls below the referencing line of 2017. See Figure 4-16.
- Section 2 and Section 54 of Location 7 were known to be corroded, the predicted years for the two sections are 2011 and 2010, which falls below the referencing line of 2017. See Figure 4-17.

From the above information, the results can be considered as providing relatively accurate predictions with 'positive error'. One would want the model to predict failures when there are failures and should not predict success when there are failures. Such a 'positive error' is tolerable from a safety point of view. However, if the model predicts failure and no failure has occurred, then the negative error can be expensive because of unnecessary repairs, but it is not unsafe.

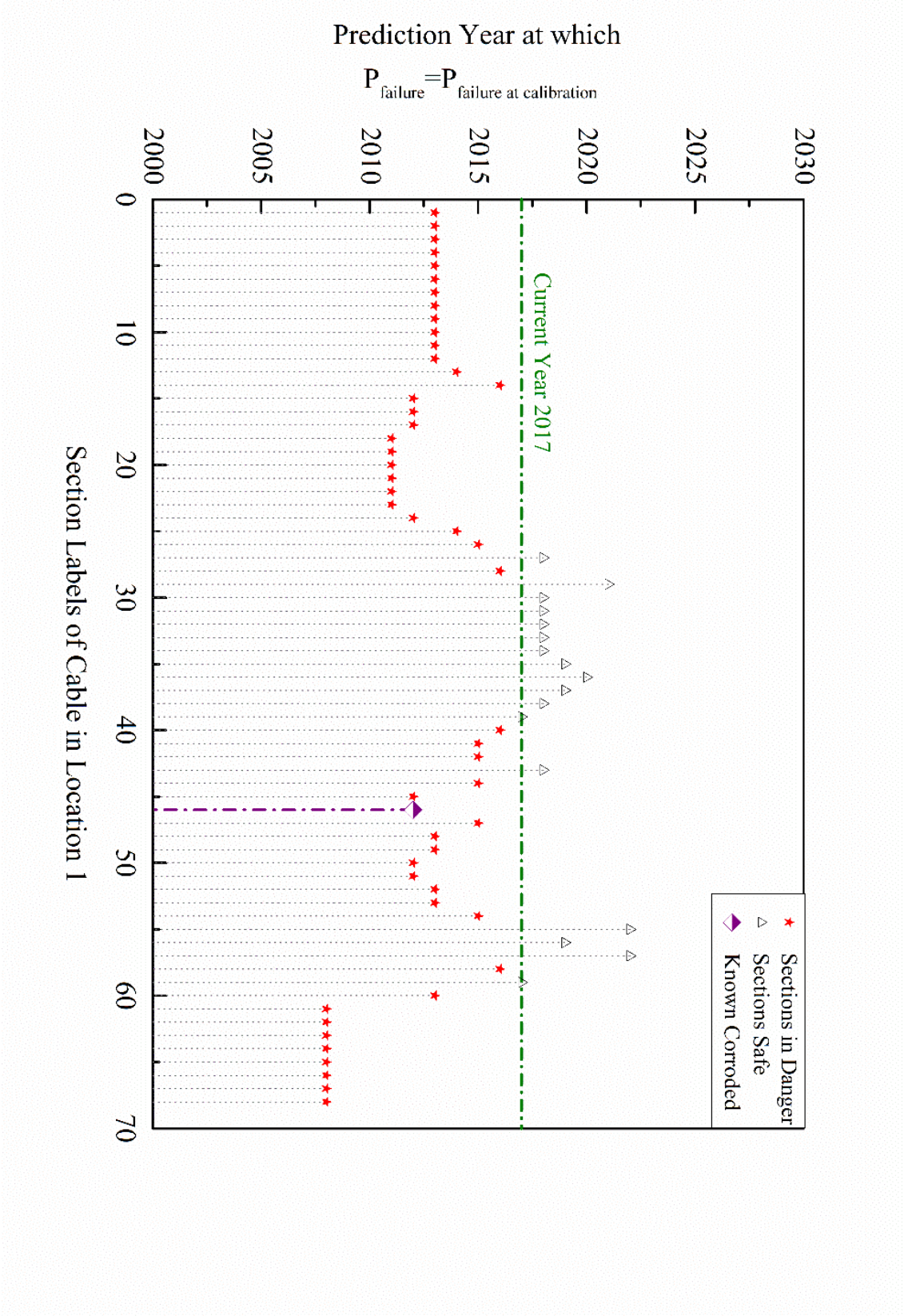

Figure 4-11: Validation of life prediction model by prediction year at which $P_{failure} = P_{failure\ at\ calibration}$ of different cable sections at Location 1 [6]

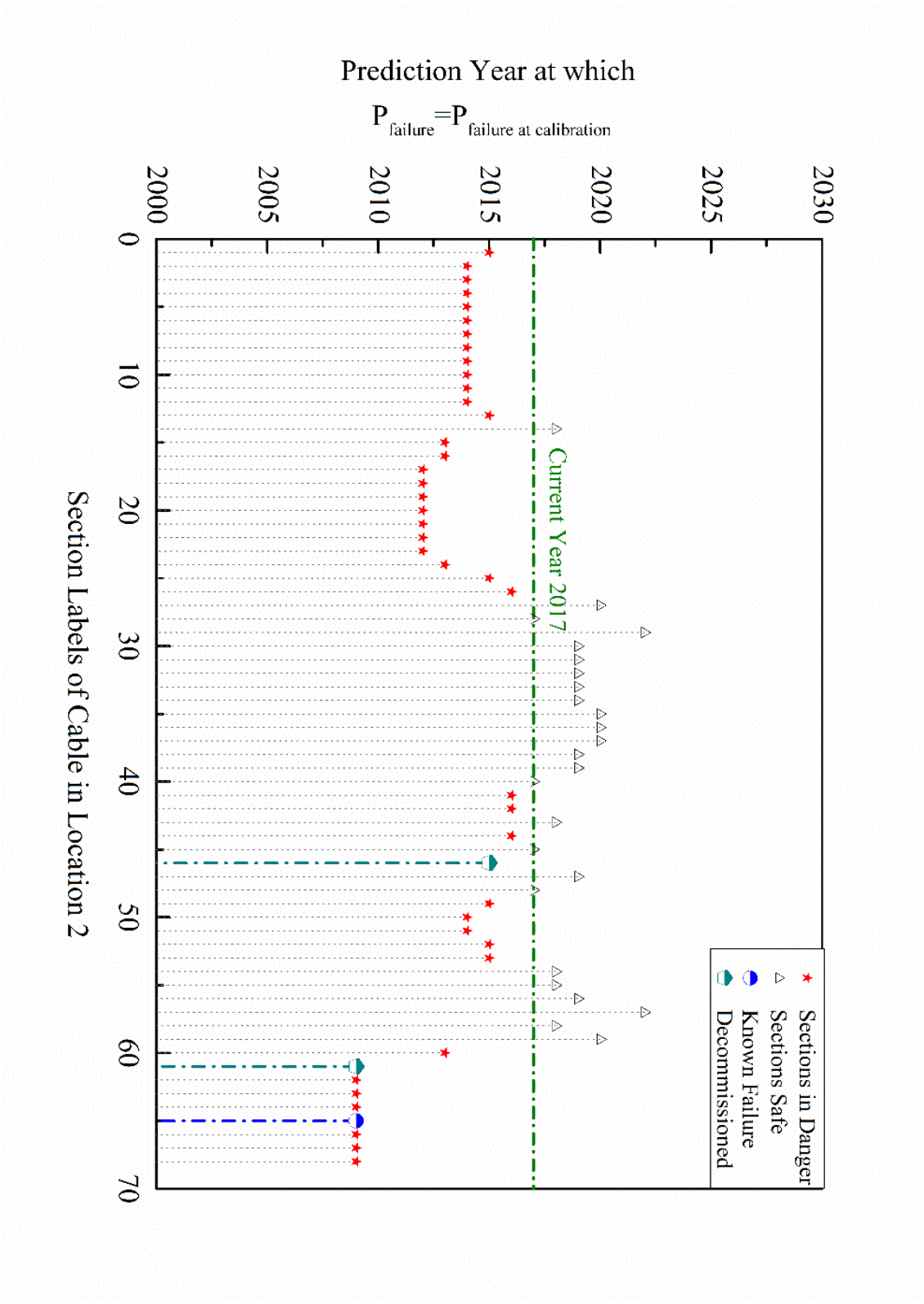

Figure 4-12: Validation of life prediction model by prediction year at which $P_{failure} = P_{failure\ at\ calibration}$ of different cable sections at Location 2 [6]

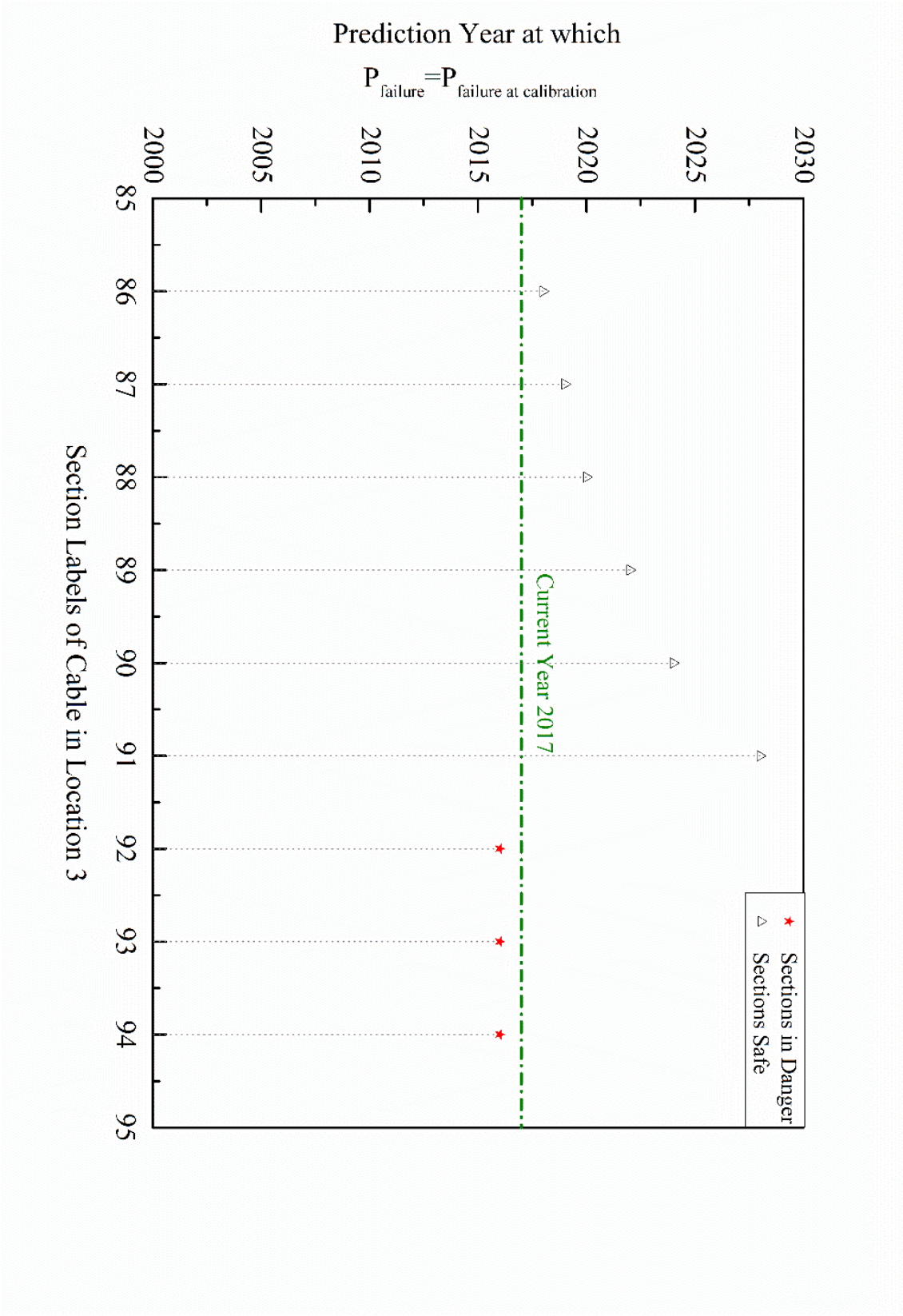

Figure 4-13: Validation of life prediction model by prediction year at which $P_{failure} = P_{failure\ at\ calibration}$ of different cable sections at Location 3 [6]

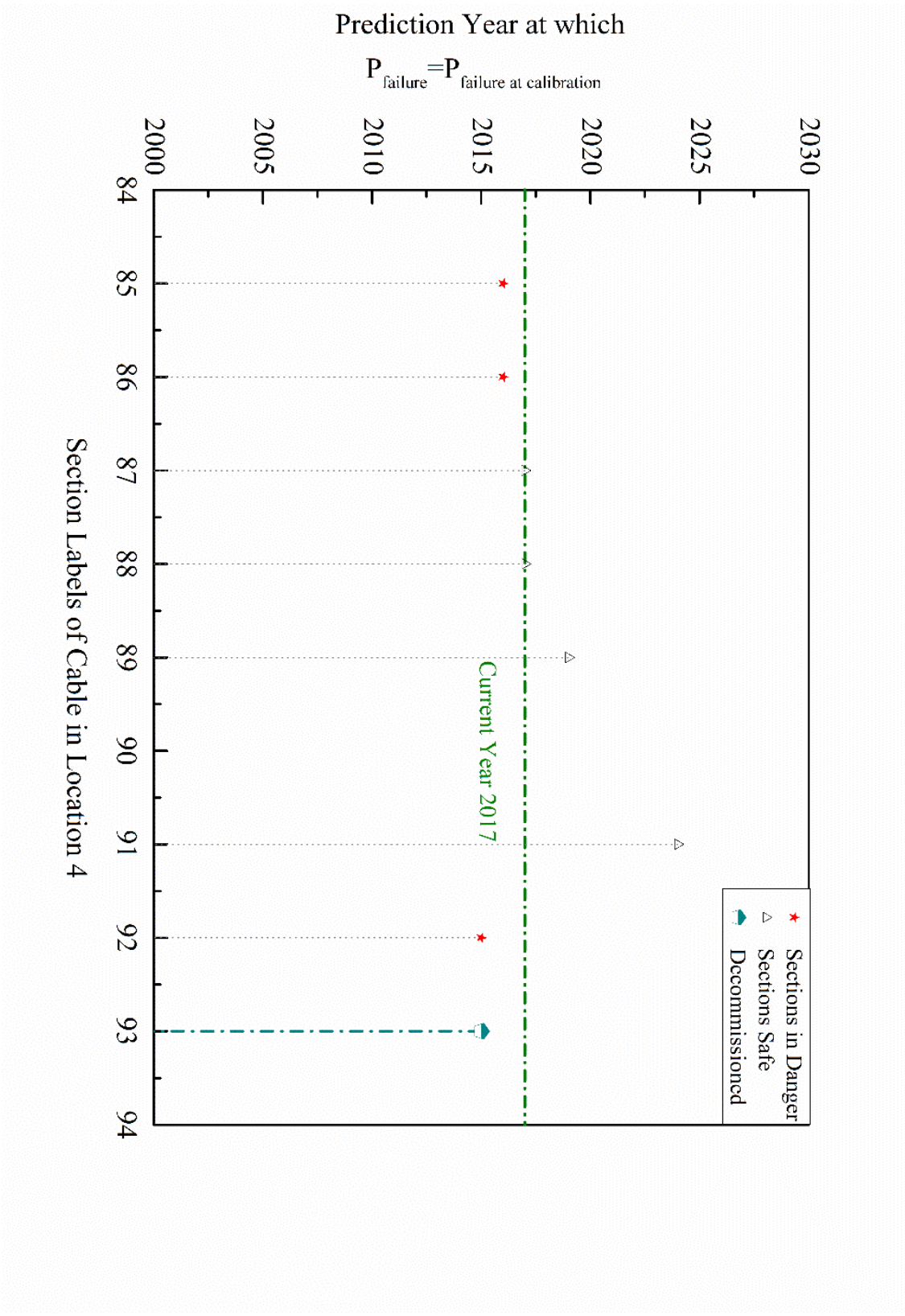

Figure 4-14: Validation of life prediction model by prediction year at which $P_{failure} = P_{failure\ at\ calibration}$ of different cable sections at Location 4 [6]

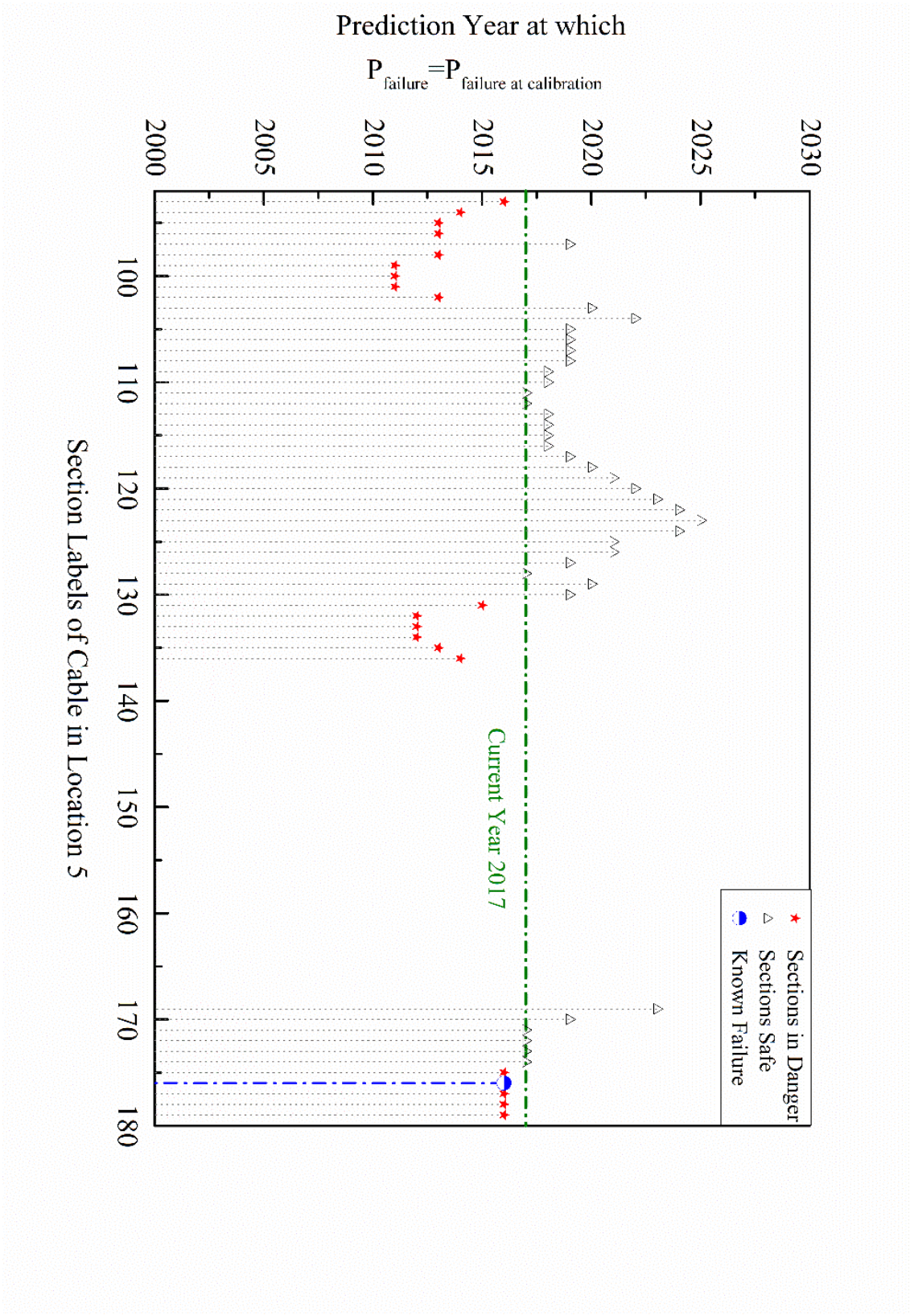

Figure 4-15: Validation of life prediction model by prediction year at which $P_{failure} = P_{failure\ at\ calibration}$ of different cable sections at Location 5 [6]

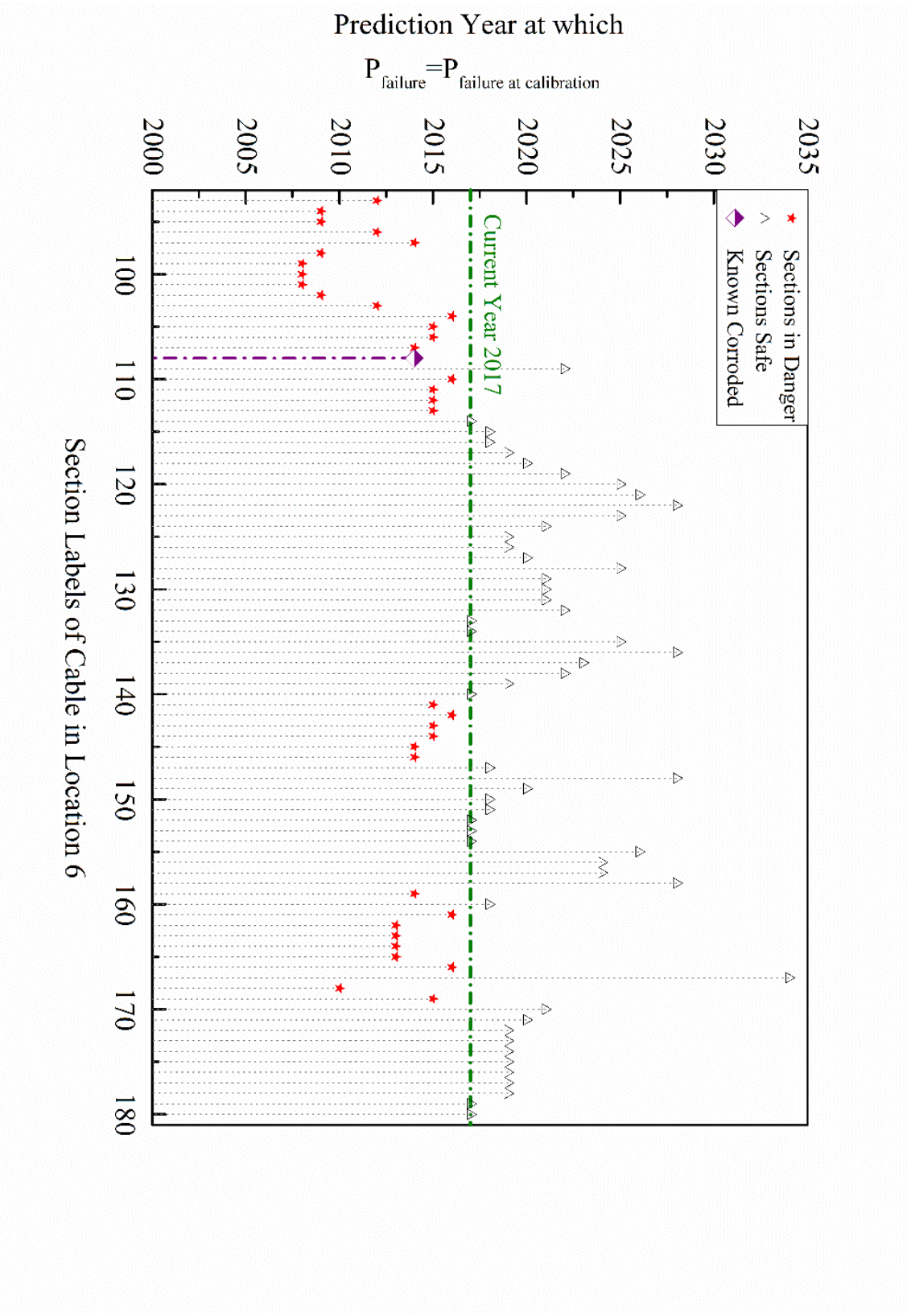

Figure 4-16: Validation of life prediction model by prediction year at which $P_{failure} = P_{failure\ at\ calibration}$ of different cable sections at Location 6 [6]

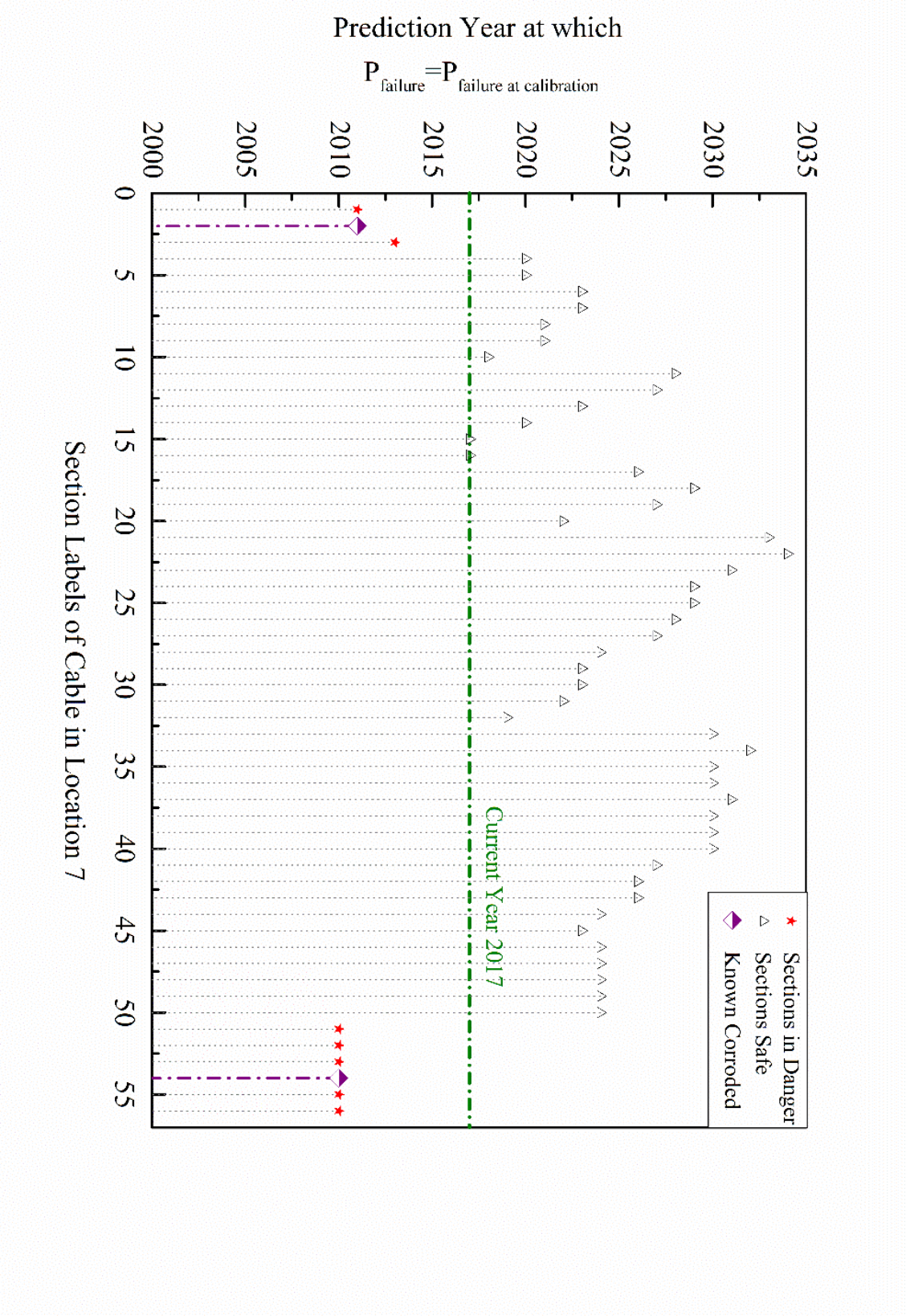

Figure 4-17: Validation of life prediction model by prediction year at which $P_{failure} = P_{failure\ at\ calibration}$ of different cable sections at Location 7 [6]

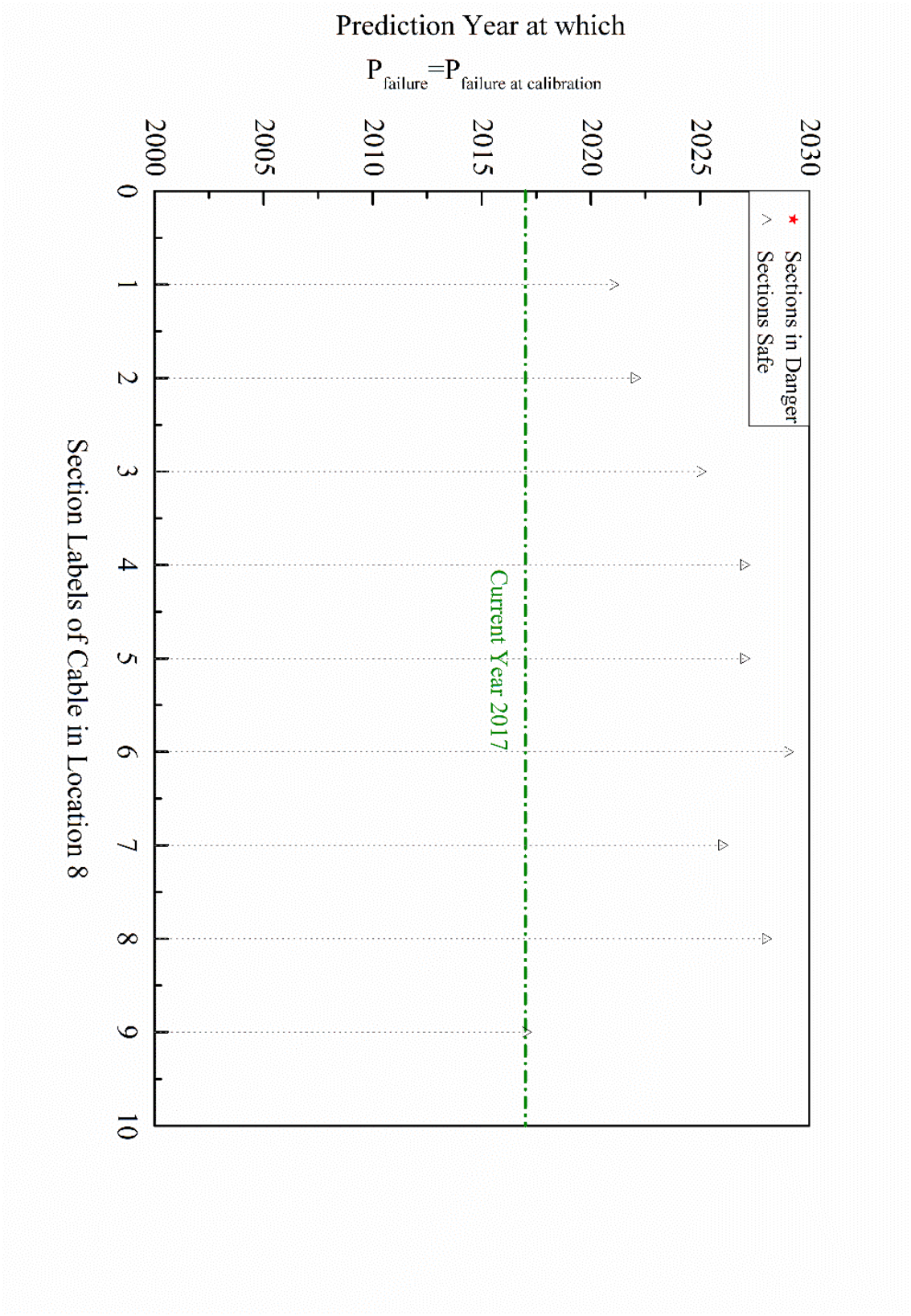

Figure 4-18: Validation of life prediction model by prediction year at which $P_{failure} = P_{failure\ at\ calibration}$ of different cable sections at Location 8 [6]

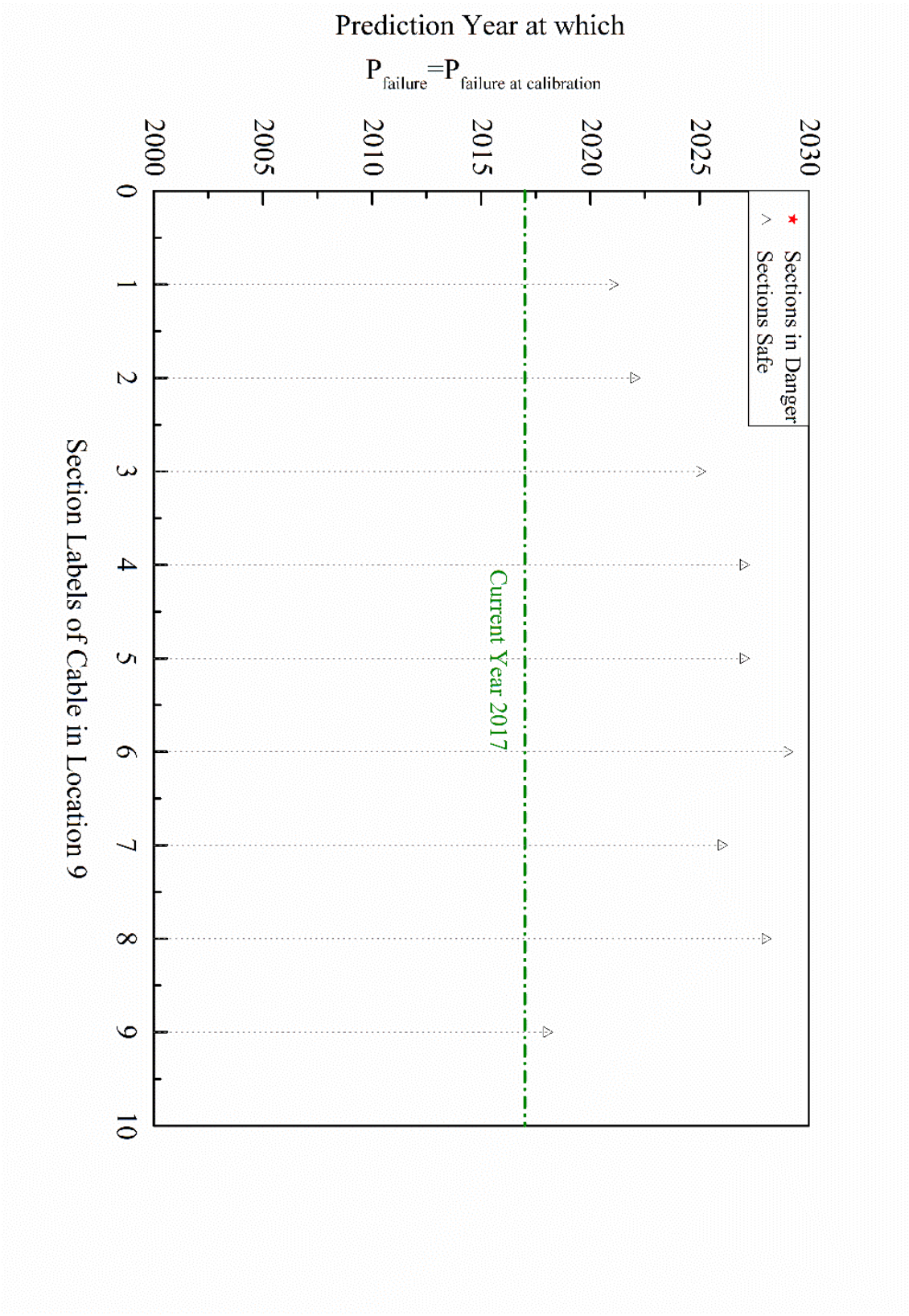

Figure 4-19: Validation of life prediction model by prediction year at which $P_{failure} = P_{failure\ at\ calibration}$ of different cable sections at Location 9 [6]

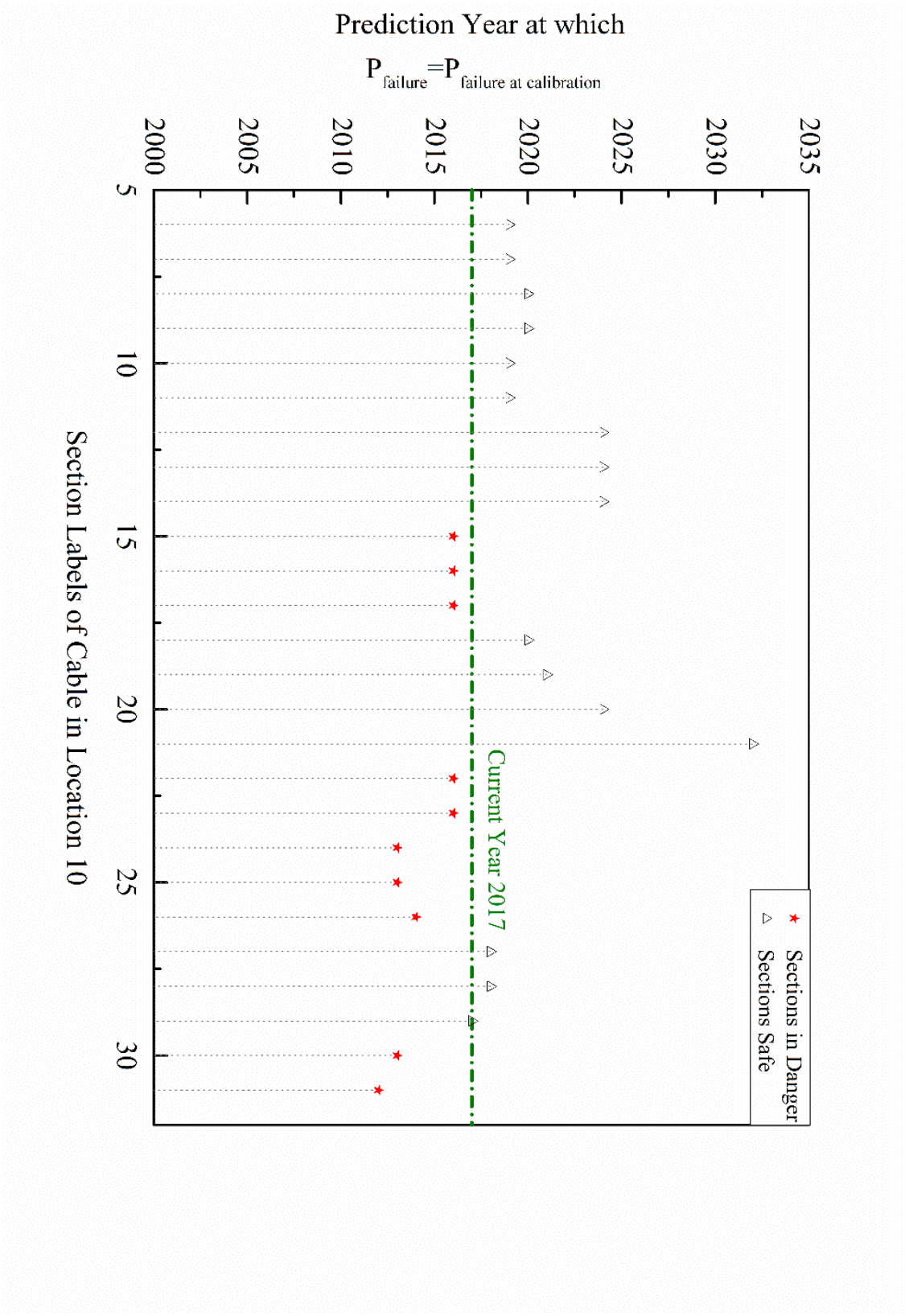

Figure 4-20: Validation of life prediction model by prediction year at which $P_{failure} = P_{failure\ at\ calibration}$ of different cable sections at Location 10 [6]

4.3 Achievements of this research chapter

This chapter provided additional insights into the entire failure process of the phosphor bronze tape in underground power transmission cables. Following an accurate Monte Carlo simulation on pit depth distributions, a probability description of pitting corrosion to crack propagation probability transfer function has been introduced in this study, covering the following points:

- A pit depth distribution model is developed. Combined with the author's previous research results on pit depth distribution on specific years [6], this study provides a model that can describe pit depth distribution for any requested point in time.
- An equation of the crack propagation in reinforced tin-bronze tape is given, under the assumption of a high mean stress and a relatively low alternating stress, for which all parameters are fixed numerically.
- A function of the pitting corrosion to crack propagation probability is given using the cumulative distribution function of the Weibull distribution, with all parameters are fixed numerically.
- A proposal for applying this $'Pit\ initiation \rightarrow Pitting\ Corrosion \rightarrow Pit - crack\ transfer \rightarrow Crack\ propagation \rightarrow Failure'$ whole process analysis to the prediction of underground power transmission cable service life is given.

5. Defining probability of failure for both the empirical-based model and the mechanism-based model

From this chapter, the rest of the research results are based on mathematical algorithms in processing the existing data and research results. Chapter 5 discusses the definition of probability of failure for both the empirical-based model applied in the power supplement industry and the mechanism-based model which is a deduction of the results from previous research Chapter 3 and Chapter 4.

The reason to develop a probability of failure model is for the service of the next Chapter 6, which discusses the model updating algorithm applying the Bayesian Inference. As for Bayesian Inference algorithm, the requirement of models are that they must be probability density functions, and the model from Chapter 4 is a life estimation model. Due to this reason, the life estimation model is transferred into a probability of failure model. This chapter is divided into two sections: the first section discusses the probability of failure from the empirical-based model and the second section gives the definition and results of the probability of failure (PoF) by the mechanism-based model.

5.1 A hypothesis based on the current industrial asset management model

The current industrial asset management model is based on the normal distribution which is pictorially shown in Figure 5-1.

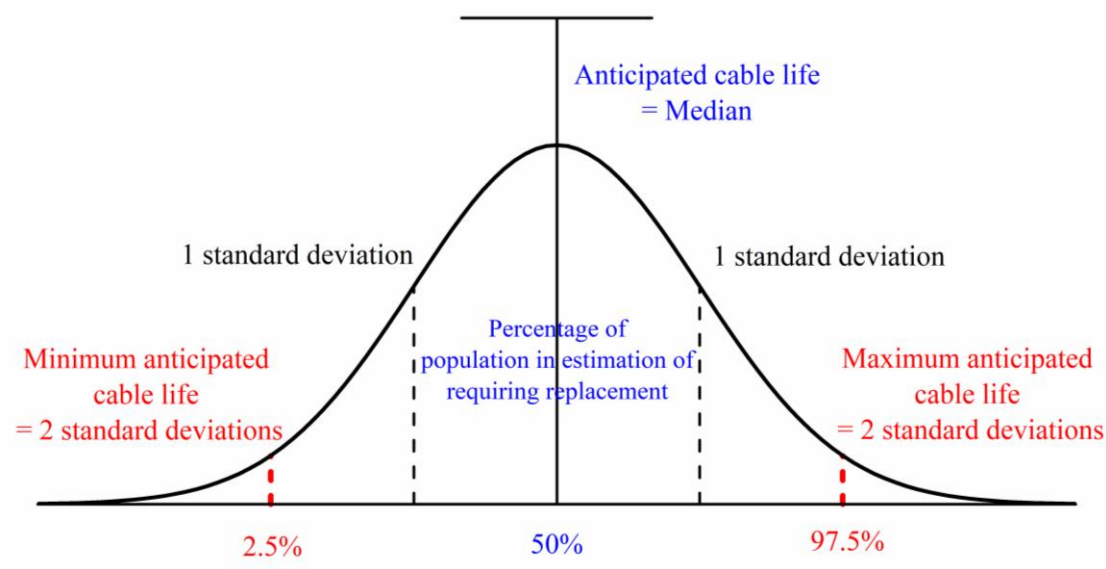

Figure 5-1: Pictorial representation of the cable replacement model in the power supplement industry

The power transmission cables being used owns a natural property, which is the anticipated life. Due to the complexity of the environment these cables are constructed and the multiple types of services these cables provide, the anticipated life for underground power transmission cables is not a fixed value, but is in a format of distribution, to be more specifically, a normal distribution which is widely used in the industry for estimations. The median of the distribution represents the life for majorities of cables. The minimum anticipated life of the cable represents the earliest anticipated failure of cable, this may be due to more heavy usage or the cable being used in a more critical environmental condition. The maximum anticipated life of the cable means the contrary of the minimum anticipated life, the cables are subject to ideal conditions and last longer than the majority of the similar cables. The minimum anticipated life and the

maximum anticipated life bonds the 95% confidence of cable life estimation distribution, which is four times the standard deviation of the distribution (4σ).

In the current definition being used in industry, cables are investigated each year and are then labelled with replacement priorities. This replacement priority can be regarded as a timescale for the criticality of the cables. The timescale is normally represented by a range of remaining life, this range varies in relation with the criticality conditions of the investigated cables. In this chapter, two cables subject to two different levels of criticality is given. Cable 1 is a critical cable with a relatively light issue, the timescale for replacing this cable is 5~10 years. Cable 2 is a critical cable with severe corrosion and requires immediate replacement, the timescale for replacing this cable is 0~2 years. These two assumed timescales for cable replacement will be used in the results section as numerical examples for the method and algorithms introduced in this research. The details of Cable 1 and Cable 2 with their assumed conditions are shown in Table 5-1.

Table 5-1: Summary of existing cable data used in this chapter

Location	**Criticality**	**Estimated Remaining Life**
Cable 1	Light	5~10
Cable 2	Severe	0~2

The anticipated life of underground power transmission cable is arguably between 30 to 70 years depending on the estimation of different power providers and research

institutes [145-148]. To demonstrate the algorithm in this paper, the median of the anticipated life is taken as 50 years and the 4σ is bounded by 30 years and 70 years, as seen in Figure 5-2. The equations in the following are all deduced in general expressions, while the figures are plotted as a typical solution for the above-mentioned values.

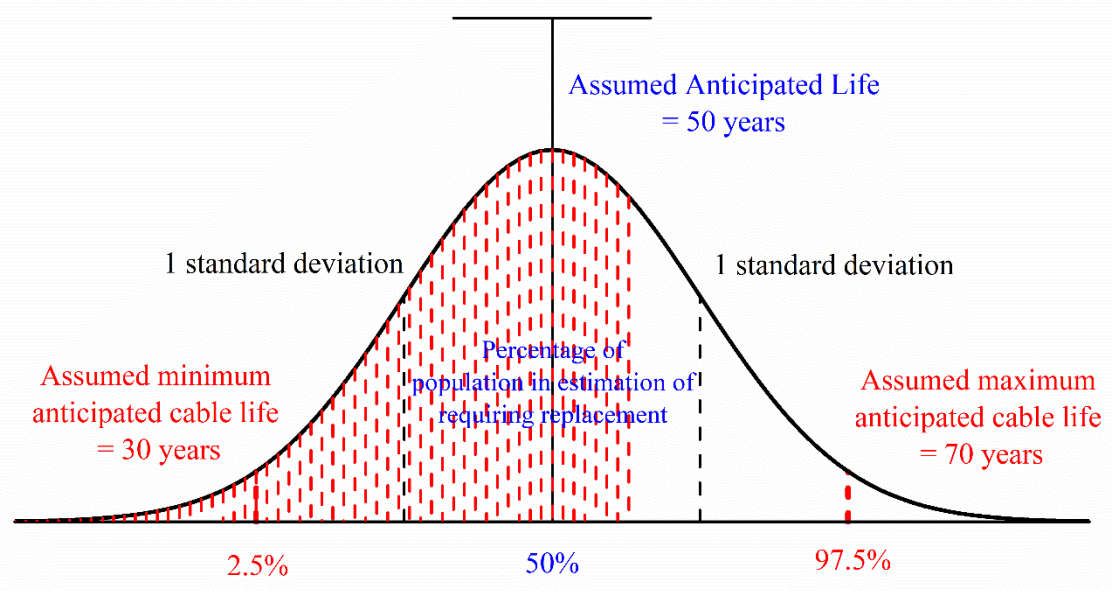

Figure 5-2: Assumed AHI=1 cable with the life anticipation distribution

The above Figure 5-1 and Figure 5-2 can be explained as: with the increase of cable life, there is a increasing percentage of cable population entering the condition that a replacement is required, the amount is the shaded area in red in Figure 5-1 and Figure 5-2. This lead to the conclusion that the older the cables get, the fewer stays in the 'safe zone' which is the unshaded area under the normal distribution bell-shaped curve. The explanation can be represented by Figure 5-3 below. Which plots the amount of cables within 'safe zone' with the increasing of cable life.

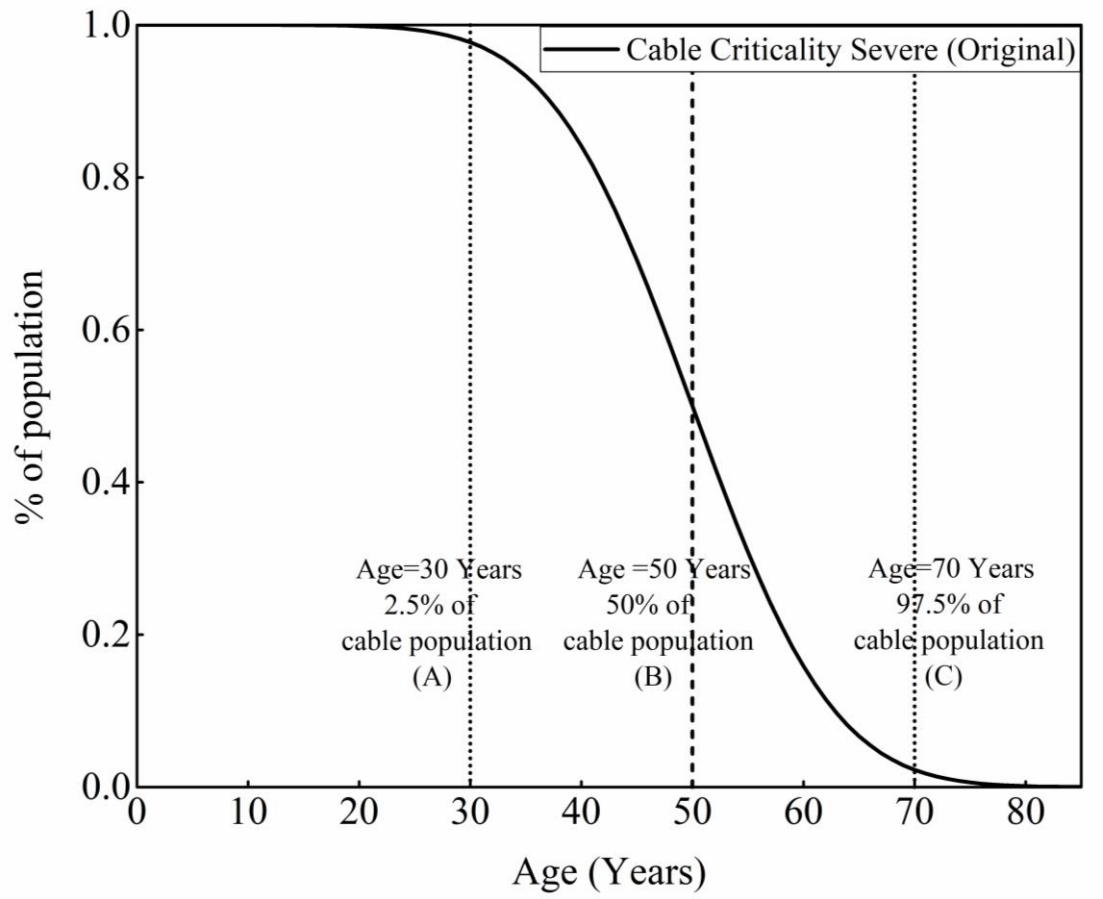

Figure 5-3: Cable with criticality evaluation of severe line plot explaining the assumed condition of Figure 5-2

The fundamental steps obtaining the empirical-based probability of failure model from the industry is based on numerical demonstration of Cable 1. The other location of cable used the same procedure of algorithm, these results are shown in the validation.

The general expression of normal distribution probability density function (PDF) is:

$$PDF_{normal} = \frac{1}{\sqrt{2\pi\sigma^2}} e^{-\frac{(x-\mu)^2}{2\sigma^2}} \quad -----(5-1)$$

The existing model in the industry extracted from [149, 150], is with no specific mathematical function given to describe the remaining asset life estimation. However, it is known that the data is a mathematical description of the normal distribution. Plus,

the 2 cables being researched, Cable 1 and Cable 2, are assumed to be with a light and severe criticality respectively. When defining the probability of failure of the empirical model used in industry, it can be explained with the assistance of Figure 5-2 and Figure 5-3 as: with the increase of cable life, there is an increasing percentage of cable population entering the condition that a replacement is required, the amount is the shaded area in red in Figure 5-2. This lead to the conclusion that the older the cables get, the fewer stays in the 'safe zone' which is the unshaded area under the normal distribution bell-shaped curve.

It can be seen in Table 5-1 that, if the evaluated cable is show obvious sign of deterioration, the cables with an assumed light criticality is with 5~10 years of replacement priority range. While the cables with an assumed severe criticality is with 0~2 years of replacement priority range. The replacement priority range can be interpreted as the upper and lower boundaries for the confidence of remaining life estimation. The lower boundary within the range is considered as a conservative estimation of the cable condition, while the upper boundary within the range is considered as a liberal estimation of the cable condition. With the above definitions, the probability of failure (PoF) functions for Cable 1 and Cable 2 in both conservative and liberal estimations are given below.

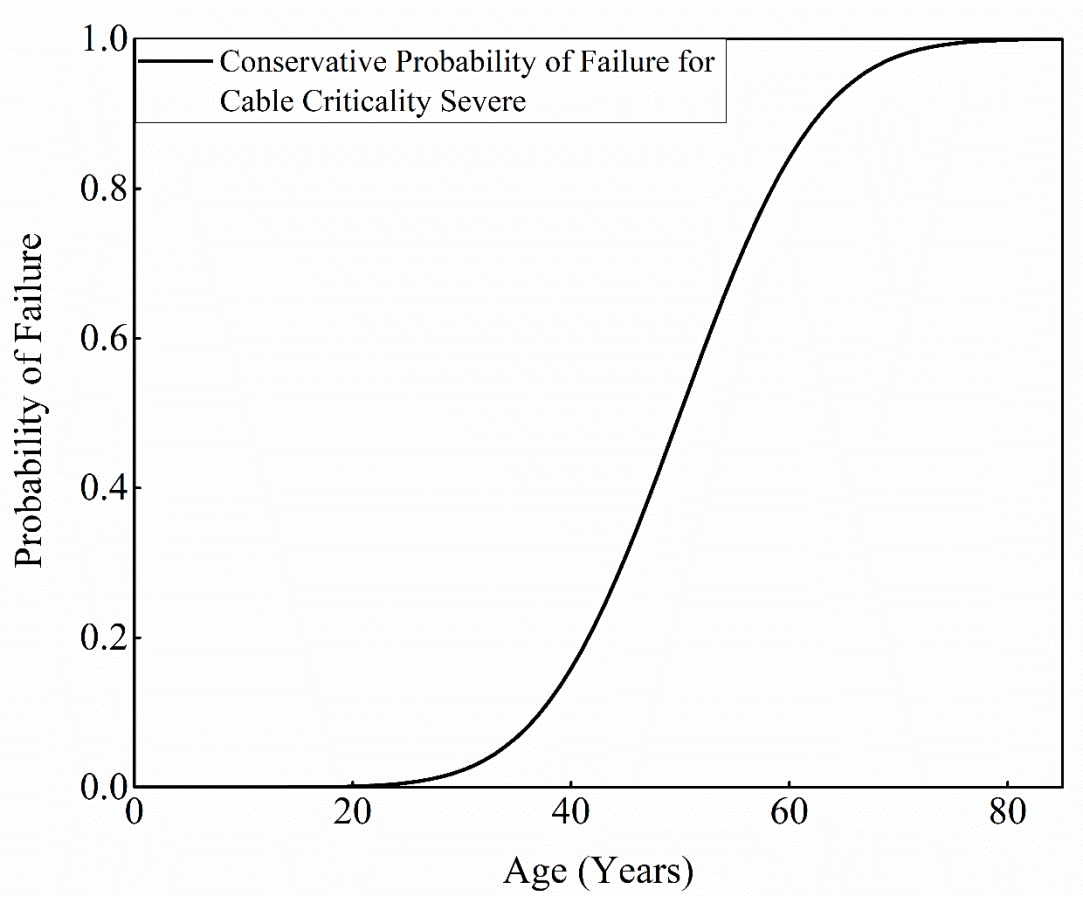

Figure 5-4: Conservative probability of failure by empirical-based model for cable with a criticality evaluation of severe

The function representing the PoF for cable with a criticality evaluation of severe is the CDF of normal distribution with parameters $\begin{cases}\mu = 50\\ \sigma = 10\end{cases}$ and can be written as:

$$PoF_{empirical} = \frac{1}{2}\left[1 + \text{erf}\left(\frac{t-\mu}{\sigma\sqrt{2}}\right)\right] - - - -(5-2)$$

Where taking

$$m = \frac{t-\mu}{\sigma\sqrt{2}} - - - -(5-3)$$

Then

$$\text{erf}(m) = \frac{2}{\sqrt{\pi}}\int_0^m e^{-r^2}dr - - - -(5-4)$$

Liberally, for the cables with a criticality evaluation of severe, there is a estimated

remaining life of 2 years. This gives the other range limit of the empirical probability of failure estimation, which can be called the 'liberal estimation of PoF'. Observing the original evaluation plot from Figure 5-3, if the cables entered the Criticality Severe zone but have a further 2 years of servicing life, the plot in Figure 5-3 would shift to the positive x-axis direction (Age axis) for 2 years in order to represent the boundaries for the cables to enter the 'Critical Zone' under the liberal approach. This is shown here in Figure 5-5.

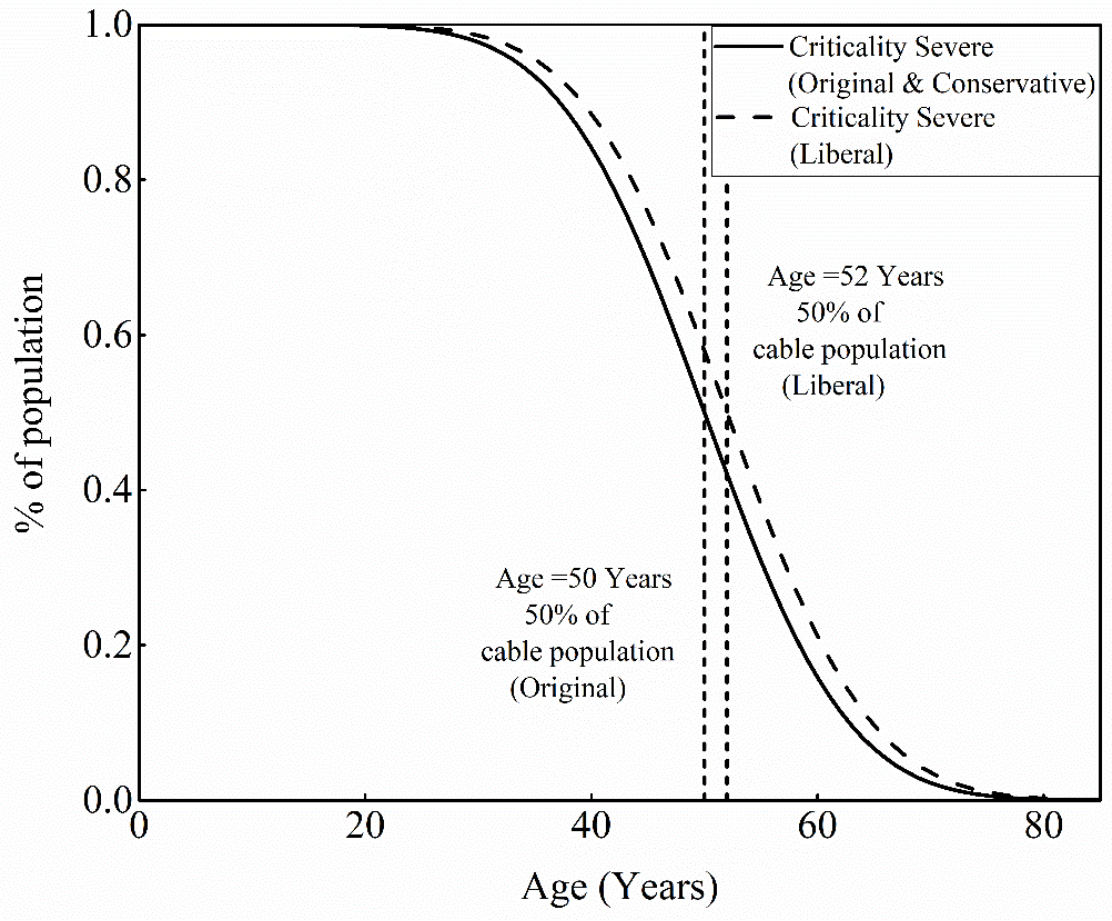

Figure 5-5: Liberal estimation shift from the original criticality severe evaluated plot

This further provides the liberal estimation of the PoF for criticality severe evaluated cables, which is interpreted as a confidence range. This range is plotted in Figure 5-6

combining the PoF estimation in conservative and liberal approaches. The liberal estimation of PoF for criticality severe evaluated cable is with parameters $\begin{cases}\mu = 52\\ \sigma = 10\end{cases}$ substituting into equations (5-2) to equation (5-4).

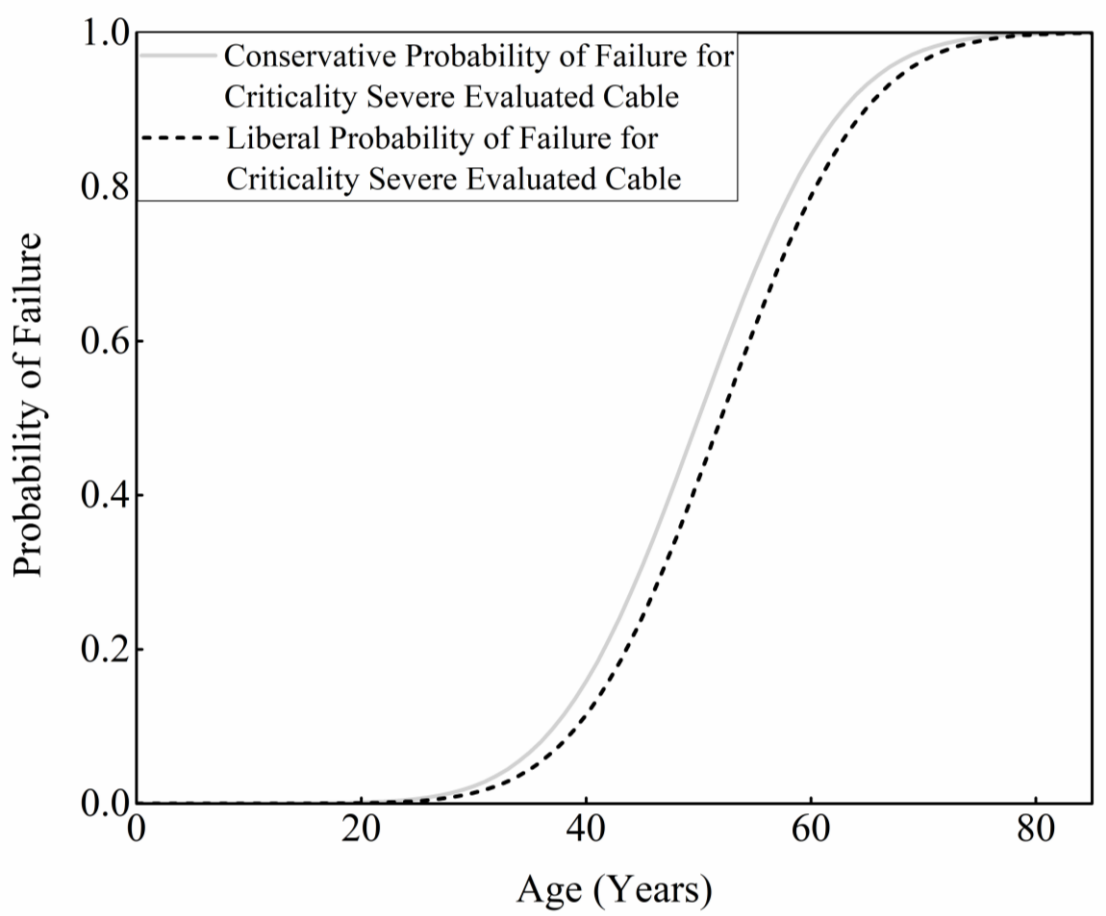

Figure 5-6: Liberal and conservative PoF by industry applied empirical model (upper and lower boundaries for criticality severe evaluated cables)

As the critical cables are assumed to be evaluated as either severe or light, it is also necessary to deduce the PoF function for criticality light evaluated cables. Repeating the procedure for criticality severe evaluated cables, the line of criticality light cables is assumed to be based on the original normal distribution parameters too. From Table 5-1, when a cable is evaluated as light criticality, there is an estimated of 5~10 years of

servicing life left, similar to the strategy of criticality severe evaluated cables, the 5 year remaining life is considered as a conservative estimation while the 10 years is taken as a liberal estimation. By shifting the plot to the positive x-axis (Age axis) of 5 years, this is the conservative plot according to which the cables currently evaluated as criticality light evaluated cable enter the 'Critical Zone'. And by shifting the plot to the positive x-axis (Age axis) of 10 years, this leads to the liberal estimation that the cables will enter the 'Critical Zone'. The plot of both the conservative and liberal estimations comparing to the original criticality evaluation plot is shown in Figure 5-7:

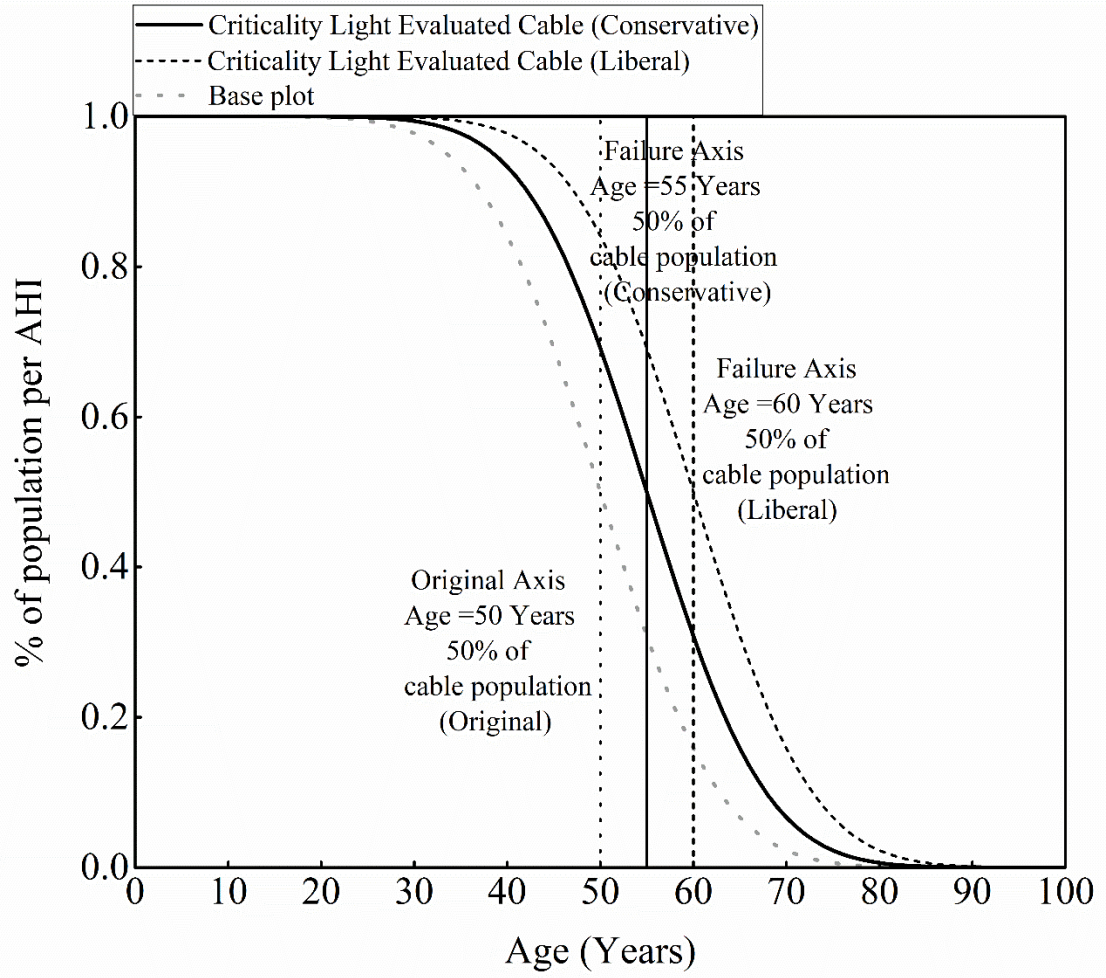

Figure 5-7: The comparison of original plot and both the conservative and liberal interpretation of estimation

The PoF function for criticality light evaluated cables is deduced from the 'Plot for estimation of failure', the conservative boundary is with anticipated normal distribution parameters of $\begin{cases}\mu = 55\\ \sigma = 10\end{cases}$. And the liberal boundary follows the anticipated normal distribution parameters of $\begin{cases}\mu = 60\\ \sigma = 10\end{cases}$. After the determination of the parameters, the function is obtained using the same method as for criticality severe evaluated cable. The probability of failure for both conservative and liberal estimations are shown below in Figure 5-8.

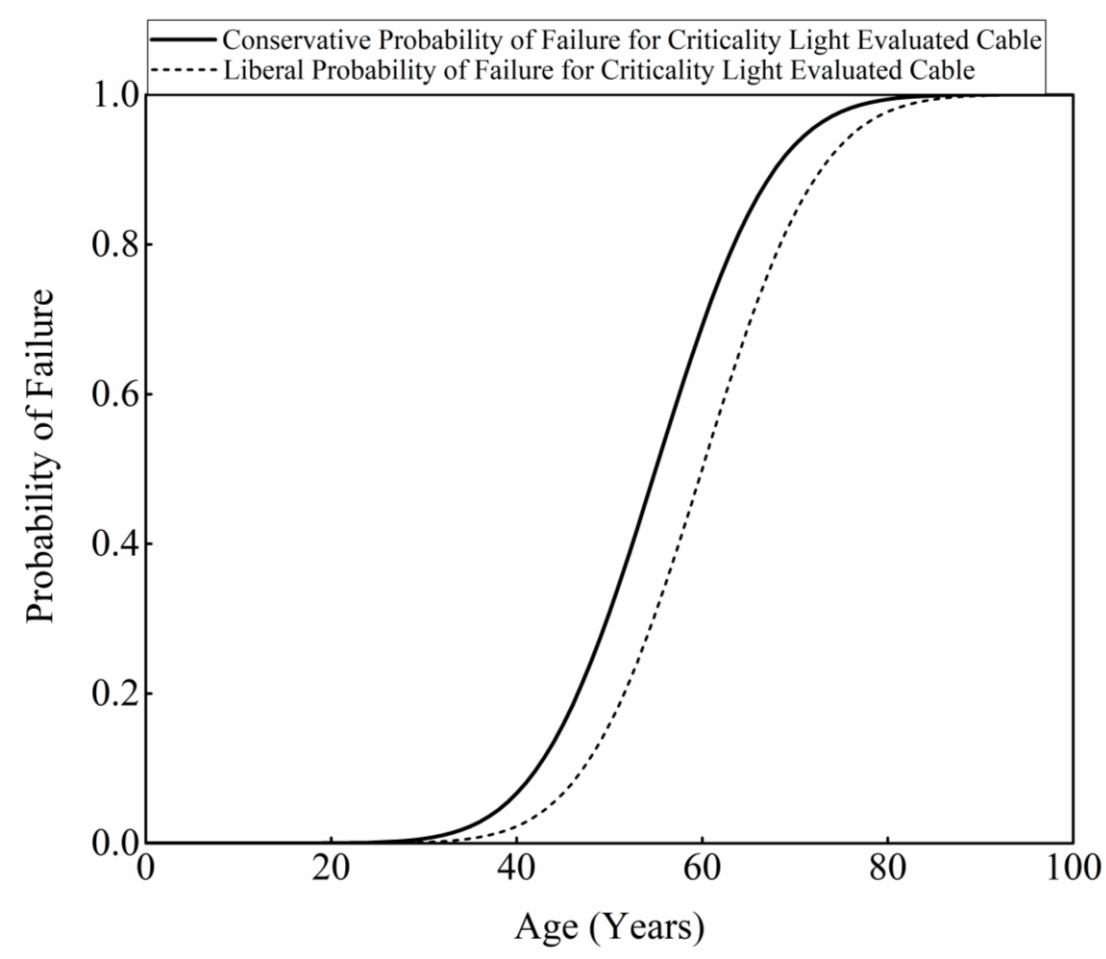

Figure 5-8: PoF plot for criticality light evaluated cable (both conservative and liberal estimations)

A pictorial representation of the probability of failure functions for all mentioned above is shown in Figure 5.

The conservative probability density function for severe criticality of cable evaluation:

$$PDF_{AHI=5_{conservative}} = \frac{1}{\sqrt{2\pi\sigma_{typical}^2}} e^{-\frac{(x-\mu_{typical})^2}{2\sigma_{typical}^2}} \quad -----(5-5)$$

The liberal probability density function for severe criticality of cable evaluation:

$$PDF_{AHI=5_{liberal}} = \frac{1}{\sqrt{2\pi\sigma_{typical}^2}} e^{-\frac{\left((x-2)-\mu_{typical}\right)^2}{2\sigma_{typical}^2}} \quad -----(5-6)$$

The conservative probability density function for light criticality of cable evaluation:

$$PDF_{AHI=4_{conservative}} = \frac{1}{\sqrt{2\pi\sigma_{typical}^2}} e^{-\frac{\left((x-5)-\mu_{typical}\right)^2}{2\sigma_{typical}^2}} \quad ----(5-7)$$

The liberal probability density function for light criticality of cable evaluation:

$$PDF_{AHI=4_{liberal}} = \frac{1}{\sqrt{2\pi\sigma_{typical}^2}} e^{-\frac{\left((x-10)-\mu_{typical}\right)^2}{2\sigma_{typical}^2}} \quad -----(5-8)$$

All the conservative and liberal estimations for criticality light and severe evaluated cables are combined for comparison and are shown in the following Figure 5-9:

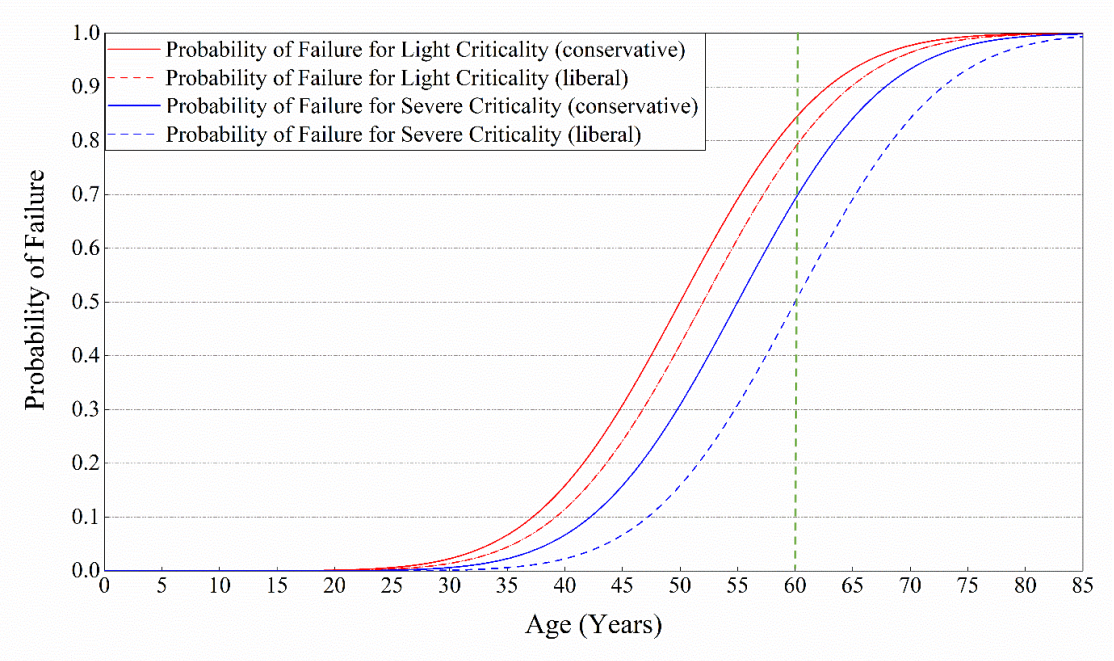

Figure 5-9: Empirical model on probability of failure for cables with light and severe criticality evaluation interpreted from industry

As observed in Figure 5-9, take year 60 as an example, for light criticality, the estimated probability of failure is within the range of 0.8 to 0.84. And for severe criticality, the estimated range is between 0.5 to 0.7. This estimation range can direct the decision making of maintenance or replace, especially when this result is applied into the estimation of invest/obtain ratio in the engineering asset management.

5.2 A corrosion fatigue mechanism-based model on cable life estimation

A corrosion fatigue mechanism based model for cable life estimation is extracted from previous work, which was described in Chapter 3 and Chapter 4. The following is a brief summary of the life estimation model:

5.2.1 Obtaining the pit depth distribution

Basically, to estimate the life of a targeting cable, a section of the tin bronze tape must be obtained in order to measure the corrosion pit depths on its surface. Then applying the Monte Carlo simulation and transfer the experimental pit depths distribution into a theoretical GEV distribution [5]. Generally, the pit depth distribution of the targeting cable at any calendar year Y (e.g. current year is 2018), can be written in the format as:

$$F(x) = \alpha \cdot (Y - commision\ year)^{0.33} - - - - - (5-9)$$

In which α follows the GEV distribution. [5] describes this procedure in detail.

5.2.2 Obtaining the pit-crack transfer pit depth

Chapter 4 introduced a pit-crack transfer probability function which can be expressed in the form of the cumulative distribution function of the Weibull distribution:

$$P(x) = 1 - e^{-(x/109.3)^{6.1}} - - - - - (5-10)$$

The pit depth distribution equation (5-9) is then multiplied by this pit-crack transfer probability equation (5-10). The pit depth with the highest probability from the product function is considered as the transfer pit depth, naming it $x_{transfer}$.

$$x_{transfer} = \max\big(F(x)P(x)\big)$$

$$= \max\left[\alpha \cdot (Y - commision\ year)^{0.33} \cdot \left(1 - e^{-(x/109.3)^{6.1}}\right)\right] - - - - - (5-11)$$

5.2.3 Processing the existing data for cable sections

In Chapter 4, 10 cables were studied leading to the publication of [5, 6]. Here data were extracted from two of these cables, which are referred as Cable 1 and Cable 2. Cable 1 is taken as the example describing the data processing. The processing of data for cable sections consist of two types: the geological data and the stress data. The geological data includes the number of cable sections, the length of each cable section and the elevation of each cable section. Two sets of geological profile data are assumed for both Cable 1 and Cable 2 to simulate the real situations. For Cable 1, this set of geological profile data is plotted in Figure 5-10, there are 57 sections of cable in Cable 1, the elevation and horizontal coordinates of the cables are hypothetical to simulate the field work scenario.

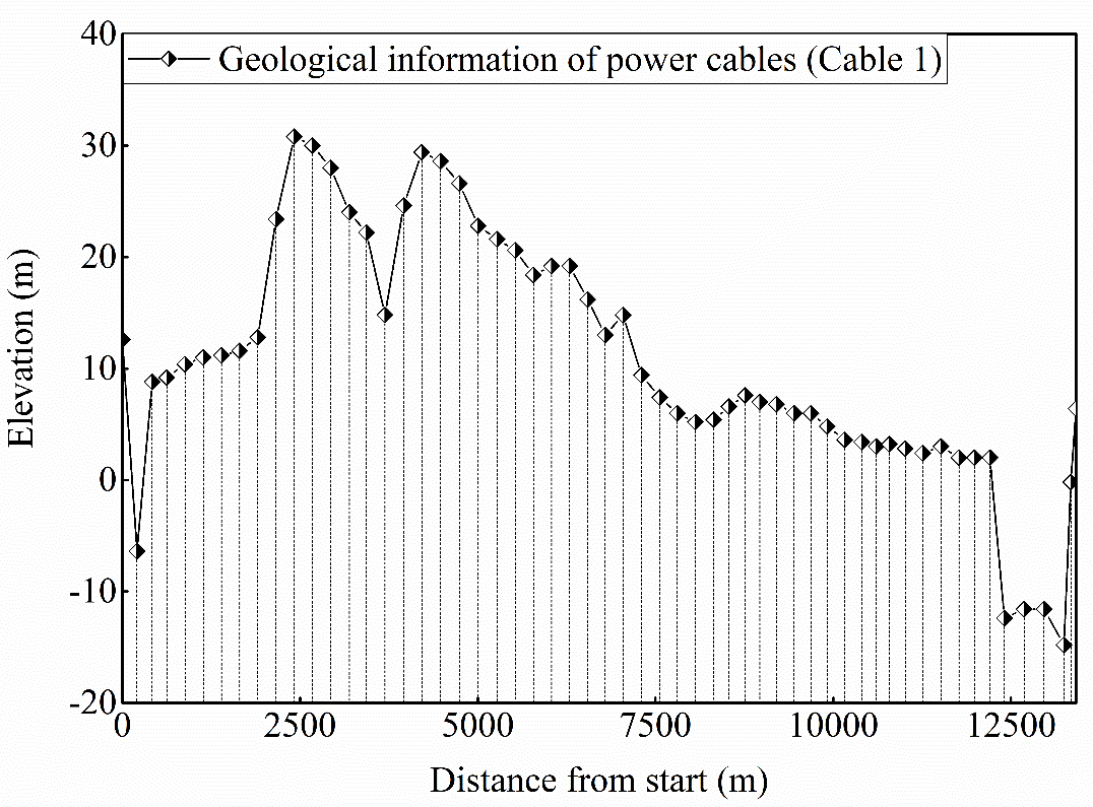

Figure 5-10: Geological data for Cable 1

From this information the length of each individual section of cable is calculated. All the sections of this cable services under a uniform alternating stress of $\sigma_{mean} = 0.69\ MPa$, but each individual section is under a different mean stress $\sigma_{mean_i}, i = 1{\sim}57$. The data of mean stress against the length of cable is plotted in Figure 5-11. The discrete points in Figure 3 are the average mean stress values, the continuous function describing the relationship between mean stresses and cable length coordinates is simulated by natural cubic splines algorithm. For 57 sections of cable it requires 56 continuous piecewise cubic functions with a smoothing factor of $p = 6 \times 10^{-4}$, covering the entire length of the power cable.

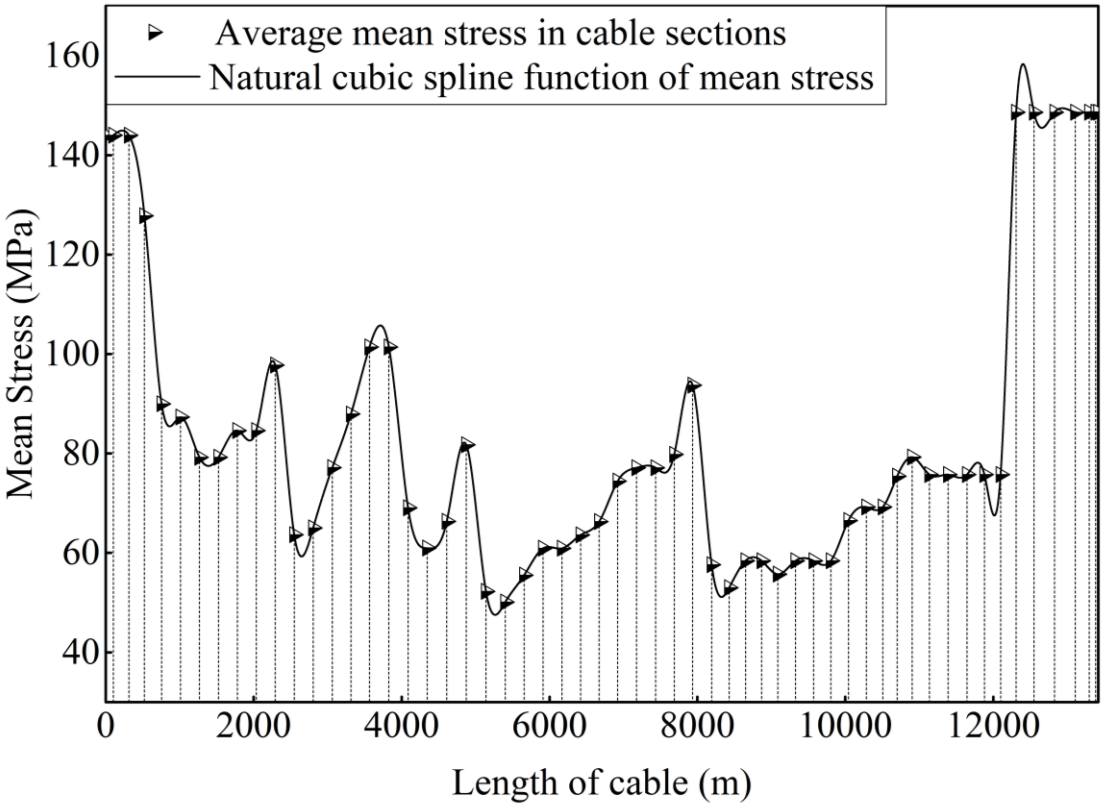

Figure 5-11: Mean stress vs Length of cable for Cable 1 (curves connecting mean stresses are simulated by natural cubic splines algorithm)

The mean stresses are assumed to be continuous throughout the entire cable for one location, without extreme changes. The approach here is to use a set of cubic equations, to create a smooth curve fitting for all the mean stresses data within each location. This is better known as the cubic spline method. The smooth factor to fit the curve to the data is specially chosen, which is the largest value that can allow the fitted curve to go through all data points. By this curve fitting approach, the equation set of mean stresses is:

$$\boldsymbol{A_1} \cdot \boldsymbol{x} = \mathbf{0} \quad ----(5-12)$$

Here $\boldsymbol{A_1}$ is the set of equation coefficients of curve fitting equation set referencing to

Cable 1 data. $\boldsymbol{x}$ is the variable set for cubic equations, as: $\begin{bmatrix} x^3 \\ x^2 \\ x \\ 1 \end{bmatrix}$. For example, after determining of the set of equations, the first and leading cubic equation is:

$$Equation_1 = -1.12 \times 10^{-7}x^3 + 0 \times x^2 + 0.029888x + 103.8308 - -(5-13)$$

The following table gives the values of coefficient matrix $\boldsymbol{A_1}$.

Table 5-2: Coefficient matrix $\boldsymbol{A_1}$ for cubic spline curve fitting of Cable 1 mean stress vs length of cable data

(Table shown in Appendix II)

By applying the same approach to the data of Cable 2, the cubic spline equation set is as:

$$\boldsymbol{A_2} \cdot \boldsymbol{x} = \boldsymbol{0} - - - -(5-14)$$

And the coefficient matrix $\boldsymbol{A_2}$ is given in Table 5-3.

Table 5-3: Coefficient matrix $\boldsymbol{A_2}$ for cubic spline curve fitting of Cable 2 mean stress vs length of cable data

(Table shown in Appendix II)

5.2.4 Defining mechanism-based probability of failure model

From the previous Chapter 4, the life estimation of underground power cable within this research can be generalised by:

$$t_{cable} = \frac{{x_{transfer}}^{0.774}}{0.108 \times (\sigma_{mean} + \Delta\sigma)^{0.453}} - - - -(5-15)$$

The combined stress $\sigma_{sum} = \sigma_{mean} + \Delta\sigma$ are known variables.

When the continuous mean stress fitting results from the above Equation (5-10) and Equation (5-11) will be substituted individually into Equation (5-12), the result is a continuous function with the result of life estimation based on the existing datasets. The life estimation of the entire power cable of Cable 1 is shown in below Figure 5-12 and the life estimation of Cable 1 is shown in below Figure 5-13.

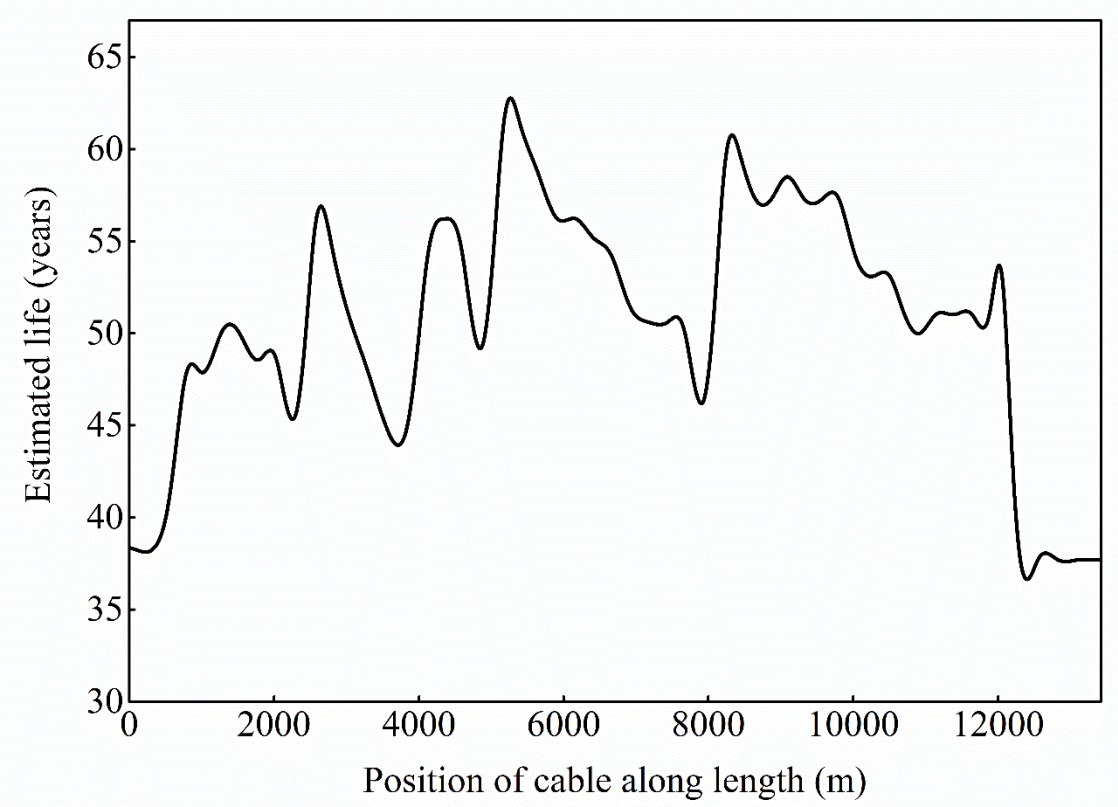

Figure 5-12: Life estimation by length of cable of Cable 1

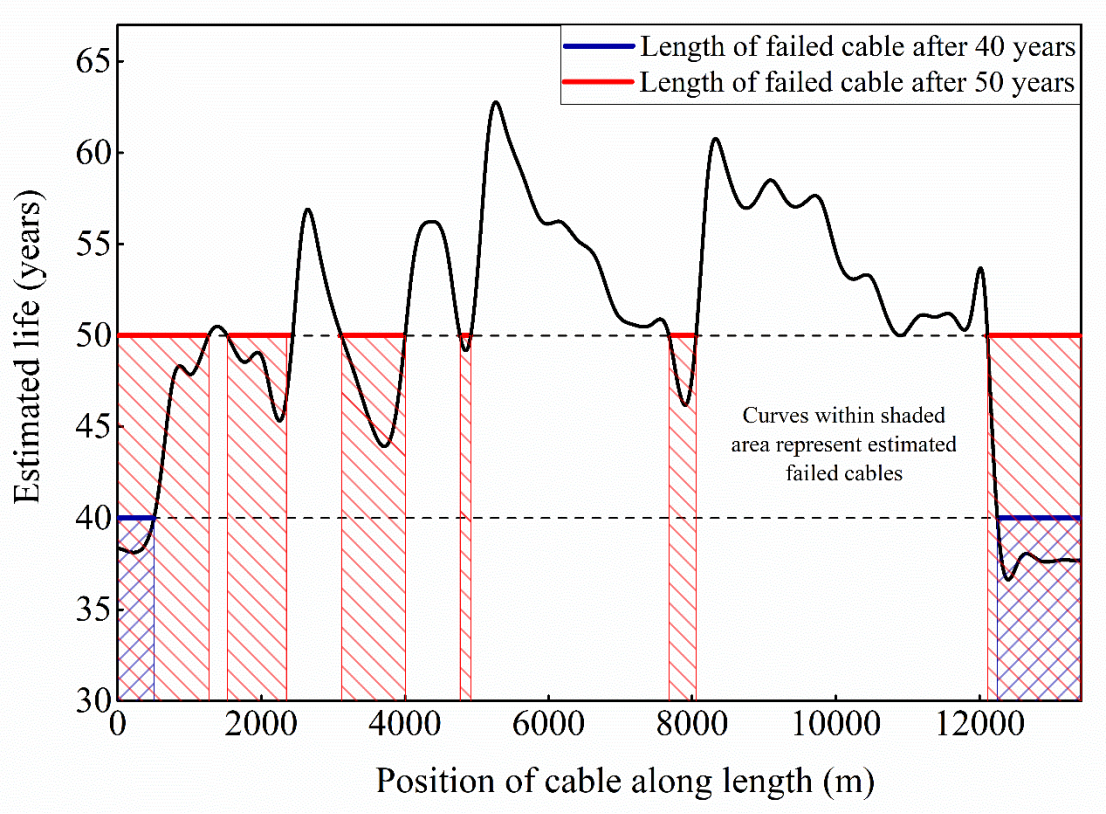

Figure 5-13: Life estimation by length of cable of Cable 1

Figure 5-13 for Cable 1 is used to explain the definition for the mechanism-based probability of failure model. The probability of failure at each year after the cable commission is defined as the percentage of the length of the estimated failed cable occupying the total length of the cable. In Figure 5-13, this definition is explained with the assistance of 40 years and 50 years after cable commission as examples. The dashed line at year 40 in Figure 5-13, cut the estimated life plot into two parts: the section of the plot above the line represents the cable with an estimated life of over 40 years, while the plot below represents the cable with an estimated life of less than 40 years (shaded in blue). The projection of the estimated life plot on the horizontal line at 40 years is the length of the cable predicted of failure. The probability of failure at year 40 is then calculated as the total length of blue straight line over the length of the entire power cable:

$$PoF_{40} = \frac{\sum l_{blue}}{L_{Cable\ 1}} - - - - - (5-16)$$

Here the l_{blue} represents the length of all predicted failed cable parts at year 40, and $L_{Cable\ 1}$ is the entire length of the cable at Cable 1.

With the same definition, at year 50, the predicted failed cable is below the horizontal dashed line at 50 years, under the shaded red areas. The total length of failed cable is the combination of the horizontal red straight lines. The probability of failure is then calculated as follows:

$$PoF_{50} = \frac{\sum l_{red}}{L_{Cable\ 1}} - - - - - (5-17)$$

Here l_{red} corresponds to the entire length of all predicted failed cable parts at year 50. It is easy to observe that under this definition, the probability of failure for the cable increases from 0 at the minimum estimated life point of the plot until reaching 100% at the maximum estimated life point of the plot.

The PoF for the cable at Cable 2 under this definition is plotted in Figure 5-14, shown in a solid blue line. Also the PoF following the same approach for Cable 1 is plotted below in Figure 5-15.

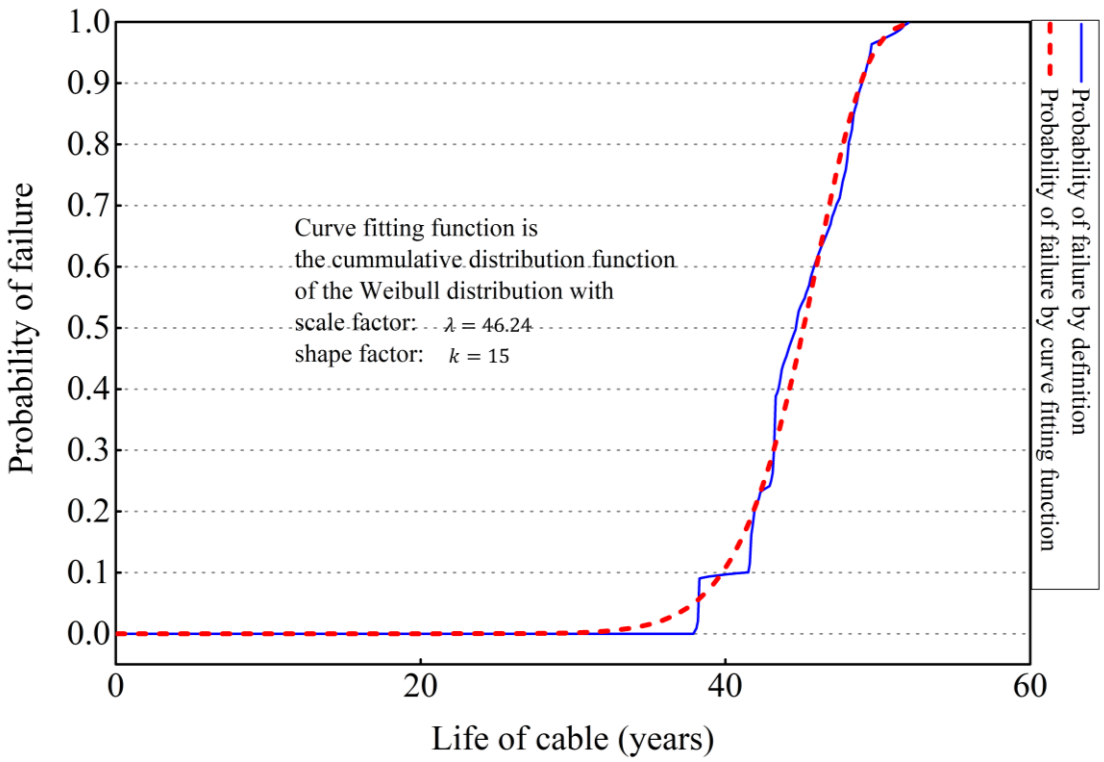

Figure 5-14: Mechanism-based probability of failure for Cable 2

The PoF plotted by the solid blue line is then fitted with a continuous function in order to be generalised mathematically. The fitted probability of failure function is a CDF of the Weibull distribution. The curve fitting technic can provide one reasonable function which can describe this result while achieving a close fit. Due to the fact that the Weibull distribution is known for its application in failure analysis [151-154] (including mechanical failure analysis), it is also used to fit the PoF in this study. The fitted function is plotted in Figure 5-14 with red dashed line in comparison with the actual result. The statistical similarity between the actual result and the fitted function is provided in Table 5-3.

Table 5-4: Statistical evaluation of similarity between the actual PoF and the fitted function describing the probability of failure for the mechanical-based model

Location	Evaluation		Function
Cable 1	$R^2 =$	0.9947	$f(t) = 1 - e^{-\left(\frac{x}{46.24}\right)^{15}}$
	$SSE =$	0.2298	
Cable 2	$R^2 =$	0.9948	$f(t) = 1 - e^{-\left(\frac{x}{53.52}\right)^{10}}$
	$SSE =$	0.3271	

The function for Location 2 with service life t as variable is:

$$f_{Location\ 2}(t) = 1 - e^{-\left(\frac{t}{46.24}\right)^{15}} \quad -----(5-18)$$

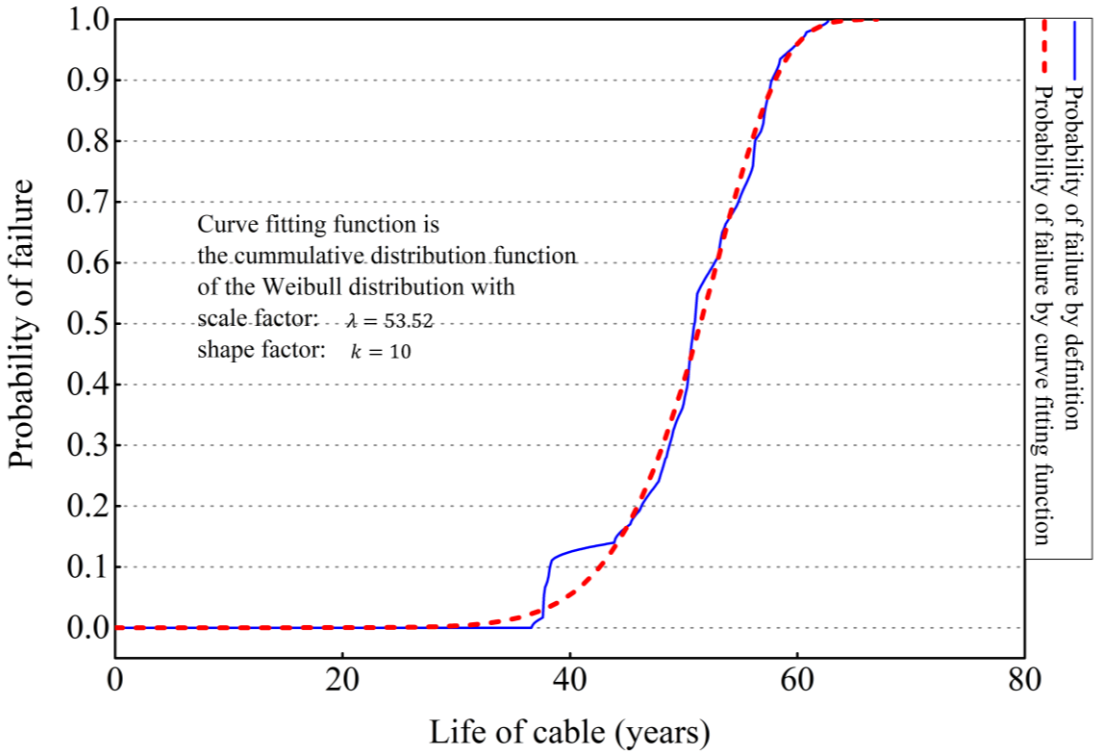

Figure 5-15: Mechanism-based probability of failure for Cable 1

The function for Cable 1 with service life t as variable is:

$$f_{Cable\ 1}(t) = 1 - e^{-\left(\frac{t}{46.24}\right)^{15}} \quad -----(5-19)$$

The evaluation to select the function that fits the best in Table 5-4 follows two standards, the R^2 and the SSE. R^2 is known as the coefficient of determination, which is the proportion of the variance in the dependent variable that is predictable from the independent variable: the higher the R^2 value, the better a function describes the dataset [155]. SE is the short form of 'sum of squared errors of prediction', it is the sum of the squares of residuals, and a small SSE value shows the model fits the data well [156].

In the final step of this chapter, the fitted functions for mechanism-based probability of failure of Cable 1 is compared with the range of the empirical-based PoF functions and are plotted and shown in the following figures.

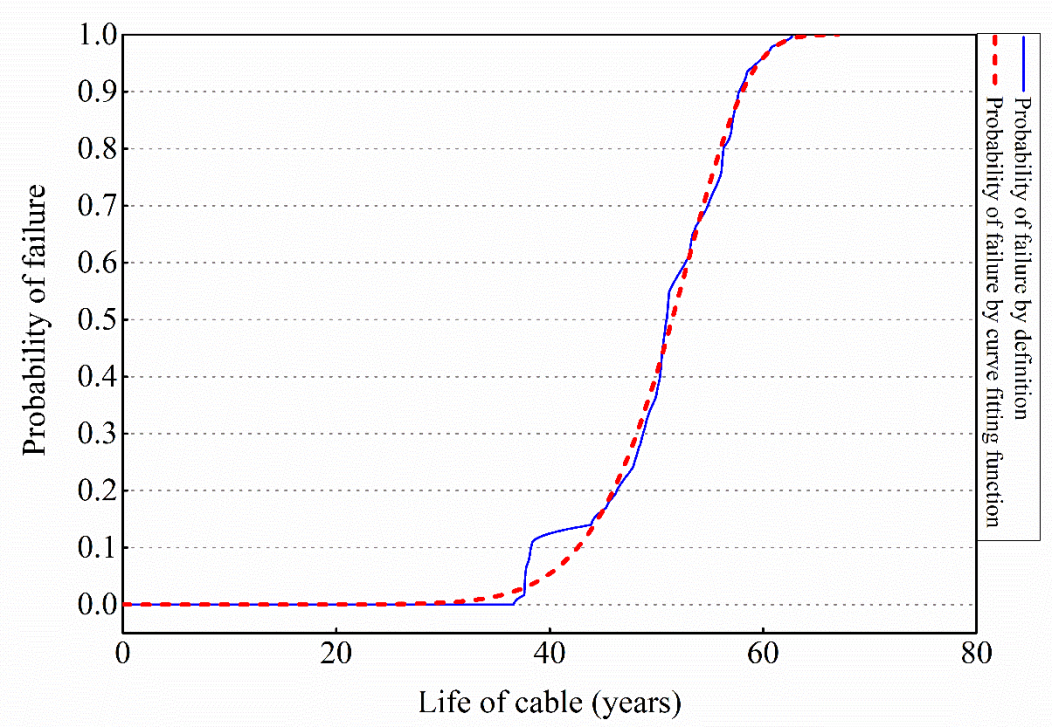

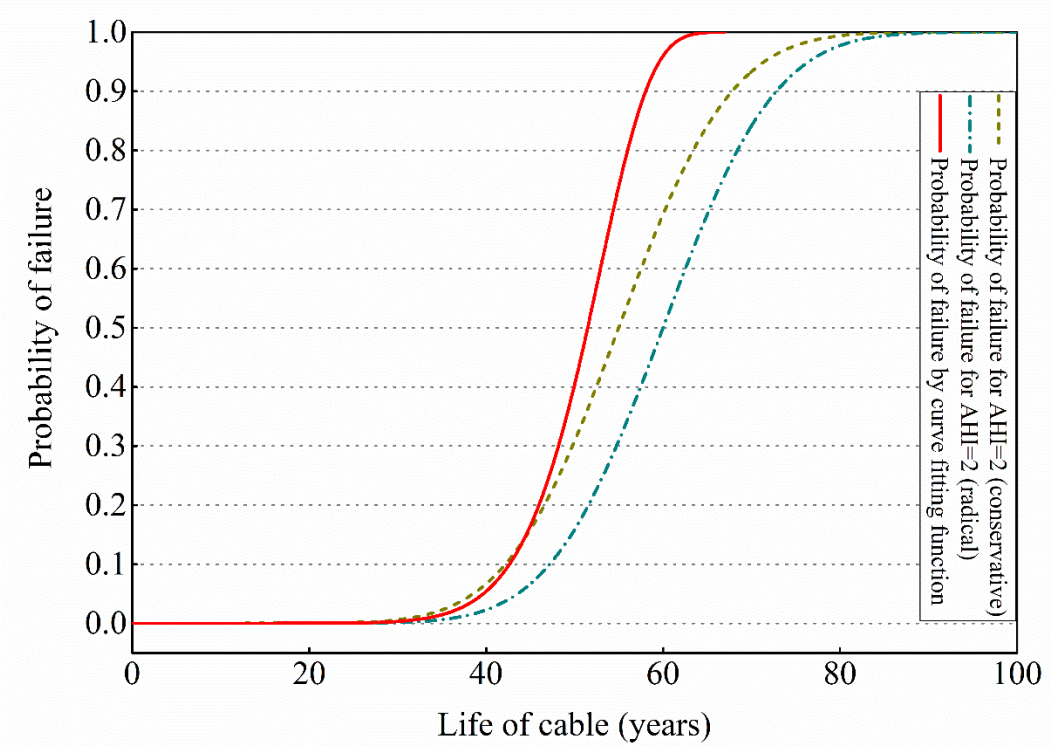

Figure 5-16: The probability of failure for Cable 1 under the definition from the mechanism-based model (Upper) The fitted function comparing to the conservative and liberal probability of failure function by empirical-based model (Lower)

In this chapter two models relating to the probability of failure for power cables are developed. An empirical-based model which is concluded from the application of the power supplement industry, this model is developed by summarizing the parameters of the existing normal distribution. A mechanism-based model is developed based on the pit depth distribution and the pit to crack transfer probability model which provided the estimation of crack propagation time, this model is developed based on a developed phosphor bronze tape entire failure model and a simulation using statistical distribution.

6. A machine-learning algorithm approach on power cable probability of failure updating

In this chapter, the mechanism-based probability of failure model is combined with the empirical-based probability of failure model using a common algorithm in the machine learning field - the Bayesian Inference algorithm. Following the results in Chapter 3, Chapter 4 and Chapter 5, the procedure of the algorithm to update the old model to achieve more accurate predictions of cable failure rate is shown in the following sections.

6.1 Fundamental Bayesian Inference modelling

Bayesian Inference is an application of Bayes' theorem [157], which can be written in this general format:

$$P(A|B) = \frac{P(B|A)P(A)}{P(B)} - - - - - - (6-1)$$

In this function:

- $P(A)$ is the prior probability, which is an estimation of probability of event A before the data of event B is observed. It is also called the marginal probability of event A.
- $P(B)$ is considered as the prior probability of event B without the influence of event A. It is also called the marginal probability of event B.
- $P(B|A)$ is the conditional probability of event B given the information of event A. It is the posterior probability of event B given the observation of event A.
- $P(A|B)$ is the conditional probability of event A given the information of event B. It is the posterior probability of event A given the observation of event B.

Chapter 5 described two probabilities of failure models. Both are continuous functions with time as the only variable. With regard to the continuous functions, the Bayesian

Inference function has another format of expression [158]:

$$p(\theta|y) = \frac{p(\theta)p(y|\theta)}{p(y)} - - - - - - (6-2)$$

Where

$$p(y) = \int p(\theta)p(y|\theta)\, d\theta - - - - - (6-3)$$

Substituting Equation (6-3) into (6-2), it can be concluded that under the condition of continuous function, the Bayesian Inference function is:

$$p(\theta|y) = \frac{p(\theta)p(y|\theta)}{\int p(\theta)p(y|\theta)\, d\theta} - - - - - (6-4)$$

The explanation of each term from the above function is shown as follows for the feasibility of its application in this research:

- $p(\theta)$ represents the probability density function derived from the probability of failure function, concluded from the empirical model applied by industry. It is a prior probability where the evidence of data was not observed or not clear.
- $p(y|\theta)$ is the probability density function derived from the probability of failure function, concluded from the mechanism-based model from Chapter 5. This conditional probability can be interpreted as follows: given the documented critical underground power cable information θ, the novel probability with new observed information y (specifically, the up to date research results in [5, 6]).
- The rest of the terms can be calculated. The difficulty is to calculate the marginal likelihood $\int p(\theta)p(y|\theta)\, d\theta$, where it is an integration of a complex function. This complicated integration requires a set of algorithms and will be discussed in the Section 6.3.

6.2 Probability density function models

From the description of section 6.1, the requirement of both functions $p(\theta)$ and $p(y|\theta)$ is that they shall both be probability density functions. Due to this requirement, the PoF functions in Chapter 4 are all transferred into probability density functions.

6.2.1 PDF for empirical-based model

As stated previously in Chapter 5, the empirical PoF model is described as the cumulative distribution function of the normal distribution with a range for each Asset Health Index evaluation. The parameters for criticality severe evaluated cables in a conservative estimation are:

$$parameters\ for\ criticality\ severe_{conservative}: \begin{cases} \mu = 50 \\ \sigma = 10 \end{cases} ----(6-5)$$

The parameters for criticality severe evaluated cables in a liberal estimation are:

$$parameters\ for\ criticality\ severe_{liberal}: \begin{cases} \mu = 52 \\ \sigma = 10 \end{cases} ----(6-6)$$

And the parameters for criticality light evaluated cables in a conservative estimation are:

$$parameters\ for\ criticality\ light_{conservative}: \begin{cases} \mu = 55 \\ \sigma = 10 \end{cases} ----(6-7)$$

The parameters for criticality light evaluated cables in a liberal estimation are:

$$arameters\ for\ criticality\ light_{liberal}: \begin{cases} \mu = 60 \\ \sigma = 10 \end{cases} ----(6-8)$$

The general form of the probability density function (PDF) of normal distribution is

given again here:

$$PDF = \frac{1}{\sqrt{2\pi\sigma^2}} e^{-\frac{(x-\mu)^2}{2\sigma^2}} ----(6-9)$$

With the above information, the PDF function for both AHI=1 cables and AHI=2 cables in conservative and liberal estimation can be written in the following functions:

$$\begin{cases} PDF_{Severe\ Criticality_{conservative}} = \frac{1}{\sqrt{2\pi\sigma_{typical}^2}} e^{-\frac{(x-\mu_{typical})^2}{2\sigma_{typical}^2}} \\ PDF_{Severe\ Criticality_{liberal}} = \frac{1}{\sqrt{2\pi\sigma_{typical}^2}} e^{-\frac{\left((x-2)-\mu_{typical}\right)^2}{2\sigma_{typical}^2}} \\ PDF_{Light\ Criticality_{conservative}} = \frac{1}{\sqrt{2\pi\sigma_{typical}^2}} e^{-\frac{\left((x-5)-\mu_{typical}\right)^2}{2\sigma_{typical}^2}} \\ PDF_{Light\ Criticality_{liberal}} = \frac{1}{\sqrt{2\pi\sigma_{typical}^2}} e^{-\frac{\left((x-10)-\mu_{typical}\right)^2}{2\sigma_{typical}^2}} \end{cases} ----(6-10)$$

6.2.2 PDF for mechanism-based model

From the results in Chapter 5, the PoF by mechanism-based model is in the cumulative density function format of the Weibull distribution, which for Cable 1 and Cable 2 the PoF functions are as follows:

$$\begin{cases} PoF_{Location\ 2} = 1 - e^{-\left(\frac{x}{46.24}\right)^{15}} \\ PoF_{Location\ 7} = 1 - e^{-\left(\frac{x}{53.52}\right)^{10}} \end{cases} ----(6-11)$$

The PDF of the Weibull distribution is in the general format of:

$$f(x|\lambda,k)=\begin{cases}0 & x<0\\ \frac{k}{\lambda}\left(\frac{x}{\lambda}\right)^{k-1}e^{-\left(\frac{x}{\lambda}\right)^{k}} & x\geq 0\end{cases}\quad -----\ (6-12)$$

- $\lambda\ is\ the\ scale\ factor$
- $k\ is\ the\ shape\ factor$

It can be concluded that based on the fitted parameters given in function set (6-11) the PDF of both Cable 1 and Cable 2 PoF functions are as:

$$\begin{cases}PDF_{Cable\ 1}=0.187\times\left(\frac{t}{53.52}\right)^{9}\times e^{-\left(\frac{t}{53.52}\right)^{10}}\\ PDF_{Cable\ 2}=0.325\times\left(\frac{t}{46.24}\right)^{14}\times e^{-\left(\frac{t}{46.24}\right)^{15}}\end{cases}----(6-13)$$

6.3 Assumptions and results of Bayesian Inference modelling

To simplify the expressions, here in, the probability of failure models stated in previous sections are replaced by:

$$\begin{cases}Empirical\ \ Probability\ of\ Failure\ Model\ PDF=F(t)\\ Mechanism-Based\ Probability\ of\ Failure\ Model\ PDF=G(t)\\ Updated\ Probability\ of\ Failure\ Model\ PDF=U(t)\end{cases}--(6-14)$$

The Bayesian Inference model stated in Section 6.1 therefore is written as:

$$U(t)=\frac{F(t)G(t)}{\int F(t)G(t)dt}-----(6-15)$$

In Equation (6-15), the terms $F(t)$ and $G(t)$ are known. The difficulty exists for the

calculation of denominator in Equation (6-15): with the multiplication of two functions, $F(t)$ being an exponential function and $G(t)$ a rational function, the analytical solution is hard to obtain. Instead, a numerical algorithm is applied to solve the problem as stated in the following sections.

6.3.1 Markov Chain Monte Carlo (MCMC) method

In this section, the purpose of the algorithm is to calculate the value of the denominator in Equation (6-15). Rewriting the denominator of Function (6-15):

$$D = \int F(t)G(t)dt \; ----- (6-16)$$

Under the strong law of large numbers (LLN) and the central limit theorem (CLT), when the numbers of sampling from the domain of t are very large and fulfil the requirement of independent sampling from function $F(t)$,the value of the integration is approximately the expectation of function $G(t)$, which can be expressed as:

$$D = \int F(t)G(t)dt = E[G(t)] \approx \frac{1}{N} \cdot \sum_{i=1}^{N} G(t_i) \; ----- (6-17)$$

The algorithm applied here to withdraw independent sampling from the function $F(t)$ is the random walk Metropolis Hastings algorithm. These steps were followed to construct the sequential independent sampling:

1) Initialise state $X_0 = [t_0]$ arbitrarily, the purpose is to construct a Markov chain containing states $X_0, X_1, X_2, \cdots, X_N \in \mathcal{X}$.
2) Let $x, x' \in \mathcal{X}$ are states in the Markov chain, propose an initial distribution $r(x'|x)$, in order to construct the Markov chain. The proposed distribution must satisfy detailed balance, where a factor $l(x'|x)$ can enable that

$$r(x'|x)f(x)l(x'|x) = r(x|x')f(x') ----(6-18)$$

In fact, this factor $l(x'|x)$ can be solved as:

$$l(x'|x) = min\left\{1, \frac{r(x|x')f(x')}{r(x'|x)f(x)}\right\} ----(6-19)$$

Define a factor in Equation (8-19) as:

$$\alpha = \frac{r(x|x')f(x')}{r(x'|x)f(x)} ----(6-20)$$

Where α is called the acceptance rate for state transfer. The acceptance rate for a successful construction of Markov Chain is around 23.4% [159]. In this current algorithm, the proposed distribution $r(x'|x)$ is set to be a Gaussian distribution which is a symmetric distribution. Only with this condition the acceptance ratio α from Function (6-20) can be simplified as:

$$\alpha = \frac{f(x')}{f(x)} ----(6-21)$$

3) Simulate a random number U from a uniform distribution $U(0,1)$, if $U < l(x'|x) = min\left\{1, \frac{f(x')}{f(x)}\right\} = min\{1, \alpha\}$, then transfer state x to state x', otherwise state x stays at x for the next round.
4) Repeat the steps from initial state $X_0 = [t_0]$ in Step 1) to Step 3) for N rounds, until the samplings become stable and convergent, these states $X_0, X_1, X_2, \cdots, X_N$ form a Markov chain independent sequential sampling from function $F(t)$.

With the above independent sequential samplings from $F(t)$, the integration result in Equation (6-17) can be obtained.

Supplied with the working example from values of parameters in Cable 1, the pit-crack transfer pit depth is $x_{transfer} = 115\ \mu m$. And the above Bayesian Inference algorithm is applied as an example to update the original Cable 1 liberal estimation of the probability of failure model. The sequential samplings in the above steps corresponding to $F(t)$ is shown in Figure 6-1, which is an example of the samplings with 10000 values. The red points are the accepted samplings for 1 trial. They are then all taken out

and form one sequence of independent sampling which is also plotted in Figure 6-2.

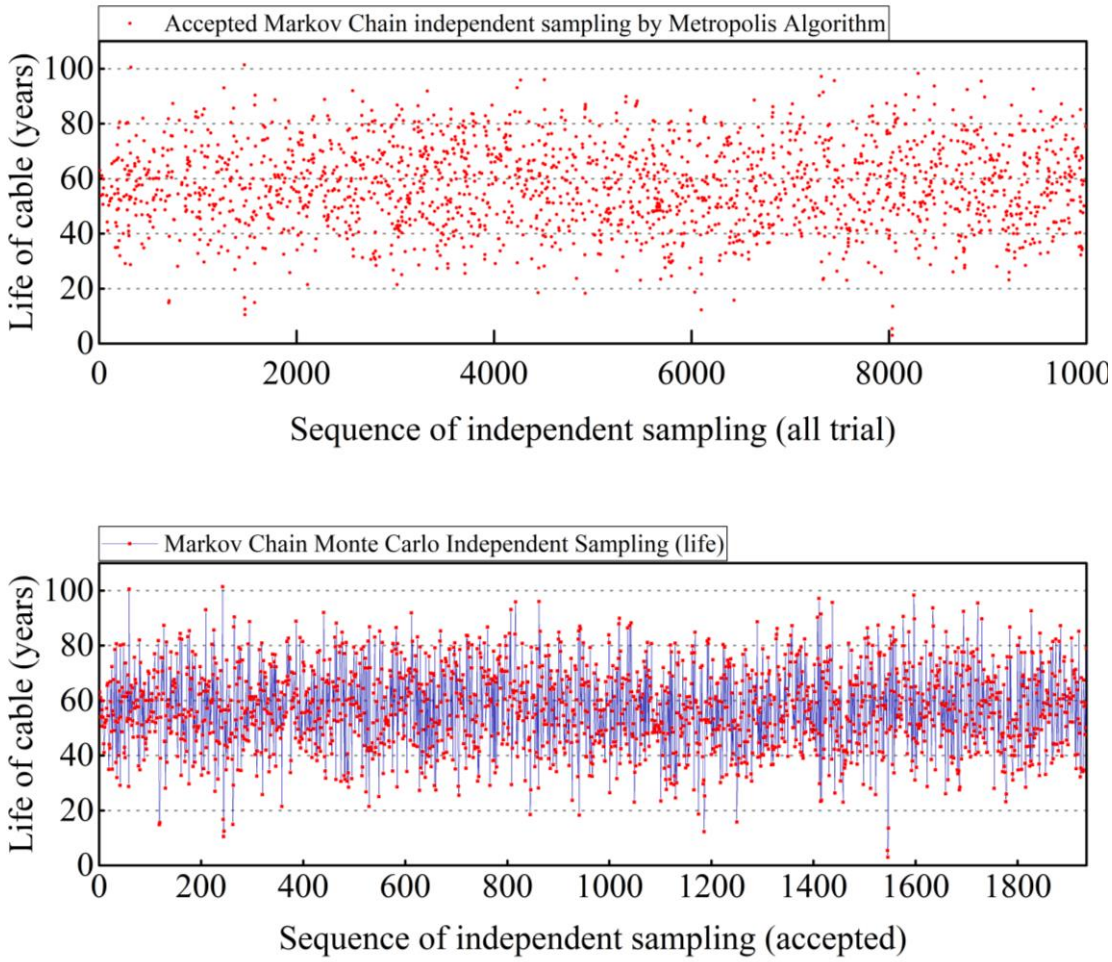

Figure 6-1: One trial of Markov Chain construction by Metropolis Hastings algorithm sampling with trial elements of 10000, among which only the accepted values are plotted (upper)Fluctuation of all the accepted values (bottom)

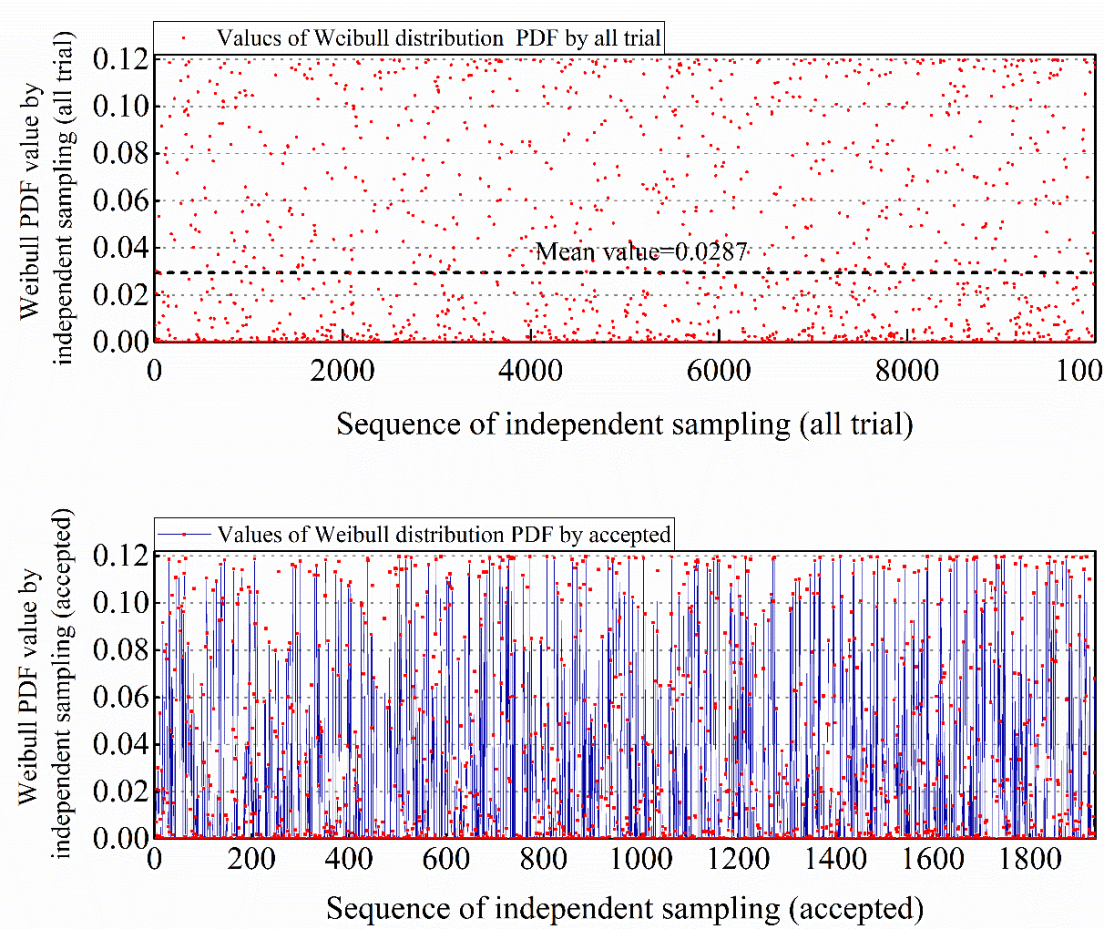

Figure 6-2: Values of $G(t_i)$ corresponding to the samplings shown in Figure 7

Due to the randomness of the Monte Carlo algorithm, the results appear to be different at small scale with each array of sequential sampling. To balance this randomness and achieve convincing and stable results, the above steps of samplings are carried out 1000 times in order to obtain an average value for the expected value of $G(t_i)$; the result is: $D \approx 0.0287$.

6.3.2 Expression of the Bayesian Inference updated model

Taking the result of the denominator and substituting the value of D into Equation (6-15), the result is the Bayesian Inference probability density. Shown as an example in Figure 6-5 is the plot of the Bayesian Inferenced probability density function for the liberal estimation.

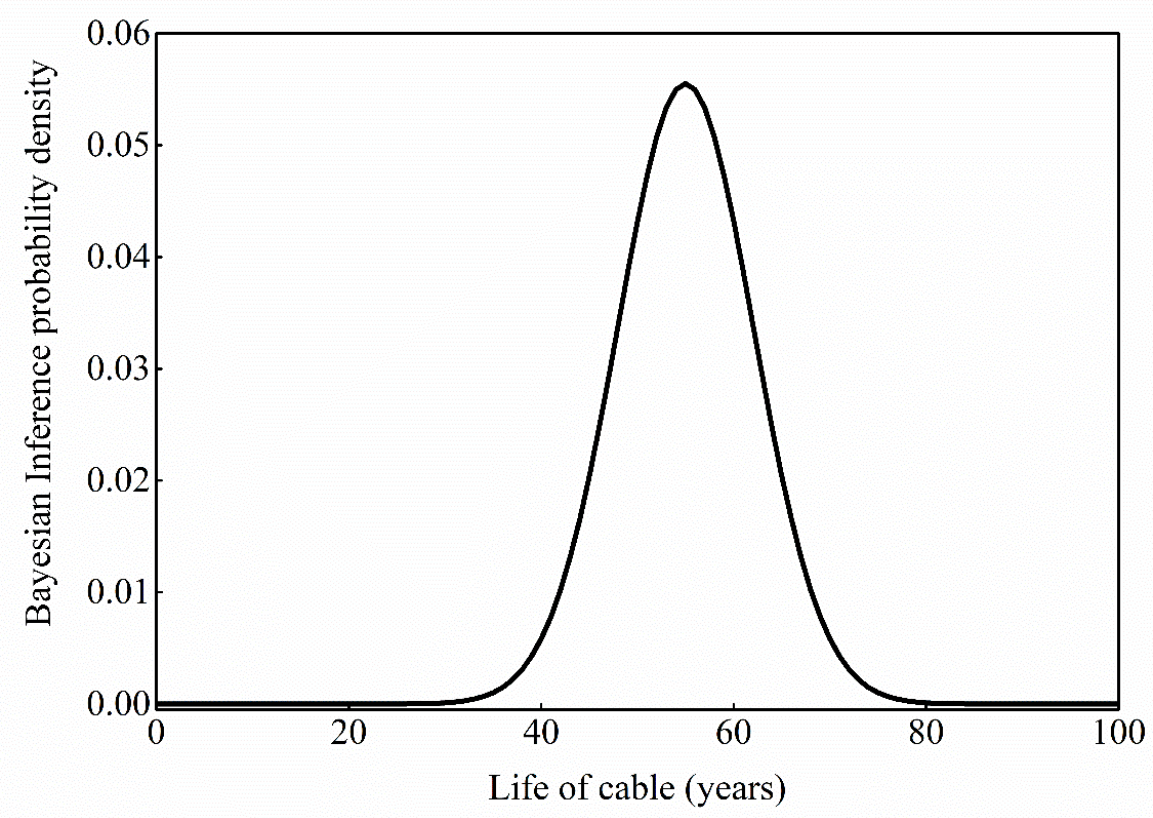

Figure 6-3: The plot of the Bayesian Inferenced probability density function of the liberal estimated model of Cable 1

When applying another curve fitting for which the result is a Gaussian distribution, the probability density function is written as follows:

$$U(t)_{Cable\ 1\ conservative} \approx 0.0559 \times e^{-\frac{(t-55)^2}{2\times 7.16^2}} \quad ----(6-22)$$

This leads to the updated probability of failure function as:

$$PoF_{Update\ Cable\ 1\ conservative} \approx \int 0.0559 \times e^{-\frac{(t-55)^2}{2\times 7.16^2}}\ dt ----(6-23)$$

The calculation of the updated PoF function for liberal estimation in Cable 1, both the conservative and liberal updated PoF function for Cable 2 are shown in Table 6-1.

Table 6-1: 'Tailored probability of failure function' for all critical locations

Location	'Tailored probability of failure function'
Cable 1 (Conservative)	$PoF_{Update\ Cable\ 1\ conservative} \approx \int 0.0559 \times e^{-\frac{(t-55)^2}{2\times 7.16^2}}\ dt$
Cable 1 (Liberal)	$PoF_{Update\ Cable\ 1\ liberal} \approx \int 0.0616 \times e^{-\frac{(t-60)^2}{2\times 6.49^2}}\ dt$
Cable 2 (Conservative)	$PoF_{Update\ Cable\ 2\ conservative} \approx \int 0.0548 \times e^{-\frac{(t-50)^2}{2\times 7.3^2}}\ dt$
Cable 2(Liberal)	$PoF_{Update\ Cable\ 2\ liberal} \approx \int 0.0571 \times e^{-\frac{(t-52)^2}{2\times 7^2}}\ dt$

6.4 Explanation of the Bayesian Inferenced models

The two plots shown here, Figure 10 and Figure 11, provide a comparison among the original conservative/liberal estimation and the updated conservative/liberal estimation for both Cable 1 and Cable 2.

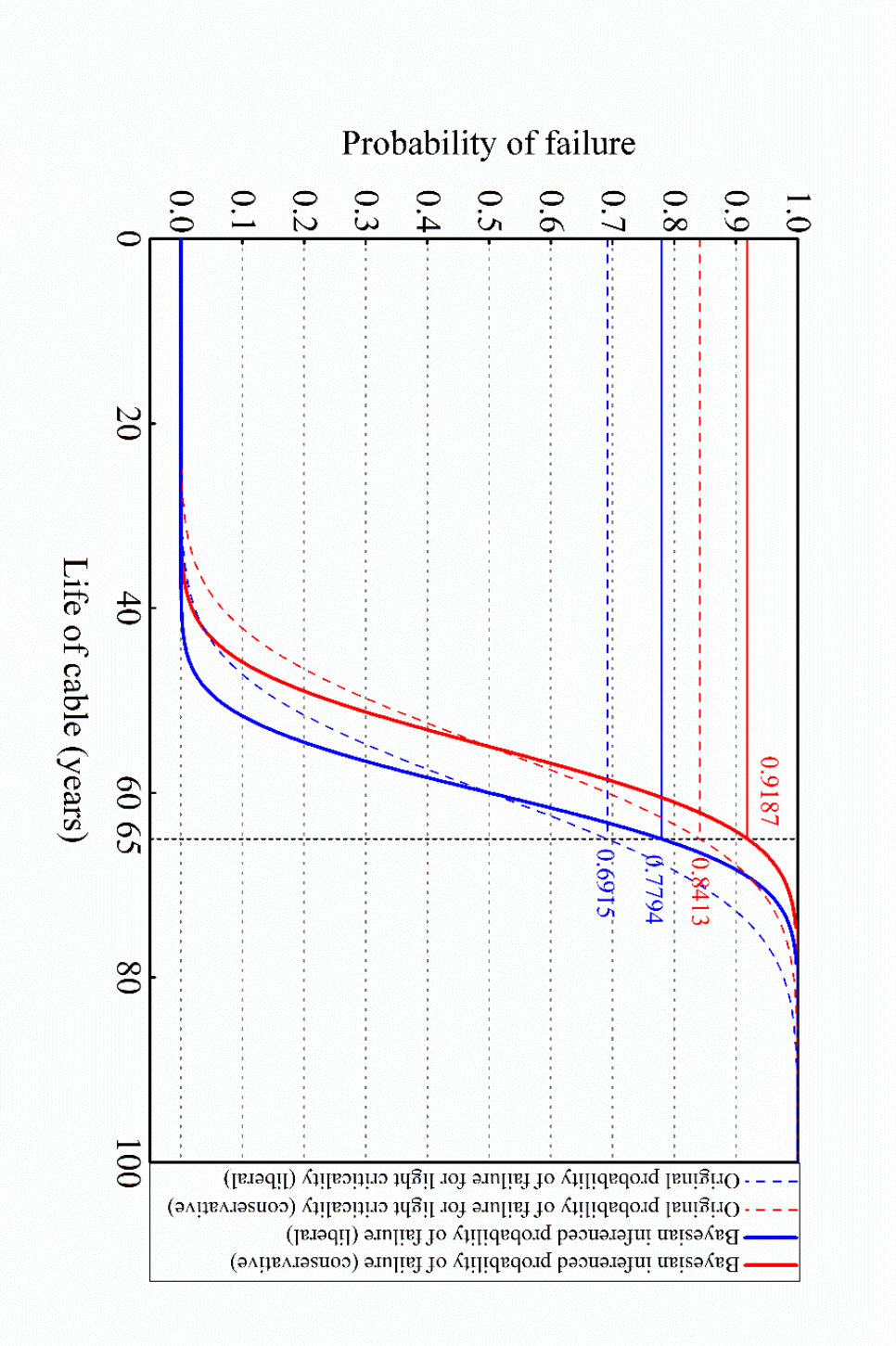

Figure 6-4: Comparison of Bayesian Inferenced model and original industrial replacement priority model for probability of failure estimation (both conservative and liberal of Cable 1)

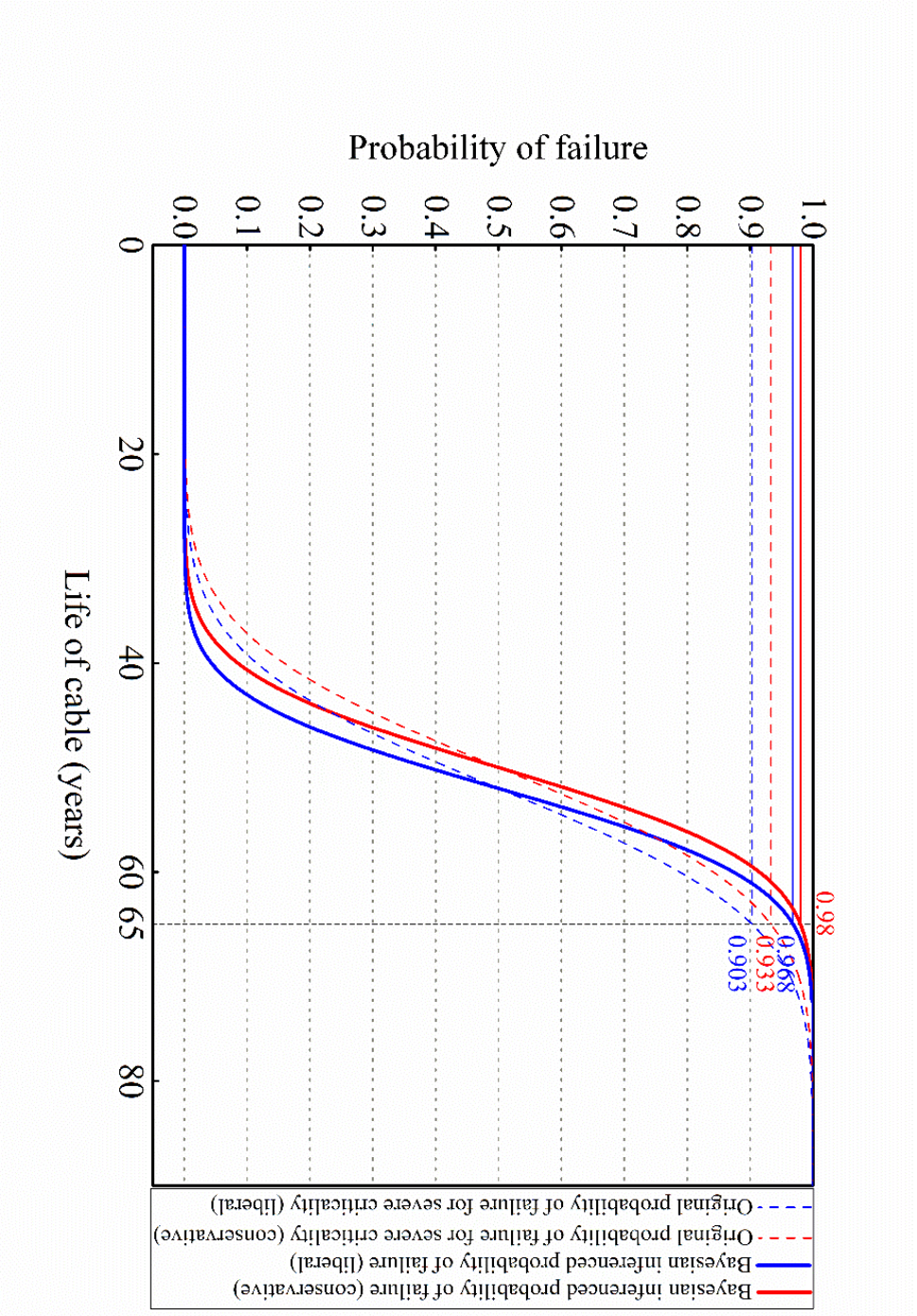

Figure 6-5: Comparison of Bayesian Inferenced model and original industrial replacement priority model for probability of failure estimation (both conservative and liberal of Cable 2)

Take the service age of 65 years as an example, for both locations, with the cable reaching higher servicing life, the probability of failure increases rapidly and are reaching higher probability values compared to the existing model. While for the relatively short service age, these are of lower probability of failure compared to the existing model. This result shows the updated model after one round of new research-based information being input into the original model and it shows the development trend of such a statistical evaluation model with the learning process. The purpose to introduce this learning model is that, with potentially large amounts of data being available in the industry, this algorithm can learn to evolve itself by adapting to any formats of further input. Thus, this algorithm can always give an output of evaluation of engineering assets based on the most complete sets of available data sources. This will enable a more versatile solution to asset management decision making than the current fixed evaluation model.

7. Conclusions

In this final chapter, conclusions are given to summarize the results and achievements of this PhD research.

7.1 Conclusion on modelling the pit depth distribution (Chapter 3)

In Chapter 3 the research focused on the pitting corrosion effect of the phosphor bronze used in underground electricity cables and the major outcomes. Reinforcing phosphor bronze tape, which was under commission for decades, was used to get pit depth distribution using the metallographic method. This data is valuable as very few studies exist on the pitting corrosion of phosphor bronze material. Pit depth is modelled using a power law and by using Monte-Carlo simulation and statistical methods. The pit growth parameter α follows a three parameter GEV distribution, and β as a fixed value of 0.33. The simple power law combined with the distribution can capture the evolution of pit growth, with validation case using two reinforcing tape samples extracted from the same site at two different years. The power law can successfully simulate pit depth distribution at different environment conditions.

7.2 Conclusion on modelling pit growth and pit to crack transfer probability (Chapter 4)

In summary, Chapter 4 provided further insights into the entire failure process of the phosphor bronze tape in underground power transmission cables. Following an accurate Monte Carlo simulation on pit depth distributions, a probability description of pitting corrosion to crack propagation probability transfer function is introduced in this study. A pit depth distribution model is developed. Combined with the author's previous research results on pit depth distribution on specific years [6], this study provides a

model that can describe pit depth distribution for any requested point in time. An equation of the crack propagation in reinforced tin-bronze tape is given, under the assumption of a high mean stress and a relatively low alternating stress, for which all parameters are fixed numerically. A function of the pitting corrosion to crack propagation probability is given using the cumulative distribution function of the Weibull distribution, with all parameters are fixed numerically. A proposal for applying this $'Pit\ initiation \rightarrow Pitting\ Corrosion \rightarrow Pit - crack\ transfer \rightarrow Crack\ propagation \rightarrow Failure'$ whole process analysis to the prediction of underground power transmission cable service life is raised.

7.3 Conclusion on modelling power transmission cable probability of failure (Chapter 5) and a machine learning approach (Bayesian Inference) to power cable probability of failure (Chapter 6)

The combined research of Chapter 5 and Chapter 6 introduced the Bayesian Inference method in combining two probability of failure models for underground power transmission cables, one being the empirical model from the industry being introduced by KEMA, based on prior experience and knowledge, the other one being the mechanism-based model which was recently developed [5, 6] based on the corrosion fatigue mechanism on phosphor bronze protection layers in cables. This combination enables a 'Tailored probability of failure' model for each cable locations. The 'Tailored probability of failure model' is of higher accuracy in estimating the probability of failure for two reasons: 1. The updated model has a more complete background information compared to the previous model. With a deeper understanding of the failure mechanism, this model fits the phenomenon of failure cases better. 2. The updated model is 'tailored' to different locations. Instead of using a universal model for all locations, this model enables the distinction of the divergent conditions at the different cable locations, and is thus more suitable for estimations.

The Bayesian Inference method applied in Chapter 6 to engineering problems creates the concept of ‘Intelligent Assets’. This concept is based on the fact that the aging and failure control is dynamic with the continuous updating of knowledge and information from the asset itself. Similar to machine learning, this is the assets’ ‘self-learning’. With each input of further information, the decisions on asset management become more accurate.

Future Work:

The newly created concept of the underground power grids ‘self-update’ in order to give a most up-to-date estimation of the probability of failure throughout its service life, introduced in this thesis, requires a continuous input of the experimental corrosion data. This study has discussed the updating of cables which started the commissions in the 1960s to 1970s, as these cables are critical at the current moment. The same research approach can be applied to all power grids containing the most recent instalments in order to give not only engineering reliability advices, but also support the decision making from a financial perspective.

Overall, this research is to provide consultancy on engineering asset management, in the decision making on strategies towards existing cables. Whether to repair a cable section, exchange a cable section or replace the entire cable line is based on the confidence to predict the probability of failure of the power cables. This leads to a significant difference in the investment of the power companies, the government and also influences greatly on the civilian’s expenses on energy resources. By applying the ‘Intelligent Asset’ approach on all power cables, it will enable a more economically accurate decision making, which will benefit all parties.

Appendix I

Working example of the DNO common network asset indices methodology [12]

Ofgem is the short form of Office of Gas and Electricity Markets and it acts as the government regulator for the electricity and downstream natural gas markets in Great Britain. In this section the asset management approach by Ofgem is introduced and to help with the understanding of the entire process, a working example is also given. The Ofgem document is published with open access which can be downloaded from its official website, but it is also attached with this thesis as a supporting document in the USB/CD submitted along with this thesis. In the following working example, all the values extracted from this document is referenced with the original page numbers and table labels for a clear rundown to follow.

As stated previously, the evaluation of cable conditions by the DNO common network asset indices methodology follows 9 steps:

1) General probability of failure
2) Normal expected life
3) Expected life
4) β_1 (initial ageing rate)
5) Initial health score
6) Current health score
7) β_2 (forecast aging rate)
8) Future health score - deterioration
9) Calculation of current and future probability of failure

This chapter is based on cable data of Location 1 mentioned in Chapter 3, for which one failure case was detected after 38 years of servicing. Following the steps of evaluation, details are given below for the working example. When referencing a certain page of the 'DNO common network asset indices methodology', this document is mentioned as 'Code' for simplification.

Step 1: General probability of failure

From the Design Code, the possibility of failure is calculated as (Code, p.30)

$$PoF = K \times \left[1 + (C \times H) + \frac{(C \times H)^2}{2!} + \frac{(C \times H)^3}{3!}\right]$$

By observation of this mathematical expression, it is easy to recognize as the Taylor Series Expansion of an exponential function, with the first four terms kept. C is a constant that controls the shape of the curve and H represent the Health Score.

Where :

- $If\ Health\ Score > 4, then\ H =$

$Health\ Score\ (Current\ or\ Future)$

- $If\ Health\ Score \leq 4, then\ H = 4$
- $K\ and\ C\ are\ constants$

The Value of both K and C are to the Code Table 21 in Appendix B (Code, p.106). From this it can be concluded that for *Pressurized Cable (EHV UG Cable (Oil) and 132 kV UG Cable (Oil))*, K-value is 2.0944%, C-value is 1.087 and Health Score Limit is 4.

Step 2: Normal Expected Life

Normal Expected Life is to be found in Table 20 Appendix B of the Code, corresponds to a Health Score of 5.5.

For *33kv UG Cable (Oil) with Lead sheath-Copper conductor*, *66kv UG Cable(Oil) with Lead sheath- Copper conductor* and *132kv UG Cable(Oil) with Lead sheath- Copper conductor*, the Normal Expected Life are all 80 years.

Step 3: Expected Life

The Expected Life calculation involves the Location Factor and the Duty Factor, and the calculation method is (Code, p.32)

$$Expected\ Life = \frac{Normal\ Expected\ Life}{(Duty\ Factor \times Location\ Factor)}$$

As in previous Step 2 the Normal Expected Life is 80 years.

$$\therefore Expected\ Life = \frac{80}{(Duty\ Factor \times Location\ Factor)}$$

Calculation of Location Factor

The general Location Factor consists of four different aspects, including:

v) Distance from coast factor

vi) Altitude factor

vii) Corrosion category factor

viii) Environment factor (indoor/outdoor)

The Distance from Coast Factor can be found in Table 22 (Code, p.106)

As the underground cable shall not be influenced by the distance from coast, it is chosen as default and equals to 1.

The Altitude Factor can be found in Table 23 (Code, p.107)

As the underground cables are buried and so should not be influenced by the altitude, therefore, the default value is also chosen here as 1.

The Corrosion Category Factor can be found in Table 24 (Code, p.107).

Although no category listed in the table fits the underground cable environment for corrosion, the underground environment is complicated, and can vary from the lowest value to the highest value. In this working example, three values are chosen for the

evaluation of cable in Location 1, the lower limit value of 0.75, the upper limit value of 1.6 and the typical default value of 1.

Represented by the group:

$$\begin{cases} Corrosion\ Factor_{min} = 0.75 \\ Corrosion\ Factor_{max} = 1.60 \\ Corrosion\ Factor_{typ} = 1.00 \end{cases}$$

The Environment Factor is determined directly as the underground power transmission cables are buried outdoor.

After obtaining all the necessary values for the Location Factor determination, under the Environment Factor classified as 'Outdoor', the calculation of Location factor is as follows in two categories (Code, p.43):

3) If the maximum of the Distance From Coast Factor, Altitude Factor and Corrosion Factor is greater than 1, which in this study case would be when $Corrosion\ Factor_{max} = 1.60$, then

$$Location\ Factor$$
$$= MAX(Distance\ From\ Coast\ Factor, Altitude\ Factor, Corrosion\ Factor)$$
$$+ \Big(\big((COUNT\ of\ factors\ greater\ than\ 1) - 1\big) \times INC\Big)$$

Here in this example only one factor is greater than one, INC in the above equation represents for Increment Constants, and can be found in Table 25 (Code, p.107). Except the Switchgear, Transformers, Submarine Cables which has an INC of 0.05, the rest of the infrastructures are with an INC of 0, as with the study of underground cables, the INC is 0.

Condition 1:

$$Location\ Factor_{Condition\ 1} = 1.6$$

4) If the maximum of the Distance From Coast Factor, Altitude Factor and Corrosion Factor is not greater than 1, which in this study case would be when $Corrosion\ Factor_{min} = 0.75$ and $Corrosion\ Factor_{typ} = 1.00$ then

$$Location\ Factor = MIN(Distance\ From\ Coast\ Factor, Altitude\ Factor, Corrosion\ Factor)$$

Here

$$Location\ Factor_{Condition\ 2} = 0.75$$

And

$$Location\ Factor_{Condition\ 3} = 1$$

Calculation of Duty Factor (Code, p47)

For the Duty Factor calculation, when dealing with cables, there are two duty factors to be considered, DF1 and DF2. The calculation for Duty Factor with both DF1 and DF2 is as follows (Code, p.48):

$$Duty\ Factor = 0.5 \times DF1 + 0.5 \times DF2$$

The Duty Factor can be checked from Table 30 (Code, p.49)

For DF1, if the maximum utilization under normal operating conditions is lower than 50%, then the minimum value for DF1 can be obtained as 0.8, in the worst case if the utilization is over 100%, then the maximum value for DF1 can achieve 1.8, listed below as

$$\begin{cases} DF1_{min} = 0.8 \\ DF1_{max} = 1.8 \end{cases}$$

For DF2, if the value for Operating Voltage/Design Voltage is lower than 40%, then the minimum value for DF2 is 0.7, but in the worst case if the value is over 70%, then the value of DF2 can achieve 1.

$$\begin{cases} DF2_{min} = 0.7 \\ DF2_{max} = 1.0 \end{cases}$$

By the above two circumstances, upper boundary and lower boundary of the duty factor can be listed as,

$$\begin{cases} Duty\ Factor_{min} = 0.8 \times 0.5 + 0.7 \times 0.5 = 0.75 \\ Duty\ Factor_{max} = 1.8 \times 0.5 + 1.0 \times 0.5 = 1.40 \end{cases}$$

Sum up from the above calculations and the range of the expected life is:

$$\begin{cases} Expected\ Life_{min} = \dfrac{Normal\ Expected\ Life}{(Duty\ Factor_{max} \times Location\ Factor_{max})} = \dfrac{80}{1.40 \times 1.60} = 35.71\ years \\ Expected\ Life_{max} = \dfrac{Normal\ Expected\ Life}{(Duty\ Factor_{min} \times Location\ Factor_{min})} = \dfrac{80}{0.75 \times 0.75} = 142.2\ years \end{cases}$$

Step 4: β_1 Initial Ageing Rate

The equation calculating the initial ageing rate is as follows (Code, p.32):

$$\beta_1 = \frac{\ln\left(\frac{H_{expected\ life}}{H_{new}}\right)}{Expected\ Life}$$

Where:

- $H_{new}\ is\ the\ Health\ Score\ of\ a\ new\ assest, equal\ to\ 0.5$
- $H_{expected\ life} is\ the\ Health\ Score\ of\ the\ asset\ when\ it\ reaches\ its\ expected\ life, equal\ to\ 5.5$

Regarding to the above Expected Life range, there is also a range for the initial ageing rate, listed as

$$\begin{cases} \beta_{1max} = \dfrac{\ln\left(\frac{5.5}{0.5}\right)}{35.71} = 0.06715 \\ \beta_{1min} = \dfrac{\ln\left(\frac{5.5}{0.5}\right)}{142.2} = 0.01686 \end{cases}$$

Step 5: Initial Health Score

The calculation for the Initial Health Score is as (Code, p.32):

$$Initial\ Health\ Score = H_{new} \times e^{(\beta_1 \times age)}$$

Where:

- $H_{new}\ is\ the\ health\ Score\ of\ the\ new\ asset, equal\ to\ 0.5$
- $Initial\ Health\ Score\ is\ capped\ at\ a\ value\ of\ 5.5$
- $\beta_1\ is\ the\ initial\ ageing\ rate$
- $age\ is\ the\ current\ age\ of\ the\ asset\ in\ years$

With the working example calculated according to the properties of Location 1, this circuit of cable started commission in the year 1970, by the year within the period of the research project and this calculation was done 2016, in total it is already with 46 years of usage. The variable:

$$age = 46\ years$$

From this the upper and lower limit of the Initial Health Score are the following:

$$\begin{cases} Initial\ Health\ Score_{min} = H_{new} \times e^{(\beta_{1min} \times age)} = 0.5 \times e^{(0.01686 \times 46)} = 1.08590 \\ Initial\ Health\ Score_{max} = H_{new} \times e^{(\beta_{1max} \times age)} = 0.5 \times e^{(0.06715 \times 46)} = 10.9765 \end{cases}$$

As 10.9765 is over the capped Initial Health Score 5.5,

$$\therefore \begin{cases} Initial\ Health\ Score_{min} = H_{new} \times e^{(\beta_{1min} \times age)} = 0.5 \times e^{(0.01686 \times 46)} = 1.08590 \\ Initial\ Health\ Score_{max} = H_{new} \times e^{(\beta_{1max} \times age)} = Capped\ Value\ of\ IHS = 5.50 \end{cases}$$

Here a compromise had to be made according to the Code, which gave the upper limit of the Initial Health Score a shrink of around 50%. As the purpose of this working example is to discover the imperfection of the method mentioned in the Code, the calculation of the values which do not follow the capped option is also given for comparison. All the un-capped calculation results in this chapter will be shown in red.

Here if the Initial Health Score is not capped:

$$\begin{cases} Initial\ Health\ Score_{min} = H_{new} \times e^{(\beta_{1min} \times age)} = 0.5 \times e^{(0.01686 \times 46)} = 1.08590 \\ Initial\ Health\ Score_{max} = H_{new} \times e^{(\beta_{1max} \times age)} = 0.5 \times e^{(0.06715 \times 46)} = 10.9765 \end{cases}$$

The values in red colour shows the calculation results following the exact same procedures but not capped by any pre-set values, the purpose is to compare the extent of difference between the capped and un-capped results.

Step 6: Current Health Score

The current Health Score is modified from the Initial Health Score, the calculation for this is (Code, p.33):

$$Current\ Health\ Score = Initial\ Health\ Score \times Health\ Score\ Factor \times Reliability\ Factor$$

Where

$$IF\ Current\ Health\ Score > Health\ Score\ Cap$$
$$THEN\ Current\ Health\ Score = Health\ Score\ Cap$$

- Current Health Score is capped at 10

Then the Current Health Score is compared with the Health Score Collar (Code, p.34)

$$IF\ Current\ Health\ Score < MAX(Health\ Score\ Collar, Reliability\ Collar)$$
$$THEN\ Current\ Health\ Score = MAX(Health\ Score\ Collar, Reliability\ Collar)$$

To calculate the Current Health Score, the Health Score Factor, or the Health Score Modifier is determined by: (Code, p.49)

iii. Observed Condition Modifier
iv. Measured Condition Modifier

Each of the condition modifier would contain three elements:

iv. A Condition Input Factor
v. A Condition Input Cap
vi. A Condition Input Collar

As stated on (Code, p.60), there are no Observed Condition Inputs for cable assets other

than Submarine Cables. For these assets:

iv) The Observed Condition Factor shall be set to 1

v) The Observed Condition Cap shall be 10

vi) The Observed Condition Collar shall be 0.5

From (Code, p.62), the Measured Condition for both EHV cable (oil) and 132kV cable (oil) are 'Leakage'.

The Measured Condition Modifier, from Table 15 (Code, p.63), for both EHV cable (oil) and 132kV cable (oil),

$$\begin{cases} Factor\ Divider\ 1 = 1.5 \\ Factor\ Divider\ 2 = 1.5 \\ Max.No.of\ Combined\ Factors = 1 \end{cases}$$

The next step is to find out the maximum and minimum value for Measured Condition Input, from Table 172 (Code, p.142), for EHV Cable (Oil) under the condition of Leakage:

$$\begin{cases} Condition\ Input\ Factor_{min} = 1.0 \\ Condition\ Input\ Factor_{max} = 2.0 \end{cases}$$
$$\begin{cases} Condition\ Input\ Cap_{min} = 10 \\ Condition\ Input\ Cap_{max} = 10 \end{cases}$$
$$\begin{cases} Condition\ Input\ Collar_{min} = 0.5 \\ Condition\ Input\ Collar_{max} = 8.0 \end{cases}$$

From Table 179 (Code, p.143), for 132kV Cable (Oil) under the condition of Leakage

$$\begin{cases} Condition\ Input\ Factor_{min} = 1.0 \\ Condition\ Input\ Factor_{max} = 2.0 \end{cases}$$
$$\begin{cases} Condition\ Input\ Cap_{min} = 10 \\ Condition\ Input\ Cap_{max} = 10 \end{cases}$$
$$\begin{cases} Condition\ Input\ Collar_{min} = 0.5 \\ Condition\ Input\ Collar_{max} = 8.0 \end{cases}$$

It can be concluded that for the cables protected by oil the factors being used are the same.

After obtaining all the factors in the Health Score Factor section, a 'Combining Factors Using a Modified Maximum and Increment (MMI)' Technique is applied for the calculation of the real Health Score Factor. (Code, p.50 & 51)

(c) Calculating the minimum value for Health Score Factor

- $Var_1 = Minimum\ of\ Factors =$

$$\min_{condition\ factor}\left(\frac{Observation\ Factor}{Leakage\ factor}\right)=1.0$$

- $Var_2 = 2nd\ Lowest\ of\ Factors = 1$
- $Var_3 = \frac{Var_2 - 1}{Factor\ Divider\ 2} = \frac{0}{1.5} = 0$
- $Combined\ Factor_{min} = Var_1 + Var_3 = 1$

(d) Calculating the maximum value for Health Score Factor

- $Var_1 = Maximum\ of\ Factors =$

$$\max_{condition\ factor}\left(\frac{Observation\ Factor}{Leakage\ factor}\right) = 2.0$$

- $Var_2 = Excluding\ Var_1$
  - $For\ remaining\ Factors\ where\ (Factor - 1) > 0, which\ is\ another\ 1$
  - $Sum\ (Factor - 1)\ for\ the\ highest\ n - 1\ of\ these; where\ n =$ $Max.No.of\ Combined\ Factors, in\ this\ case, n = 1, \therefore$

$need\ to\ sum\ up\ in\ total\ of\ 0\ factors, which\ gives\ Var_2 = 0$

- $Var_3 = \frac{Var_2}{Factor\ Divider\ 1} = 0$
- $Combined\ Factor_{max} = Var_1 + Var_3 = 2.0$

The Reliability Factor (Code, p.69) has a value between 0.6 and 1.5 with a default value of 1, written as

$$\begin{cases} Reliability\ Factor_{min} = 0.6 \\ Reliability\ Factor_{max} = 1.5 \\ Reliability\ Factor_{dft} = 1.0 \end{cases}$$

The Reliability Collar is set to be 0.5.

Summing up this section, the range of current health score is

$$\begin{cases} Current\ Health\ Score_{min} = 1.08590 \times 1.0 \times 0.6 = 0.65154 \\ Current\ Health\ Score_{max} = 5.50 \times 2.0 \times 1.5 = 16.5 > Capped\ value\ 10 = 10 \end{cases}$$

If the Current Health Score is not capped here,

$$\begin{cases} Current\ Health\ Score_{min} = 1.08590 \times 1.0 \times 0.6 = 0.65154 \\ Current\ Health\ Score_{max} = 10.9765 \times 2.0 \times 1.5 = 32.9295 \end{cases}$$

Then the Current Health Score is compared with the Health Score Collar.

Since the minimum of the Health Score Collar and Reliability Collar are both 0.5, and the minimum value from the calculation is 0.65154>0.5, so the minimum value of the Current Health Score can be kept. Moreover, the maximum Health Score Collar is 8 and the maximum value of Reliability Collar is 0.5, and 10>8, so the maximum value of Current Health Score can also be kept as 10.

Step 7: β_2 (Forecast Ageing Rate)

It can be regarded that for the current asset the age is over 10 years (Code, p.34).

$$\beta_2 = \frac{\ln\left(\frac{Current\ Health\ Score}{H_{new}}\right)}{Age}$$

$$\therefore \begin{cases} \beta_{2_{min}} = \dfrac{\ln\left(\frac{Current\ Health\ Score_{min}}{H_{new}}\right)}{Age} = \dfrac{\ln\left(\frac{0.65154}{0.5}\right)}{46} = 5.755 \times 10^{-3} \\ \beta_{2_{max}} = \dfrac{\ln\left(\frac{Current\ Health\ Score_{max}}{H_{new}}\right)}{Age} = \dfrac{\ln\left(\frac{10}{0.5}\right)}{46} = 0.06512 \end{cases}$$

If the value here is not capped, then the Forecast aging rate is as follows:

$$\begin{cases} \beta_{2_{min}} = \dfrac{\ln\left(\frac{Current\ Health\ Score_{min}}{H_{new}}\right)}{Age \times Ageing\ Reduction\ Factor_{max}} = \dfrac{\ln\left(\frac{0.65154}{0.5}\right)}{46} = 5.755 \times 10^{-3} \\ \beta_{2_{max}} = \dfrac{\ln\left(\frac{Current\ Health\ Score_{max}}{H_{new}}\right)}{Age \times Ageing\ Reduction\ Factor_{min}} = \dfrac{\ln\left(\frac{32.9295}{0.5}\right)}{46} = 0.091 \end{cases}$$

Step 8: Future Health Score – Deterioration

The Future Health Score is calculated as (Code, p.36):

$$Future\ Health\ Score = Current\ Health\ Score \times e^{\left(\beta_2/r\right)\times t}$$

Where:

- $t\ is\ the\ number\ of\ future\ years$
- $Future\ Health\ Score\ is\ capped\ at$ 15
- r is the Aging Reduction Factor

The Aging Reduction Factor is found from Table 209 (Code, p.149)

- $IF\ Current\ Health\ Score < 2, THEN\ Ageing\ Reduction\ Factor_{min} = 1$
- $IF\ Current\ Health\ Score > 5.5, THEN\ Ageing\ Reduction\ Factor_{max} = 1.5$
- $IF\ 2 \leq Current\ Health\ Score \leq 5.5, THEN\ Ageing\ Reduction\ Factor_{max} = \frac{Current\ Health\ Score-2}{7} + 1$

As here it is a working example of the method, take 20 years from 2016 as the future prediction assumption for Location 1, the variable of years in the future $t_{future-Location\ 1}$ is as follows:

$$t_{future-Location\ 1} = 20\ years$$

$$\therefore \begin{cases} Future\ Health\ Score_{min} = Current\ Health\ Score \times e^{\left(\beta_{2min}/r_{max}\right)\times t_{future-Location\ 1}} \\ \qquad = 0.65154 \times e^{\left(5.755\times10^{-3}/1.5\right)\times 20} = 0.7035 \\ Future\ Health\ Score_{max} = Current\ Health\ Score \times e^{\left(\beta_{2max}/r_{min}\right)\times t_{future-Location\ 1}} \\ \qquad = 10 \times e^{\left(0.06512/1\right)\times 20} = 36.7811 > Capped\ 15 = 15 \end{cases}$$

If the values calculated in this section are not capped, the actual values are as follows:

$$\begin{cases} Future\ Health\ Score_{min} = Current\ Health\ Score \times e^{\left(\beta_{2min}/r_{max}\right)\times t_{future-Location\ 1}} \\ \qquad = 0.65154 \times e^{\left(5.755\times10^{-3}/1.5\right)\times 20} = 0.7035 \\ Future\ Health\ Score_{max} = Current\ Health\ Score \times e^{\left(\beta_{2max}/r_{min}\right)\times t_{future-Location\ 1}} \\ \qquad = 32.9295 \times e^{\left(0.06512/1\right)\times 20} = 121.1183 \end{cases}$$

Step 9: Calculation of Current and Future Probability of Failure

It can be observed from the above calculation that the distribution of the probability of failure is of the function

$$PoF = K \times \left[1 + (C \times H) + \frac{(C \times H)^2}{2!} + \frac{(C \times H)^3}{3!}\right]$$

And the health score H, as calculated above, if being capped, can be as low as H=4 and as high as H=15,

$$\begin{cases} PoF_{\min -20\ years\ future} = 59.7\% \\ PoF_{\max -20\ years\ future} = 1827.76\% \end{cases}$$
$$\therefore 59.7\% \leq PoF_{Year\ 2036} \leq 100\%$$

Form the maximum value of the probability of failure it can be seen that at 66 years after commission for the cable in Location 1, under the worst condition it cannot last until that age. But if the condition is good without much corrosion, it can maintain functional and have a probability of failure rate at 66 years for as low as 59.7%.

If the calculated value is not capped here, the values would be:

$$0.0804\% \leq PoF \leq 815000\%$$

Apparently until here the un-capped value does not make sense anymore, as the probability of failure cannot achieve anywhere beyond 100%, so the capped value is useful for the lower value of calculation, but cannot reflect the worst condition that happen on the power cables as the actual value is far more serious than 100%.

Appendix II

Table of matrixes in Chapter 5

Table 5-2: Coefficient matrix $\boldsymbol{A_1}$ for cubic spline curve fitting of Cable 1 mean stress vs length of cable data

Coefficient of x^3	Coefficient of x^2	Coefficient of x	Coefficient of constant term
-1.12E-07	0	0.029888	103.8308
1.39E-07	-7.95E-05	0.011122	109.4081
-4.14E-08	2.19E-05	-0.00288	109.4114
2.69E-08	-8.24E-06	0.00043	109.4095
-2.63E-08	1.11E-05	0.001128	109.4104
3.07E-09	-8.15E-06	0.001862	109.9698
1.44E-08	-5.82E-06	-0.00167	109.9699
9.07E-09	5.08E-06	-0.00185	109.41
-1.59E-08	1.19E-05	0.002426	109.4102
-9.07E-08	-1.08E-07	0.005416	110.5306
2.23E-07	-6.65E-05	-0.01084	110.5276
-5.44E-07	9.41E-05	-0.00425	107.1858
1.21E-06	-0.00031	-0.05584	103.8168
-1.42E-06	0.000631	0.028151	89.89969
8.53E-07	-0.00048	0.067382	115.143
-3.10E-07	0.00017	-0.01194	115.1687
8.64E-08	-6.28E-05	0.014791	117.947
1.25E-09	1.34E-06	-0.00042	119.0706
1.25E-09	2.29E-06	0.000494	119.07
-4.58E-08	3.21E-06	0.001852	119.3504
1.00E-07	-2.97E-05	-0.00449	119.3489
-1.46E-07	4.20E-05	-0.00156	117.9518
1.86E-08	-6.51E-05	-0.0072	117.9488

1.92E-07	-5.12E-05	-0.03628	112.3687
-4.86E-07	9.14E-05	-0.02633	103.1651
1.18E-06	-0.00025	-0.06469	95.6175
-1.77E-06	0.000564	0.006793	81.70213
1.83E-06	-0.00068	-0.02053	91.45303
-1.23E-06	0.000626	-0.03348	72.65294
4.36E-07	-0.00027	0.052197	83.77749
-1.04E-07	4.06E-05	-0.00369	86.58405
1.01E-07	-3.67E-05	-0.00273	86.57846
-1.19E-07	3.85E-05	-0.00228	85.18165
1.03E-07	-4.95E-05	-0.00501	85.17834
-4.13E-08	2.90E-05	-0.01023	82.39108
6.30E-08	-2.13E-06	-0.00346	80.99922
-1.25E-07	4.55E-05	0.007473	81.00141
1.90E-07	-5.07E-05	0.006146	83.78763
-2.05E-07	9.39E-05	0.017076	85.18296
9.99E-08	-6.06E-05	0.025435	92.15772
-2.76E-07	1.55E-05	0.01396	96.34282
7.57E-07	-0.0002	-0.03199	96.33226
-1.03E-06	0.000379	0.014506	87.98338
1.11E-06	-0.00043	0.002542	99.34395
-1.31E-06	0.000482	0.017823	90.98814
1.33E-06	-0.00058	-0.0102	105.1802
-8.09E-07	0.00048	-0.03796	86.14604
2.50E-07	-0.00015	0.047867	94.50206
-1.38E-07	4.46E-05	0.02071	101.2029

-3.86E-08	-5.97E-05	0.016895	107.0593
3.03E-07	-8.80E-05	-0.01922	107.0574
-4.54E-07	0.000139	-0.00661	101.4857
5.04E-07	-0.00021	-0.026	101.1928
-2.12E-07	0.000175	-0.03581	88.93536
-3.09E-07	1.14E-05	0.012438	87.74073
8.96E-07	-0.00024	-0.04778	85.97097
-1.32E-06	0.000488	0.019909	73.44661
2.09E-06	-0.00057	-0.0032	88.39446
-1.84E-06	0.000883	0.068643	82.86941
-5.77E-07	-0.00019	0.203222	116.3206
1.10E-06	-0.00053	0.062452	144.2174
-2.72E-07	0.000138	-0.0171	144.2403
7.20E-08	-3.66E-05	0.004547	144.2274
-1.87E-08	9.66E-06	-0.00122	144.2307
4.80E-09	-2.54E-06	0.000328	144.2298
-1.36E-09	6.86E-07	-8.57E-05	144.23
6.80E-10	-2.20E-07	1.79E-05	144.23
-7.07E-10	8.27E-08	-2.55E-06	144.23

Table 5-3: Coefficient matrix $\boldsymbol{A_2}$ for cubic spline curve fitting of Cable 2 mean stress vs length of cable data

Coefficient of x^3	Coefficient of x^2	Coefficient of x	Coefficient of constant term
-2.68E-07	0	0.01187	143.9927
-3.96E-07	-0.00017	-0.02376	143.9913
1.52E-06	-0.00042	-0.1478	127.7808
-1.16E-06	0.000636	-0.09776	90.0268
5.10E-07	-0.00025	0.000214	87.28334
-8.65E-08	0.000138	-0.02965	79.20596
-3.24E-07	7.15E-05	0.023955	79.20237
7.42E-07	-0.00018	-0.00308	84.58935
-1.54E-06	0.000392	0.051795	84.62277
1.82E-06	-0.00079	-0.04998	97.7765
-8.26E-07	0.000608	-0.09635	63.6664
8.55E-09	-2.49E-05	0.052723	64.98166
9.29E-08	-1.82E-05	0.04155	77.13916
-1.47E-07	5.20E-05	0.050081	87.9424
-4.84E-07	-5.84E-05	0.048483	101.4434
1.06E-06	-0.00044	-0.08187	101.4246
-5.13E-07	0.000384	-0.09624	69.05568
3.72E-07	-1.61E-05	-0.00087	60.94116
-1.19E-06	0.000277	0.067753	66.35557
1.42E-06	-0.00066	-0.03471	81.70391
-6.52E-07	0.00047	-0.08646	52.29075
9.33E-08	-4.03E-05	0.02538	50.10255
-1.52E-07	3.12E-05	0.023057	55.51245

1.92E-07	-8.53E-05	0.009246	60.90656
-1.33E-07	6.23E-05	0.003369	60.91325
1.81E-07	-3.90E-05	0.009265	63.60686
-2.49E-07	9.69E-05	0.023718	66.3143
1.24E-07	-9.00E-05	0.025444	74.40627
-7.93E-08	5.69E-06	0.003831	77.11203
5.40E-07	-5.60E-05	-0.00923	77.10381
-1.56E-06	0.000352	0.065092	79.83102
1.81E-06	-0.00082	-0.05055	93.70627
-7.98E-07	0.000578	-0.11157	57.62608
-1.32E-07	1.31E-05	0.027954	53.00334
3.78E-08	-7.44E-05	0.014388	58.40831
2.33E-07	-4.97E-05	-0.0126	58.40804
-2.20E-07	0.000103	-0.00091	55.71453
4.97E-08	-5.55E-05	0.010569	58.4073
2.22E-07	-1.93E-05	-0.00763	58.40828
-3.24E-07	0.000137	0.019886	58.41546
6.85E-08	-9.43E-05	0.02996	66.50608
2.74E-07	-4.47E-05	-0.00359	69.20795
-3.23E-07	0.000138	0.017231	69.21597
-1.28E-07	-5.04E-05	0.03431	75.41804
3.13E-07	-0.00013	-0.00208	79.2356
-1.90E-07	9.07E-05	-0.01086	75.73502
2.25E-07	-5.24E-05	-0.00122	75.72586
-7.99E-07	0.00012	0.016007	75.74023
3.33E-06	-0.00045	-0.06096	75.68873

-5.42E-06	0.001737	0.22113	75.81745
2.88E-06	-0.00167	0.235313	148.547
-6.28E-07	0.000415	-0.06697	148.6651
1.76E-07	-0.00011	0.017589	148.622
-8.56E-08	3.58E-05	-0.00373	148.6326
6.32E-08	-1.26E-05	0.000645	148.6285
-3.42E-08	3.64E-06	-0.00012	148.631

References:

1. *Undergrounding high voltage electricity transmission lines*. 2015, Warwick: National Grid.
2. *Undergrounding high voltage electricity transmission lines - The technical issues*. Vol. 4. January 2015, Warwick, UK: National Grid.
3. *Oil-Filled Cable*. [cited 2018 Oct 12]; Available from: https://encyclopedia2.thefreedictionary.com/Oil-Filled+Cable.
4. TAIHAN, *Oil Filled Power Cable*. TAIHAN ELECTRIC WIRE CO., LTD.
5. Zhou, H., et al., *Measurement and Modeling of Pitting Depth Distribution for Phosphor Bronze Tapes Used in Underground Power Transmission Cables.* CORROSION, 2017. **73**(7): p. 844-852.
6. Zhou, H., et al., *Life prediction of phosphor bronze reinforcing tape used in underground power cables* CORROSION, 2018. **74**(5): p. 530-542.
7. Müller, M., *Theoretical Considerations on Corrosion Fatigue Crack Initiation.* Metall. Trans. , 1982. **13A**(4): p. 649-655.
8. Le Son, K., et al., *Remaining useful life estimation based on stochastic deterioration models: A comparative study.* Reliability Engineering & System Safety, 2013. **112**(Supplement C): p. 165-175.
9. McAlinden, B. *Electricity transmission and distribution*. 2014 [cited 2018 March]; Available from: https://www.ice.org.uk/knowledge-and-resources/briefing-sheet/electricity-transmission-and-distribution.
10. Amadi-Echendu, J.E., et al., *What Is Engineering Asset Management?*, in *Definitions, Concepts and Scope of Engineering Asset Management*, J.E. Amadi-Echendu, et al., Editors. 2010, Springer London: London. p. 3-16.
11. *Network Output Measures Methodology*. 2010, UK: National Grid.
12. *DNO COMMON NETWORK ASSET INDICES METHODOLOGY*. 2017, UK: Office of Gas and Electricity Markets.
13. *Corrosion: Understanding the Basics*. 2000, ASM International.
14. Ke, W., *Progress in public inquiry concerning corrosion in Chinese industrial and natural environments.* CORROSION & PROTECTION, 2004. **25**(1): p. 1-8.
15. *Introduction and Overview of Electrochemical Corrosion*, in *Fundamentals of Electrochemical Corrosion*. 2000, ASM International.
16. *UNIFORM CORROSION (GENERAL CORROSION)*. [cited 2018 May 9th]; Available from: https://www.materials.sandvik/en/materials-center/corrosion/wet-corrosion/general-corrosion/.

17. Frankel, G.S. and N. Sridhar, *Understanding localized corrosion.* Materials Today, 2008. **11**(10): p. 38-44.
18. *Galvanic Corrosion*. [cited 2018 May 9th]; Available from: https://www.nace.org/Corrosion-Central/Corrosion-101/Galvanic-Corrosion/.
19. Mitchell, J. *The Galvanic Series-the essential guide*. 2017 [cited 2018 Oct 16th]; Available from: https://www.engineeringclicks.com/galvanic-series/.
20. *Crevice Corrosion*. [cited 2018; Available from: https://www.nace.org/Corrosion-Central/Corrosion-101/Crevice-Corrosion/.
21. *Pitting Corrosion*. [cited 2018; Available from: https://www.nace.org/Pitting-Corrosion/.
22. *Intergranular Corrosion*. [cited 2018; Available from: https://www.nace.org/Corrosion-Central/Corrosion-101/Intergranular-Corrosion/.
23. Antkyr. *Microscope view of a polished cross section of a material attacked by intergranular corrosion*. 2005 [cited 2018 Oct 16th]; Available from: https://en.wikipedia.org/wiki/Intergranular_corrosion#/media/File:Intergranular_corrosion.JPG.
24. *Dealloying (selective leaching)*. [cited 2018; Available from: https://www.nace.org/Dealloying/.
25. *Graphitization*. [cited 2018; Available from: https://www.corrosionpedia.com/definition/607/graphitization.
26. *Stress Corrosion Cracking (SCC)*. [cited 2018; Available from: https://www.nace.org/Corrosion-Central/Corrosion-101/Stress-Corrosion-Cracking-(SCC)/.
27. *Corrosion Fatigue*. [cited 2018; Available from: https://www.nace.org/Corrosion-Central/Corrosion-101/Corrosion-Fatigue/.
28. Esaklul, K.A., *13 - Hydrogen damage A2 - El-Sherik, A.M*, in *Trends in Oil and Gas Corrosion Research and Technologies*. 2017, Woodhead Publishing: Boston. p. 315-340.
29. Khajavi, M.R., et al., *Failure analysis of bank front boiler tubes.* Engineering Failure Analysis, 2007. **14**(4): p. 731-738.
30. D.Port, R. and H. M.Herro, *The Nalco Guide to BOiler Failure Analysis*. 1985: McGraw-Hill, Inc.
31. Lamping, G.A. and S.R. Institute, *Manual for Investigation and Correction of Boiler Tube Failures*. 1985: Electric Power Research Institute.
32. Soltis, J., *Passivity breakdown, pit initiation and propagation of pits in metallic materials – Review.* Corrosion Science, 2015. **90**: p. 5-22.
33. Böhni, H., *Breakdown of Passivity and Localized Corrosion Processes.* Langmuir, 1987. **3**(6): p. 924-930.
34. P.R.Roberge, *Recognizing the Forms of Corrosion*, in *Corrosion Engineering*. 2008, McGraw Hill Professional, Access Engineering.

35. G.S.Frankel, *Pitting corrosion of metals: a review of the critical factors.* Journal of Electrochemical Society, 1998. **145**(6): p. 13.
36. E.J.Dolley, B.Lee, and R.P.Wei, *The effect of pitting corrosion on fatigue life.* Fatigue and Fracture of Engineering Materials and Structures, 2000. **23**: p. 6.
37. C.Blanc and G.Mankowski, *Susceptibility to Pitting Corrosion of 6056 Aluminium Alloy.* Corrosion Science, 1997. **39**(5): p. 11.
38. H.Ezuber, A.El-Houd, and F.El-Shawesh, *A study on the corrosion behavior of aluminum alloys in seawater.* Materials and Design, 2008. **29**: p. 5.
39. E.McCafferty, *Sequence of steps in the pitting of aluminum by chloride ions.* Corrosion Science, 2003. **45**: p. 18.
40. R.P.Wei, *Environmental considerations for fatigue cracking.* Fatigue and Fracture of Engineering Materials and Structures, 2002. **25**: p. 10.
41. C.Pan, et al., *Pitting corrosion of 304ss nanocrystalline thin film.* Corrosion Science, 2013. **73**: p. 12.
42. D.Nakhaie and M.H.Moayed, *Pitting corrosion of cold rolled solution treated 17-4 PH stainless steel.* Corrosion Science, 2014. **80**: p. 9.
43. W.Tian, et al., *Metastable pitting corrosion of 304 stainless steel in 3.5% NaCl solution.* Corrosion Science, 2014. **85**: p. 8.
44. F.Caleyo, et al., *Probability distribution of pitting corrosion depth and rate in underground pipelines: A Monte Carlo study.* Corrosion Science, 2009. **51**: p. 10.
45. D.G.Kingerley and M.J.Longster, *Stress corrosion of phosphor-bronze reinforcing tapes on underground power cables.* Corrosion Science, 1974. **14**(2).
46. F.Maurizio, et al., *Corrosion fatigue of phosphor-bronze reinforcing tapes on underground power transmission cables- Failure analysis.* Submitted to Corrs. Eng. Sci. Techn., 2016.
47. V.F.Lucey, *Developments Leading to the Present Understanding of the Mechanism of Pitting Corrosion of Copper.* British Corrosion Journal, 1972. **7**(1): p. 6.
48. M.H.Mohd, et al., *A time-variant corrosion wastage model for subsea gas pipelines.* Ships and Offshore Structures, 2014. **9**(2): p. 16.
49. W.Harara, *Pit-depth measurement on large diameter pipes by tangential radiography using a Co-60 gamma-ray source.* Russian Journal of Nondestructive Testing, 2004. **40**(11): p. 7.
50. R.Baboian, ed. *Corrosion Tests and Standards: Application and Interpretation - Second Edition*. ed. R.Baboian, et al. 2005, ASTM International: Baltimore, MD. 882.
51. J.A.Mock, *A guide to nondestructive testing.* Materials Engineering, 1969. **69**.
52. Kingerley, D.G. and M.J. Longster, *Stress corrosion of phosphor-bronze reinforcing tapes on underground power cables.* Corros. Sci., 1974. **14**(2): p. 165-167.

53. Maurizio, F., et al., *Corrosion fatigue of phosphor - bronze reinforcing tapes on underground power transmission cables - Failure analysis.* Submitted to Engineering Failure Analysis.
54. Hoeppner, D.W., *Model for prediction of fatigue lives based upon a pitting corrosion fatigue process*, in *Fatigue Mechanisms*, J.T. Fong, Editor. 1979, ASTM STP675: Philadelphia PA. p. 841.
55. Y.Kondo and R.P.Wei, *Proceedings of EVALMAT89*. Approach on quantitative evaluation of corrosion fatigue crack initiation condition. 1989, Kobe, Japan: Iron & Steel Institute of Japan.
56. Y.Kondo, *Prediction of Fatigue Crack Initiation Life Based on Pit Growth.* Corrosion Science, 1989. **45**(1): p. 7-13.
57. Amiri, M., et al., *A continuum damage mechanics model for pit-to-crack transition in AA2024-T3.* Corrosion Science, 2015. **98**: p. 678-687.
58. Rokhlin, S.I., et al., *Effect of pitting corrosion on fatigue crack initiation and fatigue life.* Engineering Fracture Mechanics, 1999. **62**(4–5): p. 425-444.
59. Xie, C., et al., *Corrosion Reliability Analysis Considering the Coupled Effect of Mechanical Stresses.* ASCE-ASME Journal of Risk and Uncertainty in Engineering Systems, Part B: Mechanical Engineering, 2016. **2**(3): p. 031001-031001.
60. M.Romanoff, *Underground Corrosion.* NBS Circular 579, National Bureau of Standard, Washington, DC, 1957.
61. D.G.Harlow and R.P.Wei, *Probability approach for prediction of corrosion and corrosion fatigue life.* AIAA JOURNAL, 1994. **32**(10): p. 2073-2078.
62. D.G.Harlow and R.P.Wei, *A probability model for the growth of corrosion pits in aluminum alloys induced by constituent particles.* Engineering Fracture Mechanics, 1998. **59**(3): p. 305-325.
63. J.Rajasankar and N.R.Iyer, *A probability-based model for growth of corrosion pits in aluminium alloys.* Engineering Fracture Mechanics, 2006. **73**: p. 553-570.
64. J.L.Alamilla and E.Sosa, *Stochastic modelling of corrosion damage propagation in active sites from field inspection data.* Corrosion Science, 2008. **50**(7): p. 9.
65. M.Chookah, M.Nuhi, and M.Modarres, *A probabilitistic physics-of-failure model for prognostic health management of strucutres subjuect to pitting and corrosion-fatigue.* Reliability Engineering and System Safety, 2011. **96**: p. 10.
66. Bechhoefer, E., A.P.F. Bernhard, and D. He, *Use of Paris Law for Prediction of Component Remaining Life.* Conference Paper in IEEE Aerospace Conference Proceedings, 2008: p. 8.
67. Brown, E.N., S.R. White, and N.R. Sottos, *Fatigue crack propagation in microcapsule-toughened epoxy.* J Mater Sci 2006. **41**: p. 8.
68. Olurin, O.B., et al., *Fatigue crack propagation in aluminium alloy foams.* International Journal of Fatigue, 2001. **23**: p. 8.

69. Pugno, N., et al., *A generalized Paris' law for fatigue crack growth.* Journal of the Mechanics and Physics of Solids, 2006. **54**: p. 17.
70. Turnbull, A., L.N. McCartney, and S. Zhou, *A model to predict the evolution of pitting corrosion and the pit-to-crack transition incorporating statistically distributed input parameters.* Corrosion Science, 2006. **48**(8): p. 2084-2105.
71. Engelhardt, G. and D.D. Macdonald, *Unification of the deterministic and statistical approaches for predicting localized corrosion damage. I. Theoretical foundation.* Corros. Sci., 2004. **46**(11): p. 2755-2780.
72. G. Engelhardt, et al., *Deterministic Prediction of Corrosion Damage in Low Pressure Steam Turbines* Power Plant Chem., 2004. **6**(11): p. 647.
73. Turnbull, A. and S. Zhou, *Pit to crack transition in stress corrosion cracking of a steam turbine disc steel.* Corrosion Science, 2004. **46**(5): p. 1239-1264.
74. A.Valor, et al., *Stochastic modeling of pitting corrosion: a new model for initiation and growth of multiple corrosion pits.* Corrosion Science, 2007. **49**(2): p. 20.
75. J.C.Velazquez, et al., *Statistical modelling of pitting corrosion: extrapolation of the maximum pit depth-growth.* International Journal of Electrochemical Science, 2014. **9**: p. 15.
76. C.C.Nathan and C.L.Dulaney, *Localized Corrosion*. 1984: NACE.
77. A.K.Sheikh, J.K.Boah, and D.A.Hansen, *Statistical modeling of pitting corrosion and pipeline reliability.* Corrosion, 1990. **46**(3): p. 8.
78. T.Johnsen and R.Hilfer, *Statistical prediction of corrosion front penetration.* Physical Review E - Statistical Physics, Plasmas, Fluids, and Related Interdisciplinary Topics, 1997. **55**(5 A): p. 10.
79. D.G.Harlow and R.P.Wei, *A Probability Model for the Growth of Corrosion Pits in Aluminum Alloys Induced by Constituent Particles.* Engineering Fracture Mechanics, 1998. **59**(3): p. 21.
80. G.Engelhardt and D.D.Macdonald, *Deterministic Prediction of Pit Depth Distribution.* Corrosion, 1997. **54**(6): p. 11.
81. S.Komukai and K.Kasahara, *On the requirements for a reasonable extreme value prediction of maximum pits on hot-water-supply copper tubing.* Journal of Research of the National Institute of Standards and Technology, 1994. **99**(4): p. 6.
82. T.Isogai, Y.Katano, and K.Miyata, *Models and inference for corrosion pit depth data.* Extremes, 2004. **7**: p. 18.
83. A.Valor, et al., *Markov Chain models for the stochastic modeling of opitting corrosion.* Mathematical Problems in Engineering, 2013. **2013**: p. 13.
84. M.K.Cavanaugh, R.G.Buchheit, and N.Birbilis, *Modeling the environmental dependence of pit growth using neural network approaches.* Corrosion Science, 2010. **52**: p. 8.
85. T.Shibata, *1996 W.R. Whitney Award lecture: statistical and stochastic*

approaches to localized corrosion. Material und Organismen, 1996. **52**(11): p. 18.
86. J.Rajasankar and N.R.Iyer, *A probability-based model for growth of corrosion pits in aluminium alloys.* Engineering Fracture Mechanics, 2006. **73**: p. 18.
87. D.G.Harlow and R.P.Wei, *Probability approach for prediction of corrosion and corrosion fatigue life.* AIAA JOURNAL, 1994. **32**(10): p. 6.
88. C.I.Ossai, *Pipeline corrosion prediction and reliability analysis: a systematic approach with Monte Carlo simulation and degradation models.* International Journal of Science & Technology Research 2013. **2**(3): p. 12.
89. K.R.Davey, O.Lavigne, and P.Shah, *Establishing an atlas of risk of pitting of metals at sea – demonstrated for stainless steel AISI 316L in the Bass Strait.* Chemical Engineering Science, 2016. **140**: p. 5.
90. C.I.Ossai, B.Boswell, and I.J.Davies, *Application of Markov modelling and Monte Carlo simulation technique in failure probability estimation — a consideration of corrosion defects of internally corroded pipelines.* Engineering Failure Analysis.
91. N.Murer and R.G.Buchheit, *Stochastic modeling of pitting corrosion in aluminum alloys.* Corrosion Science, 2013. **69**: p. 10.
92. *Review of the Electricity Transmission Asset Management Policies and Processes as adopted by National Grid Electricity Transmission (NGET) within England & Wales*. 2006, KEMA Limited.
93. Martin, D., et al., *An updated model to determine the life remaining of transformer insulation.* IEEE Transactions on Power Delivery, 2015. **30**(1): p. 395-402.
94. Khalifa, M., F. Khan, and J. Thorp, *Risk-based maintenance and remaining life assessment for gas turbines.* Journal of Quality in Maintenance Engineering, 2015. **21**(1): p. 100-111.
95. Segovia, M., et al., *Predicting remaining life of transmission tower steelwork components*, in *Risk, Reliability and Safety*. 2016, CRC Press: London, UK.
96. Ahmadzadeh, F. and J. Lundberg, *Remaining useful life prediction of grinding mill liners using an artificial neural network.* Minerals Engineering, 2013. **53**(Supplement C): p. 1-8.
97. Animah, I. and M. Shafiee, *Condition assessment, remaining useful life prediction and life extension decision making for offshore oil and gas assets.* Journal of Loss Prevention in the Process Industries, 2017.
98. Su, Y., et al., *A one-dimensional integral approach to calculating the failure probability of geotechnical engineering structures.* Computers and Geotechnics, 2017. **90**(Supplement C): p. 85-95.
99. Wang, W., et al., *Comparative analysis of failure probability for ethylene cracking furnace tube using Monte Carlo and API RBI technology.* Engineering Failure Analysis, 2014. **45**(Supplement C): p. 278-282.

100. Zhou, J., W. Zhao, and W. Mao, *Least Favorable Probability of Failure for 5- and 10-story RC Frame Structures with Vertical Irregularities.* Journal of Earthquake Engineering, 2015. **19**(7): p. 1158-1180.
101. Liang, G., et al., *A transformer replacement decision method based on probabilty assessment of failure rate.* Energy and Power Engineering, 2017. **9**: p. 748-755.
102. Seo, J., et al., *A Study on the Probability of Failure Model Based on the Safety Factor for Risk Assessment in a Water Supply Network.* Procedia Engineering, 2015. **119**(Supplement C): p. 206-215.
103. Kioumarsi, M.M., et al., *The effect of interference of corrosion pits on the failure probability of a reinforced concrete beam.* Engineering Structures, 2016. **114**(Supplement C): p. 113-121.
104. Jamali, A., et al., *Probability of failure for uncertain control systems using neural networks and multi-objective uniform-diversity genetic algorithms (MUGA).* Engineering Applications of Artificial Intelligence, 2013. **26**(2): p. 714-723.
105. Qiao, L., J. Shi, and W. An, *An application of systemic prediction evaluation parameters for neural network remaining useful life predictions models.* 2015 IEEE Conference on Prognostics and Health Management (PHM), 2015: p. 1-4.
106. Wang, H.-W., T.-X. Xu, and W.-Y. Wang, *Remaining Life Prediction Based on Wiener Processes with ADT Prior Information.* Quality and Reliability Engineering International, 2016. **32**(3): p. 753-765.
107. A.Mosallam, K.Medjaher, and N.Zerhouni, *Data-driven prognostic method based on Bayesian approaches for direct remaining useful life prediction.* Journal of Intelligent Manufacturing, 2016. **27**(5): p. 1037-1048.
108. Tenenbaum, J.B., T.L. Griffiths, and C. Kemp, *Theory-based Bayesian models of inductive learning and reasoning.* Trends in Cognitive Sciences, 2006. **10**(7): p. 309-318.
109. Xu, F. and J.B. Tenenbaum, *Word learning as Bayesian inference.* Psychological Review, 2007. **114**(2): p. 245-272.
110. Davis, R.H., D.B. Edelman, and A.J. Gammerman, *Machine-learning algorithms for credit-card applications.* IMA Journal of Management Mathematics, 1992. **4**(1): p. 43-51.
111. Perrin, B.-E., et al., *Gene networks inference using dynamic Bayesian networks.* Bioinformatics, 2003. **19**(suppl_2): p. ii138-ii148.
112. Zelterman, D., *Bayesian Artificial Intelligence.* Technometrics, 2005. **47**(1): p. 101-102.
113. Andrieu, C., et al., *An Introduction to MCMC for Machine Learning.* Machine Learning, 2003. **50**(1): p. 5-43.
114. E.Tipping, M., *Sparse Bayesian learning and the relevance vector machine.* Journal of Machine Learning Research, 2001. **1**: p. 211-244.

115. Minka, T.P., *Expectation propagation for approximate Bayesian inference*, in *Proceedings of the Seventeenth conference on Uncertainty in artificial intelligence*. 2001, Morgan Kaufmann Publishers Inc.: Seattle, Washington. p. 362-369.
116. Tenenbaum, J.B. and T.L. Griffiths, *Generalization, similarity, and Bayesian inference.* Behavioral and Brain Sciences, 2002. **24**(4): p. 629-640.
117. P.C.Paris, M.P.Gomez, and W.E.Anderson, *A rational analytic theory of fatigue.* The Trend in Engineering, 1961. **13**: p. 9-14.
118. Zhang, J., X.D. He, and S.Y. Du, *A simple engineering approach in the prediction of the effect of stress ratio on fatigue threshold.* International Journal of Fatigue, 2003. **25**(9): p. 935-938.
119. Taylor, D., *A Compendium of Fatigue Thresholds and Growth Rates*. 1985: Engineering Materials Advisory Services Limited.
120. Smith, K., T. Topper, and P. Watson, *A stress-strain function for the fatigue of metals(Stress-strain function for metal fatigue including mean stress effect).* Journal of materials, 1970. **5**: p. 767-778.
121. Walker, K., *The effect of stress ratio during crack propagation and fatigue for 2024-T3 and 7075-T6 aluminum*, in *Effects of environment and complex load history on fatigue life*. 1970, ASTM International.
122. Klesnil, M. and P. Lukáš, *Effect of stress cycle asymmetry on fatigue crack growth.* Materials Science and Engineering, 1972. **9**: p. 231-240.
123. International, A., *Standard Guide for Preparation of Metallographic Specimens*. 2011.
124. International, A., *Standard Guide for Examination and Evaluation of Pitting Corrosion*. 2005.
125. Watkins, J.C., *An Introduction to the Science of Statistics: From Theory to Implementation*.
126. Fougères, A.L., S. Holm, and H. Rootzén, *Pitting Corrosion: Comparison of Treatments With Extreme-Value–Distributed Responses.* Technometrics, 2006. **48**(2): p. 262-272.
127. Mohd, M.H., et al., *A time-variant corrosion wastage model for subsea gas pipelines.* Ships and Offshore Structures, 2014. **9**(2): p. 16.
128. Aankul, A. *T-test using Python and Numpy*. 2017 [cited 2018 April 8th]; Available from: https://towardsdatascience.com/inferential-statistics-series-t-test-using-numpy-2718f8f9bf2f.
129. SCHWENK, W., *Theory Of Stainless Steel Pitting.* CORROSION, 1964. **20**(4): p. 129t-137t.
130. Rosenfeld, I.L. and I.S. Danilov, *Electrochemical aspects of pitting corrosion.* Corrosion Science, 1967. **7**(3): p. 129-142.
131. Isaacs, H.S. and G. Kissel, *Surface Preparation and Pit Propagation in Stainless Steels.* Journal of The Electrochemical Society, 1972. **119**(12): p. 1628-1632.

132. Mankowski, J. and Z. Szklarska-Smialowska, *Studies on accumulation of chloride ions in pits growing during anodic polarization.* Corrosion Science, 1975. **15**(6): p. 493-501.
133. Pistorius, P.C. and G.T. Burstein, *Metastable pitting corrosion of stainless steel and the transition to stability.* Philosophical Transactions of the Royal Society of London. Series A: Physical and Engineering Sciences, 1992. **341**(1662): p. 531-559.
134. Frankel, G.S., et al., *Metastable Pitting of Stainless Steel.* CORROSION, 1987. **43**(7): p. 429-436.
135. Ernst, P., et al., *The mechanism of lacy cover formation in pitting.* Corrosion Science, 1997. **39**(6): p. 1133-1136.
136. Ernst, P. and R.C. Newman, *Pit growth studies in stainless steel foils. I. Introduction and pit growth kinetics.* Corrosion Science, 2002. **44**(5): p. 927-941.
137. Ernst, P. and R.C. Newman, *Pit growth studies in stainless steel foils. II. Effect of temperature, chloride concentration and sulphate addition.* Corrosion Science, 2002. **44**(5): p. 943-954.
138. Ghahari, S.M., et al., *In situ synchrotron X-ray micro-tomography study of pitting corrosion in stainless steel.* Corrosion Science, 2011. **53**(9): p. 2684-2687.
139. Almuaili, F.A., et al., *Strain-induced reactivation of corrosion pits in austenitic stainless steel.* Corrosion Science, 2017. **125**: p. 12-19.
140. Ghahari, M., et al., *Synchrotron X-ray radiography studies of pitting corrosion of stainless steel: Extraction of pit propagation parameters.* Corrosion Science, 2015. **100**: p. 23-35.
141. Y.Kondo, *Prediction of Fatigue Crack Initiation Life Based on Pit Growth.* Corrosion Science, 1989. **45**(1): p. 5.
142. McCafferty, E., *Pit Initiation on Aluminum as a Queueing Process.* J. Electrochem. Soc., 2010. **157**(11): p. 6.
143. Cavanaugh, M.K., N. Birbilis, and R.G. Buchheit, *Modeling pit initiation rate as a function of environment for Aluminum alloy 7075-T651.* Electrochimica Acta, 2012. **59**: p. 336-345.
144. Kunz, L. and L. Collini, *Mechanical properties of copper processed by Equal Channel Angular Pressing – a review.* Frattura ed Integrità Strutturale, 2012. **19**: p. 15.
145. *Critical components, Underground cables*. [cited 2018; Available from: https://www.hydro.mb.ca/projects/system_renewal/components.shtml.
146. *Undergrounding high voltage electricity transmission lines*. 2015; Available from: https://www.nationalgrid.com/sites/default/files/documents/39111-Undergrounding_high_voltage_electricity_transmission_lines_The_technical_issues_INT.pdf.

147. *Overview of the Potential for Undergrounding the Electricity Networks in Europe*. 2003, ICF Consulting: London, United Kindom.
148. *Transmission & Distribution Infrastructure*. 2014, Harris Williams & Co.
149. *Statistics: Overhead Lines and Underground Cables*, in *Aging of the System-Impact on Planning*. 2000, CIGRE: Paris, France.
150. Buhari, M. and S. Awadallah, *Modelling of Ageing Distribution Cable for Replacement Planning*. Vol. 1. 2015.
151. Lihou, D.A. and G.D. Spence, *Proper use of data with the Weibull distribution.* Journal of Loss Prevention in the Process Industries, 1988. **1**(2): p. 110-113.
152. Seal, C.K. and A.H. Sherry, *Weibull distribution of brittle failures in the transition region.* Procedia Structural Integrity, 2016. **2**: p. 1668-1675.
153. Thomason, J.L., *On the application of Weibull analysis to experimentally determined single fibre strength distributions.* Composites Science and Technology, 2013. **77**: p. 74-80.
154. Gourier, C., et al., *Mechanical analysis of elementary flax fibre tensile properties after different thermal cycles.* Composites Part A: Applied Science and Manufacturing, 2014. **64**: p. 159-166.
155. Glantz, S.A. and B.K. Slinker, *Primer of Applied Regression and Analysis of Variance*. 1990: McGraw-Hill, Health Professions Division.
156. Draper, N.R. and H. Smith, *Applied Regression Analysis, Third Edition*. Wiley Series in Probability and Statistics. 1998: John Wiley & Sons, Inc.
157. Berger, J.O., *Statistical Decision Theory and Bayesian Analysis*. Springer Series in Statistics. 1985: Springer-Verlag New York.
158. Gelman, A., et al., *Bayesian Data Analysis*, ed. F. Dominici, et al. 2014, New York: Taylor & Francis Group.
159. Roberts, G.O. and J.S. Rosenthal, *General state space Markov chains and MCMC algorithms.* Probab. Surveys, 2004. **1**: p. 20-71.